

## POPULATION PROPERTIES OF BROWN DWARF ANALOGS TO EXOPLANETS\*

JACQUELINE K. FAHERTY<sup>1,2,9</sup>, ADRIC R. RIEDEL<sup>2,3</sup>, KELLE L. CRUZ<sup>2,3,11</sup>, JONATHAN GAGNE<sup>1, 10</sup>, JOSEPH C. FILIPPAZZO<sup>2,4,11</sup>, ERINI LAMBRIDES<sup>2</sup>, HALEY FICA<sup>2</sup>, ALYCIA WEINBERGER<sup>1</sup>, JOHN R. THORSTENSEN<sup>8</sup>, C. G. TINNEY<sup>7,12</sup>, VIVIENNE BALDASSARE<sup>2,5</sup>, EMILY LEMONIER<sup>2,6</sup>, EMILY L. RICE<sup>2,4,11</sup>

*Draft version May 26, 2016*

### ABSTRACT

We present a kinematic analysis of 152 low surface gravity M7-L8 dwarfs by adding 18 new parallaxes (including 10 for comparative field objects), 38 new radial velocities, and 19 new proper motions. We also add low- or moderate-resolution near-infrared spectra for 43 sources confirming their low-surface gravity features. Among the full sample, we find 39 objects to be high-likelihood or new bona fide members of nearby moving groups, 92 objects to be ambiguous members and 21 objects that are non-members. Using this age calibrated sample, we investigate trends in gravity classification, photometric color, absolute magnitude, color-magnitude, luminosity and effective temperature. We find that gravity classification and photometric color clearly separate 5-130 Myr sources from > 3 Gyr field objects, but they do not correlate one-to-one with the narrower 5 -130 Myr age range. Sources with the same spectral subtype in the same group have systematically redder colors, but they are distributed between 1-4 $\sigma$  from the field sequences and the most extreme outlier switches between intermediate and low-gravity sources either confirmed in a group or not. The absolute magnitudes of low-gravity sources from *J* band through *W3* show a flux redistribution when compared to equivalently typed field brown dwarfs that is correlated with spectral subtype. Low-gravity late-type L dwarfs are fainter at *J* than the field sequence but brighter by *W3*. Low-gravity M dwarfs are > 1 mag brighter than field dwarfs in all bands from *J* through *W3*. Clouds, which are a far more dominant opacity source for L dwarfs, are the likely cause. On color magnitude diagrams, the latest-type low-gravity L dwarfs drive the elbow of the L/T transition up to 1 magnitude redder and 1 magnitude fainter than field dwarfs at *M<sub>J</sub>* but are consistent with or brighter than the elbow at *M<sub>W1</sub>* and *M<sub>W2</sub>*. We conclude that low-gravity dwarfs carry an extreme version of the cloud conditions of field objects to lower temperatures, which logically extends into the lowest mass directly imaged exoplanets. Furthermore, there is an indication on CMD's (such as *M<sub>J</sub>* versus (*J-W2*)) of increasingly redder sequences separated by gravity classification although it is not consistent across all CMD combinations. Examining bolometric luminosities for planets and low-gravity objects, we confirm that (in general) young M dwarfs are overluminous while young L dwarfs are normal compared to the field. Using model extracted radii, this translates into normal to slightly warmer M dwarf temperatures compared to the field sequence while lower temperatures for L dwarfs with no obvious correlation with assigned moving group.

*Keywords:* Astrometry— stars: low-mass— brown dwarfs

\*THIS PAPER INCLUDES DATA GATHERED WITH THE 6.5 METER MAGELLAN TELESCOPES LOCATED AT LAS CAM-PANAS OBSERVATORY, CHILE.

<sup>1</sup> Department of Terrestrial Magnetism, Carnegie Institution of Washington, Washington, DC 20015, USA; jfaherty@carnegiescience.edu

<sup>2</sup> Department of Astrophysics, American Museum of Natural History, Central Park West at 79th Street, New York, NY 10034; jfaherty@amnh.org

<sup>3</sup> Department of Physics & Astronomy, Hunter College, 695 Park Avenue, New York, NY 10065, USA

<sup>4</sup> Department of Engineering Science & Physics, College of Staten Island, 2800 Victory Blvd., Staten Island, NY 10301 USA

<sup>5</sup> Department of Astronomy, University of Michigan, 1085 S. University, Ann Arbor, MI 48109

<sup>6</sup> Department of Physics & Astronomy, Columbia University, Broadway and 116th St., New York, NY 10027 USA

<sup>7</sup> School of Physics, UNSW Australia, 2052. Australia

<sup>8</sup> Department of Physics and Astronomy, Dartmouth College, Hanover NH 03755, USA

<sup>9</sup> Hubble Fellow

<sup>10</sup> Sagan Fellow

<sup>11</sup> Physics Program, The Graduate Center, City University of New York, New York, NY 10016

<sup>12</sup> Australian Centre for Astrobiology, UNSW Australia, 2052. Australia

### 1. INTRODUCTION

At masses  $<\sim 75 M_{Jup}$  – the H-burning mass limit –, the interior of a source changes significantly. Below this mass limit, electron degeneracy pressure sufficiently slows contraction that the core of a given object is prevented from ever reaching the temperatures required for nuclear fusion (Hayashi & Nakano 1963, Kumar 1963). As a consequence, the evolution of substellar mass objects produces a temperature, age, and mass degeneracy that leads to an important, and at times completely indistinguishable, overlap in the physical properties of the lowest mass stars, brown dwarfs and planets.

Objects with masses  $<\sim 75 M_{Jup}$  cool through their lives with spectral energy distributions evolving as their atmospheric chemistry changes with decreasing temperatures. The spectral classification for sources in the range (3000 K  $> T_{eff} > 250$  K) corresponds to late-type M, L, T and Y with each class defined by the effects of changing molecular species available in the photosphere (Kirkpatrick 2005, Burgasser et al. 2002a, Cushing et al. 2011). At the warmest temperatures, the atmosphere is too hot

for the condensation of solids (Allard & Hauschildt 1995; Lodders 1999). But as the  $T_{eff}$  falls below 2500 K, both liquid (e.g. Fe) and solid (e.g. CaTiO<sub>3</sub>, VO) mineral and metal condensates settle into discrete cloud layers (Ackerman & Marley 2001; Tsuji et al. 1996b,a; Woitke & Helling 2004; Allard et al. 2001).

As temperatures cool further, cloud layers form at such deep levels in the photosphere that they have little or no impact on the emergent spectrum. This transition between “cloudy” to “cloudless” objects occurs rapidly over a narrow temperature range (1200-1400 K, corresponding to the transition between L-type and T-type spectra) and drives extreme photometric, spectroscopic, and luminosity changes (Burgasser et al. 2002b, Tinney et al. 2003, Faherty et al. 2012, 2014a, Dupuy & Liu 2012, Radigan et al. 2012, Artigau et al. 2009). Violent storms (like those seen on Jupiter), along with magnetic-activity-inducing aurorae, have been noted as environmental conditions likely to be present at the L-T transition (Metchev et al. 2015, Radigan et al. 2012, Apai et al. 2013, Hallinan et al. 2015, Buenzli et al. 2014, Gillon et al. 2013, Buenzli et al. 2015, Faherty et al. 2014a, Burgasser et al. 2014).

Confounding our understanding of cloud formation in low-temperature atmospheres is mounting evidence for a correlation between cloud properties and youth. Low surface gravity brown dwarfs, thought to be young, have unusually red near to mid-infrared colors and a fainter absolute magnitude through  $\sim 2.5 \mu\text{m}$  when compared to their older spectral counterparts with field surface gravities (Faherty et al. 2012, Faherty et al. 2013, Filippazzo et al. 2015, Liu et al. 2013, Gagné et al. 2015b). Metchev & Hillenbrand (2006) made the first connection between age and cloudiness in their study of the young companion HD 203030B, whose transition to the cloud-free T spectral class appears to be delayed by the presence of thick clouds. In a detailed study of the prototypical isolated, young brown dwarf 2M0355+1133, Faherty et al. (2013) found that the deviant colors and fainter absolute magnitudes were best explained by enhanced dust, or thick photospheric clouds, shifting flux to longer wavelengths. At the coldest temperatures, where clouds should all but have dispersed below the photosphere in field brown dwarfs, Burgasser et al. (2010b) studied the T8 dwarf Ross 458 C and found clouds must be considered as an important opacity source for young T dwarfs.

Exoplanet studies have independently found similar trends with age and cloud properties. The young planetary mass companions 2M1207 b ( $< 10 M_{Jup}$ ) and HR8799 b ( $< 10 M_{Jup}$ ), are exceedingly red in the near-infrared and up to 2 magnitudes fainter than field brown dwarfs of similar  $T_{eff}$  (Marois et al. 2008, 2010, Mohanty et al. 2007). To reproduce their anomalous observables, theorists have developed “enhanced” cloudy atmospheric models with non-equilibrium chemistry (Marley et al. 2012, Barman et al. 2011a,b, Madhusudhan et al. 2011) in which lower surface gravity alters the vertical mixing which then leads to high altitude clouds with differing physical composition (e.g. thicker or thinner aggregations).

In general, M, L, T, and Y classifications identify brown dwarfs. If the source is older ( $> 2 - 3 \text{ Gyr}$ ), late-type M and early L dwarfs are stars. But if the source is young ( $< 1 \text{ Gyr}$ ), even those warmer classifi-

cations will describe an object that is  $< 75 M_{Jup}$ . To date, all directly imaged giant exoplanets have observable properties which lead to their classification squarely in this well-studied regime. Planetary mass companions such as 2M1207 b, 51 Eri b,  $\beta$  Pictoris b, ROXs 42B b, and the giant planets orbiting HR8799, have observables that are similar to L or T brown dwarfs (Chauvin et al. 2004, Macintosh et al. 2015, Lagrange et al. 2010, Marois et al. 2008, 2010, Currie et al. 2014, Kraus et al. 2014). Furthermore, there exists a population of “classical” brown dwarfs that overlap in effective temperature, age – many in the same moving group – , and mass with directly observed planetary mass companions (e.g. PSO 318, SDSS1110, 0047+6803, Liu et al. 2013, Gagné et al. 2015c, Gizis et al. 2012, 2015). Studies of these two populations in concert may resolve questions of the formation of companions versus isolated equivalents as well as untangle atmosphere, temperature, age, and metallicity effects on the observables.

In this work we examine this new population of suspected young, low surface gravity sources that are excellent exoplanet analogs. In section 2 we explain the sample examined in this work and in section 3 we describe the imaging and spectral data acquired. In section 4 we review new near-infrared spectral types designated in this work and in section 5 we discuss how we measured new radial velocities. In section 6 we assess the likelihood of membership in nearby moving groups such as  $\beta$  Pictoris, AB Doradus, Argus, Columba, TW Hydrea, and Tucana Horologium. In section 7 we review the diversity of the whole sample in spectral features, infrared colors, absolute magnitudes, bolometric luminosities and effective temperatures. In section 8 we place the young brown dwarf sample in context with directly imaged planetary mass companions. Conclusions are presented in section 9.

## 2. THE SAMPLE

Given the age-mass degeneracy of substellar mass objects and an age range of  $\sim 5 - 130 \text{ Myr}$  for groups such as TW Hydrea (5-15 Myr; Weinberger et al. 2013),  $\beta$  Pictoris (20-26 Myr; Binks & Jeffries 2014, Malo et al. 2014), and AB Doradus (110 - 130 Myr; Barenfeld et al. 2013, Zuckerman et al. 2004) the target temperature for our sample was  $T_{eff} < 3000 \text{ K}$ , or, equivalently, sources with spectral types of M7 or later. This cut-off restricted us to  $< 0.07 M_{\odot}$  or the classic brown dwarf boundary (Kumar 1963, Hayashi & Nakano 1963).

The suspicion of membership in a nearby moving group should be accompanied by observed signatures of youth as kinematics alone leave doubt about chance contamination from the field sample. As such, for this work we focused on  $> M7$  objects with confirmed spectral signatures of low-gravity in either the optical or the infrared. We note that while there are isolated T dwarfs thought to be young (e.g. SDSS 1110, Gagné et al. 2015a, CF-BDSIR 2149, Delorme et al. 2012), their spectral peculiarities appear to be subtle making them more difficult to identify and investigate (see also Best et al. 2015).

For isolated late-type M and L dwarfs suspected to be young, there are strong spectral differences in the strength of the alkali lines and metal oxide absorption bands as well as the shape of the near-infrared  $H$ - band ( $\sim 1.65 \mu\text{m}$ ) compared to older field age counterparts (e.g.

Lucas et al. 2001; Gorlova et al. 2003; Luhman et al. 2004; McGovern et al. 2004; Allers et al. 2007; Rice et al. 2010, 2011, Patience et al. 2012; Faherty et al. 2013). Physically this can be explained by a change in the balance between ionized and neutral atomic and molecular species, as a result of lower surface gravity and, consequently, lower gas densities in the photospheric layers (Kirkpatrick et al. 2006). Furthermore, a lower surface gravity is linked to an increase in collision induced H<sub>2</sub> absorption (see e.g. Canti et al. 2013, Tokunaga & Kobayashi 1999). Changes in the amount of this absorption result in the *K*-band ( $\sim 2.2 \mu\text{m}$ ) being suppressed (or enhanced) and the shape of the *H* band being modified to cause the “peaky” *H* band relative to water opacity seen in young sources (see Rice et al. 2011).

The collection of brown dwarfs with spectral signatures of a low-surface gravity is increasing<sup>13</sup>. Gagné et al. (2014c, 2015b,c) presented a bayesian analysis of the brown dwarf population looking for potential new moving group members and uncovered numerous low-gravity sources. Allers & Liu (2013) presented a near-infrared spectroscopic study of a large number of known sources. Aside from those extensive studies, objects have been reported singly in paper (e.g. Kirkpatrick et al. 2006, Liu et al. 2013, Gagné et al. 2014a,b, 2015a, Faherty et al. 2013, Rice et al. 2010, Gizis et al. 2012, Gauza et al. 2015) or included as a subset to a larger compilation of field objects (e.g. Cruz et al. 2007, Kirkpatrick et al. 2010, Reid et al. 2007, Thompson et al. 2013). The objects within this paper were drawn from the literature as well as our ongoing search for new low-surface gravity objects.

The 152<sup>14</sup> low-surface gravity objects examined in this work are listed in Table 1 with their coordinates, spectral types, gravity classifications (optical and infrared as applicable), 2MASS and WISE photometry. There are 48 sources in this sample that are lacking an optical spectral type and 8 sources lacking an infrared spectral type. Of the 96 objects with both optical and near-infrared data, there are 67 sources (70%) that have a different optical spectral type than the infrared although the majority are within 1 subtype of each other.

For assigning a gravity designation, there are two classification systems based on spectral features. The Cruz et al. (2009) system uses optical spectra and assigns a low-surface gravity ( $\gamma$ ), intermediate gravity ( $\beta$ ), or field gravity (‘—’ in Table 1 and throughout) based on the strength of metal oxide absorption bands and alkali lines. In certain cases a classification of  $\delta$  is also used for objects that look more extreme than  $\gamma$  (see Gagné et al. 2015b). In this work we label objects as  $\delta$  in tables but plot them and discuss them along with  $\gamma$  sources. On the Cruz et al. (2009) scheme,  $\gamma$  and  $\beta$  objects are thought to be younger than the Pleiades (age  $< \sim 120$  Myr, Stauffer et al. 1998). The Allers & Liu (2013) system uses near-infrared spectra and evaluates spectral indices to assign a very low-gravity (vl-g), intermediate gravity (int-g), or

<sup>13</sup> Our group maintains a listing of known isolated field objects noted as having gravity sensitive features on a web-based compendium [http://www.bdnyc.org/young\\_bds](http://www.bdnyc.org/young_bds)

<sup>14</sup> While this paper was awaiting acceptance, Aller et al. (2016) reported a sample of AB Doradus late-type M and L dwarfs. Those objects are not included in this analysis but should be considered in future work.

field gravity (fld-g) to a given source. As discussed in Allers & Liu (2013), the optical and near-infrared gravity systems are broadly consistent. However, to anchor either requires an age-calibrated sample to ground the gravity designations as age-indicators.

Figure 1 shows a histogram distribution of the spectral subtypes in the optical and the infrared highlighting the gravity classification. There are 51 objects classified optically as  $\gamma$  and 80 with the equivalent infrared classification. There are 27 objects classified optically as  $\beta$  and 57 with the equivalent infrared classification. Of the objects which have both optical and infrared gravity designations, 16 sources (17%) have different gravity classifications from the two methods and 23 objects (24%) have a low-gravity infrared classification but are not noted as peculiar in the optical. For simplification of the text (and in large part because the two systems are generally consistent), we have adopted the convention that any object classified as vl-g or int-g in the infrared is referred to as  $\gamma$  or  $\beta$  (respectively) in the text, Tables, and Figures.

### 3. DATA

The sample of 152 M7-L8 ultracool dwarfs comprising our sample were placed on follow-up programs – either imaging (parallax, proper motion), spectroscopy (radial velocity) or both – to determine kinematic membership in a nearby moving group. Below we describe the data collected for the suspected young brown dwarf sample.

#### 3.1. Parallax and Proper Motion Imaging

The astrometric images for this program were obtained using three different instruments and telescopes in the northern and southern hemispheres. We report parallaxes for eight low-gravity and ten field dwarfs. For 19 objects, we report proper motion alone as we lack enough epochs to decouple parallaxes. An additional 13 objects have not yet been imaged by either the northern or southern instruments, and so we report proper motions using the time baseline between 2MASS and WISE.

##### 3.1.1. Northern Hemisphere Targets

For Northern Hemisphere astrometry targets, we obtained *I*-band images with the MDM Observatory 2.4m Hiltner telescope on Kitt Peak, Arizona. Parallaxes are being measured for both low-surface gravity and field ultracool dwarfs and for this work we report 5 of the former and 10 of the latter (field dwarfs used for comparison in the analysis discussed in Section 7).

For most observations at MDM, we used a thinned SITe CCD detector (named “echelle”) with 2048x2048 pixels and an image scale of  $0''.275 \text{ pixel}^{-1}$ . This suffered a hardware failure and was unavailable for some of the runs. As a substitute, we began using “Nellie”, a thick, frontside-illuminated STIS CCD which gave  $0''.240 \text{ pixel}^{-1}$ . The change in instrument made no discernible difference to the astrometry. Table 2 gives the pertinent astrometric information. In addition to the parallax imaging, we took *V*-band images and determined  $V - I$  colors for the field stars for use in the parallax reduction and analysis. For a single target field (1552+2948) we used SDSS colors instead. The reduction and analysis was similar to that described in Thorstensen (2003) and Thorstensen et al. (2008), with some modifications.

Parallax observations through a broadband filter are subject to differential color refraction (DCR). The effective wavelength of the light reaching the detector for each star will depend on its spectral energy distribution. Consequently, the target and reference stars can be observed to have different positions depending on how far from the zenith the target is observed at each epoch. In previous studies we approximated the  $I$ -band DCR correction as a simple linear trend with  $V - I$  color, amounting to 5 mas per unit  $V - I$  per unit  $\tan z$  (where  $z$  is the zenith distance of each observation). We checked this by explicitly computing the correction for stars of varying color using library spectra from Pickles (1998), a tabulation of the  $I$  passband from Bessell (1990), and the atmospheric refraction as a function of wavelength appropriate to the observatory's elevation. The synthesized corrections agreed very well with the empirically-derived linear correction. However, the library spectra did not extend to objects as red as the present sample and most are so faint in  $V$  that we could not measure  $V - I$  accurately. We therefore computed DCR corrections using the spectral classifications of our targets and spectra of L and T-dwarfs assembled by Neill Reid<sup>15</sup>. The resulting corrections typically amounted to  $\sim 25$  mas per unit  $\tan z$ , that is, the DCR expected on the basis of the linear relation for a star with  $(V - I) \approx 5$ .

To minimize DCR effects, we restricted the parallax observations to hour angles within  $\pm 2$  h of the meridian. The effect of DCR on parallax is mainly along the east-west (or  $X$ ) direction, and the  $X$ -component of refraction is proportional to  $\tan z \sin p$ , where  $p$  is the parallactic angle. This quantity averaged 0.12 for our observations, reflecting a slight westward bias in hour angle, and its standard deviation was 0.15. We are therefore confident that the DCR correction is not affecting our results unduly.

As in previous papers, we used our parallax observations to estimate distances using a Bayesian formalism that takes into account proper motion, parallax, and a plausible range of absolute magnitude (Thorstensen 2003). For these targets we assumed a large spread in absolute magnitude, so that it had essentially no effect on the distance, and used a velocity distribution characteristic of a disk population to formulate the proper-motion prior. For most of the targets, the parallax  $\pi$  was precise enough that the Lutz-Kelker correction and other Bayesian priors had little effect on the estimated distance, which was therefore close to  $1/\pi$ .

Table 3 lists our measured parallaxes and proper motions and Table 4 shows the comparison with literature values for four sources with previously reported values. In the case of MDM measured proper motions, they are relative to the reference stars, and not absolute. Although the formal errors of the proper motions are typically  $1\text{-}2$  mas  $\text{yr}^{-1}$ , this precision is spurious in that the dispersion of the reference star proper motions is usually over 10 mas  $\text{yr}^{-1}$ , so the relative zero point is correspondingly uncertain.

### 3.1.2. Southern Hemisphere Targets

We observed 16 of the most southernly targets with the Carnegie Astrometric Planet Search Camera (CAP-

SCam) on the 100-inch du Pont telescope and five with the FourStar imaging camera (Persson et al. 2013) on the Magellan Baade Telescope. In the case of both programs, we are continually imaging objects for the purpose of measuring parallaxes. However, for this work we report parallaxes (and proper motions) for only 3 objects with CAPSCam. The remaining 18 objects (13 – CAPSCam, 5 – FourStar) need more epochs to decouple parallax from proper motion and will be the subject of a future paper.

A description of the CAPSCam instrument and the basic data reduction techniques are described in Boss et al. (2009) and Anglada-Escudé et al. (2012). CAPSCam utilizes a Hawaii-2RG HyViSI detector filtered to a bandpass of 100 nm centered at 865 nm with 2048 x 2048 pixels, each subtending 0.196'' on a side. CAPSCam was built to simultaneously image bright target stars in a 64 x 64 pixel guide window allowing short exposures while obtaining longer exposures of fainter reference stars in the full frame window (e.g. Weinberger et al. 2013). The brown dwarfs targeted in this program were generally fainter than the astrometric reference stars so we worked with only the full frame window. Data were processed as described in Weinberger et al. (2013). For exposure times, we used 30s - 120s for our bright targets and 150s - 300s for our faint targets with no coadds in an 8 - 12 point dither pattern contained in a 15'' box. Pertinent astrometric information for parallax targets is given in Table 2.

FourStar is a near-infrared mosaic imager (Persson et al. 2013) with four 2048 x 2048 Teledyne HAWAII-2RG arrays that produce a 10.9' x 10.9' field of view at a plate scale of 0.159'' pixel $^{-1}$ . Each target was observed with the J3 (1.22–1.36  $\mu\text{m}$ ) narrow band filter and centered in chip 2. This procedure has proven successful in our astrometric program for late-T and Y dwarfs (e.g. Tinney et al. 2012, 2014, Faherty et al. 2014b). Exposure times of 15s with 2 coadds in an 11 point dither pattern contained in a 15'' box were used for each target. The images were processed as described in Tinney et al. (2014).

In the case of the 18 proper motion only targets from either CAPSCam or FourStar, we combine our latest image with that of 2MASS ( $\Delta t$  listed in Table 5). Proper motions were calculated using the astrometric strategy described in Faherty et al. (2009). Results are listed in Table 5.

For three CAPSCam targets there is sufficient data to solve for both proper motions and parallaxes. For these sources, the astrometric pipeline described in Weinberger et al. (2013) was employed. Table 3 lists our measured parallaxes and proper motions and Table 4 shows the comparison with literature values for 0241-0326.

## 3.2. Low and Medium Resolution Spectroscopy

### 3.2.1. FIRE

We used the 6.5m Baade Magellan telescope and the Folded-port InfraRed Echelle (FIRE; Simcoe et al. 2013) spectrograph to obtain near-infrared spectra of 36 sources. Observations were made over 7 runs between 2013 July and 2014 September. For all observations, we used the echelle mode and the 0.6'' slit (resolution  $\lambda/\Delta\lambda \sim 6000$ ) covering the full 0.8 - 2.5  $\mu\text{m}$  band with a spatial resolution of 0.18''/pixel. Exposure times for

<sup>15</sup> Available at <http://www.stsci.edu/~inr/ultracool.html>

each source and number of images acquired are listed in Table 6. Immediately after each science image, we obtained an A star for telluric correction and obtained a ThAr lamp spectra. At the start of the night we obtained dome flats and Xe flash lamps to construct a pixel-to-pixel response calibration. Data were reduced using the FIREHOSE package which is based on the MASE and SpeX reduction tools (Bochanski et al. 2009, Cushing et al. 2004, Vacca et al. 2003).

### 3.2.2. IRTF

We used the 3m NASA Infrared Telescope Facility (IRTF) to obtain low-resolution near-infrared spectroscopy for 10 targets. We used either the  $0''.5$  slit or the  $0''.8$  slit depending on conditions. All observations were aligned to the parallactic angle to obtain  $R \equiv \lambda / \Delta\lambda \approx 120$  spectral data over the wavelength range of  $0.7 - 2.5 \mu\text{m}$ . Exposure times for each source and number of images acquired are listed in Table 6. Immediately after each science observation we observed an A0 star at a similar airmass for telluric corrections and flux calibration, as well as an exposure of an internal flat-field and Ar arc lamp. All data were reduced using the SpeXtool package version 3.4 using standard settings (Cushing et al. 2004, Vacca et al. 2003).

### 3.2.3. TSpec

We used the Triple Spectrograph (TSpec) at the 5 m Hale Telescope at Palomar Observatory to obtain near-infrared spectra of two targets. TSpec uses a 1024 x 2048 HAWAII-2 array to cover simultaneously the range from  $1.0$  to  $2.45 \mu\text{m}$  (Herter et al. 2008). With a  $1.1 \times 43''$  slit, it achieves a resolution of  $\sim 2500$ . Observations were acquired in an ABBA nod sequence with an exposure time per nod position of 300s (see Table 6) so as to mitigate problems with changing OH background levels. Observations of A0 stars were taken near in time and near in airmass to the target objects and were used for telluric correction and flux calibration. Dome flats were taken to calibrate the pixel-to-pixel response. Data were reduced using a modified version of Spextool (see Kirkpatrick et al. 2011).

## 3.3. High Resolution Spectroscopy

### 3.3.1. Keck II NIRSPEC

The Keck II near-infrared SPECtrograph (NIRSPEC) is a Nasmyth focus spectrograph designed to obtain spectra at wavelengths from  $0.95 - 5.5 \mu\text{m}$  (McLean et al. 1998). It offers a choice of low-resolution and cross-dispersed high resolution spectrographic modes, with optional adaptive optics guidance. In high-resolution mode, it can achieve resolving powers of up to  $R=25000$  using a 3 pixel entrance slit, with two orders visible on the output spectrum (selectable by filter).

Multiple observations of 17 sources were taken in high resolution mode on Keck II on 14, 15, and 16 September 2008, using the NIRSPEC-5 filter to obtain H-band spectra in Order 49 ( $1.545 - 1.570 \mu\text{m}$ ). Observational data for each source are listed in Table 7. The data were reduced using the IDL-based spectroscopy reduction package REDSPEC. Many of our observations had very low signal-to-noise, and so multiple exposures were co-added before extracting spectra. We tested this procedure by

using objects with sufficient signal-to-noise prior to co-adding, and by comparing individual against co-added spectra. The resulting individual exposure spectra were almost identical to those obtained by co-adding prior to running REDSPEC reductions. Heliocentric radial velocity corrections were calculated with the IRAF task *rvcorrect*, and applied using custom python code.

### 3.3.2. Gemini South Phoenix

The Phoenix instrument (previously on Gemini South) is a long-slit, high resolution infrared echelle spectrograph, designed to obtain spectra between  $1 - 5 \mu\text{m}$  at resolutions between  $R=50000$  and  $R=80000$ . Spectra are not cross-dispersed, leaving only a narrow range of a single order selectable by order-sorting filters.

Observations of 18 sources were taken during semester 2007B and 2009B using the H6420 filter to select H-band spectra in Order 36 ( $1.551 - 1.558 \mu\text{m}$ ). Spectra were reduced using the supplied IDL Phoenix reduction codes. Observational data for each source are listed in Table 7.

### 3.3.3. Magellan Clay MIKE

The Magellan Inamori Kyocera Echelle (MIKE) on the Magellan II (Clay) telescope is a cross-dispersed, high resolution optical spectrograph, designed to cover the entire optical spectrum range (divided into two channels, blue:  $0.32 - 0.48 \mu\text{m}$ , and red:  $0.44 - 1.00 \mu\text{m}$ ) at a resolving power of  $R \sim 28,000$  (blue) and  $R \sim 22,000$  (red) using the  $1.0''$  slit. The output spectra contain a large range of overlapping echelle orders, each covering roughly  $0.02 \mu\text{m}$  of the red optical spectrum.

Red-side spectra were taken on 4 July 2006, 1 November 2006, and 2 November 2006. The observations comprise 17 target and standard spectra, with additional B-type and white dwarf flux calibrators. Observational data for each source are listed in Table 7. Spectra were reduced using the IDL MIKE echelle pipeline<sup>16</sup>, and orders 38 – 52 ( $0.92 - 0.65 \mu\text{m}$ ) were extracted from every spectrum. Many of those orders were unusable for our purposes, and were not used in the final solutions. Telluric atmospheric features dominate the wavebands covered by orders 38 (telluric  $O_2$ ), 45 (A band), and 50 (B band). The orders higher (bluer) than 44 typically had insufficient signal due to the extreme faint and red colors of the target objects.

## 4. NEW NEAR-INFRARED SPECTRAL TYPES

We obtained spectra with FIRE, SpeX, and TSpec for 43 targets to investigate near-infrared signatures of youth. Each object had either demonstrated optical low-surface gravity features, but were missing (or had poor) near infrared data, or had low signal to noise near infrared spectra. Determining the spectral type and gravity classification for peculiar sources has its difficulties. Primarily because one wants to ground the peculiar object type by comparing to an equivalent field source. However, as will be seen in section 7, the low gravity sequence does not easily follow from the field sequence. In the infrared, Allers & Liu (2013) have presented a method for determining gravity classification using indices. Alternatively, the population of low gravity

<sup>16</sup> <http://web.mit.edu/burles/www/MIKE/> checked 19 JUNE 2014

sources (especially earlier L types) has grown in number such that templates of peculiar sources can be made for comparison (e.g. Gagné et al. 2015b, Cruz et al. submitted). For this work, we have defaulted to a visual match to templates or known sources – grounded by their optical data – as our primary spectral typing method. However we also check each source against indices to ensure consistency.

In the case of each new spectrum, we visually compared to the library of spectra in the SpeX prism library<sup>17</sup> as well as the low gravity templates discussed in Gagné et al. 2015b. For the FIRE and TSpec echelle spectra, we first binned them to prism resolution ( $\sim 120$ ). This visual check to known objects gave the match we found most reliable for this work in both type and gravity classification and it is listed in the “SpT adopted” column in Table 9. Figures 3 - 4 show two example spectra (prism and binned down FIRE data) compared visually to both field and very low gravity sources, as representations of our spectral typing method.

As a secondary check, we report the indices analysis of each object. A near infrared spectral subtype is a required input for evaluating the gravity classification with the Allers & Liu (2013) system so we first applied the subtype indices (as described in Allers & Liu 2013) and list the results in the “SpT Allers13” column in Table 9. Once we had determined the closest near infrared type, we evaluated the medium resolution (for FIRE and TSpec data) and/or the low resolution gravity indices (for Prism data). We list the results of each in Table 9. In general we found that matching visually to low gravity templates or known objects versus using indices were consistent within 1 subtype.

## 5. RADIAL VELOCITIES

Radial velocities from NIRSPEC, Phoenix, and MIKE were calculated using a custom python routine, which uses cross-correlation with standard brown dwarfs to achieve  $1 \text{ km s}^{-1}$  radial velocity precision. Useable spectra have resolving power of  $R=20,000$  or higher, and generally signal-to-noise of at least 20. All data were corrected to heliocentric radial velocity by shifting the wavelength grid. Brown dwarf standards – sourced primarily from Blake et al. (2010) – were observed and corrected with the same settings as the targets, and paired with objects of matching spectral type. Given that our radial velocity sample is bimodal with peaks at L0 and L4, our spectra are fit against relatively few standards.

The python code calculates radial velocities on the fly, and operates on optical and infrared data without modification. The radial velocity inputs were the wavelength, flux, and uncertainty data as three one-dimensional arrays, for both the target and the standard. The target and standard spectra were first cropped to only the portion where they overlap, and then interpolated onto a log-normal wavelength grid.

From there, 5000 trials were conducted with different randomized Gaussian noise added to the wavelength grids of the target and standard, according to the per-element uncertainties. This was done to account for the uncertainties on the fluxes and to provide a method of quantifying the uncertainty on the output radial velocity.

<sup>17</sup> <http://pono.ucsd.edu/~adam/browndwarfs/spexprism/>

For each of the 5000 trials, the two spectra were cross-correlated to produce a wavelength shift between them. A small 400-element region around the peak of the cross-correlation function was fit with a Gaussian and a linear term, to locate the exact peak of the cross-correlation on a sub-element basis. The widths (and therefore per-measurement errors) of the cross-correlation peak were discarded, assumed to be accounted for in the actual spread of the resulting set of peaks.

The results of the 5000 trials formed (in well-determined cases) a Gaussian histogram centered on the radial velocity shift between the two systems. The width of that Gaussian was taken to represent the uncertainty in the measured radial velocity. This pixel shift was converted into  $\text{km s}^{-1}$  radial velocity, and corrected for the known velocity of the standard. Semi-independent verification of the radial velocities was accomplished by measuring the velocity relative to two different standards, or where available, using multiple orders from the same spectrum.

The process was sensitive to virtually all unwanted processes that produce features in the brown dwarf spectra. Chief among these were cosmic rays and detector hot pixels, which were pixel-scale events removed from the spectra prior to interpolation onto the grid and provide very little signal in the RV correlation. The most important effect was telluric lines, which appeared like normal spectral features but did not track the radial velocity of the star. These were dealt with by identifying orders whose contamination was severe enough to produce discordant radial velocities and avoiding them in the analysis.

Table 7 lists the final radial velocity values for each source. Table 8 shows a comparison of sources for which there was a literature value.

### 5.1. Instrument-specific Differences

MIKE data has multiple echelle orders, and all stars were measured against two L2 dwarf standards: LHS 2924 and BRI 1222-1221 (Mohanty et al. 2003). All orders were examined by eye, and determinations were made as to whether they contained sufficient signal for a believable radial velocity. This was corroborated by cross-checking the result against other orders from the same star and radial velocity. Some orders had broader cross-correlation functions, and the Gaussian was fit to a 200 pixel region around the peak rather than the standard 100 pixels. In other orders, a small a-physical secondary peak in the final results appeared, and was removed from the Gaussian fit for the final radial velocity for that order.

After visual inspection, the most consistent orders – both within the match between the two stars, and between the two standards – were combined into a weighted mean and weighted standard deviation. For all stars, the results of orders 39-44, collectively covering  $0.77\mu\text{m} - 0.89\mu\text{m}$  – were deemed sufficiently reliable (despite the presence of telluric water features) to be used in the final result.

## 6. COMPUTING KINEMATIC PROBABILITIES IN NEARBY YOUNG MOVING GROUPS

Among the 152 brown dwarfs investigated for kinematic membership in this work, we report 37 new radial velocities, 8 new parallaxes, and 33 new proper motions

(13 of which are reported as new from 2MASS to WISE proper motion measurements). In total 27 targets have full kinematics (a parallax, proper motion and radial velocity), and the remaining 123 have only partial kinematics – 16 have a parallax and proper motion but no radial velocity, 26 have radial velocity and proper motion but no parallax, and 81 have proper motions but no parallax or radial velocity measurement. All astrometric information for this sample is listed in Table 10.

As discussed in Section 2, there are 51 objects classified optically as  $\gamma$  and 80 with the equivalent infrared classification. There are also 27 objects classified optically as  $\beta$  and 57 with the equivalent infrared classification. Given the gravity indications, we regard each object as a potentially young source and investigate membership in a group within 100 pc of the Sun. To assess the likelihood of membership, we employed four different tools to examine the available kinematic data:

- BANYAN-I Bayesian statistical calculator (Malo et al. 2013) and its successor,
- BANYAN-II (Gagné et al. 2014d),
- LACEwING (Riedel 2015), and
- Convergent point method of Rodriguez et al. (2013).

The plurality of measurements in combination with a visual inspection of an objects kinematics against bona fide members listed in (Malo et al. 2013) along with the individual kinematic boxes of Zuckerman & Song (2004) drove our decision on group membership.

The four different methods test for membership in different sets of groups - LACEwING considers 14 distinct groups, BANYAN I and II consider 7 groups (or 8 including the “Old” object classification), and the convergence method tests for membership in 6 groups. Each method has its benefits and flaws. For instance Banyan I is a fast bayesian formalism that uses flat priors but assumes (probably unrealistically) that radial velocity, and proper motion in a given direction are Gaussian. Banyan II deals better with transforming measurements to probabilities based on the distribution of known members (does not assume a Gaussian distribution) however it likely has incomplete/imperfect lists of bona fide members. LACEwING is similar to Banyan I in its assumption that radial velocity, and proper motion in a given direction are Gaussian but it requires fitting a model to a (arguably much cleaner list of) bona fide members of multiple groups not covered by the other methods. The convergent point method is a simple yet different approach that estimates the probability of membership in a known group by measuring the proper motions in directions parallel and perpendicular to the location of a given groups convergent point. Unfortunately, this method does not take into account measured radial velocities or distances. Given the benefits and flaws of each method, we chose to take the output of each into consideration as we decided on membership for each target. For an adequate comparison, we only considered membership in six groups: TW Hydrae,  $\beta$  Pictoris, Tucana Horologium, Columba, Argus (which is not tested by the Convergence code), and AB Doradus. All other groups could not be consistently checked. Therefore they may be mentioned (e.g.

Chamaeleon near, Octans, Hyades) but are only considered tentative until further kinematic investigation.

Furthermore, the output of each code should be viewed slightly differently. In Malo et al. (2013), the authors adopt a membership probability threshold of 90% to recover bona fide members. Banyan II supplements with a contamination probability and finds this number should be  $<$  a few percent with a high membership probability (we impose  $>$  90% based on Banyan I) in order to recover bona fide members (Gagné et al. 2014d). LACEwING (as described in Riedel 2015) finds  $<$  20% - 60% is low probability and  $>$  60% is high probability for group membership. Convergent point reports distinct probabilities for each group between 0 - 100% (hence objects can have  $>$  90% probability of membership in more than one group). As with Banyan I, we impose  $>$  90% as a high probability threshold for membership on convergent point as well.

In assessing the membership probability, we found four different categories for describing an object:

- *Non-member, NM*: An object that is kinematically eliminated from falling into a nearby group regardless of future astrometric measurements
- *Ambiguous member, AM*: An object that requires updated astrometric precision because it could either belong to more than one group or it can not be differentiated from the field
- *High-likelihood member, HLM*: An object that does not have full kinematics but is regarded as high confidence ( $>$  90% in Banayan I,  $>$  90% in Banyan II with  $<$  5% contamination,  $>$  90% in convergent point,  $>$  60% in LACEwING) in three of the four codes, and
- *Bona fide member, BM*: An object regarded as a high-likelihood member with full kinematics (parallax, proper motion, radial velocity) demonstrating that it is in line with known higher mass bona fide members of nearby groups.

### 6.1. Full Kinematic Sample

For the 28 targets with full kinematics, we compute the XYZ spatial positions and UVW velocities following the formalism of Johnson & Soderblom (1987), which employs U/X in the direction of the Galactic center, providing a right-handed coordinate system. In general, the resulting values are limited by the parallax precision. For these 28 objects, visual inspection against the positions and velocities of the bona fide members in each group (as listed by Malo et al. 2013) gave an obvious and strong indication of membership. We used the four other methods listed above as confirmation for the visual inspection. The XYZ spatial positions and UVW velocities for systems with full kinematic information are given in Table 11. A visual example of the phase-space motions of 0045+1634, a new bona fide member of Argus, is shown in Figure 2. Among the full kinematic sample, we found 11 objects stand out as bona fide members, 9 objects are classified as ambiguous, and 8 are classified as non-members. The outcome of assessing the likelihood of membership from each kinematic method is listed in Table 12.

### 6.2. Partial Kinematic Sample

Having only partial kinematics for 124 objects limits our ability to definitively place these targets in a nearby group. As stated above, the BANYAN I/II, Convergent Point, and LACEwING methods use varying techniques to yield membership probabilities. We list the outcomes of assessing the likelihood of membership for each source in Table 12. As can be seen from this tabulation, the results varied across methods. In the case of an object like 2322-6151, all methods yield a probability of membership in the Tucana Horologium moving group with three of the 4 yielding  $> 90\%$  membership. The most difficult cases were objects like 1154-3400, where each method yielded a moderate to high probability in a different group (Banyan I and Banyan II both predict Argus, LACEwING predicts TW Hydrae, and Convergent point predicts Chameleon-near). Our approach to the analysis was to be conservative with group membership to eliminate assigning objects to groups that were uncertain. In all we concluded that there were 28 objects to be regarded as high likelihood members (HLM) of a known group, 83 objects that were ambiguous (AM), and 13 objects that were non-members (NM). Adding the full kinematic sample the final tally is 28 high likelihood members (HLM), 11 bona fide group members (BM), 92 ambiguous (AM), and 21 non-members (NM).

### 6.3. Comparison with Previous Works

Among the 152 brown dwarfs examined in this work, 11 are newly identified as low-gravity and 141 have been previously discussed in the literature for membership in a nearby moving group (e.g. Gagné et al. 2015b,c). Several of the objects – 2M0355, PSO318, 0047+6803, 1741-4642, 2154-1055, 0608-2753 – have been the subject of single-object papers (Faherty et al. 2013, Liu et al. 2013, Schneider et al. 2014, Gagné et al. 2014a,b, Rice et al. 2010). The remaining 129 objects were examined for membership in a nearby group primarily by Gagné et al. (2014d) – hereafter G14 –, and Gagné et al. 2015b – hereafter G15 – using BANYAN II.

There are 69 objects from our sample included in G14, 73 objects in G15 and 6 in both. In G14, there is a hierarchical probability structure that categorizes potential members as: (1) Bona fide, (2) High probability, (3) Moderate probability and, (4) Low Probability<sup>18</sup>. That structure is not used in G15, but replaced by noting the probability of membership in a group (multiple groups if deemed necessary) along with its contamination potential.

Of the 69 objects from our sample examined in G14, three objects – 2M0355, 2M0123, and TWA 26 – were declared bona fide members of AB Doradus, Tucana Horologium, and TW Hydrae respectively. A further 29 objects were deemed high probability members of Argus (2), AB Doradus (5),  $\beta$  Pictoris (4), Columba (4), and Tucana Horologium (14). Ten objects were deemed modest probability members of AB Doradus (3),  $\beta$  Pictoris (3), Columba (1), Argus (1), and Tucana Horologium (2). Eight objects were deemed low probability members of Argus (1), AB Doradus (1),  $\beta$  Pictoris (4), and

TW Hydrae (2). There were also 16 objects designated as young field sources (aka “no group membership possible”) and 3 objects designated as peripheral members or contaminants in a group.

In Table 12, we use our new kinematics and show the predictions from BANYAN I, BANYAN II, LACEwING, the convergent point and our plurality decision based on reviewing the results from all four methods with updated astrometric measurements for many of the sources. For the G14 overlap, we agree with 2M0355, 2M0123, and TWA 26 being considered bona fide members. Among the high-likelihood sample from G14 we add a new radial velocity, parallax, and/or proper motion to 19 of the 29 objects and confirm 11 objects as high-likelihood members and demote 5 objects to ambiguous or non-member. Our re-evaluation of the kinematics also leads us to demote 3 objects to ambiguous members rather than considering them high-likelihood sources in a given group. Among the moderate and low probability objects in G14, we add new kinematics to 8 objects and find 5 remain ambiguous and 3 are demoted to non-members. Our re-evaluation of the kinematics finds that 15 of the low or moderate probability sources are ambiguous therefore we can not say anything about membership. The remaining 19 sources that were young field, periphery, or contaminants in G14 are ambiguous or non-members in our analysis.

For the 67 objects in G15, we add three new kinematic points. One object is deemed high-likelihood while the other 2 are ambiguous. Otherwise, our re-evaluation of the kinematics leads us to classify 13 objects as high-likelihood members of groups while the remaining 54 are ambiguous (52) or non-members (2).

In all, we find that when the Bayesian II analysis predictions find group members have a high-likelihood of membership in a single group ( $> 99\%$ ) while yielding a contamination probability of  $< 1\%$ , the various kinematic methods are consistent in their predictions and we take this to mean that the source is a reliable member.

## 7. DIVERSITY OF YOUNG BROWN DWARFS

Each one of these moving group members is a possible benchmark for examining the evolutionary properties of the brown dwarf and directly imaged exoplanet populations. In this section we evaluate the homogeneity and diversity of the sample as a whole as well as the subsamples from each moving group.

### 7.1. Do Gravity Classifications Correspond With Age?

In total there are 51 optically classified  $\gamma$  objects (80 infrared classified equivalents) as well as 27 optically classified  $\beta$  objects (57 infrared equivalents). We confirm 20 (28) of the  $\gamma$  objects and 5 (7) of the  $\beta$  objects respectively as high confidence or bona fide members of moving groups. There are an additional 19 (44)  $\gamma$  objects and 17 (41)  $\beta$  objects regarded as ambiguous members to a known group, and 12 (10)  $\gamma$  objects and 5 (8)  $\beta$  objects found to be non members. As stated in Section 2,  $\gamma$  classified sources have spectral features indicating that they are a lower surface gravity than the  $\beta$  classified objects. Furthermore,  $\beta$  classified sources are subtly but distinctively different from the field sample, indicating – as noted in Allers & Liu 2013 and Cruz et al. 2009 – that they are also younger but not to the extent of the  $\gamma$

<sup>18</sup> See the G14 paper for a detailed description of how to interpret each probability category'

objects. The age calibrated sample allows us to test how well gravity features trace the age of an object.

In Table 13, we list the new members of each group as well as their optical and/or near-infrared spectral and gravity classification. As stated in section 6.1, nine bona fide objects have full kinematics. For the 28 sources missing a radial velocity or parallax but regarded as high confidence members to a group, we list the kinematically predicted radial velocity and/or parallax from BANYAN II – checked to be consistent with LACEWING predictions – in parentheses in Table 13.

In TW Hydreae and  $\beta$  Pictoris, which are the two youngest groups at  $\sim 10$  and  $\sim 20$  Myr respectively, there are nine M7 or later objects, all of which have a gravity classification of  $\gamma$  in both the infrared and optical. In AB Doradus, the oldest association at  $\sim 110$  - 130 Myr, there are eight sources with 4 optical  $\gamma$  (6 infrared) and 1 optical  $\beta$  (2 infrared) objects. Similarly, in Tucana Horologium, where we have the most number of bona fide or high-likelihood members, 20 M7 or later, there are 9 optical  $\gamma$  (10 infrared) and 3 optical  $\beta$  (5 infrared) objects.

Splitting the sample of BM/HLM objects into  $< 25$  Myr ( $\beta$  Pictoris, TW Hydreae),  $\sim 40$  Myr (Tucana Horologium, Columba, Argus), and  $> 100$  Myr (AB Doradus) categories, and using the default spectral type and gravity classes used in plots within this text, we find there are (9  $\gamma$ , 0  $\beta$ ) in  $< 25$  Myr, (14  $\gamma$ , 8  $\beta$ ) in  $\sim 40$  Myr, and (6 $\gamma$ , 2  $\beta$ ) in  $> 100$  Myr associations. While these are still small numbers, the lack of a correlation of numbers of ( $\gamma$ ,  $\beta$ ) objects as a function of bin, indicates that spectral features do not correspond one to one with age. We note that there are 25 objects that have both an infrared and optical spectral type and while 6 have differing gravity classifications, 19 are consistent with each other affirming the diversity. Clearly, what have been assigned as gravity sensitive features are influenced by secondary parameters (see also discussions in Allers & Liu 2013, Liu et al. 2013, G15).

## 7.2. Photometric Properties: What Do the Colors Tell Us?

The majority of flux for a brown dwarf emerges in the infrared. Interestingly, an enormous amount of diversity among the population can be found by examining infrared colors alone (e.g. Kirkpatrick et al. 2008, Faherty et al. 2009, 2013, Schmidt et al. 2010).

As quantified in Tables 15 - 16 and visualized in Figures 5 - 14, the scatter for “normal” sources is pronounced, especially among the mid- to late- L dwarfs. Past works have attributed this to variations in effective temperature, metallicity, age, or atmosphere conditions (Faherty et al. 2013, Kirkpatrick et al. 2008, Patten et al. 2006, Knapp et al. 2004).

In Figures 5 - 14 we plot infrared color combinations for the population. These can be used to examine trends or lack thereof among the new age-calibrated sample. The spread for “normal” objects (grey shaded area) in Figures 5 - 14 was created by isolating sources without peculiar spectral features (e.g. subdwarfs, low-gravity objects, and unresolved binaries were eliminated), and only keeping sources with photometric uncertainties in the color shown  $< 0.2$  mag. The list was gathered from

the dwarfarchives<sup>19</sup> compendium and supplemented with the large ultra cool dwarf surveys from Schmidt et al. (2010), Mace et al. (2013), Kirkpatrick et al. (2011), and West et al. (2008) (for M dwarfs).

For the low gravity sample, spectral types, as well as gravity classifications, are from optical data unless only infrared was available. We note that most sources plotted have spectral type uncertainties of 0.5. However, as can be seen in Table 1, low-gravity sources can have up to a 2 type difference in subtype, as well as differing gravity indications between the optical and the infrared. We investigated whether isolating the smaller samples of optical only or infrared only yielded different trends than this mixed sample, but found similar results in all cases. Hence we default to optical classifications and designations where available, as this is the wavelength range where the original spectral typing schemes for this expected temperature range were created.

Overplotted on the grey field sequences in Figures 5 - 14 are the individual  $\gamma$  or  $\beta$  low-gravity objects. We have color coded each source by the group it has been assigned or labeled it as “young field?” for those with ambiguous or non conforming group kinematics. We have also given the  $\beta$  and  $\gamma$  objects different symbols so their trends could be highlighted. Tables 17 - 18 give the infrared color of each source as well as its deviation from the mean (see Tables 15 - 16) of normal objects in its spectral subtype.

In general, the  $\gamma$  and  $\beta$  sources are systematically redder than the mean for their subtype with the deviation from “normal” increasing with later spectral subtypes. Objects are most deviant from normal in the ( $J$ - $W2$ ) color (Figure 8) where they are an average of  $2\sigma$  (or up to 1.85 mag) redder than the subtype mean value across all types, and least deviant in the ( $J$ - $H$ ) color (Figure 5) where they are an average of  $\sim 0.7\sigma$  (or up to 0.6 mag) redder than the subtype mean value across all types. Typically, the  $\gamma$  sources mark the extreme red photometric outliers for each subtype bin, although there are a handful of extreme  $\beta$  sources (e.g. 0153-6744, an infrared L3  $\beta$ ).

The difference in age between the oldest moving group investigated and the average age for field sources is more than  $\sim 3$  Gyr (field age references Burgasser et al. 2015, Seifahrt et al. 2010, Faherty et al. 2009). As shown in Figures 5 - 14, the difference in photometric properties across this large age gap is distinct. We also investigated the more subtle age difference changes to the photometric properties across the 5 - 130 Myr sample. Isolating the sources that are confidently associated with a moving group, we conclude that there is no obvious correlation between the extreme color of an object and the age of the group. For example, 5-15 Myr TW Hydreae late-type M and L dwarfs, 25 Myr  $\beta$  Pictoris spectral equivalents and 30 - 50 Myr Tucana Horologium spectral equivalents have similar photometric colors. The exceptions are TWA27A and TWA28, which are  $2-5\sigma$  redder than similar objects in several colors. We note that Schneider et al. (2012a,b) postulate that these sources may have disks hence their surroundings may be contributing to the colors.

Comparing internally within the same moving group (assumed to have the same age and metallicity) we find

<sup>19</sup> <http://www.dwarfarchives.org>

that objects of the same spectral subtype show a large diversity in their photometric colors. The best example is at L0 where there are 5 Tucana Horologium members. The objects have systematically redder colors, but they are distributed between  $1-4\sigma$  from the field mean indicating that since this is a coeval group, diversity must be driven by yet another parameter. We note that depending on the exact formation mechanism, metallicity variations can not be completely outruled as also contributing to the diversity among objects in the same group.

Plotted as grey symbols throughout Figures 5 - 14 are objects that are kinematically ambiguous or unassociated with any known group. Many of these sources, (such as the L4 $\gamma$  1615+4953 and the very oddly reddened M8 $\gamma$  0435-1441 – see discussion in Allers & Liu 2013 and Cruz et al. 2003), are among the reddest objects for their spectral bins and rival the associated kinematic members in their spectral and photometric peculiarities. Conversely, there are several  $\beta$  sources, such as the L2 $\beta$  0510-1843, that fall within the normal range in each color and are only subtly spectrally different than field sources. Unfortunately, with no group association, we can not comment on the likelihood of age differences driving the diversity. It is likely that within this sample, there are objects in moving groups not yet recognized, as well as sources that are not young but mimic low surface gravity features due to secondary parameters (e.g. atmosphere or metallicity variations).

### 7.3. Flux Redistribution to Longer Wavelengths for Younger Objects

As discussed in section 7.2 above, low surface gravity brown dwarfs are systematically redder for their given spectral types. Hence, one might expect that they would not logically follow the absolute magnitude sequence of field equivalents. Figures 15 - 20 show  $M_J$  through  $M_{W3}$  versus spectral type for all low surface gravity sources with parallaxes or, in a select few cases, with kinematic distances. In Table 13 we mark the 25 sources for which we lack a parallax but have assumed the kinematic distance to a moving group since the object was assessed as a high-likelihood member. The grey area throughout each figure is the polynomial relation for the field population at each band recalculated with all known brown dwarfs with parallaxes. We list all new relations for both field and low gravity objects used in or calculated for this work in Table 19. Throughout Figures 15 - 20, individual low surface gravity objects are over plotted and color coded by group membership and given a symbol representing their gravity designation. The lower portion of each figure shows the deviation of each low-gravity source from the mean absolute magnitude value of the spectral subtype.

#### 7.3.1. Trends with Spectral Type

Focusing on the objects associated with known groups, there is a distinct difference between the behavior of low-gravity late-type M dwarfs and L dwarfs. In Figure 15, which shows the  $M_J$  band trend, the TW Hydrae and Tucana Horologium late-type M's are  $\sim 2$  magnitudes brighter than the field relations whereas the L dwarfs are normal to  $\sim 1$  mag fainter than the field relations. Moving to longer wavelengths, the flux shifts. By

$M_{W3}$ , nearly all sources regardless of spectral type have brighter absolute magnitudes than the field polynomial. One plausible explanation for this redistribution of flux is dust grains in the photosphere that absorb and reradiate at cooler temperatures (hence longer wavelengths). Equally likely is the possibility that there exists thicker clouds or that there are higher lying clouds in the atmospheres of these sources (e.g. Marocco et al. 2013, Hiranaka et al. 2015, Faherty et al. 2013).

One main consequence of the young sources deviating from the field in some bands and not in others, is that the polynomial relations that use spectral type and photometry to obtain distances, are inappropriate for low-surface gravity objects. At bluer near-infrared bands, they would over estimate distances, whereas at redder near-infrared bands they would under-estimate. In Table 19 we have taken this into account and present new spectrophotometric polynomials for suspected young sources at J through W3 bands. As discussed in Filippazzo et al. (2015), the flux redistribution hinges around  $K$  band. As a result, we recommend this spectral distance polynomial relation for suspected young sources.

#### 7.3.2. Trends with Age

Overall, we find that there is a clear difference in the behavior of the absolute magnitudes as a function of spectral type for the  $> \sim 3$  Gyr field trends in each band compared to the behavior of the low surface gravity sources. Narrowing in on the 5 - 130 Myr range and comparing equivalent spectral type sources in differing groups (such as the L7 sources in AB Doradus and  $\beta$  Pictoris or the Tucana Horologium late- M and L dwarfs) we find that there is no obvious correlation with age and absolute magnitude trend. In the case of PSO318 ( $\sim 25$  Myr), 1119-1137, and 1147-2040 ( $\sim 5$  -15 Myr) versus 0047+6803 ( $\sim 110$ -130 Myr) or TWA 27A ( $\sim 5$ -15 Myr) versus 0123-6921 ( $\sim 30$ -50 Myr), the sources switch in brightness depending on the band, but stay within  $1\sigma$  of each other from  $J$  ( $\sim 1.25\mu$  m) through  $W2$  ( $\sim 4.6\mu$  m). By  $M_{W3}$  ( $\sim 11.56\mu$  m), TWA 27 A is over 1 magnitude brighter than 0123-6921 although this might be due to a disk and not due to the source (Schneider et al. 2012a,b). Regardless, it does not appear that the younger sources show an extreme version of the overall trend indicating that whatever causes the flux redistribution compared to the field ( $> 3$  Gyr sample) has a near equal impact from  $\sim 5$ -15 Myr through  $\sim 110$ -130 Myr.

#### 7.3.3. Trends with Non-Group Members and Expanded Explanations for Diversity

The sources with non-conforming group kinematics (grey points) do not all trace the behavior of the bona fide/high-likelihood members. For instance, all but 2 of the  $\gamma$  or  $\beta$  “Young Field?” M7-L1 objects stay within the polynomial for each band. Furthermore, all but one of those are classified as  $\beta$ , which is the more subtly altered gravity type. Conversely, the L3 and L4  $\gamma$  and  $\beta$  sources move from within the field polynomial band to being  $1-2\sigma$  brighter than equivalent sources between  $M_J$  and  $M_{W3}$ .

There are several explanations for why a spectroscopically classified low gravity object looks normal in other parameters. Photometric variability may contribute slightly to their position on spectrophotometric diagrams

(e.g. Allers et al. 2016) but it is unlikely to contribute in a significant way. As shown in works such as Radigan et al. (2014), and Metchev et al. (2015), large amplitude photometric variations ( $> 5\%$ ) among brown dwarfs are rare. Alternatively, rotational velocity could contribute in a substantial way because it influences global circulation on a given source which causes or disrupts cloud patterns. In this same vein, the distribution of clouds by latitude on a given object may not be homogeneous in structure or grain size. Consequently, (as first proposed by Kirkpatrick et al. 2010) our viewing angle (e.g. pole-on or equatorial on) would impact the spectral and photometric appearance. Unfortunately, there is little information on the rotational velocity distribution of the young brown dwarf sample so testing this parameter will require additional data.

The simplest explanation is that sources falling within “normal” absolute magnitude and luminosity plots with non-conforming kinematics to any known group may not be young. Aganze et al. (2016) showed this to be the case for the d/sdM7 object GJ 660.1B that had a peculiar near infrared spectrum which hinted that it was young. However this object was co-moving with a higher mass, low-metallicity star refuting that suggestion. In the case of GJ 660.1 B, a low-metallicity likely helped to mimic certain spectral features of youth. In lieu of the fact that there may be some older contaminants in the sample, we present all new relations in Table 19 to be inclusive of all objects in this work with parallaxes as well as only objects that are considered bona fide or high likely members of groups.

#### 7.4. Color Magnitude Trends for Young Brown Dwarfs

Color magnitude diagrams have been discussed at length in the literature as a diagnostic of temperature, gravity, metallicity, and atmosphere properties of the brown dwarf population (e.g. Liu et al. 2013, Faherty et al. 2012, 2013, Filippazzo et al. 2015, G15, Dupuy & Liu 2012, Patten et al. 2006). Figures 21 - 31 show the full suite of infrared color magnitude diagrams using JHK (2MASS) and W1W2 (WISE) photometry for the field parallax sample omitting binaries, subdwarfs, spectrally peculiar sources and those with absolute magnitude uncertainties  $> 0.5$  in any band. On each plot we color code objects by spectral ranges of  $< M9$ , L0-L4, L5-L9, T0-T4, and  $> T5$  and we highlight the low surface gravity objects by their gravity classification. The latest type sources in our sample are labeled on each plot. On select plots, we have also labeled the M dwarf members of  $\beta$  Pictoris and TW Hydrae.

For completeness of the discussion, we have included the one confirmed isolated T dwarf member of a moving group in the analysis (SDSS1110, T5.5, Gagné et al. 2015a) as well as the L7 wide companion VHS 1256 B (Gauza et al. 2015). While the latest-type L dwarfs push the elbow of the L/T transition to an extreme red/faint color/magnitude, SDSS 1110 falls near spectral equivalents on all color magnitude diagrams. As discussed in Gagné et al. 2015c and Filippazzo et al. 2015, this source appears  $\sim 150$  K cooler than equivalents but does not exhibit the extreme color-magnitude properties as seen with the L dwarfs.

Looking at a given absolute magnitude across all plots and comparing field objects to low surface gravity ob-

jects, we find that the latter can be more than a 1 magnitude redder. The most extreme behavior can be seen on Figures 24 and 25 which exploits the largest wavelength difference in color ( $J - W2$ ) and as discussed in section 7.2 is where the low-gravity objects are the most extreme photometric outliers.

As was discussed in section 7.3, there is a distinct difference in the diversity of absolute magnitudes between young M dwarfs and L dwarfs. Using the color coding as a visual queue in Figures 21 - 31, the M dwarfs fall redder than the field sequence but they also scatter to brighter magnitudes. For the W2 color difference plots (e.g.  $M_{JHK}$  vs  $(J-W2)$ ,  $(H-W2)$ , or  $(K-W2)$ ), we label the position of the M dwarfs in TW Hydrae and  $\beta$  Pictoris as they are strikingly red and bright at these wavelengths and well separated from the field population.

Comparatively, the L dwarfs flip in their behavior and can be seen as redder but fainter than field sources. Focusing on Figures 21 - 22, and 26 which use JHK photometry only, the latest type sources (e.g. PSO318, 0047+6803, 2244+2043, 1119-1137, 1147-2040) are not only redder but they also drive the elbow of the L/T transition  $\sim 1$  magnitude fainter than the field (notably in  $M_J$ ). Moving to longer wavelengths, this behavior reverses. By Figures that evaluate colors against  $M_{W1}$  ( $\sim 3.4\mu m$ ) or  $M_{W2}$  (e.g. Figure 23 or 28) the latest type sources are consistent with or slightly brighter than the elbow. Hence as discussed in section 7.3 and Filippazzo et al. (2015), the flux redistribution of young L dwarfs seems to hinge very close to the  $K$  band. Indeed the color magnitude diagram that appears to smoothly and monotonically transition objects from late-M to T dwarfs is the  $M_K$  vs  $(K-W2)$  plot in Figure 30. There is a 10 magnitude difference between the warmest to the coolest objects and the magnitude seems to monotonically decrease with reddening color showing only a hint of an L/T transition elbow at  $M_K=13/M_{W2}=12$ . On this plot, the low-surface gravity sequence lies  $\sim 1$  magnitude brighter than the field with the exception of a small fraction of the sample appearing normal (including the AB Doradus T dwarf SDSS1110).

The L/T transition induces a turning elbow on most color magnitude plots. This feature is brought on when the clouds dissipate as one moves from warmer L dwarfs to cooler T dwarfs and  $CH_4$  begins to dominate as an opacity source all conspiring to drive the source colors blueward. The demonstration that these young sources are redder and fainter than the field sequence in the near-infrared indicates that the clouds must persist through lower temperatures (fainter) and represent an extreme version of the conditions present for field age equivalents (redder). The brightening of sources at W1 and W2 at extreme red colors likely holds clues to the composition and structure of the clouds as it is a reflection of the flux redistribution to longer wavelengths as discussed in section 7.3 above.

For colors and magnitudes evaluated across JH or K and W1 or W2 (e.g. Figure 27 which shows  $M_H$  vs  $H-W1$ ), the latest type objects pull the low-gravity sequence redder than the field while maintaining a small spread in absolute magnitude from 0103+1935 through PSO318. Interestingly this indicates similarities in these sources not readily apparent in current spectral data.

Lastly, on Figures 21 - 31 we have given  $\gamma$  and  $\beta$  classified sources different symbols to investigate whether trends between the two could be identified. Throughout, there is a hint that the sequence of  $\gamma$  classified objects is redder than that of the  $\beta$  sources. This is most prominent on Figures 23 - 24 where only four  $\beta$  L dwarfs rival  $\gamma$  sources in color and/or magnitude. On other figures such as 21, there appears to be more mixing between the two gravity classifications. As has been stated throughout this work, spectral type and the corresponding gravity classification are difficult to evaluate and can differ between optical and infrared spectra or from low resolution to medium resolution data. The data as viewed in this work, seems to indicate that the  $\gamma$  classified sources are distinct on color magnitude diagrams from the  $\beta$  classified sources with some mixing likely due to a non-uniform spectral typing methodology.

### 7.5. The Bolometric Luminosities and Effective Temperatures of Young Objects

One expects that younger brown dwarfs should have inflated radii compared to equivalent temperature sources given that they are still contracting. Consequently, one would expect that  $\gamma$  and  $\beta$  objects would be overluminous when compared to their field age equivalents. A rough estimate using the Burrows et al. (2001) evolutionary models indicates that 10 Myr (50 Myr) objects with masses ranging from 10 to 75  $M_{Jup}$  have radii that are 25% to 75% (13% to 50%) larger than 1 - 3 Gyr dwarfs with equivalent temperatures. Since  $L_{bol}$  scales as  $R^2$ , one might expect that this age difference translates into younger objects being 1.5x - 3.0x (1.3x - 2.3x) overluminous compared to the field.

Initially, studies categorized low surface gravity brown dwarfs as “underluminous” compared to field sources based on examining near-infrared absolute magnitude trends alone (e.g. Faherty et al. 2012). However as discussed in section 7.3, flux shifts to longer wavelengths beyond the  $H$  and  $K$  bands at lower gravities, so that some absolute magnitude bands might be fainter but  $L_{bol}$ ’s are not underluminous compared to the field (Faherty et al. 2013, Filippazzo et al. 2015). In fact, Filippazzo et al. (2015) carefully evaluated  $L_{bol}$  values for all brown dwarfs with parallaxes (or kinematic distances in the case of high likelihood moving group members) and presented up to date relations between observables and calculated  $L_{bol}$ ’s. In that work,  $\beta$  and  $\gamma$  objects were found to split along the M/L transition whereby M dwarfs were overluminous and L dwarfs were within to slightly below the sequence when compared to field objects.

To investigate  $L_{bol}$  trends among the age calibrated sample, we first calculate values for sources reported here-in using the technique described in Filippazzo et al. (2015). In that work, the authors integrate under the combined optical and near-infrared photometry and spectra as well as the WISE photometry and mid infrared spectra where available. As described in previous sections, we use parallaxes where available but supplement with kinematic distances when a source was regarded as a high likelihood member to a group (see values in parentheses in Tables 13 and 10). All  $L_{bol}$ ,  $T_{eff}$ , and Mass values are listed in Table 14 as well as Table 13 for members only.

Figure 32 shows  $L_{bol}$  as a function of spectral type for

all objects compared to the field polynomial from Filippazzo et al. (2015). Also overplotted is the polynomial fit for objects in groups (labeled as GRP in Table 19). We highlight bona fide and high-likelihood brown dwarf moving group members as well as the unassociated  $\gamma$  and  $\beta$  objects with differing symbols and colors.

Focusing on the age calibrated sample, we find that late-type M dwarfs assigned to groups are overluminous compared to the field. The L dwarfs assigned to a group are mixed, with the majority falling within the field polynomial relations and a small number falling slightly above. Comparing group-to-group differences, the 5-15 Myr TW Hydreae M8 and M9 objects are  $\sim$ 5x more luminous than the field while the 30-50 Myr Tucana Horologium source is  $\sim$ 2x more luminous. Interestingly, the TW Hydreae,  $\beta$  Pictoris, and AB Doradus L7’s have near equal  $L_{bol}$  values, all near the mean value for their subtype.

Comparing the  $\gamma$  and  $\beta$  gravity sources without membership to the field and high-likelihood group members, we find that – with the exception of the M7.5 0335+2342 which is highly suspect to be a  $\beta$  Pictoris member (see note in Table 13) – all non-members fall within the polynomial relations for the field. This trend indicates that the late-M non-member  $\gamma$  and  $\beta$  sources may not be young (see discussion in subsection 7.3.3 and section 7.6). Indeed, 1022+0200 is a late-M non-member with full kinematics. When we compare the UV velocity of this source to that of the Eggen & Iben (1989) criterion for young stars, we find it falls outside of it hinting that it may be drawn from the older disk population. It remains unclear how to interpret the non-member L dwarfs as this trend is in line with group assigned equivalents.

The result of  $L_{bol}$ ’s for  $\gamma$  and  $\beta$  gravity L dwarfs looking like field sources or in some cases underluminous, implies that they are cooler than their field spectral equivalents. In other words, low-gravity or atmospheric conditions potentially induced at a younger age, mimic spectral features of a warmer object. As young sources are typed on a scheme anchored by field objects, they are incorrectly grouped with warmer sources. They certainly stand out in photometric, spectroscopic, and band by band absolute magnitude comparisons with field sources (e.g. all of section 7). However the low gravity sequence does not logically or easily follow off of the field sequence. Figure 33 shows the  $T_{eff}$  values for  $\gamma$  and  $\beta$  sources calculated using the method described in Filippazzo et al. (2015) along with the polynomial and residuals for field objects (from Filippazzo et al. 2015) and group members (from Table 19). As noted in Filippazzo et al. (2015) – with the exception of a few – while M dwarfs are similar if not warmer for their given spectral subtype, the L dwarfs are up to 100-300K cooler. Examining the 5-130 Myr age calibrated objects within this sample, we can not isolate a trend of younger objects being increasingly cooler than older equivalent sources. For example, PSO318 and 0047+6803 are equivalent temperatures even though there is a  $\sim$ 100 Myr difference in age.

### 7.6. Unmatched objects with Signatures of Youth

Among the 152 objects in this sample with reported spectral signatures of youth in either the optical or the near-infrared, we confidently find that 39 ( $\sim$ 25%) are high-likelihood or bona fide members of nearby mov-

ing groups. There are 92 ( $\sim 61\%$ ) dubbed ambiguous either because their kinematics overlap with more than one group (including the old field) and they need better astrometric measurements to differentiate, or there is not strong enough evidence with the current astrometry to definitively call it high-likelihood or bona fide. There are 21 objects ( $\sim 14\%$ ) for which we have enough information to declare them as non-members to any known group assessed in this work. Among the non-members, there are 4 optically classified (3 infrared classified) M dwarfs and 15 optically classified (17 infrared classified) L dwarfs with 12 optically (10 infrared) classified  $\gamma$  objects and 5 optically (8 infrared) classified  $\beta$  objects. Several of these objects have extreme infrared colors (see Figures 5 - 14). For instance, 1615+4953 is classified in the optical as an L4 $\gamma$  and rivals the most exciting late-type objects in its deviant infrared colors. However, current kinematics do not show a high probability of membership in any group despite its having a proper motion and radial velocity. Similarly, 0435-1441 is strikingly red in  $JHK$ , shows both optical and infrared signatures of youth, and its spectrum needs to be de-reddened ( $E(B-V)=1.8$ ). While it is in the direction of the nearby star-forming region MBM 20, the distance noted for that cluster (112 - 161 pc) would drive unrealistic absolute magnitudes and  $L_{bol}$  values for this source.

The current census of young, but, unassociated late- M and L dwarfs is similar to what has emerged in studies of early M dwarfs with multiple signatures of youth (e.g. X-ray, UV and IR-excess, Lithium). A significant portion of objects in the studies of Rodriguez et al. (2013) and Shkolnik et al. (2011, 2012) are strong candidates for being 5 - 130 Myr objects via their spectral and photometric properties but their kinematics are inconclusive and their age cannot be determined by a group assignment. Likely, there are a number of groups waiting to be uncovered that may account for this overabundance of young, low mass objects. Alternatively, after 5 - 130 Myr sources have been dynamically moved from their origins such that tracing back their history to any collection of objects is beyond our capability.

## 8. COMPARISONS WITH DIRECTLY IMAGED EXOPLANETS

Several of the objects discussed herein are in the same moving groups as directly imaged exoplanets or planetary mass companions. For example, there are two bona fide or high-likelihood brown dwarfs in the  $\beta$  Pictoris moving group, home to the 11-13 Jupiter mass planet  $\beta$  Pictoris b and the newly discovered 2 - 3 Jupiter mass planet 51 Eri b (Bonnefoy et al. 2013, 2014, Males et al. 2014, Macintosh et al. 2015), 20 in the Tucana Horologium association which houses the 10 - 14  $M_{Jup}$  planetary mass companion AB Pictoris b (Chauvin et al. 2005, Bonnefoy et al. 2010) as well as the 12 - 15  $M_{Jup}$  planetary mass companion 2M0219 b (Artigau et al. 2015), and seven in the TW Hydriæ Association which is the home of the 3 - 7  $M_{Jup}$  planetary mass companion 2M1207 b (Chauvin et al. 2004, Patience et al. 2012). As such, the brown dwarfs discussed herein should be considered siblings of the directly imaged planets as one can assume that they are co-eval, and share formation conditions and dynamical histories. The mode of formation for the brown dwarfs versus the directly imaged

exoplanets remains a question but will likely drive distinct differences in the observables of each population. In this section, we look to place the young brown dwarf sample in context with related exoplanet members.

### 8.1. Similarities of Brown Dwarfs and Imaged Exoplanets on Color Magnitude Diagrams

Young isolated brown dwarfs are far easier to accumulate data on than directly imaged exoplanet equivalents because they do not have a bright star to block when observing. The collection of currently known giant exoplanets, generally have only infrared ( $J, H, K, L', M'$ ) photometric measurements. Near-infrared spectroscopy is possible for some although this requires considerable telescope time and advanced instrumentation (e.g. Oppenheimer et al. 2013, Macintosh et al. 2015, Hinkley et al. 2015, Bonnefoy et al. 2013, Patience et al. 2012).

Figures 35 - 41 show a full suite of near-infrared color magnitude diagrams with the same brown dwarf sample as in Figures 21 - 31 however we now compliment each with directly imaged exoplanets and color code sources by their respective moving groups. For L' band photometry of the brown dwarfs, we have used the small sample of MLT sources with measured MKO L' – primarily from Golicowski et al. (2004) – to convert the WISE W1 band photometry which has comparable wavelength coverage. The polynomial relation used for converting between bands is listed in Table 19.

As with the young brown dwarfs discussed herein, an observable feature of note for the exoplanets is that they are redder and fainter than the field brown dwarf population in near-infrared color magnitude diagrams. This is exemplified by the positions of HR8799 b and 2M1207 b both of which sit  $\sim 1$  mag below the L dwarf sequence in Figures 35, 36, and 37. To explain their position on near-infrared color magnitude diagrams, several authors have proposed thick or high-lying photospheric clouds in their atmospheres (Bowler et al. 2010b, Madhusudhan et al. 2011, Hinz et al. 2010, Marley et al. 2012, Skemer et al. 2012, Currie et al. 2011). An alternative theory proposed by Tremblin et al. (2016) has recently emerged that proposes cloudless atmospheres with thermo-chemical instabilities may invoke some of the features seen here-in. Further investigation of those models is required before we can appropriately comment on how well they may reproduce the large sample presented in this work.

The young brown dwarf sequence in many ways mirrors that of the directly imaged exoplanets but for warmer (or older) objects. From the warmest (at M7) to the coolest (at L7) the low-gravity brown dwarfs are redder and fainter than their field counterparts. As can be seen on each Figure, the low-gravity sequence appears to logically extend through many of the directly imaged exoplanets. Interestingly, the youngest exoplanets (those in Taurus, Upper Scorpius, and  $\rho$  Ophiuchus; Kraus et al. 2014, Currie et al. 2014) are redder than either the field or the low-gravity sequences indicating that – assuming formation differences do not drastically alter the available compositions – the atmosphere or gravity effects are most pronounced close to formation.

By color combinations using L' band, the youngest planetary mass objects such as ROXs12 b, DH Tau b, and GQ Lup b are nearly 2 magnitudes redder and  $> 2$  magnitudes brighter than the field sequence. Con-

versely, the lowest temperature planets around HR8799 fall within or close to the T dwarf sequence. The exception is HR8799 b which has a significantly redder ( $J-L$ ) color than the field sequence as well as the young brown dwarf sequence. It is also  $\sim 2$  magnitudes fainter in  $M_L$  than the low-gravity sequence which extends redward in Figure 38 with minimal scatter in  $M_L$ . Skemer et al. (2012) have noted that the  $3.3\mu\text{m}$  photometry (not plotted) for the HR8799 planets is brighter than predicted by evolutionary or atmosphere models. As in Barman et al. (2011a), Skemer et al. (2012) use thick cloudy non-equilibrium chemistry models and remove  $\text{CH}_4$  to fit the data. Similarly, none of the isolated late-type L dwarfs labeled on Figures 35 - 41 have  $\text{CH}_4$  in their near infrared spectra even though 1119-1137, 1147-2040, PSO318 and 0047+6803 have calculated  $T_{eff}$ s which should allow for detectable  $\text{CH}_4$ . Interestingly only the planetary mass companion 2M1207 b rivals the far reaching red sequence of the young brown dwarfs, yet that source is lacking an L' or equivalent band detection. Hence at this point the late-type young brown dwarf sequence prevails over the exoplanet sequence in their extreme L' colors even as the earliest type youngest planetary mass sources prevail at slightly bluer magnitudes.

The latest-type low-gravity brown dwarfs, and the known directly imaged exoplanets push the L/T transition to cooler temperatures and redder colors. Interestingly we have two sets of objects in the same group that span either side of the famed L/T transition. 0047+6803 ( $T_{eff}=1227 \pm 30$  K, Mass= 9 - 15  $M_{Jup}$ ) and SDSS1110 ( $T_{eff}= 926 \pm 18$ , Mass= 7 - 11  $M_{Jup}$ ) are both in the  $\sim 110$  - 130 Myr AB Doradus moving group. PSO318 ( $T_{eff}= 1210 \pm 41$ , Mass= 5 - 9  $M_{Jup}$ ) and 51 Eri b ( $T_{eff}= 675 \pm 75$ , Mass= 2 - 12  $M_{Jup}$ ) are both in the  $\sim 25$  Myr  $\beta$  Pictoris moving group. The two sets differ by  $\sim 100$  Myr in age. Comparing 0047+6803 to PSO318 we find they have similar spectral types, have  $T_{eff}$  within  $1\sigma$  but may differ in mass by up to  $\sim 10 M_{Jup}$ . Both push the L/T transition redder on multiple color magnitude diagrams in Figures 21 - 31 and Figures 35 - 41. Overall PSO318 and 0047+6803 have similar absolute magnitudes (see Figures 15 - 20) although PSO318 can be significantly redder in specific colors. 51 Eri b and SDSS1110 are thought to have similar spectral types but differ in mass and  $T_{eff}$  by as much as 344 K and 5  $M_{Jup}$  respectively. Interestingly, 51 Eri b is  $\sim 2$  mag fainter in  $M_{JHL}$  than SDSS 1110. Comparing its position on Figures 35, 38 and 40, 51 Eri b appears much more like the T8 Ross 458 C thought to be 150 - 800 Myr (Burgasser et al. 2010b). Regardless for both groups we see that by the time we have reached the mid to late-T dwarf phase, sources are back on or very close to, the field sequence. As cloud clearing is thought to happen at the L/T transition, we surmise this is further evidence that much of the diversity seen among the young, warm exoplanet and brown dwarf population is atmosphere related.

A note of caution when looking for similarities on color magnitude diagrams between brown dwarfs and giant exoplanets comes in the way of comparing the newly discovered L7 companion VHS1256 B to HR8799 b. In Gauza et al. (2015), the authors noted a similarity of this companion and the giant exoplanet. On Figure 37, the two have enticingly similar near-infrared values. However, Figure 42 shows the near-infrared spectrum of each ob-

ject as well as a field L7 to demonstrate strong differences in H-band. Clearly there is some commonality between the two sources, but color magnitude combinations alone do not give a full enough picture to draw conclusions.

The directly imaged companion GJ 504 b is another example of how we require multiple color magnitude diagram plots to begin exploring the potential characteristics of a single object (Kuzuhara et al. 2013). GJ 504 b is nearly 1 magnitude redder than late-type T dwarfs in  $M_{JHK}$  vs ( $J-K$ ) or ( $H-K$ ) diagrams (Figures 37 and 39), but it appears normal in  $M_{JH}$  vs ( $J-H$ ) plots (Figure 35). Recent work by Fuhrmann & Chini (2015) suggest the primary may not be young therefore this source may not be planetary mass. Regardless it is a low mass T dwarf orbiting at  $< 50$  AU, potentially formed in a disk around a nearby star hence it may be characteristically different than equivalent temperature T dwarfs (see e.g. Skemer et al. 2015).

### 8.1.1. Bolometric Luminosities

Comparing the bolometric luminosities ( $L_{bol}$ ) across the sample of field objects, new bona fide or high-likelihood moving group members, and directly imaged exoplanets allows us to investigate how the flux varies across the sample. For the directly imaged exoplanets, we use the  $L_{bol}$  values reported in the literature (see Males et al. 2014, Bonnefoy et al. 2014, Currie et al. 2014).

As discussed in both section 7.5 and Filippazzo et al. (2015), the young M dwarfs are overluminous for their spectral type while the young L's are normal to slightly underluminous. Several authors have noted this peculiarity among the directly imaged exoplanets as well (e.g. Bowler et al. 2013, Males et al. 2014). Examining the two populations together allows us to investigate whether there is an obvious age-associated correlation within the scatter. The youngest objects in Figure 43 are the directly imaged exoplanets such as ROXs 42B b, and 1RXS1609 b which belong to star forming regions at just a few Myr of age. These sources appear overluminous in comparison to equivalent sources regardless of how late their spectral type (e.g. 1RXS1609b which is thought to resemble an L4). The latest type planets that have direct, comparable data – 2M1207 b, HR8799 b, 51 Eri b – are all  $\sim 1 \sigma$  or more below the field sequence indicating that they are either far cooler than the latest L dwarfs or there is unaccounted flux in the bolometric luminosity calculations. Interestingly, this appears to be where the young brown dwarf and the directly imaged exoplanet comparisons diverge. The latest type exoplanets in equivalent age groups to the isolated brown dwarfs, are either far cooler than any currently discovered young brown dwarf equivalent, or the physical conditions diverge (e.g. atmosphere conditions, chemistry, other).

### 8.1.2. Masses from combining Evolutionary Models with $L_{bol}$ , and Age

In Figure 34, we combine the  $L_{bol}$  values with the ages of the moving group members to estimate masses. In Table 14 we also list masses calculated from the spectral energy distribution analysis as described in Filippazzo et al. (2015). Over-plotted on Figure 34 with the young brown dwarfs are directly imaged planetary and brown dwarf mass companions with  $L_{bol}$  values collected

from the literature. The models from Saumon & Marley (2008)(solid) and Baraffe et al. (2015) (dashed) are shown with lines of equal mass color coded as stars ( $> 75 M_{Jup}$ , blue) brown dwarfs ( $> 13 M_{Jup}$ , green) and planets ( $< 13 M_{Jup}$ , red).

It is unclear how each one of the objects in this sample formed however, using the  $13 M_{Jup}$  boundary as a mass distinguisher between brown-dwarf and planet-type objects, we find that there are close to 9 solitary objects with masses  $< 13 M_{Jup}$ . Several of those sources lie in an ambiguous area where low mass brown dwarfs and planetary mass objects cross (30 - 130 Myr between masses of 10 - 20  $M_{Jup}$ ).

With the exception of Y type objects whose age is still undetermined (e.g. W0855, Luhman 2014), 1119-1137, 1147-2040, and PSO318 are the lowest mass isolated sources categorized. PSO 318 has a lower luminosity than  $\beta$  Pictoris b, the  $11 - 13 M_{Jup}$  planet in the same association while 1119-1137 and 1147-2040 are significantly more luminous than their sibling exoplanet 2M1207b. Interestingly, the AB Doradus equivalently typed L7 member, 0047+6803, is higher mass than all of these sources even though its bolometric luminosity is comparable. Similarly, 0355+1133 which is in the same group as 0047+6803, shares photometric anomalies with PSO318 (near-infrared and mid infrared color) and spectral anomalies with 2M1207b yet it is much higher mass.

The overlap in masses of the directly imaged exoplanets and isolated brown dwarfs invites questions of formation given co-evolving groups. Whether the latter was formed via star formation processes or ejected after planetary formation processes is yet to be seen and requires further investigation.

## 9. CONCLUSIONS

In this work we investigate the kinematics and fundamental properties of a sample of 152 suspected young brown dwarfs. We present near-infrared spectra and confirm low-surface gravity features for 43 of the objects designating them either intermediate ( $\beta$ ) or very low ( $\gamma$ ) gravity sources. We report 18 new parallaxes (10 field objects for comparison and 8 low surface gravity), 19 new proper motions, and 38 new radial velocities and investigate the likelihood of membership in a nearby moving group. We use four kinematic membership codes (1) BANYAN I, (2) BANYAN II, (3) LACEWING, and (4) Convergent method, as well as a visual check of the available space motion for each target against known members of well known nearby kinematic groups to determine the likelihood of co-membership for our sources. We categorize objects as (1) bona fide -BM, (2) high-likelihood -HLM, (2) ambiguous -AM, or (3) non-member -NM of nearby moving groups. We find 39 sources are bona fide or high-likelihood members of known associations (8 in AB Doradus, 1 in Argus, 2 in  $\beta$  Pictoris, 1 in Columba, 7 in TW Hydreae, and 20 in Tucana Horologium). A further 92 objects have an ambiguous status and 21 objects are not members of any known group evaluated in this work.

Examining the distribution of gravity classifications between different groups we find that the youngest association (TW Hydreae) has only very low-gravity ( $\gamma$ ) sources associated with it but slightly older groups such as Tucana Horologium (9 optically classified, 10 infrared

classified  $\gamma$  objects and 3 optically classified, 5 infrared classified  $\beta$  objects) and AB Doradus (4 optically classified, 6 infrared classified  $\gamma$  objects and 1 optically classified, 2 infrared classified  $\beta$  objects) show a mix of both intermediate ( $\beta$ ) and very low-gravity sources. This diversity is evidence that classically delegated gravity features in the spectra of brown dwarfs are influenced by other parameters such as metallicity or (more likely) atmospheric conditions.

We investigate colors for the full sample across the suite of MKO, 2MASS and WISE photometry ( $J, H, K_s, W1, W2, W3$ ). In color versus spectral type diagrams, we find that the  $\gamma$  and  $\beta$  classified objects are distinct from the field ( $> 3$  Gyr sources). They are most deviant from the field sequence in the ( $J-W2$ ) color where they are an average of  $2\sigma$  redder than the subtype mean. They are least deviant in the ( $J-H$ ) color where they are an average of  $0.7\sigma$  redder than the subtype mean. Based on the 5 -130 Myr age calibrated sample, we conclude that the extent of deviation in infrared color is not indicative of the age of the source (meaning redder does not translate to younger). In any given color a  $\gamma$  or a  $\beta$  object – whether confirmed in a group or not – may mark the extreme outlier for a given subtype. We find that the L0 dwarfs in Tucana Horologium (expected to have the same,  $T_{eff}$ , age and metallicity) deviate from the field sequence of infrared colors by between 1 and  $4\sigma$  (depending on the particular color examined). Assuming clouds are the source of the diversity, we conclude that there is a variation in cloud properties between otherwise similar objects.

Examination of the absolute magnitudes for the parallax sample indicates a clear flux redistribution for low- and intermediate-gravity brown dwarfs (compared to field brown dwarfs) from near-infrared to wavelengths at (and longer than) the WISE W3 band. There is also a clear correlation of this trend with spectral subtype. The M dwarfs are  $1-2\sigma$  brighter than field equivalents at  $J$  band but  $4-5\sigma$  brighter at W3. The L dwarfs are  $1-2\sigma$  fainter at  $J$  band but  $1-2\sigma$  brighter at W3. Clouds, which are a far more dominant opacity source for L dwarfs, are likely the cause.

Sources that are not confirmed in groups do not all trace the same behavior in absolute magnitude or color indicating that some sources may not be young. Variations in atmospheric conditions or metallicity likely drive the diversity.

On color-magnitude diagrams, the low-surface gravity brown dwarfs pull the elbow of the field L/T transition significantly redder and fainter with the most extreme case being the  $M_J$  vs ( $J-W2$ ) plot where young objects are up to 1 mag redder than the field sequence. Conversely, the  $M_K$  versus ( $K-W2$ ) plot shows a 10 magnitude difference between the warmest and coolest brown dwarfs yet seems to monotonically decrease in magnitude with reddening color. On this figure there is little evidence for an L/T transition elbow and the young objects form a secondary sequence that is  $\sim 1$  mag redder than the field sequence. Interestingly as we move to longer wavelengths the effect reverses and the latest type objects pull the elbow of the L/T transition back up as they are equivalent or slightly brighter than field equivalents at  $M_{W1,W2}$ . Comparing the sequence of  $\gamma$  and  $\beta$  classified sources on CMD's compared to the field, we

find a hint that the two are distinct with the former redder than the latter. This trend is clearest on the  $M_J$  versus ( $J-W2$ ) figure although there is still a small mix of  $\gamma$  and  $\beta$  sources at extreme colors for a given absolute magnitude.

Comparing the low-gravity sample with directly imaged exoplanets on color magnitude diagrams we find that the former sequence logically extends through the latest type planets on multiple color magnitude diagrams. The small collection of hot, planetary mass objects in star forming regions such as  $\rho$  Ophiuchus and Taurus are strikingly red, bright, and luminous compared to either the field sequence or the low-gravity objects indicating that the atmosphere and/or gravity effects that drive the population diversity may be pronounced close to formation. Comparing  $\beta$  Pictoris members 51 Eri b (mid T dwarf) and PSO318 (late L dwarf) with AB Doradus members SDSS1110 (mid T dwarf) and 0047+6803 (late L dwarf) we find that even though the members differ by  $\sim 100$  Myr, the late-type L's similarly push the elbow of the L/T transition redder and fainter whereas the T dwarfs appear on or very close to the field sequence. We surmise that this behavior, seen in two sets of objects at different ages across the L/T transition where cloud clearing is thought to be significant, is evidence that much of the diversity seen among young warm exoplanet and brown dwarfs is atmosphere related.

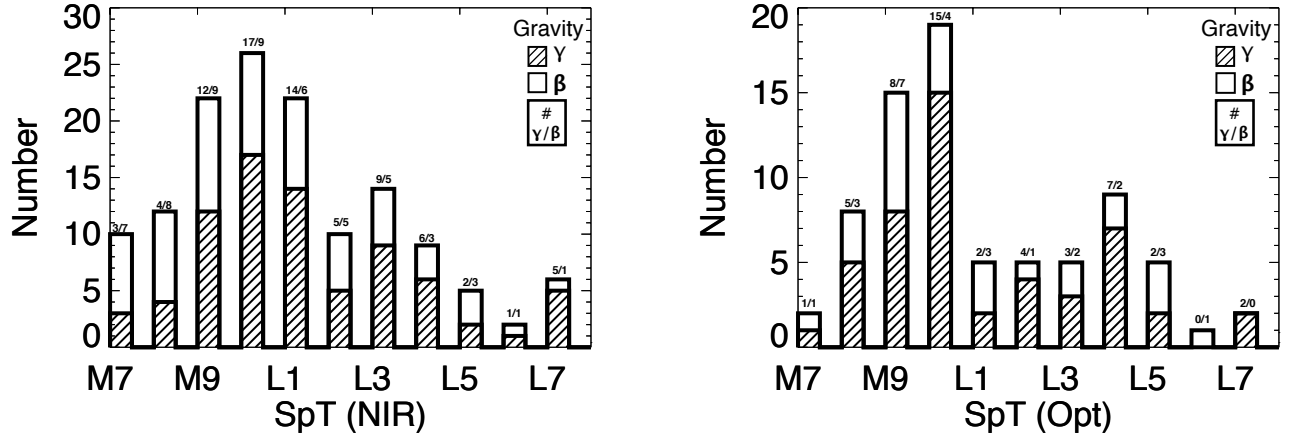


**Figure 1.** The distribution of objects analyzed in this work organized by spectral subtype and gravity classification in either the near-infrared (left) or optical (right). For ease of labels in this work, we have chosen to label VL-G and INT-G objects classified using the Allers & Liu (2013) spectral indices as  $\gamma$  and  $\beta$  respectively. On this plot we also show the number of  $\gamma$  and  $\beta$  at each subtype as a ratio of  $\# \gamma / \# \beta$ .

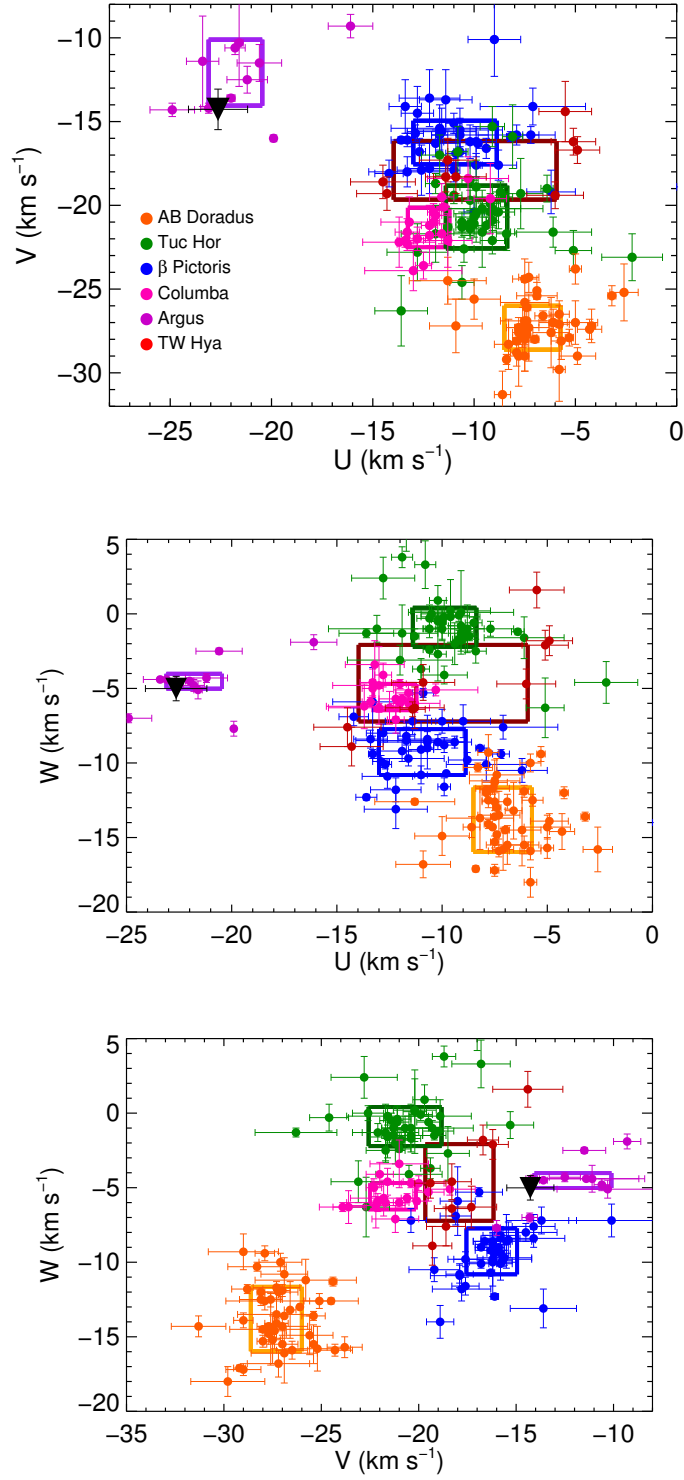


**Figure 2.** The UVW properties of 0045+1634 (black filled triangle) compared to those of the members of the nearby young groups. Solid rectangles surround the furthest extent of highly probable members from Torres et al. (2008) but their distribution does not necessarily fill the entire rectangle.

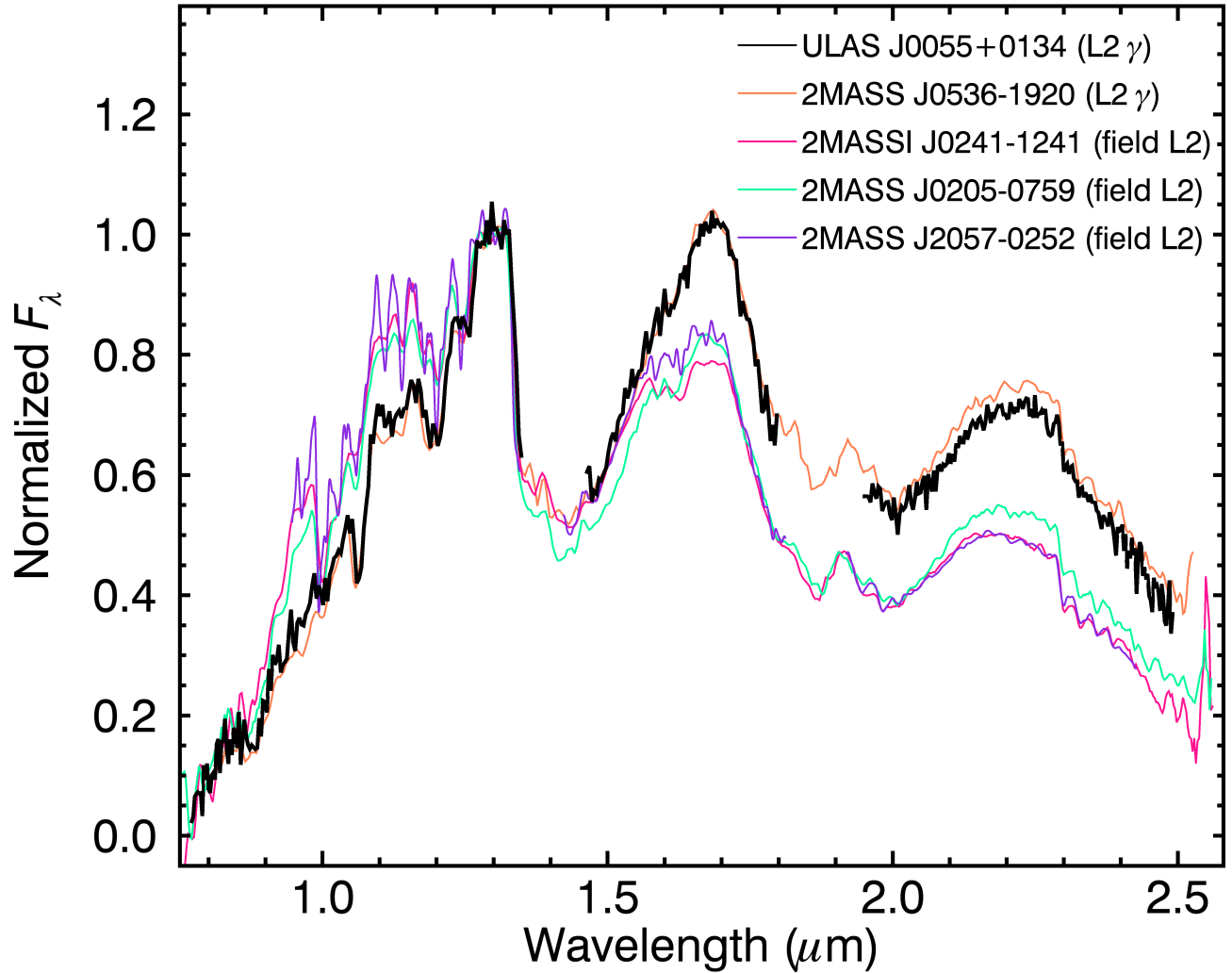


**Figure 3.** The SpeX prism spectrum of 0055+0134 over-plotted with a sample of field and very low-gravity subtype equivalents.

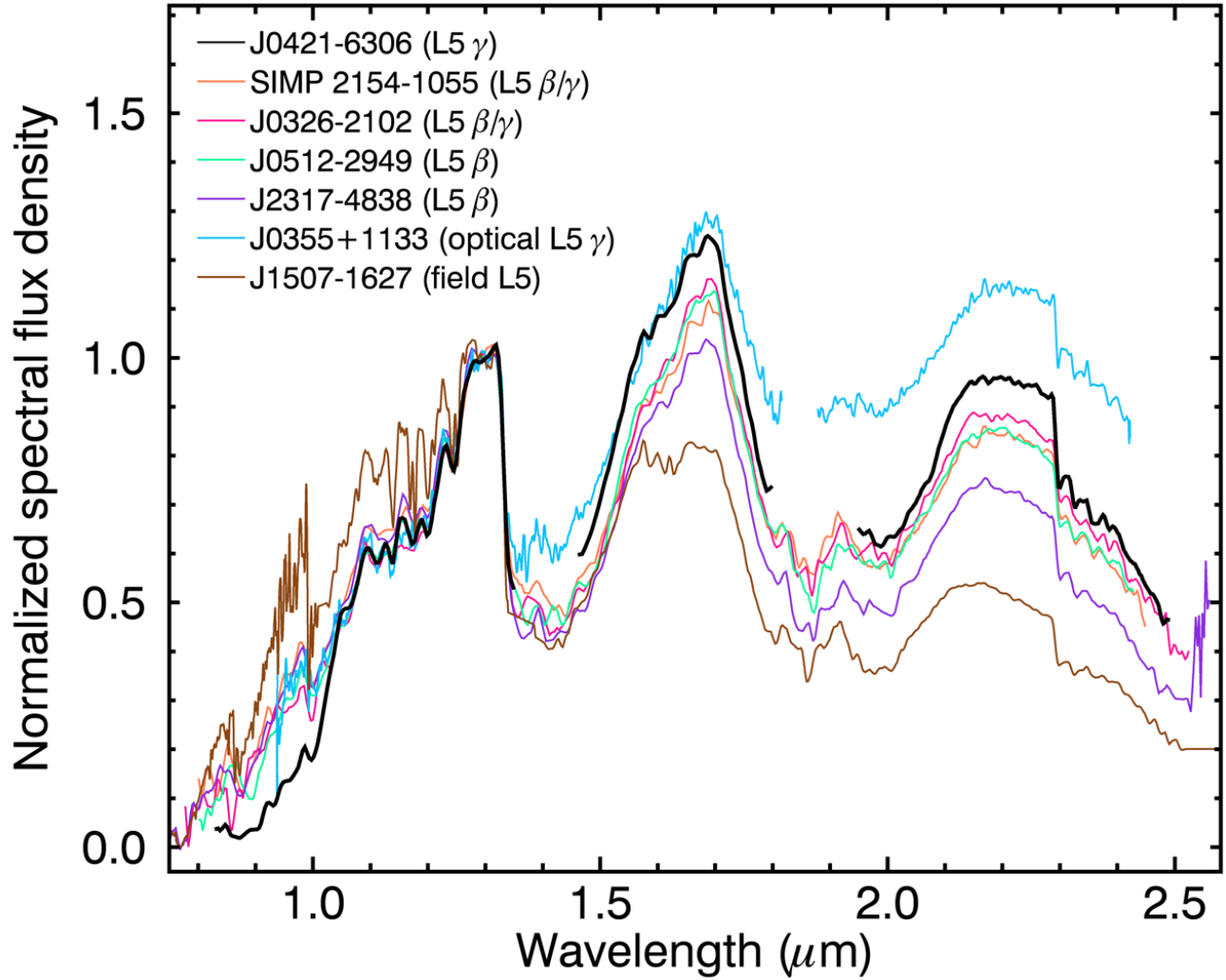


**Figure 4.** The FIRE spectrum of 0421-6306 binned to prism resolution and over-plotted with a sample of field and very low-gravity subtypes.

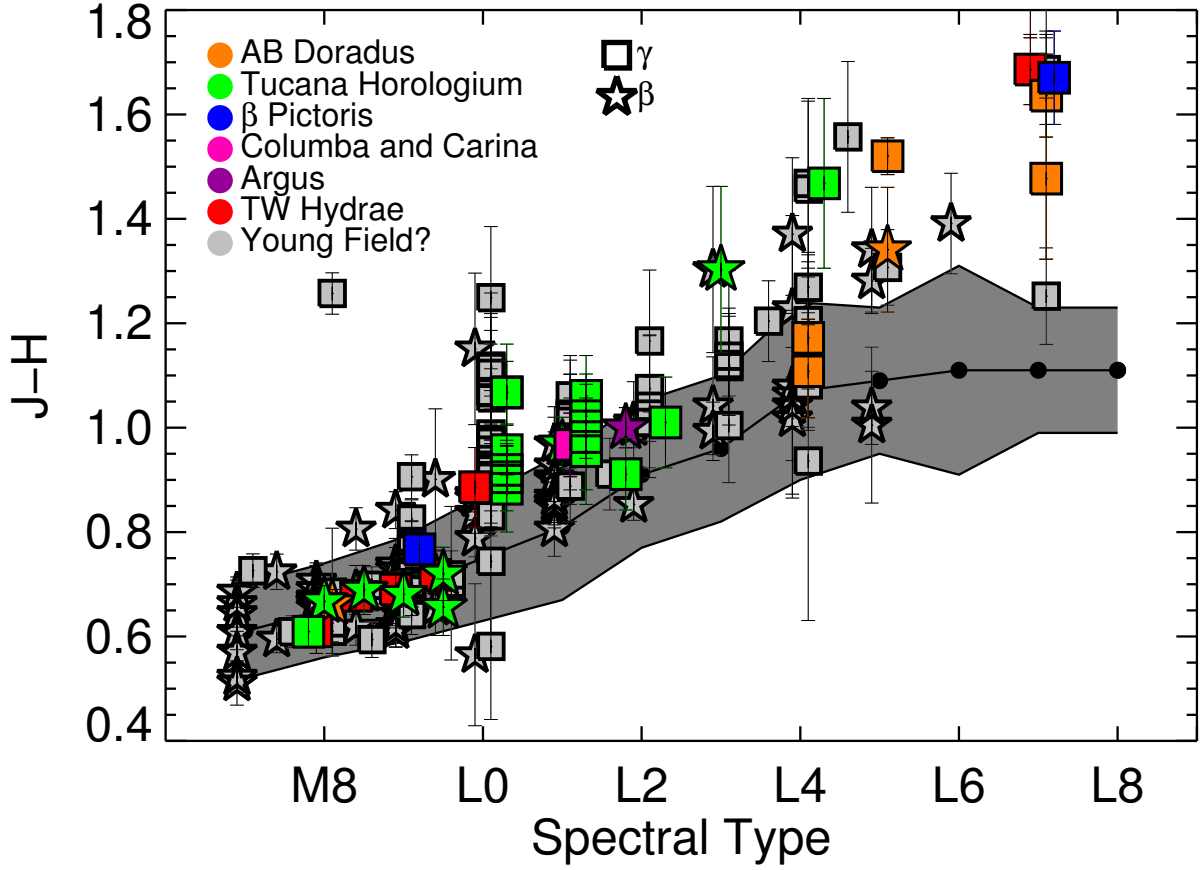


**Figure 5.** The distribution of J-H color as a function of spectral type. The black filled circle at each subtype is the mean value and the grey filled area marks the standard deviation spread. The isolated sources that compose this “normal” sample have no spectral peculiarities (e.g. subdwarfs, low-gravity, unresolved binarity), and were only included if they had a photometric uncertainty in each band  $< 0.2$  mag. The full list was gathered from the dwarfarchives compendium and supplemented with the large ultra cool dwarf surveys from Schmidt et al. (2010), Mace et al. (2013), Kirkpatrick et al. (2011), and West et al. (2008) (for M dwarfs). Individual filled squares or five-point stars are  $\gamma$  or  $\beta$  (respectively) classified objects. Spectral types, as well as gravity classifications, are from optical data unless only infrared was available. We note that most sources plotted have spectral type uncertainties of 0.5. Objects are color coded by group assignments (or lack-thereof) discussed in this work. 2MASS photometry is used for  $JHK_s$  bands.

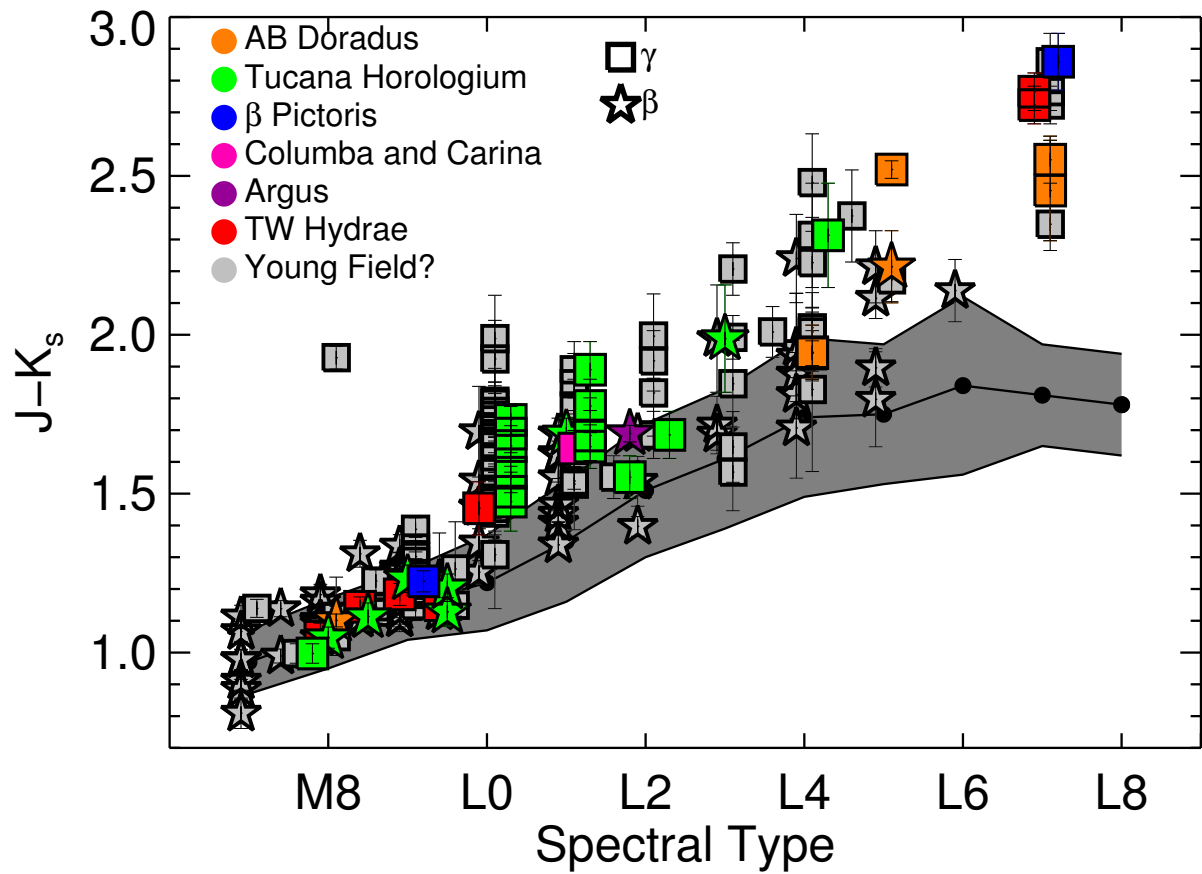


**Figure 6.** The distribution of  $J-K_s$  color as a function of spectral type. Symbols are as described in Figure 5.

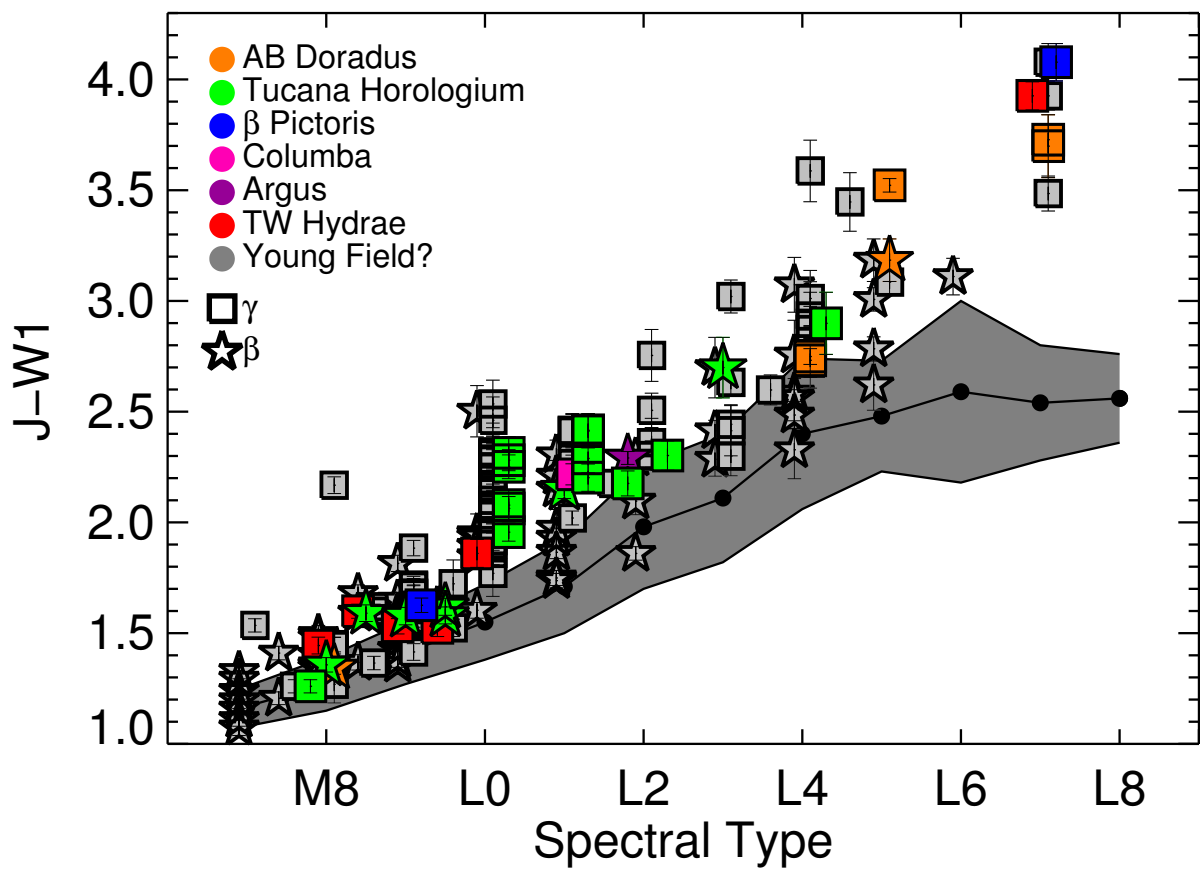


**Figure 7.** The distribution of J-W1 color as a function of spectral type. Symbols are as described in Figure 5.

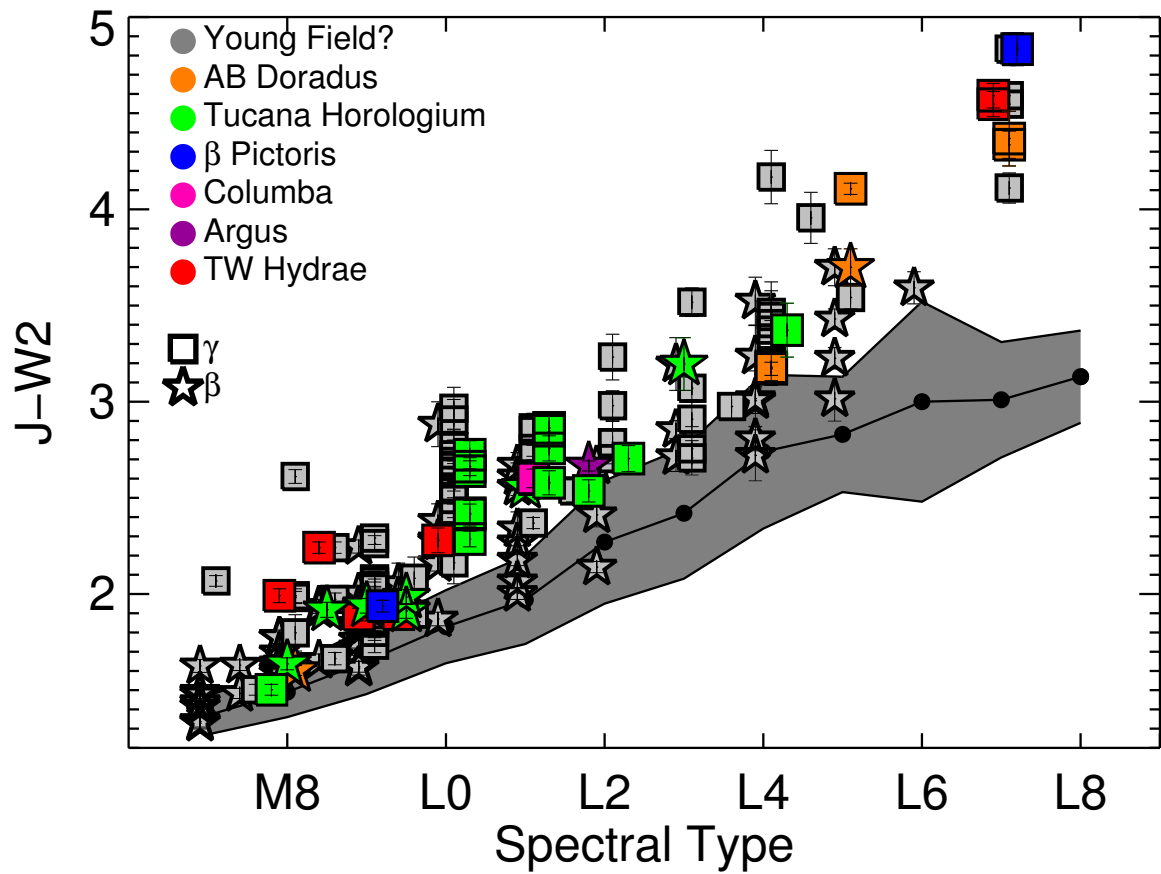


**Figure 8.** The distribution of J-W2 color as a function of spectral type. Symbols are as described in Figure 5.

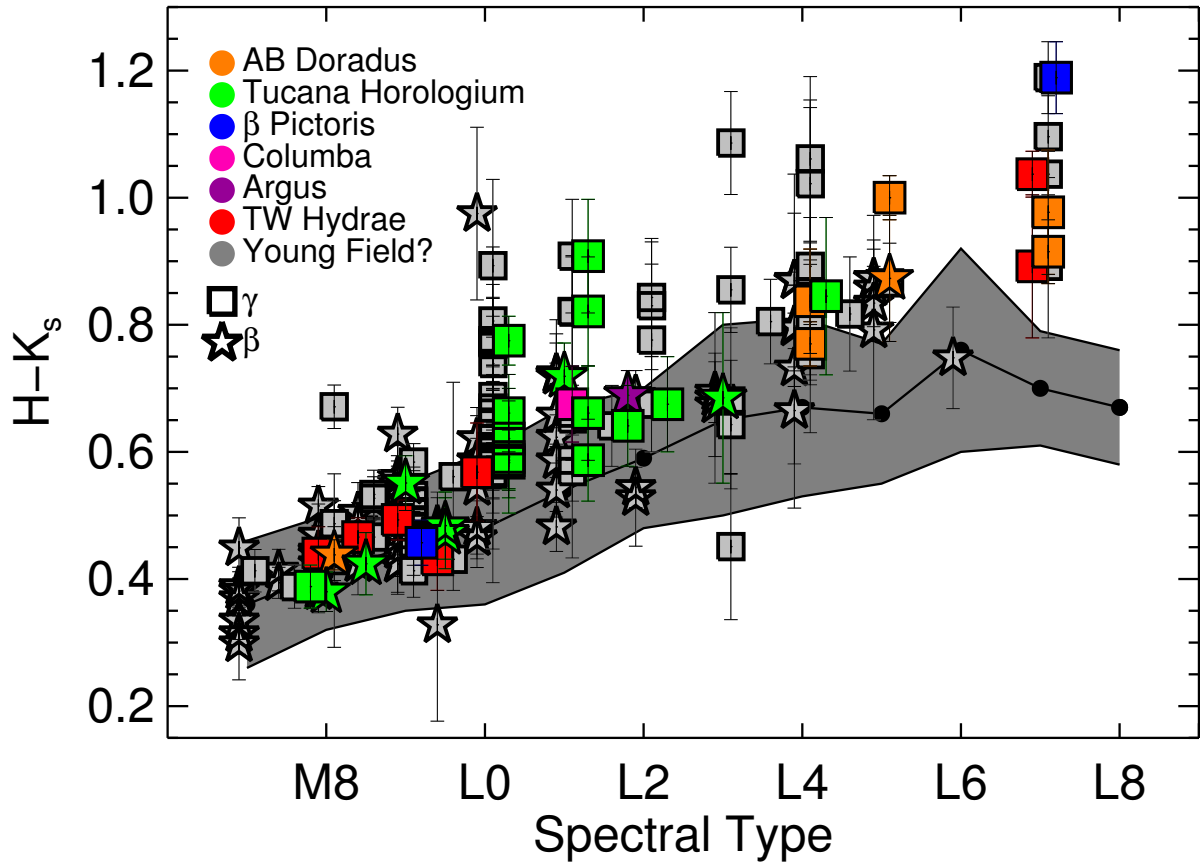


**Figure 9.** The distribution of  $H-K_s$  color as a function of spectral type. Symbols are as described in Figure 5.

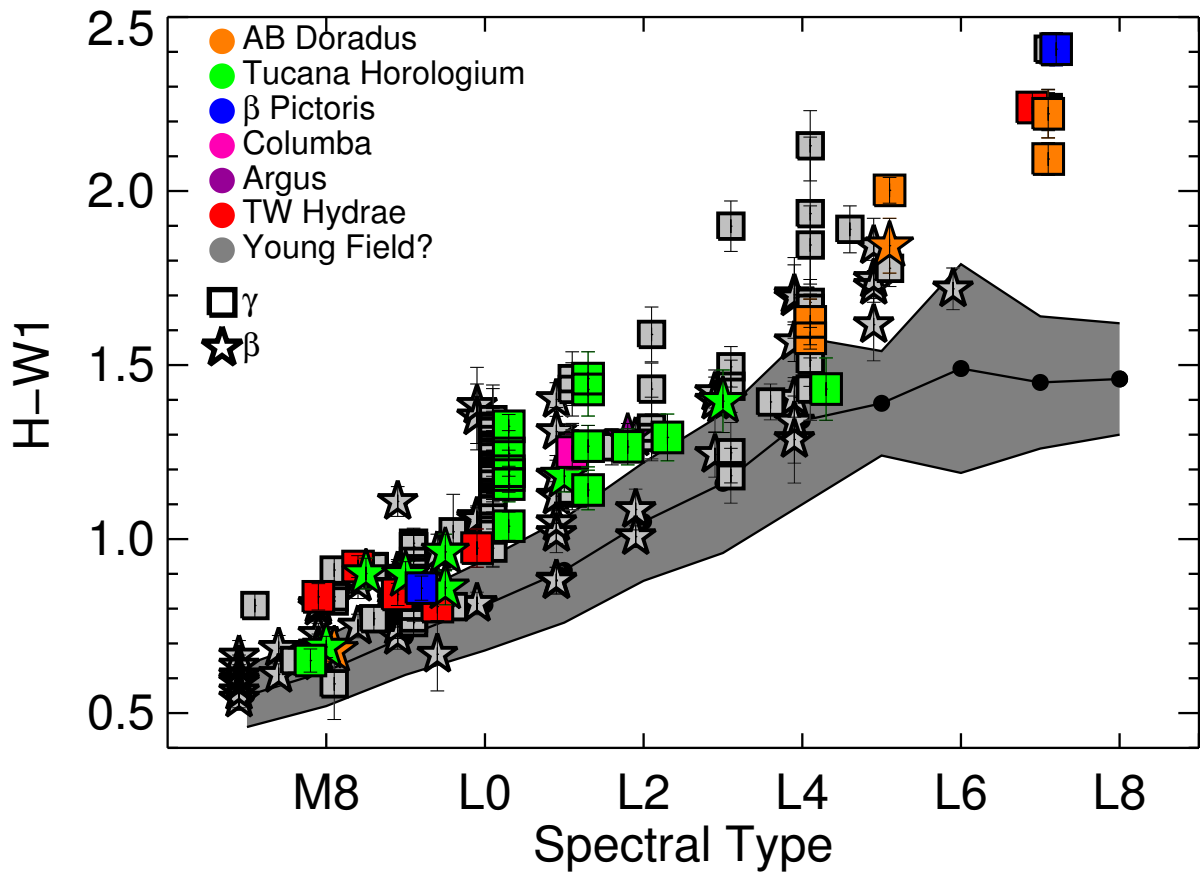


**Figure 10.** The distribution of H-W1 color as a function of spectral type. Symbols are as described in Figure 5.

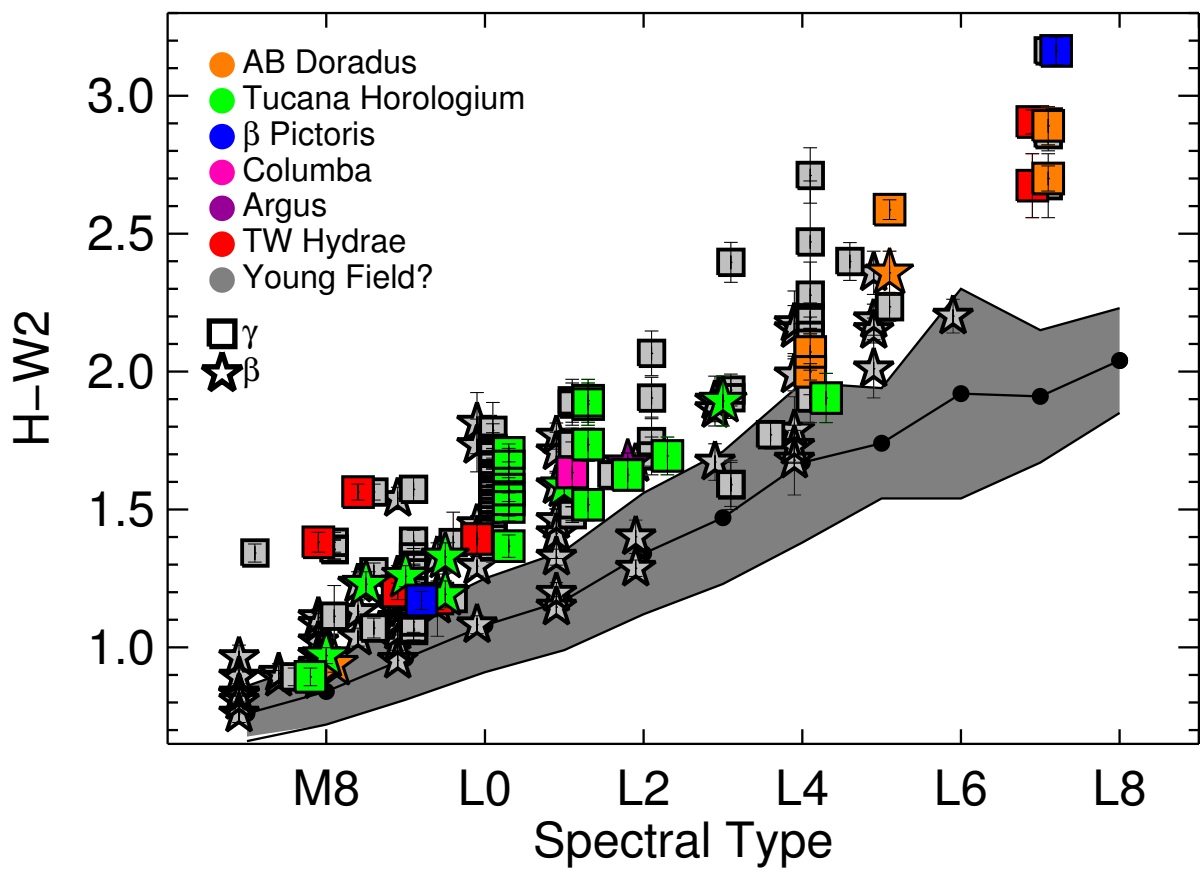


**Figure 11.** The distribution of H-W2 color as a function of spectral type. Symbols are as described in Figure 5.

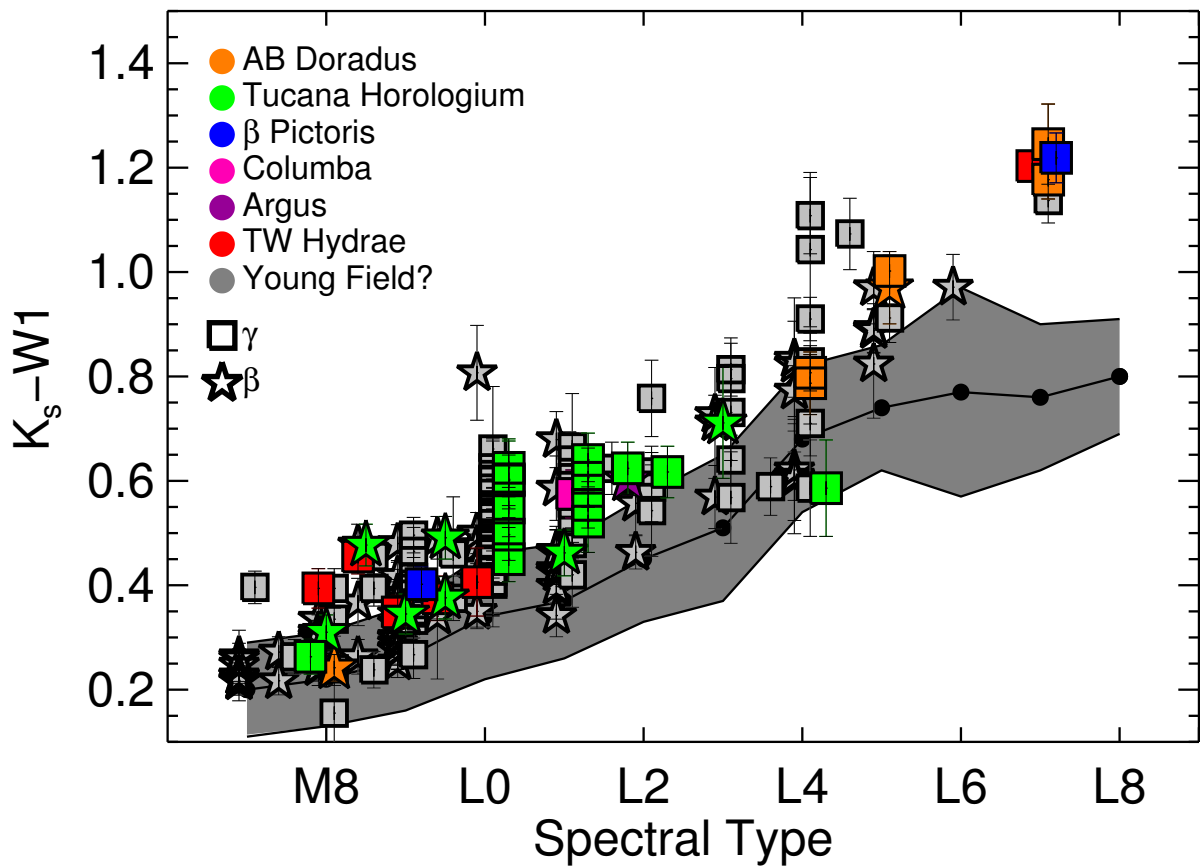


**Figure 12.** The distribution of  $K_s$ -W1 color as a function of spectral type. Symbols are as described in Figure 5.

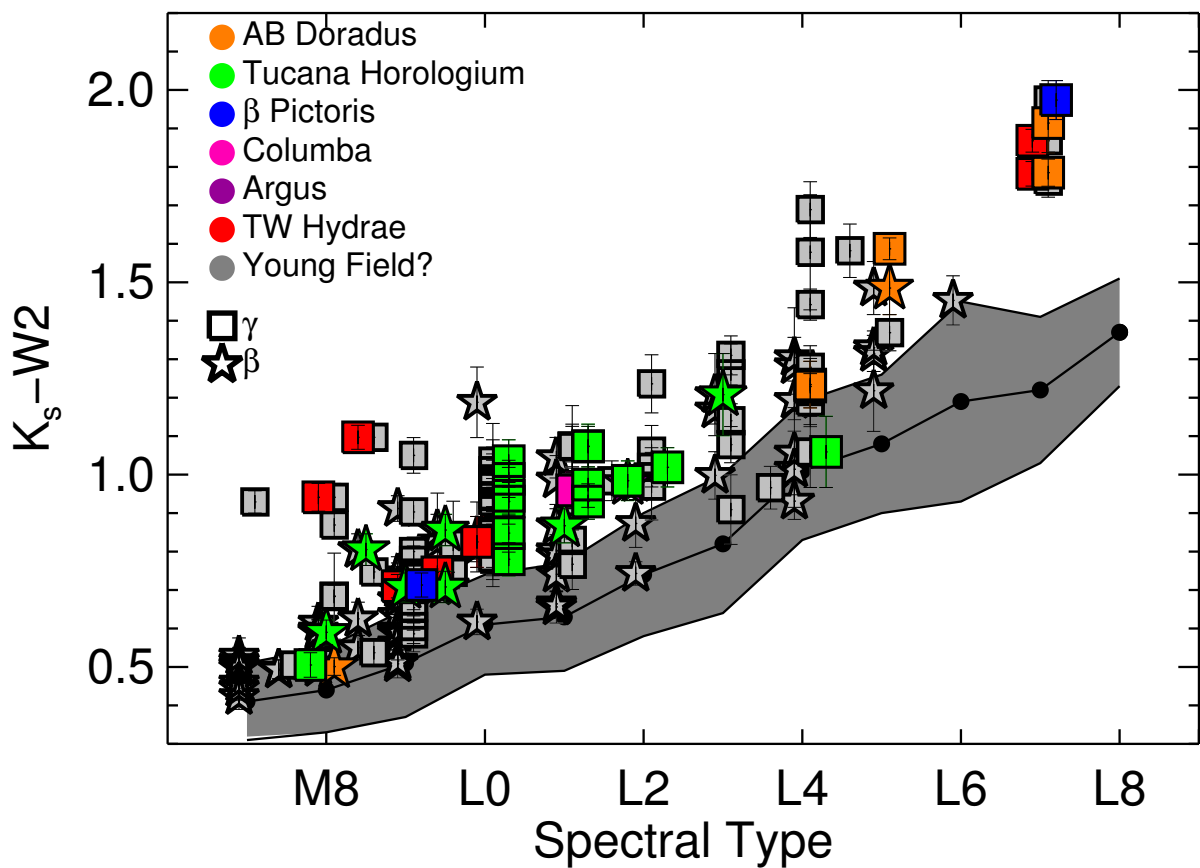


**Figure 13.** The distribution of  $K_s$ -W2 color as a function of spectral type. Symbols are as described in Figure 5.

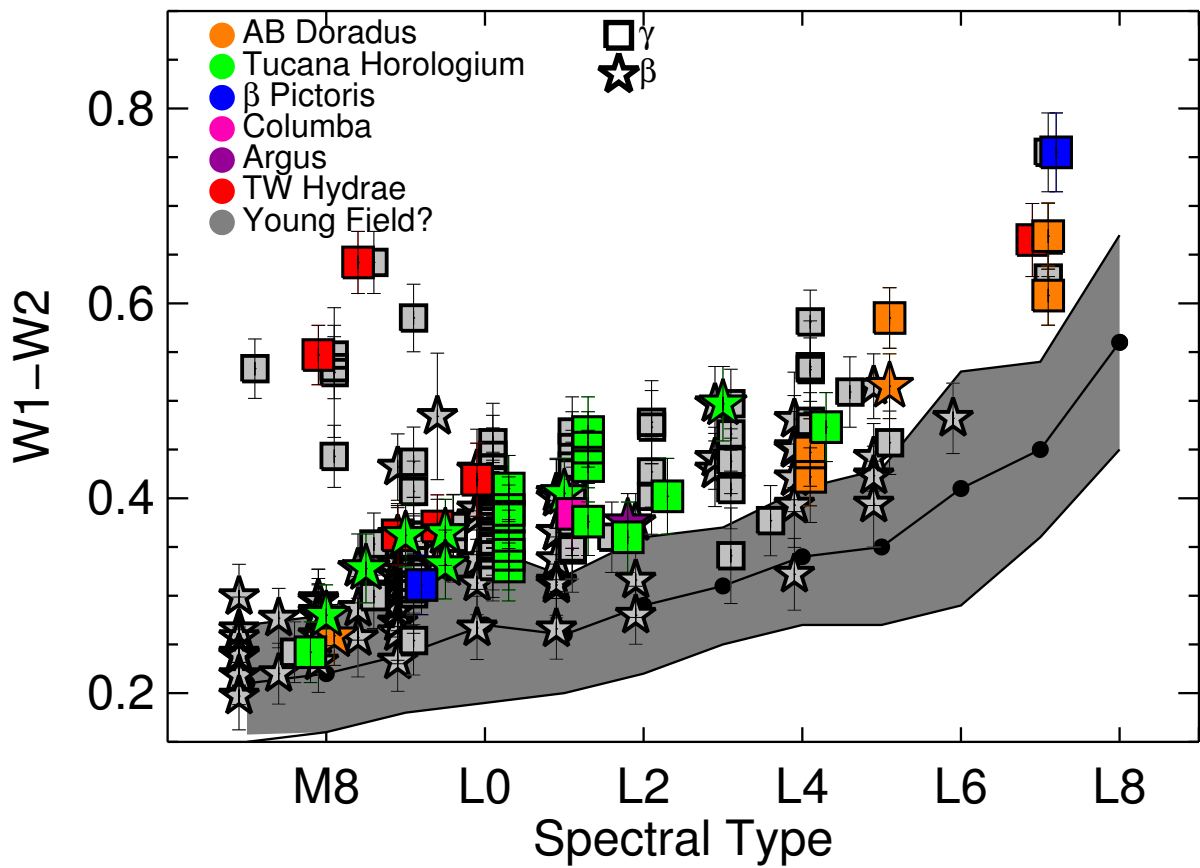


**Figure 14.** The distribution of W1-W2 color as a function of spectral type. Symbols are as described in Figure 5.

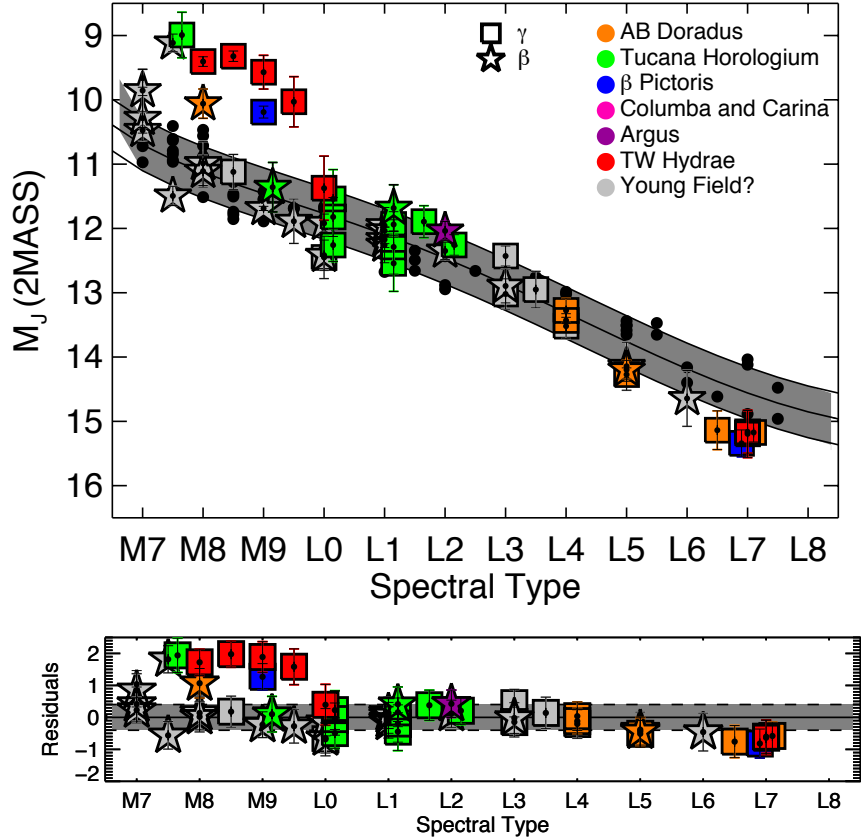


**Figure 15.** The spectral type versus  $M_J$  plot. The field polynomial listed in Table 19 is represented by the grey area. All  $JHK$  photometry is from 2MASS. Over-plotted are objects in this work with measured parallaxes or estimated kinematic distances from high confidence group membership. Symbols distinguish very low ( $\gamma$ ) from intermediate ( $\beta$ ) gravity sources. Objects are color coded by group membership. For demonstration on the  $M_J$  plot only, we also overplot individual field objects (with  $M_{Jer} < 0.5$ ) as black filled circles. Residuals of individual  $\gamma$  and  $\beta$  objects against the field polynomial are shown in the lower panel.

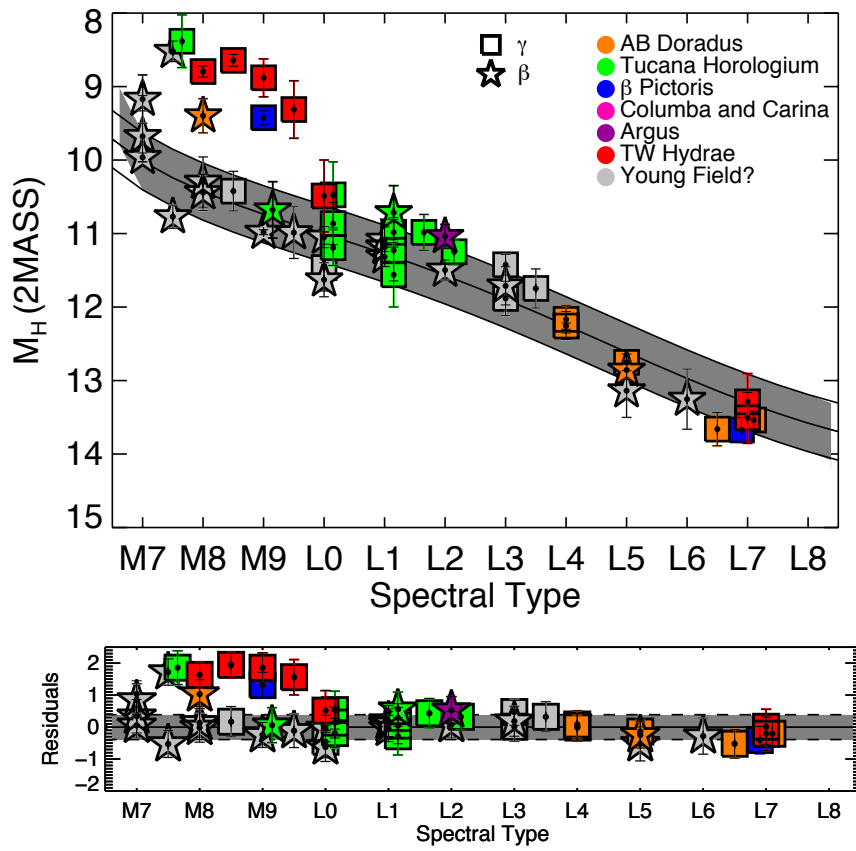


**Figure 16.** The spectral type versus  $M_H$  plot with residuals against polynomial relations (lower panel). Symbols are as described in Figure 15.

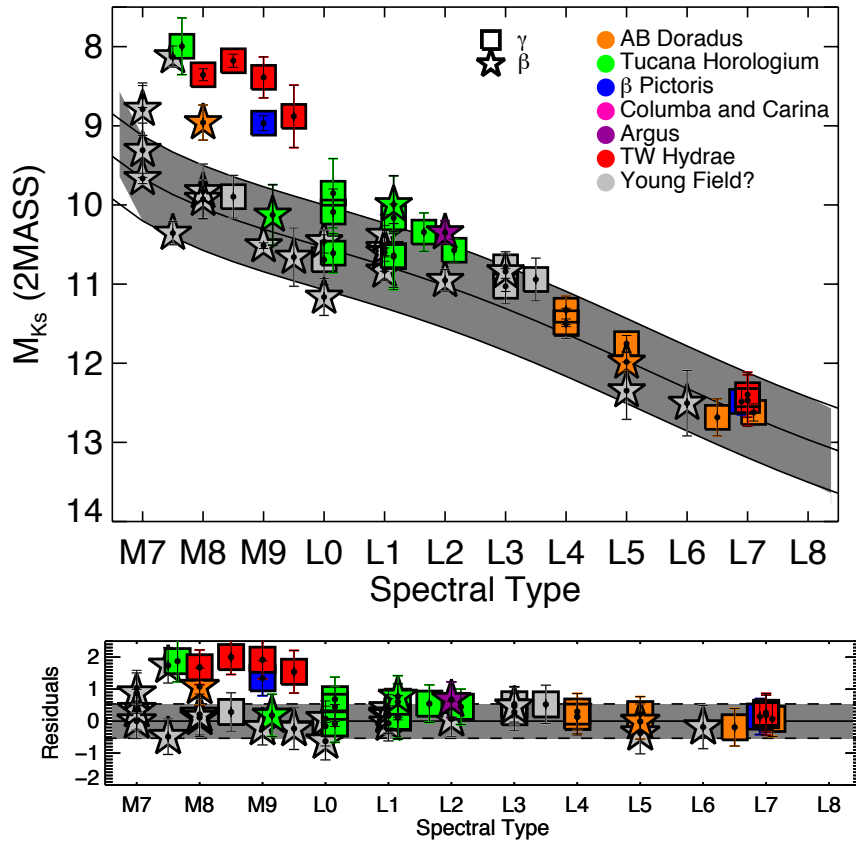


**Figure 17.** The spectral type versus  $M_{Ks}$  plot with residuals against polynomial relations (lower panel). Symbols are as described in Figure 15.

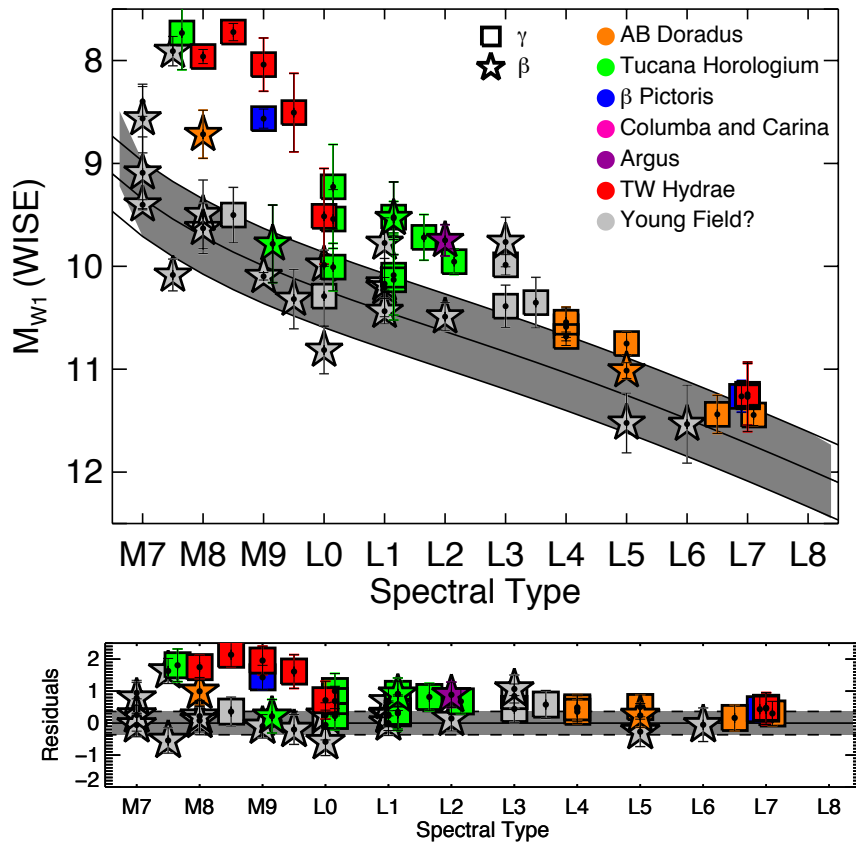


**Figure 18.** The spectral type versus  $M_{W1}$  plot with residuals against polynomial relations (lower panel). Symbols are as described in Figure 15.



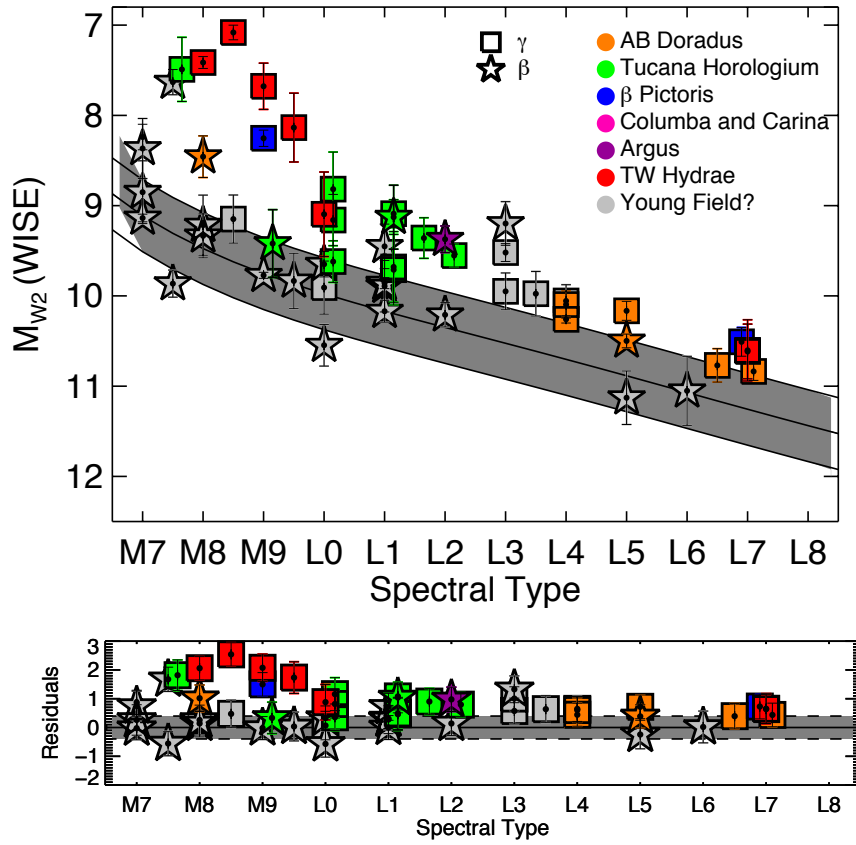


**Figure 19.** The spectral type versus  $M_{W2}$  plot with residuals against polynomial relations (lower panel). Symbols are as described in Figure 15.

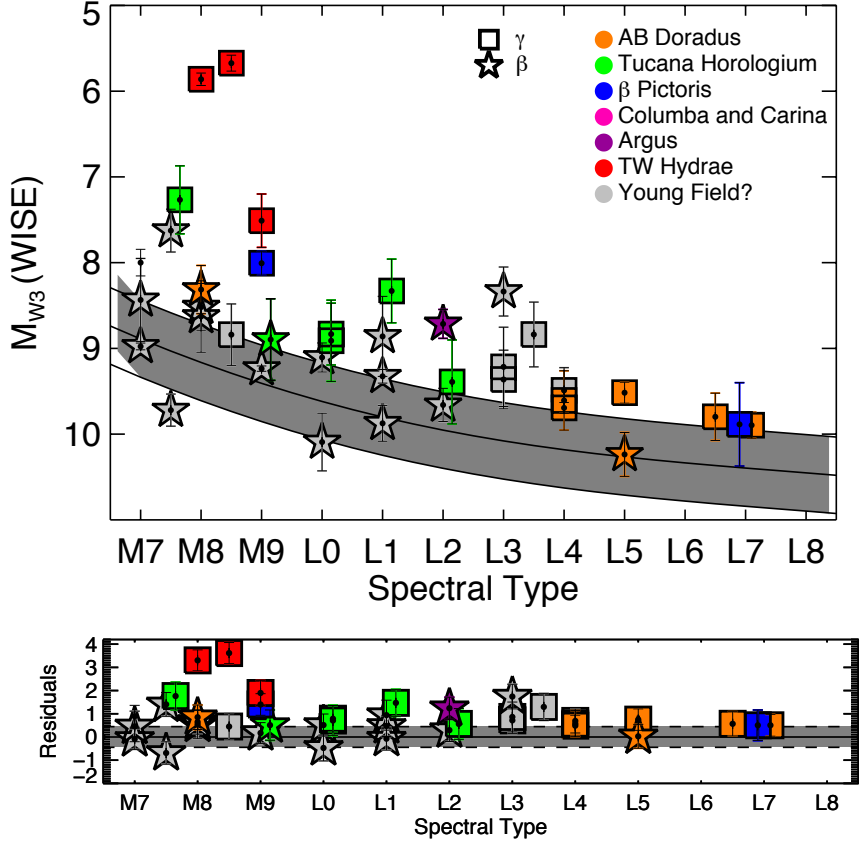


**Figure 20.** The spectral type versus  $M_{W3}$  plot with residuals against polynomial relations (lower panel). Symbols are as described in Figure 15.

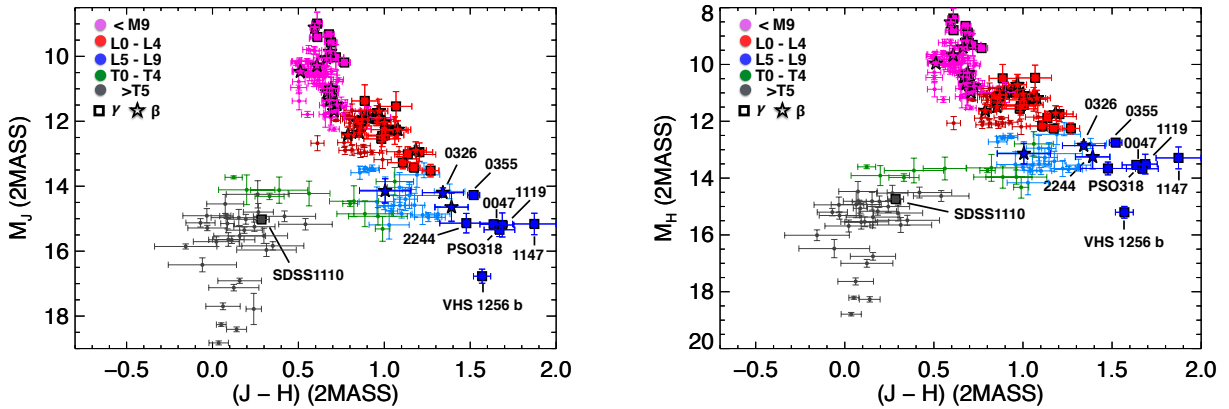


**Figure 21.** The  $(J-H)$  versus  $M_J$  (left) and  $M_H$  (right) color magnitude diagram for late-type M through T dwarfs (Y dwarfs where photometry is available). All  $JHK$  photometry is on the MKO system. Objects have been color coded by spectral subtype. Binaries, subdwarfs, spectrally peculiar sources and those with absolute magnitude uncertainties  $> 0.5$  have been omitted. Low-gravity objects are highlighted as bold filled circles throughout. Objects of interest discussed in detail within the text have been labeled.

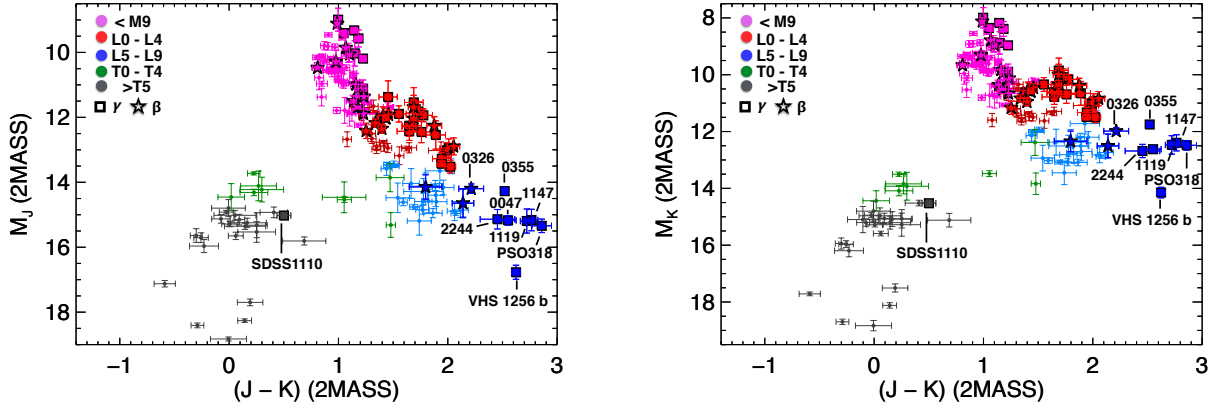


**Figure 22.** The  $(J-K)$  versus  $M_J$  (left) and  $M_K$  (right) color magnitude diagram. Symbols are as described in Figure 21.

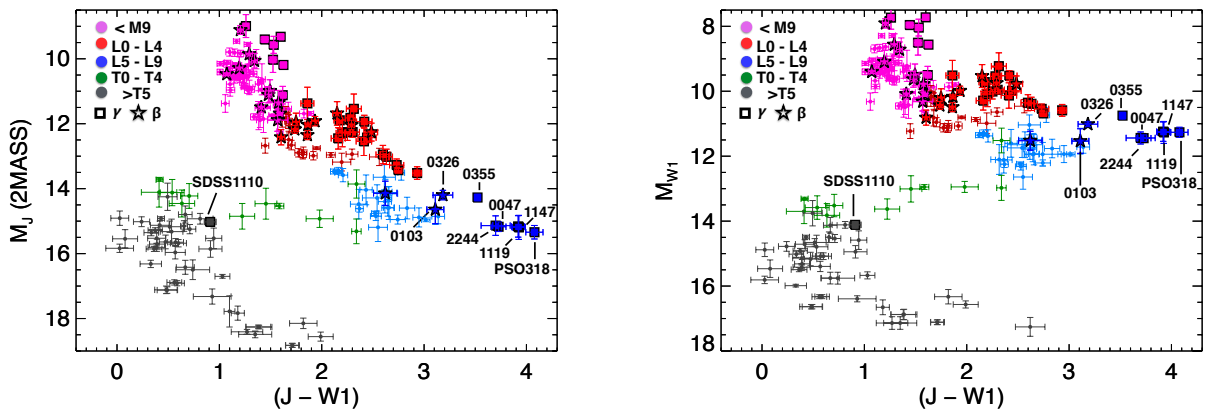


**Figure 23.** The  $(J-W_1)$  versus  $M_J$  (left) and  $M_{W_1}$  (right) color magnitude diagram. Symbols are as described in Figure 21.

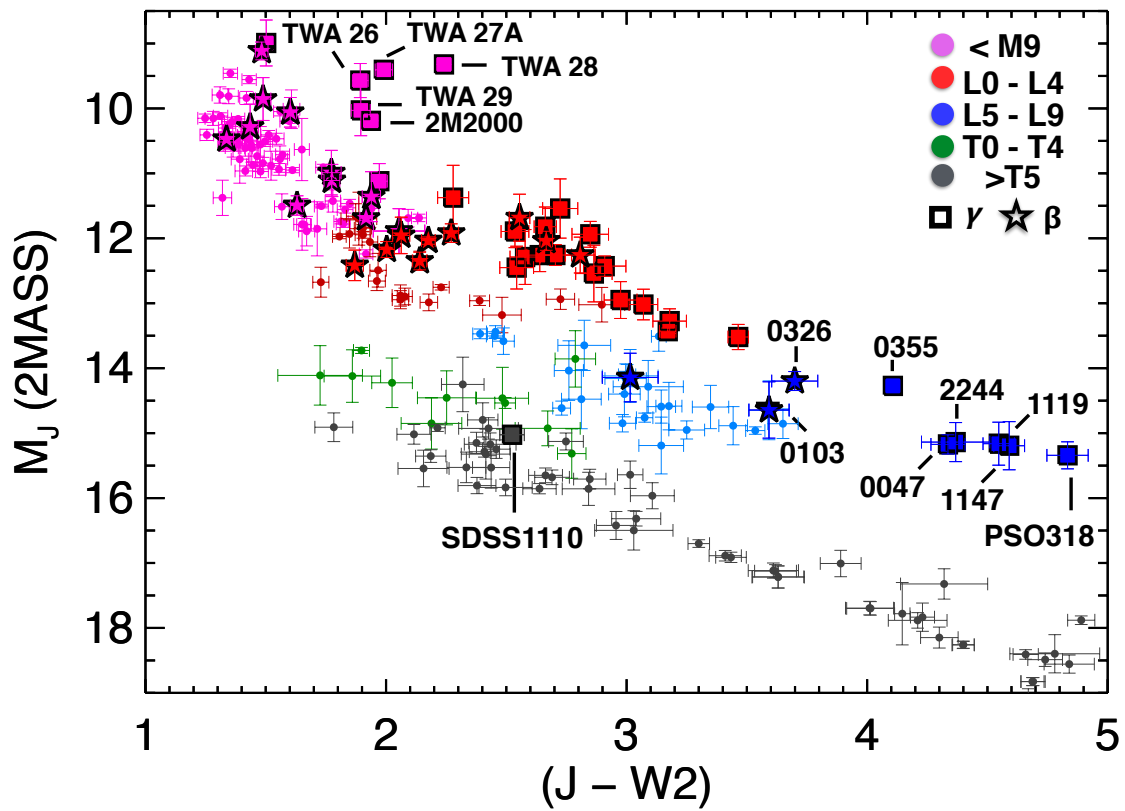


**Figure 24.** The  $(J-W2)$  versus  $M_J$  color magnitude diagram. Symbols are as described in Figure 21.

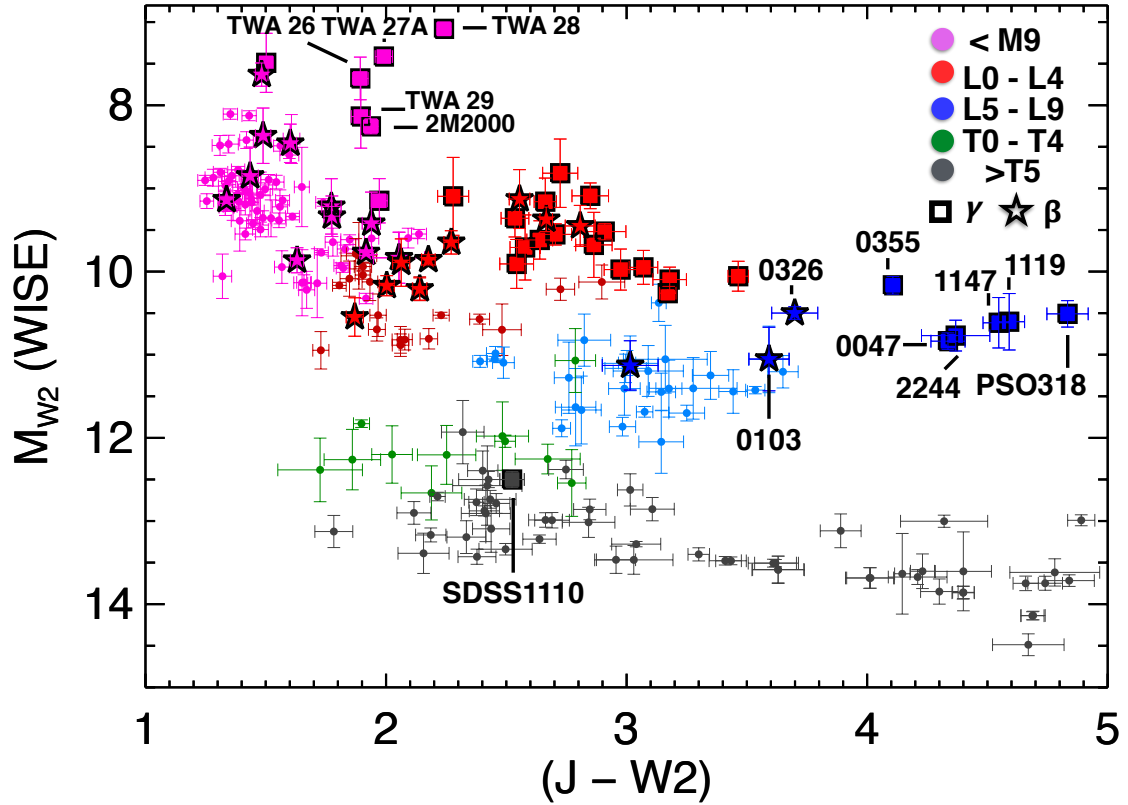


**Figure 25.** The  $(J - W2)$  versus  $M_{W2}$  (right) color magnitude diagram. Symbols are as described in Figure 21.

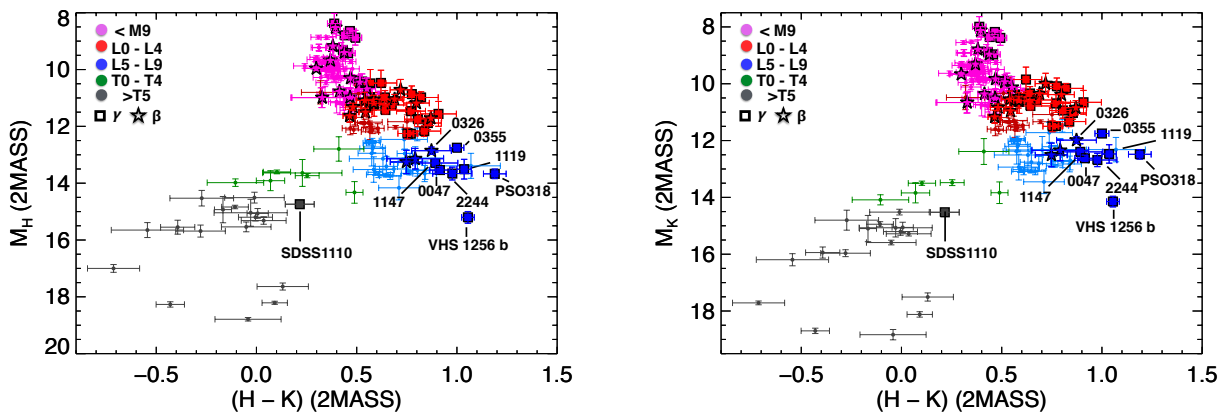


**Figure 26.** The  $(H - K)$  versus  $M_H$  (left) and  $M_K$  (right) color magnitude diagram. Symbols are as described in Figure 21.

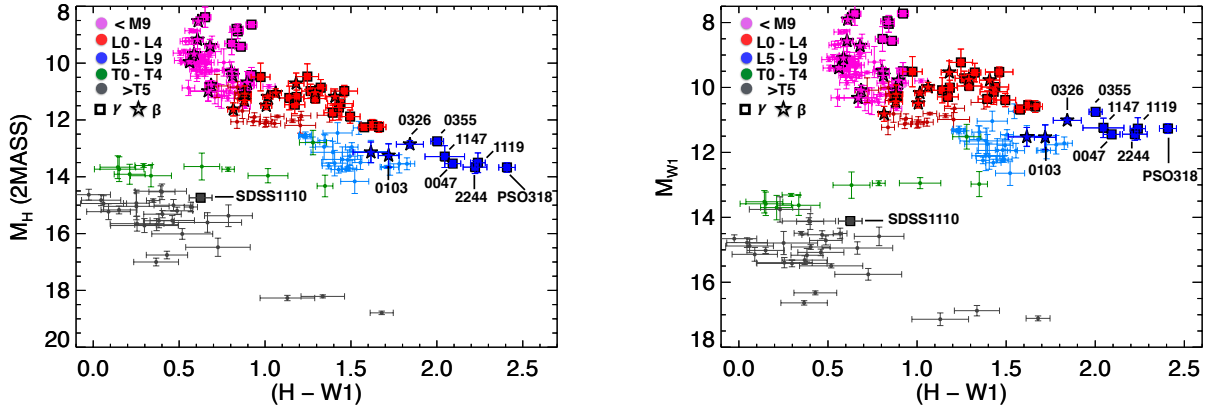


**Figure 27.** The  $(H - W_1)$  versus  $M_H$  (left) and  $M_{W_1}$  (right) color magnitude diagram. Symbols are as described in Figure 21.

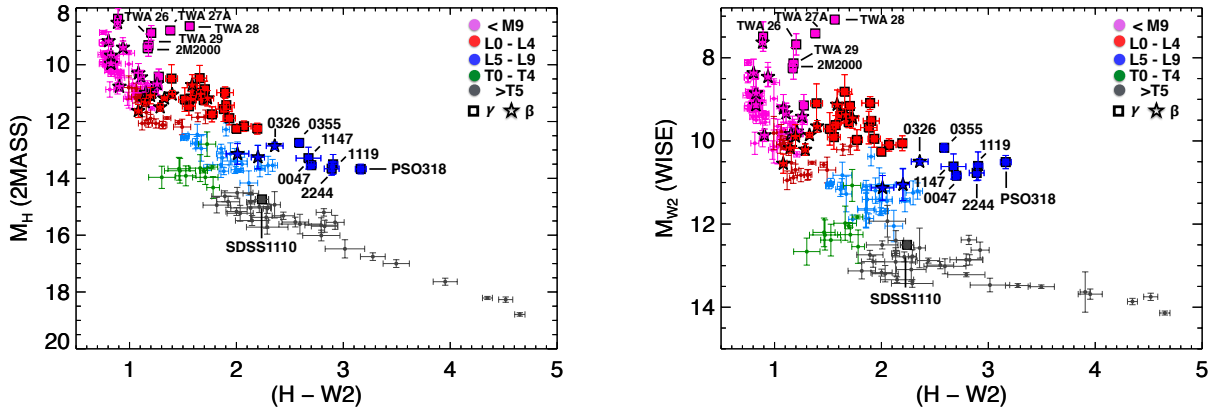


**Figure 28.** The  $(H - W_2)$  versus  $M_H$  (left) and  $M_{W_2}$  (right) color magnitude diagram. Symbols are as described in Figure 21.

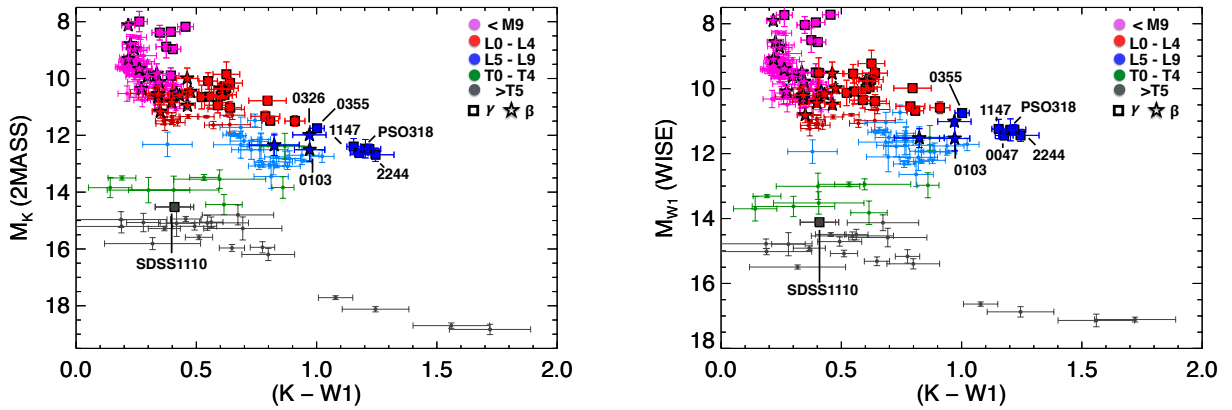


**Figure 29.** The  $(K - W_1)$  versus  $M_K$  (left) and  $M_{W_1}$  (right) color magnitude diagram. Symbols are as described in Figure 21.



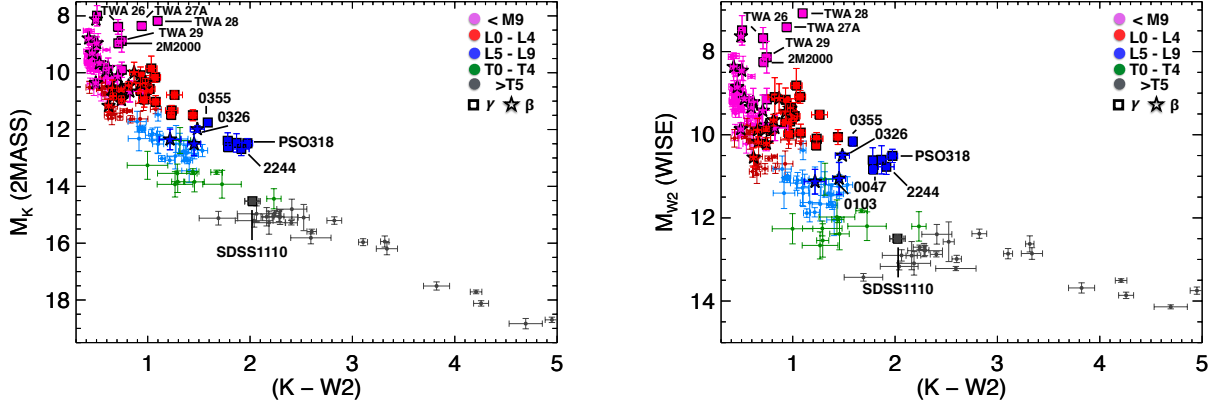


**Figure 30.** The  $(K-W2)$  versus  $M_K$  (left) and  $M_{W2}$  (right) color magnitude diagram. Symbols are as described in Figure 21.

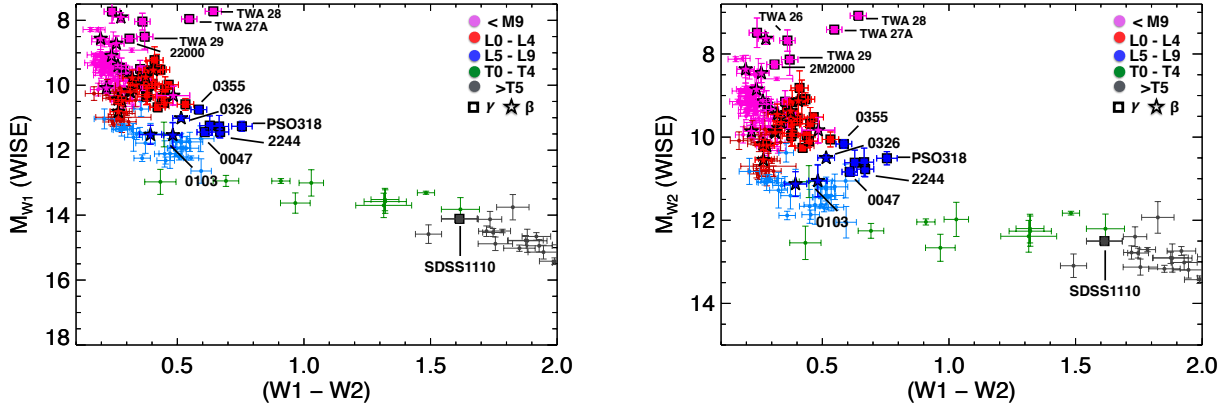


**Figure 31.** The  $(W1-W2)$  versus  $M_{W1}$  (left) and  $M_{W2}$  (right) color magnitude diagram. Symbols are as described in Figure 21.

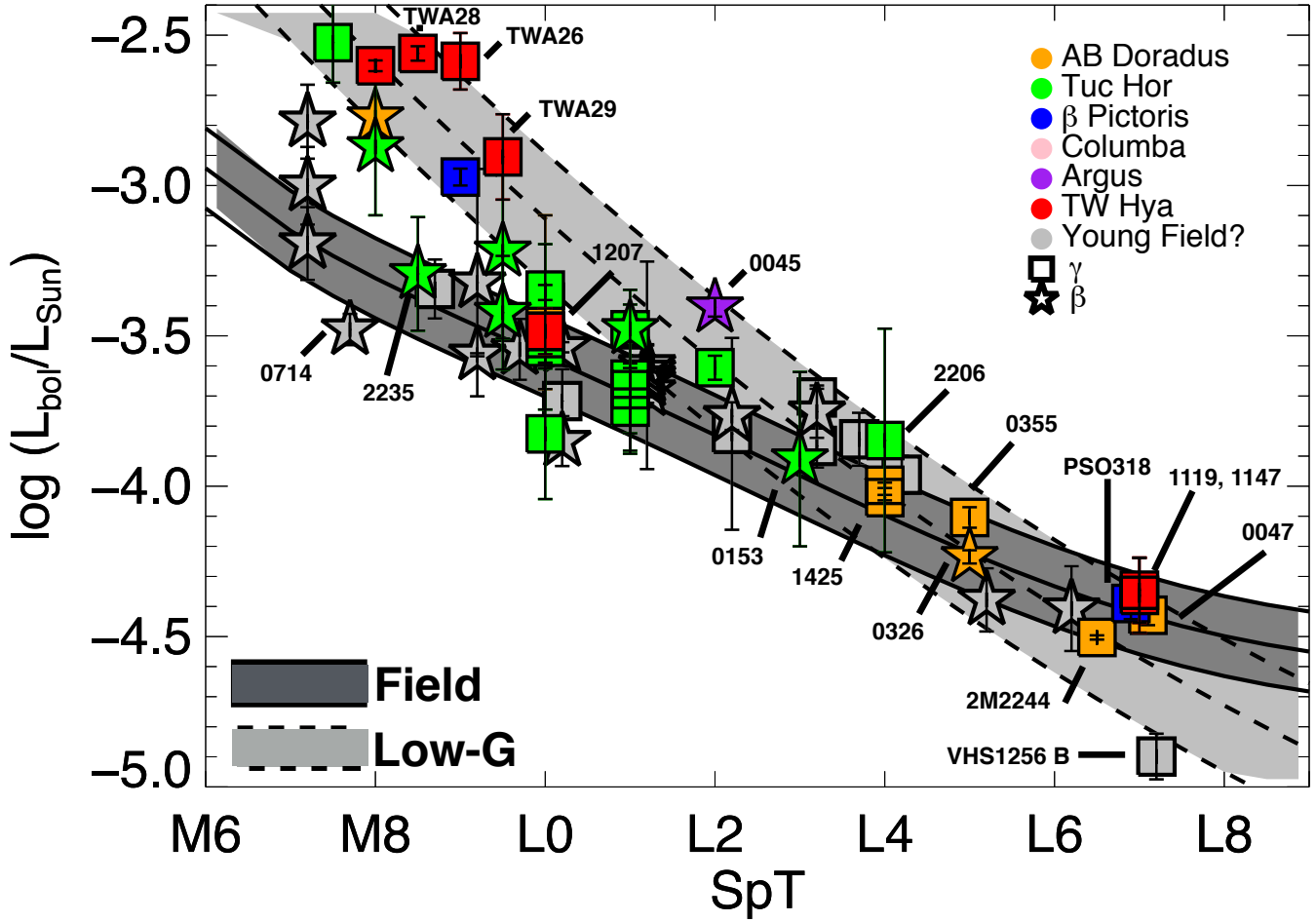


**Figure 32.** The spectral type versus bolometric luminosity plot. The field polynomial and residuals from Filippazzo et al. (2015) is represented by the grey area. Over-plotted are objects in this work with measured parallaxes or estimated kinematic distances from high confidence group membership.  $L_{bol}$  values were calculated as described in Filippazzo et al. (2015). Symbols distinguish very low ( $\gamma$ ) from intermediate ( $\beta$ ) gravity sources. Objects are color coded by group membership.

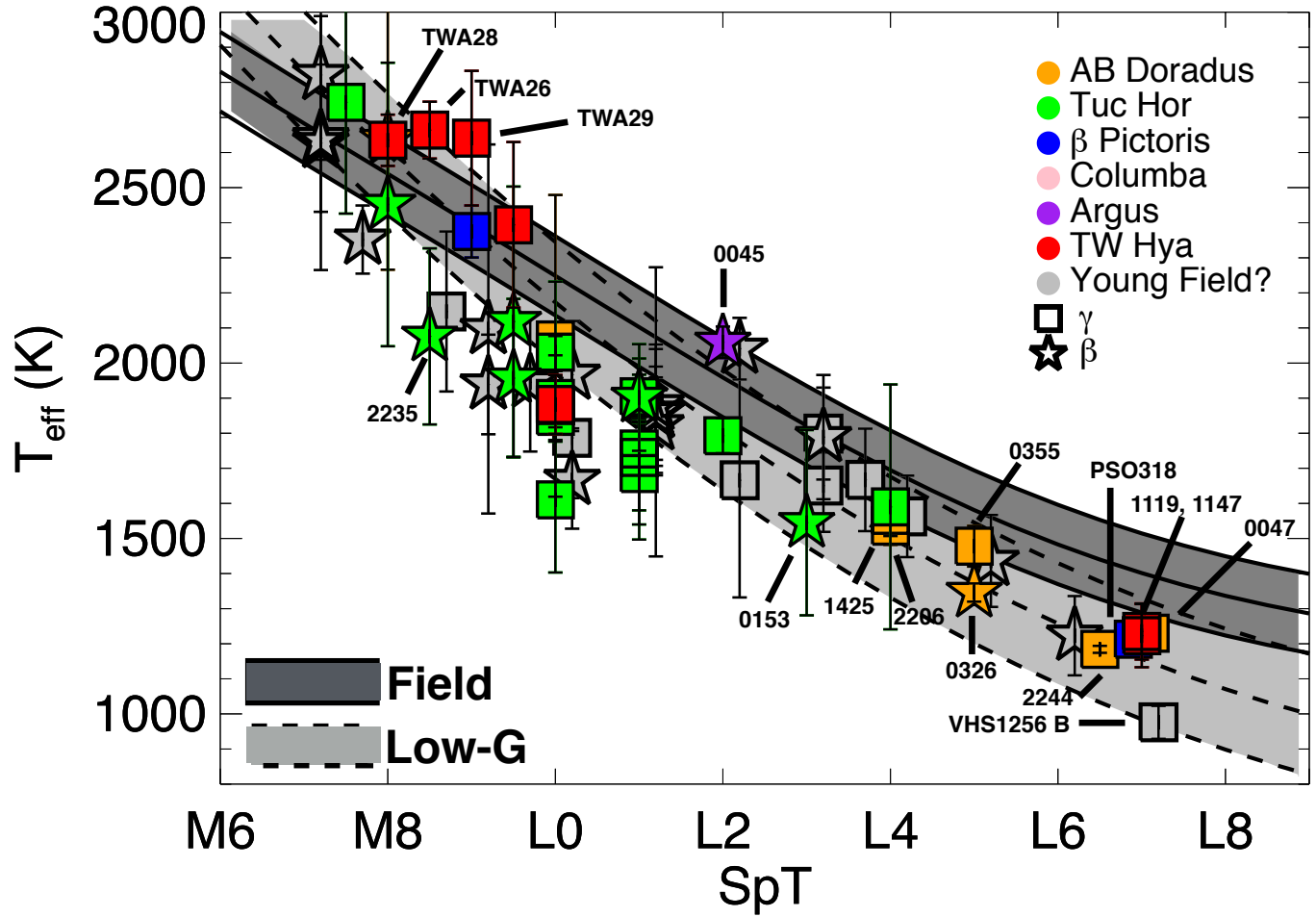


**Figure 33.** The spectral type versus  $T_{\text{eff}}$  plot. Symbols are as described in Figure 32.

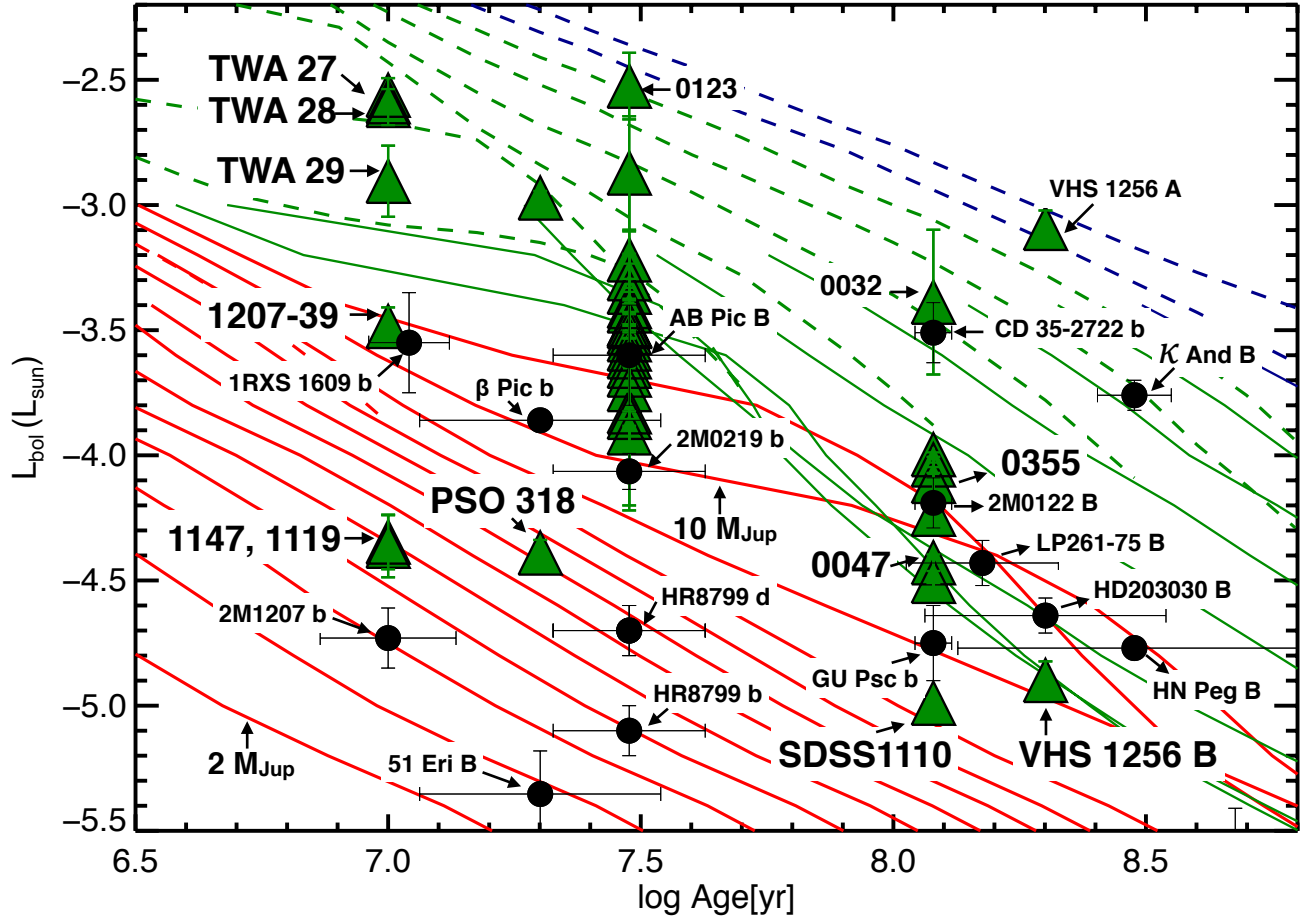


**Figure 34.** The age versus bolometric luminosity plot with model isochrone tracks at constant mass from Saumon & Marley (2008) (solid lines) and Baraffe et al. (2015) (dashed lines). We have color coded  $< 13 M_{Jup}$  tracks in red,  $13 M_{Jup} < M < 75 M_{Jup}$  tracks in green and  $> 75 M_{Jup}$  blue. Over-plotted are both the young brown dwarfs discussed in this work and directly imaged exoplanets with measured quantities.

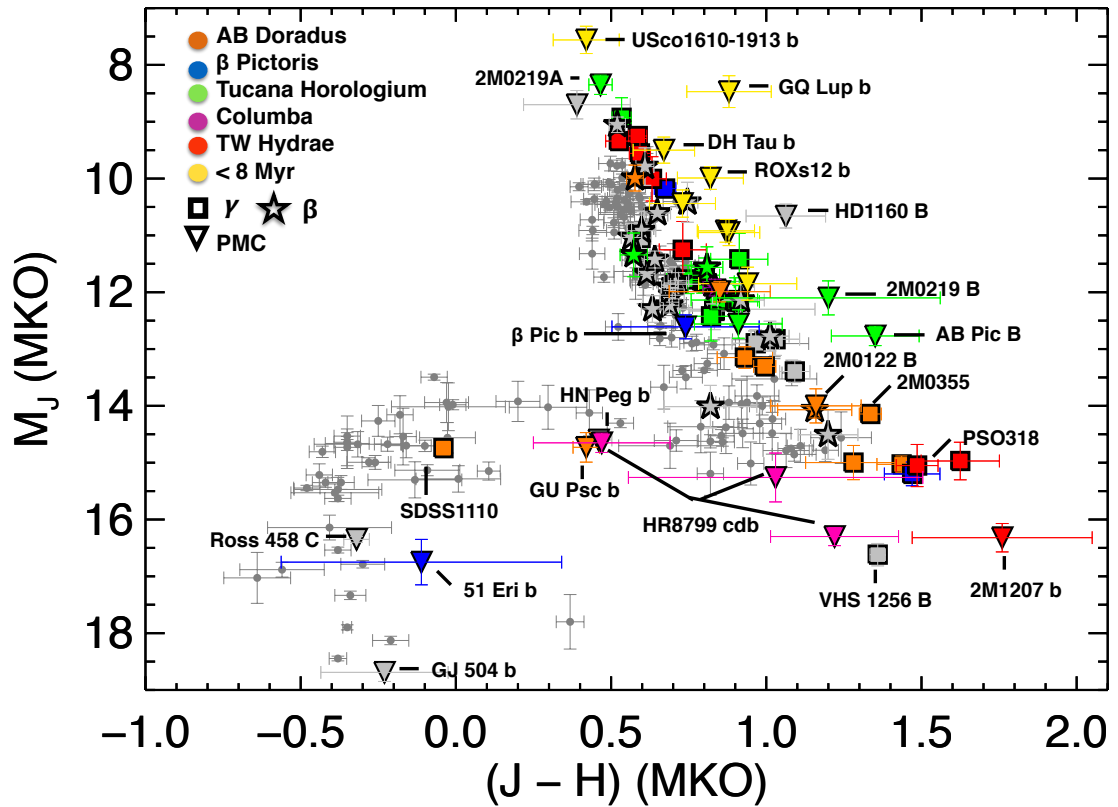


**Figure 35.** The  $(J-H)$  versus  $M_J$  color magnitude diagram for brown dwarfs and directly imaged planetary mass companions. All photometry is on the MKO system. For the brown dwarfs lacking MKO L' photometry, WISE W1 mags were converted using a polynomial listed in Table 19. Objects have been color coded by nearby moving group membership and those of interest discussed in detail within the text have been labeled.

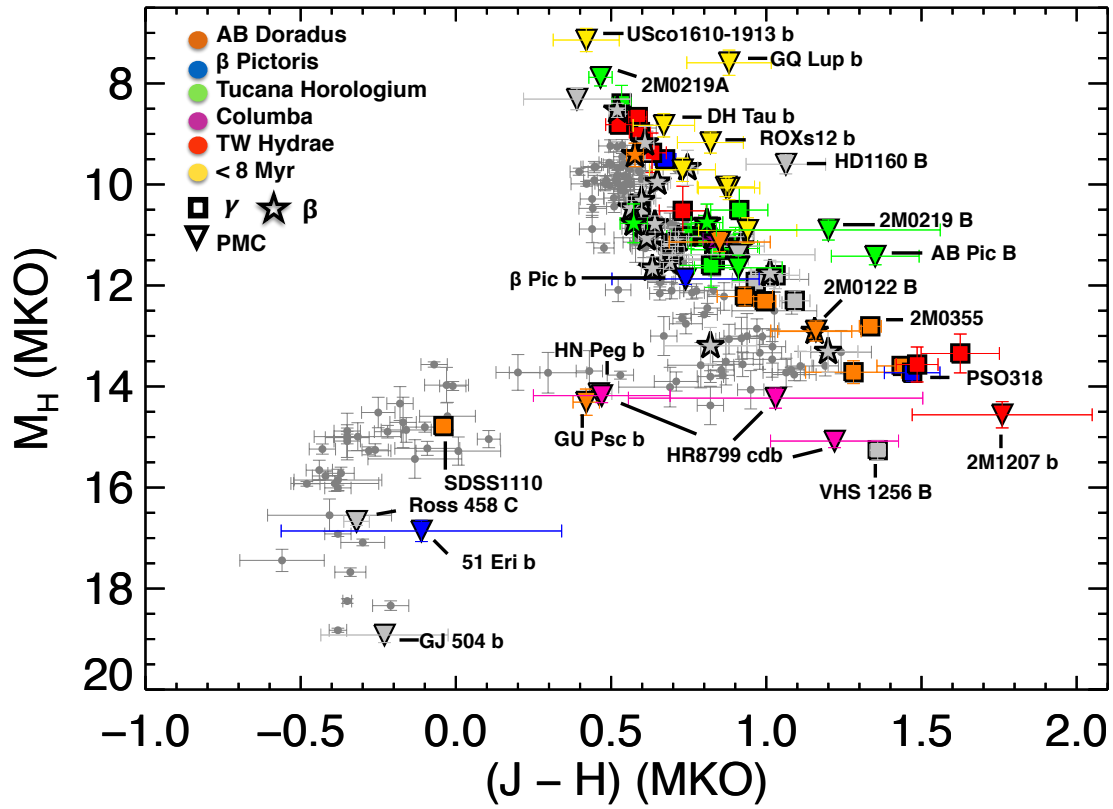


**Figure 36.** The  $(J-H)$  versus  $M_H$  (right) color magnitude diagram for brown dwarfs and directly imaged planetary mass companions. Symbols are as described in Figure 35.

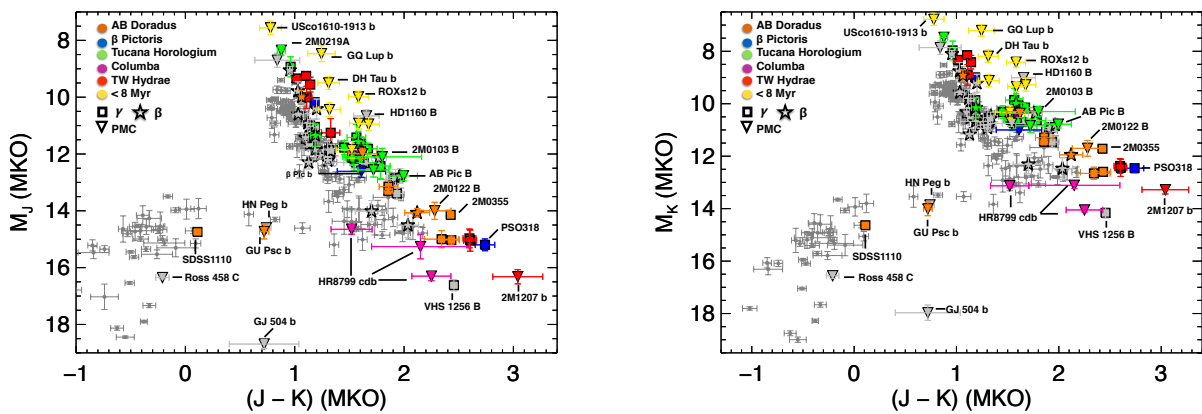


**Figure 37.** The  $(J-K)$  versus  $M_J$  (left) and  $M_K$  (right) color magnitude diagram for brown dwarfs and directly imaged planetary mass companions. Symbols are as described in Figure 35.

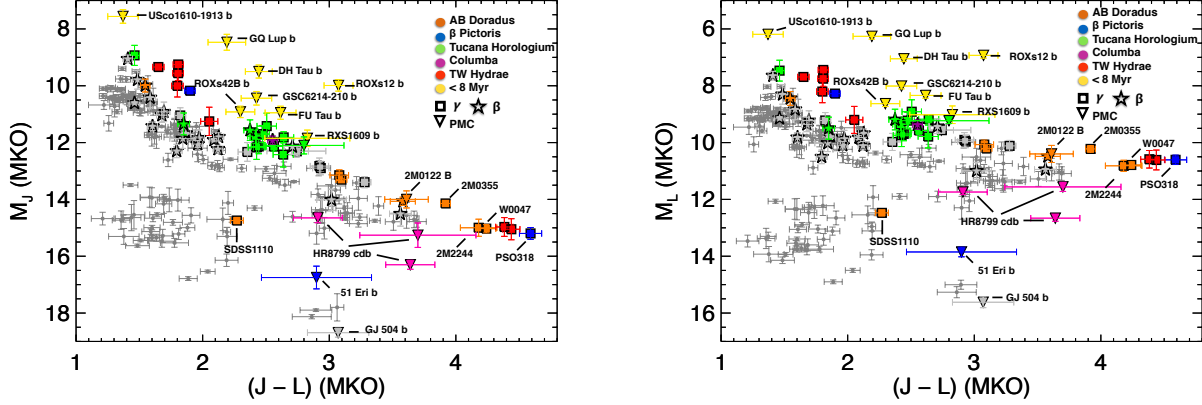


**Figure 38.** The  $(J-L)$  versus  $M_J$  (left) and  $M_L$  (right) color magnitude diagram for brown dwarfs and directly imaged planetary mass companions. Symbols are as described in Figure 35.

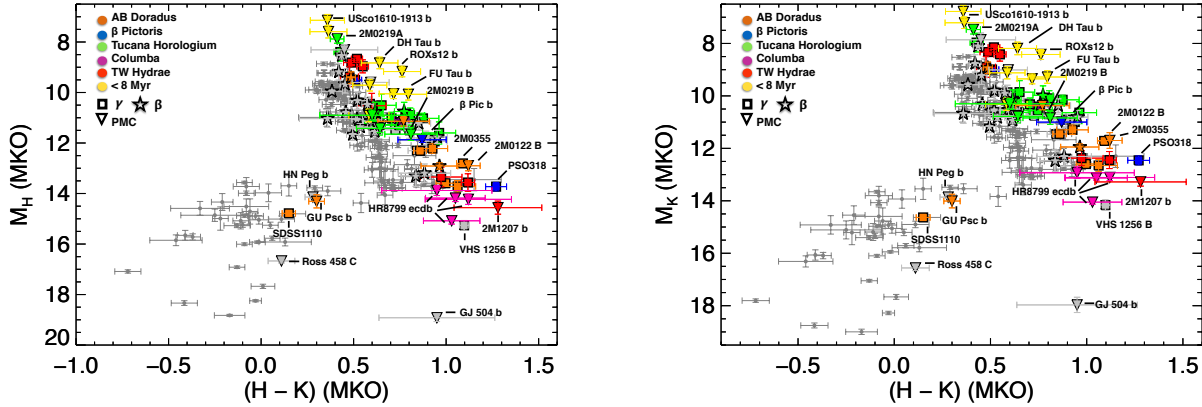


**Figure 39.** The  $(H-K)$  versus  $M_H$  (left) and  $M_K$  (right) color magnitude diagram for brown dwarfs and directly imaged planetary mass companions. Symbols are as described in Figure 35.

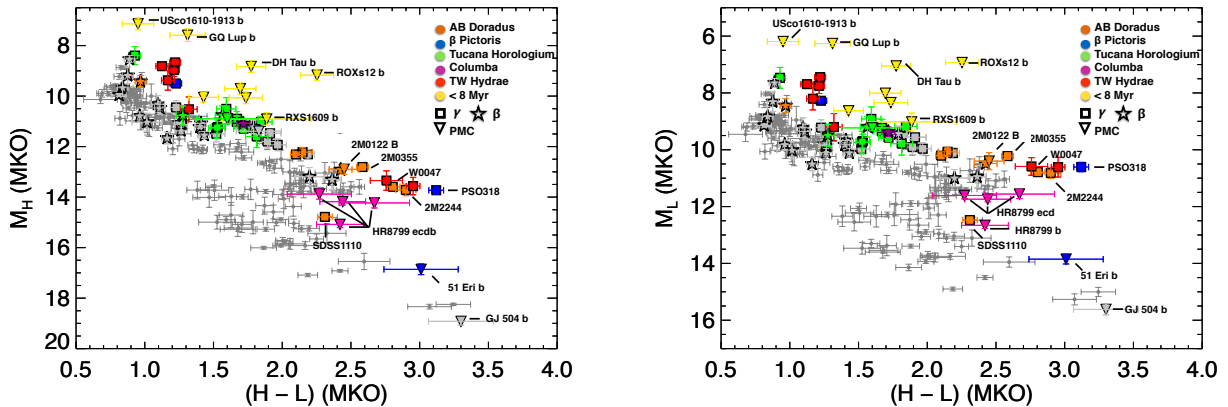


**Figure 40.** The  $(H-L)$  versus  $M_H$  (left) and  $M_L$  (right) color magnitude diagram for brown dwarfs and directly imaged planetary mass companions. Symbols are as described in Figure 35.

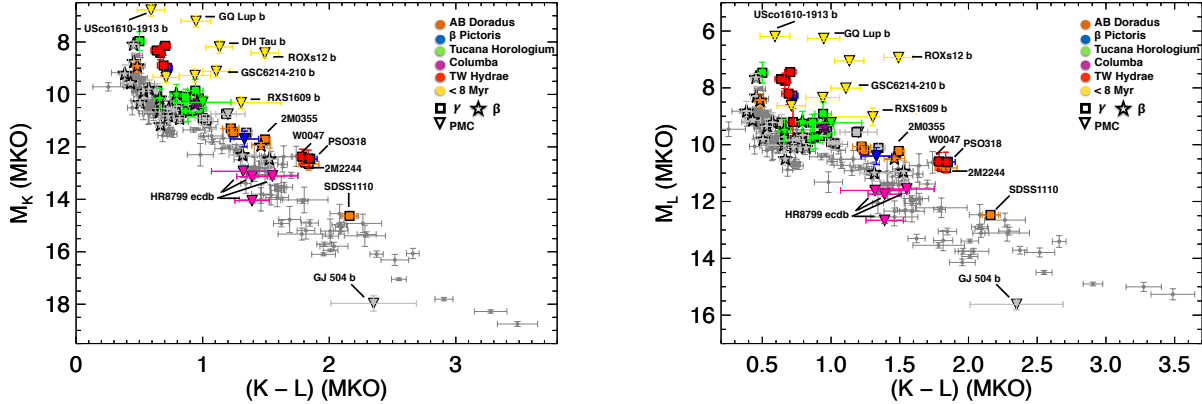


**Figure 41.** The  $(K-L)$  versus  $M_K$  (left) and  $M_L$  (right) color magnitude diagram for brown dwarfs and directly imaged planetary mass companions. Symbols are as described in Figure 35.

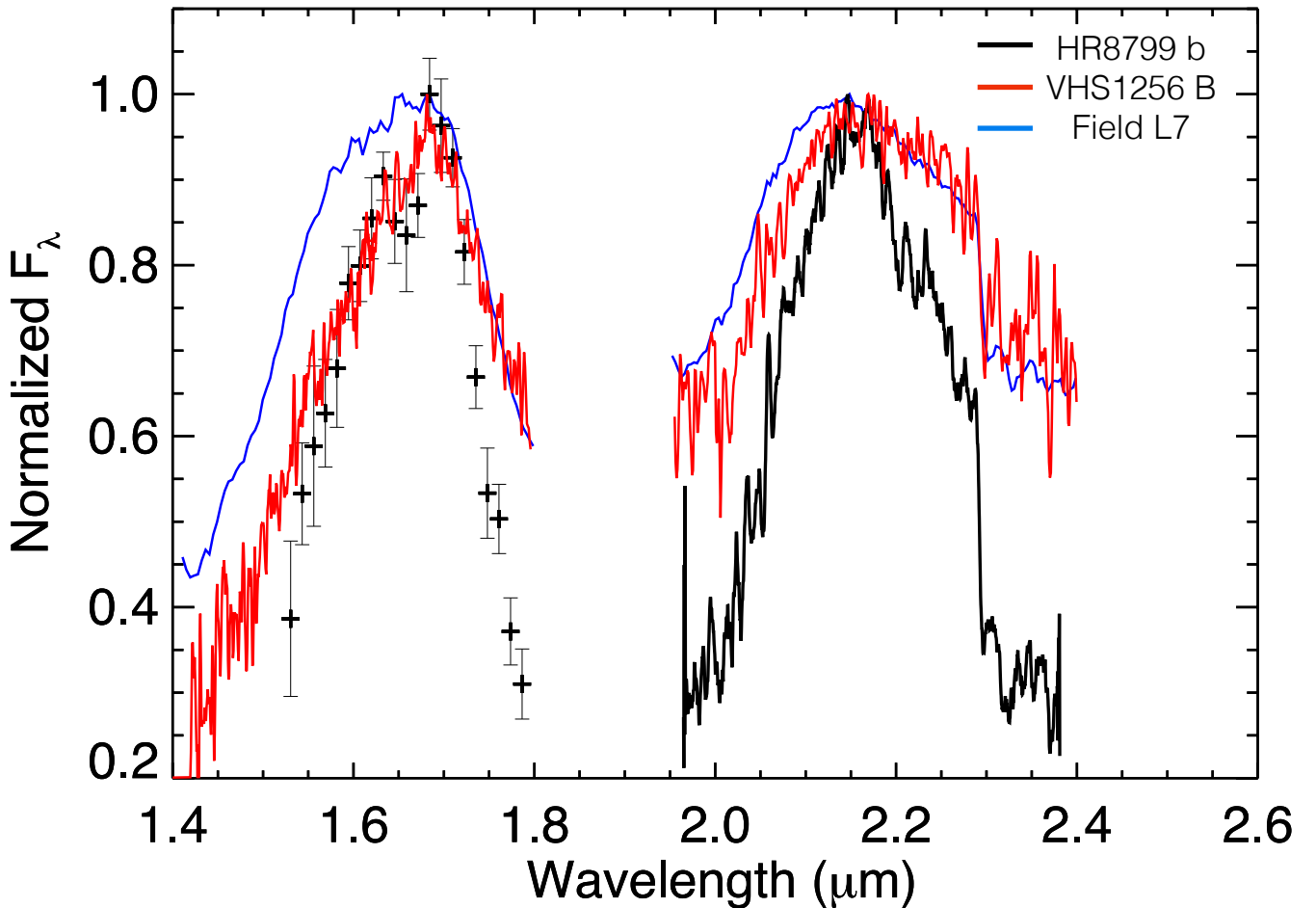


**Figure 42.** The near-infrared spectrum comparison of HR8799 b (black, from Oppenheimer et al. 2013, Barman et al. 2011a), VHS 1256 B (red, from Gauza et al. 2015), and a field L7 (Gagné et al. (2015b)).

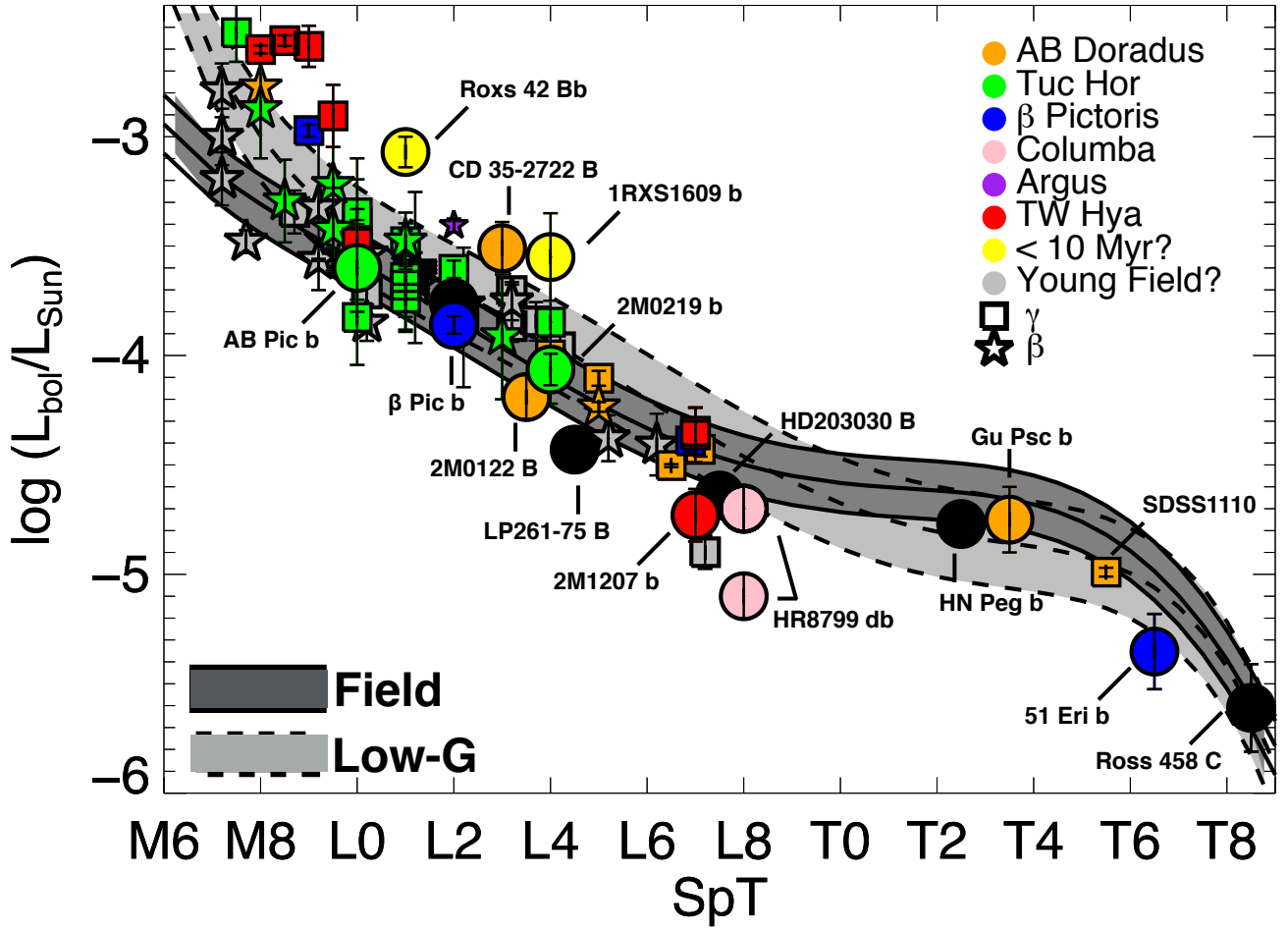


**Figure 43.** The spectral type versus bolometric luminosity plot for brown dwarfs and directly imaged planets.  $L_{bol}$  values and spectral types for planets have been taken from the literature with the exception of HR8799bd and 2M1207b which we delegate as L8 objects to represent their nature as late-type objects. Symbols are as in Figure 32.

**Table 1**  
Photometric Properties of Low Surface Gravity Dwarfs

2MASS Designation	SpT OpT (2)	SpT IR (3)	J 2MASS (4)	H 2MASS (5)	K 2MASS (6)	W1 WISE (7)	W2 WISE (8)	W3 WISE (9)	W4 WISE (10)	Ref (11)	
00011217+1535355	--	L4 $\beta$	15.522 ± 0.061	14.505 ± 0.052	13.71 ± 0.043	12.938 ± 0.023	12.517 ± 0.026	11.498 ± 0.177	8.953 ± -	5	
00040288-6410358	L1 $\gamma$	L1 $\gamma^a$	15.786 ± 0.071	14.831 ± 0.073	14.010 ± 0.045	13.370 ± 0.025	12.937 ± 0.027	12.178 ± 0.244	9.161 ± -	15, 27	
00182834-6703130	--	L0 $\gamma$	15.457 ± 0.057	14.48 ± 0.061	13.711 ± 0.039	13.171 ± 0.025	12.768 ± 0.026	12.763 ± 0.445	9.046 ± -	5	
00191296-6226005	--	L1 $\gamma$	15.64 ± 0.06	14.618 ± 0.054	13.957 ± 0.051	13.351 ± 0.025	12.883 ± 0.026	12.378 ± 0.262	9.114 ± -	5	
00192626+4614078	M8 -	M8 $\beta$	12.603 ± 0.017	11.940 ± 0.021	11.502 ± 0.011	11.260 ± 0.023	11.001 ± 0.020	10.857 ± 0.070	9.401 ± -	7, 5	
00274197+0503417	M9.5 $\beta$	L0 $\beta^a$	16.189 ± 0.092	15.288 ± 0.099	14.960 ± 0.115	14.619 ± 0.036	14.135 ± 0.054	12.239 ± -	8.890 ± -	6, 27, 36	
00303013-1450333	L7 -	L4-L6 $\beta$	16.278 ± 0.112	15.273 ± 0.1	14.481 ± 0.1	13.657 ± 0.028	12.263 ± 0.034	12.275 ± -	9.149 ± -	18, 5	
00325584-4405058	L0 $\gamma$	L0 $\beta$	14.776 ± 0.32	13.857 ± 0.32	13.270 ± 0.35	12.820 ± 0.025	12.490 ± 0.025	11.726 ± 0.187	9.289 ± -	2, 6, 27	
003323.86-152130	L4 $\beta$	L1 $\beta$	15.286 ± 0.056	14.208 ± 0.051	13.410 ± 0.039	12.801 ± 0.025	12.479 ± 0.027	11.888 ± 0.247	8.879 ± -	2, 6, 27	
00344300-4102266	--	L1 $\beta$	15.707 ± 0.066	14.807 ± 0.064	14.084 ± 0.056	13.498 ± 0.026	13.098 ± 0.03	12.596 ± 0.394	9.285 ± -	5	
00374306-5846229	L0 $\gamma$	--	15.374 ± 0.050	14.259 ± 0.051	13.590 ± 0.044	13.125 ± 0.026	12.928 ± 0.027	12.557 ± 0.380	9.324 ± -	2	
00381489-6403529	--	M9.5 $\beta$	14.523 ± 0.03	13.867 ± 0.045	13.395 ± 0.033	12.904 ± 0.024	12.539 ± 0.024	11.746 ± 0.175	9.374 ± -	5	
00425923+1142104	--	M9 $\beta$	14.754 ± 0.036	14.074 ± 0.042	13.514 ± 0.027	13.237 ± 0.026	12.918 ± 0.03	12.175 ± -	9.151 ± -	5	
00452143+1634446	L2 $\beta$	L2 $\gamma^a$	13.059 ± 0.018	12.059 ± 0.034	11.370 ± 0.019	10.768 ± 0.023	10.393 ± 0.019	9.735 ± 0.040	8.424 ± 0.261	2, 6, 27	
00461841+0715177	M9 $\beta$	L0 $\delta$	13.885 ± 0.036	13.178 ± 0.034	12.550 ± 0.025	11.709 ± 0.026	11.139 ± 0.022	11.024 ± 0.181	9.024 ± -	1, 5, 27	
00470038+6803543	L7 ( $\gamma?$ )	L6-L8 $\gamma$	15.604 ± 0.068	13.968 ± 0.041	13.053 ± 0.029	11.876 ± 0.023	11.268 ± 0.020	10.327 ± 0.072	9.095 ± 0.453	34, 35	
00550664+0134365	L2 $\gamma$	L2 $\gamma^a$	16.436 ± 0.114	15.270 ± 0.074	14.440 ± 0.068	13.682 ± 0.027	13.204 ± 0.033	11.988 ± -	8.477 ± -	27, 36	
00584253-0651239	L0 -	L1 $\beta$	14.311 ± 0.023	13.444 ± 0.028	12.904 ± 0.032	12.562 ± 0.025	12.248 ± 0.027	11.692 ± 0.411	8.739 ± -	18, 5	
01033203+1935361	L6 $\beta$	L6 $\beta$	16.288 ± 0.079	14.897 ± 0.055	14.149 ± 0.058	13.178 ± 0.024	12.696 ± 0.027	12.334 ± 0.325	8.290 ± -	8, 5	
01174748-3403258	L1 $\beta$	L1 $\beta^a$	15.178 ± 0.034	14.209 ± 0.038	13.490 ± 0.036	13.028 ± 0.025	12.623 ± 0.026	11.802 ± 0.186	9.215 ± -	7, 6, 27	
01205114-5203349	--	L1 $\gamma$	15.642 ± 0.071	14.66 ± 0.072	13.752 ± 0.053	13.23 ± 0.026	12.778 ± 0.026	11.847 ± 0.168	8.949 ± -	5	
01231125-6921379	M7.5 $\gamma$	--	12.320 ± 0.019	11.711 ± 0.024	11.323 ± 0.024	11.060 ± 0.023	10.818 ± 0.021	10.595 ± 0.062	9.426 ± -	4	
01244599-5745379	L0 $\gamma$	--	16.308 ± 0.104	15.059 ± 0.088	14.320 ± 0.088	13.773 ± 0.026	13.342 ± 0.032	12.449 ± 0.313	8.908 ± -	2, 27	
01262109+1428057	L4 $\gamma$	L2 $\gamma$	16.172 ± 0.214	16.172 ± 0.218	15.280 ± 0.145	14.237 ± 0.029	13.702 ± 0.037	12.379 ± -	9.127 ± -	21, 6	
01294256-0822550	M5 -	M7 $\beta$	10.655 ± 0.021	10.085 ± 0.023	9.771 ± 0.023	9.545 ± 0.022	9.327 ± 0.02	9.206 ± 0.032	8.891 ± 0.458	17, 5	
01415823-4633574	L0 $\gamma$	--	14.832 ± 0.041	13.875 ± 0.024	13.100 ± 0.030	12.551 ± 0.024	12.170 ± 0.022	11.921 ± 0.212	9.243 ± -	2, 6, 28	
01531463-6744181	L2 -	L3 $\beta$	16.412 ± 0.134	15.109 ± 0.086	14.424 ± 0.103	13.713 ± 0.026	12.514 ± 0.028	12.514 ± 0.28	9.335 ± -	1, 5	
02103857-3015313	L0 $\gamma$	--	15.066 ± 0.047	14.161 ± 0.050	13.500 ± 0.042	13.003 ± 0.026	12.652 ± 0.026	11.934 ± 0.195	9.355 ± -	5, 27	
02212859-6831400	M8 $\beta$	--	13.965 ± 0.033	13.275 ± 0.032	12.806 ± 0.037	12.471 ± 0.024	12.192 ± 0.023	11.604 ± 0.107	9.614 ± -	27	
02215494-5412054	M9 $\beta$	--	13.902 ± 0.031	13.221 ± 0.031	12.670 ± 0.030	12.325 ± 0.024	11.963 ± 0.022	11.440 ± 0.122	9.481 ± -	1, 13, 27	
02253464-5815067	L0 $\gamma$	--	15.070 ± 0.048	14.003 ± 0.036	13.420 ± 0.042	12.819 ± 0.024	12.431 ± 0.024	11.644 ± 0.154	9.466 ± -	2	
02251947-5837295	M9 $\beta$	M9 $\gamma^a$	13.738 ± 0.025	13.058 ± 0.025	12.560 ± 0.026	12.234 ± 0.024	11.926 ± 0.023	11.994 ± 0.190	9.218 ± -	27, 36	
02265658-5327032	--	L0 $\delta$	15.403 ± 0.044	14.346 ± 0.045	13.752 ± 0.045	13.219 ± 0.025	12.783 ± 0.026	11.58 ± 0.14	8.64 ± 0.256	5	
02292794-0053282	--	L0 $\gamma$	16.490 ± 0.099	15.746 ± 0.099	15.182 ± 0.138	14.720 ± 0.032	14.328 ± 0.045	12.679 ± -	8.724 ± -	6	
02340093-6442068	L0 $\gamma$	--	15.325 ± 0.062	14.442 ± 0.055	13.850 ± 0.069	13.247 ± 0.025	12.905 ± 0.026	12.619 ± 0.279	9.494 ± -	5	
02410564-5511466	--	L1 $\gamma$	15.387 ± 0.057	14.326 ± 0.058	13.739 ± 0.038	13.185 ± 0.025	12.809 ± 0.026	12.249 ± 0.242	9.349 ± -	5	
02411151-0326587	L0 $\gamma$	--	15.799 ± 0.064	14.811 ± 0.053	14.040 ± 0.049	13.638 ± 0.025	13.256 ± 0.026	12.766 ± 0.415	9.000 ± -	14, 6	
02501167-0151295 <sup>f</sup>	--	M7 $\beta$	12.886 ± 0.026	12.278 ± 0.021	11.909 ± 0.017	11.691 ± 0.023	11.451 ± 0.022	11.035 ± 0.158	8.827 ± -	5	
02530084+1652532 <sup>d</sup>	M6.5 -	M7 $\beta^d$	8.394 ± 0.021	7.883 ± 0.037	7.585 ± 0.043	7.322 ± 0.027	7.057 ± 0.02	6.897 ± 0.017	6.718 ± 0.076	20, 25, 5	
02535980+3206373	M7 $\beta$	--	13.616 ± 0.021	12.931 ± 0.020	12.550 ± 0.023	12.324 ± 0.025	12.077 ± 0.024	11.808 ± 0.250	8.930 ± -	27, 36	
02583123-1520536	--	L3 $\beta$	15.908 ± 0.072	14.866 ± 0.06	14.192 ± 0.055	13.623 ± 0.025	13.194 ± 0.028	12.578 ± 0.305	9.542 ± -	5	
03032042-7312300	--	--	16.137 ± 0.107	15.096 ± 0.085	14.320 ± 0.084	13.777 ± 0.025	13.350 ± 0.026	12.288 ± 0.167	9.344 ± 0.341	15	
03164512-2848521	L0 -	--	14.578 ± 0.039	13.772 ± 0.035	13.114 ± 0.035	12.649 ± 0.023	12.312 ± 0.023	11.743 ± 0.125	9.364 ± -	7, 5	
03231002-4631237	L0 $\gamma$	--	15.854 ± 0.069	15.386 ± 0.086	14.541 ± 0.089	13.955 ± 0.025	13.482 ± 0.032	12.994 ± 0.025	12.193 ± 0.160	9.180 ± -	5, 27
03264235-2102057	L5 $\beta$	--	16.134 ± 0.093	14.793 ± 0.075	13.920 ± 0.065	12.950 ± 0.024	12.435 ± 0.023	12.173 ± 0.203	9.663 ± -	5, 27	
03350208+2342356	M8.5 -	M7.5 $\beta$	12.250 ± 0.017	11.655 ± 0.020	11.261 ± 0.014	11.044 ± 0.023	10.767 ± 0.020	10.762 ± 0.130	8.932 ± -	12, 6	
03393521-3525440	M9 $\beta$	--	10.725 ± 0.018	10.017 ± 0.020	9.550 ± 0.021	9.133 ± 0.022	8.808 ± 0.019	8.272 ± 0.017	7.997 ± 0.110	12, 6, 27	
03420931-2904317	L0 $\beta$	--	15.918 ± 0.085	15.353 ± 0.106	14.378 ± 0.085	13.777 ± 0.027	13.54 ± 0.032	12.673 ± -	9.237 ± -	5	
03421621-6817321	L4 $\gamma$	--	16.854 ± 0.138	15.386 ± 0.086	14.541 ± 0.089	13.955 ± 0.025	13.482 ± 0.032	12.994 ± 0.025	9.723 ± -	5	
03550477-1032415	M8.5 $\beta$	--	13.08 ± 0.025	12.462 ± 0.024	11.975 ± 0.023	11.712 ± 0.024	11.425 ± 0.022	10.865 ± 0.095	8.627 ± 0.309	5, 36	
03552337+1133437	L5 $\gamma$	--	14.050 ± 0.020	12.530 ± 0.029	11.530 ± 0.019	10.528 ± 0.023	9.943 ± 0.021	9.294 ± 0.038	8.317 ± -	2, 5, 21	
03572695-4417305	L0 $\beta$	--	14.367 ± 0.029	13.531 ± 0.025	12.910 ± 0.026	12.475 ± 0.023	12.086 ± 0.021	11.600 ± 0.084	9.318 ± -	14, 27	
04062677-3812102	L0 $\gamma$	--	16.768 ± 0.126	15.711 ± 0.101	15.110 ± 0.116	14.449 ± 0.030	14.100 ± 0.041	12.520 ± -	9.097 ± -	15, 6	
04185879-4507413	--	L3 $\gamma$	16.163 ± 0.084	15.046 ± 0.074	14.595 ± 0.088	13.864 ± 0.027	13.455 ± 0.03	12.783 ± -	9.642 ± -	5	
04210718-6306022	L5 $\beta$	--	15.565 ± 0.048	14.284 ± 0.040	13.450 ± 0.022	12.558 ± 0.022	12.135 ± 0.021	11.598 ± 0.095	9.245 ± -	2, 27	
04351455-1414468	M8 $\gamma$	--	11.879 ± 0.029	10.622 ± 0.027	9.951 ± 0.021	9.711 ± 0.024	9.268 ± 0.021	9.136 ± 0.034	8.514 ± 0.310	27, 36	



Table 1 — *Continued*

2MASS Designation	SpT OpT (2)	SpT IR (3)	J 2MASS (4)	H 2MASS (5)	K 2MASS (6)	W1 WISE (7)	W2 WISE (8)	W3 WISE (9)	W4 WISE (10)	Ref <sup>e</sup> (11)
17111353+2326333	L0 $\gamma$	L1 $\beta^a$	14.499 $\pm$ 0.024	13.668 $\pm$ 0.030	13.060 $\pm$ 0.026	12.581 $\pm$ 0.024	12.226 $\pm$ 0.024	11.662 $\pm$ 0.152	9.334 $\pm$ –	3, 6, 27
17260007+1538190	L3.5 $\gamma$	L3 $\gamma^a$	15.669 $\pm$ 0.063	14.465 $\pm$ 0.045	13.660 $\pm$ 0.049	13.071 $\pm$ 0.025	12.694 $\pm$ 0.026	11.556 $\pm$ 0.157	9.309 $\pm$ –	5, 27
17410280+4612218	—	L6-L8 $\gamma^a$	15.734 $\pm$ 0.075	14.438 $\pm$ 0.054	12.396 $\pm$ 0.021	12.301 $\pm$ 0.025	11.475 $\pm$ 0.023	11.432 $\pm$ 0.190	8.541 $\pm$ –	5, 27
18212815+1414010	L4.5 —	L4 $\rho^a$	13.431 $\pm$ 0.021	12.396 $\pm$ 0.017	11.650 $\pm$ 0.019	10.853 $\pm$ 0.023	10.475 $\pm$ 0.020	9.928 $\pm$ 0.052	9.067 $\pm$ 0.534	27, 29, 30
19350976+6200473	—	L1 $\gamma$	16.254 $\pm$ 0.105	15.293 $\pm$ 0.094	14.724 $\pm$ 0.098	14.059 $\pm$ 0.029	13.65 $\pm$ 0.039	12.881 $\pm$ –	8.559 $\pm$ –	5
19355595-2846343	M9 $\gamma$	M9 $\gamma^a$	13.953 $\pm$ 0.024	13.180 $\pm$ 0.020	12.710 $\pm$ 0.028	12.347 $\pm$ 0.026	11.910 $\pm$ 0.025	10.519 $\pm$ 0.076	8.636 $\pm$ –	27, 36
19564700+7542270	L0 $\gamma$	L2 $\gamma^a$	16.154 $\pm$ 0.102	15.036 $\pm$ 0.096	14.230 $\pm$ 0.066	13.693 $\pm$ 0.027	13.249 $\pm$ 0.031	12.678 $\pm$ –	9.171 $\pm$ –	2, 27
20004841-7523070	M9 $\gamma$	M9 $\gamma^a$	12.734 $\pm$ 0.023	11.967 $\pm$ 0.026	11.510 $\pm$ 0.024	11.108 $\pm$ 0.023	10.797 $\pm$ 0.020	10.550 $\pm$ 0.069	8.548 $\pm$ –	4, 5, 27
20025073-0521524	L5 $\beta$	L5-L7 $\gamma^a$	15.316 $\pm$ 0.049	14.278 $\pm$ 0.035	13.420 $\pm$ 0.035	12.532 $\pm$ 0.023	12.090 $\pm$ 0.026	11.441 $\pm$ 0.209	8.818 $\pm$ –	3, 5, 27
20113196-5048112	—	L3 $\gamma$	16.423 $\pm$ 0.109	15.257 $\pm$ 0.081	14.577 $\pm$ 0.082	14.009 $\pm$ 0.031	13.668 $\pm$ 0.038	12.431 $\pm$ –	9.084 $\pm$ –	5
20135152-2806020	M9 $\gamma$	M9 $\gamma^a$	14.242 $\pm$ 0.028	13.461 $\pm$ 0.027	12.940 $\pm$ 0.026	12.525 $\pm$ 0.028	12.163 $\pm$ 0.027	11.877 $\pm$ 0.276	8.663 $\pm$ –	1, 6, 27
20282203-5637024	—	M8.5 $\gamma$	13.837 $\pm$ 0.021	13.243 $\pm$ 0.021	12.71 $\pm$ 0.027	12.472 $\pm$ 0.022	12.173 $\pm$ 0.024	12.298 $\pm$ 0.315	8.669 $\pm$ –	5
20334473-5635338	—	L0 $\gamma$	15.718 $\pm$ 0.088	15.137 $\pm$ 0.109	14.244 $\pm$ 0.081	13.817 $\pm$ 0.027	13.415 $\pm$ 0.034	12.376 $\pm$ –	9.27 $\pm$ –	5
20391314-1126531	M8 —	M7 $\beta$	13.792 $\pm$ 0.024	13.129 $\pm$ 0.038	12.68 $\pm$ 0.028	12.465 $\pm$ 0.023	12.166 $\pm$ 0.024	12.596 $\pm$ 0.538	9.04 $\pm$ –	7, 5
20575409-0252302	L1.5 —	L2 $\beta$	13.121 $\pm$ 0.021	12.268 $\pm$ 0.022	11.724 $\pm$ 0.023	11.261 $\pm$ 0.022	10.981 $\pm$ 0.020	10.431 $\pm$ 0.079	8.906 $\pm$ –	7, 25, 27
21140802-2251358 <sup>b,c</sup>	—	L6-L8 $\gamma^a$	17.294 $\pm$ 0.08	15.624 $\pm$ 0.045	14.435 $\pm$ 0.04	13.216 $\pm$ 0.026	12.461 $\pm$ 0.031	11.838 $\pm$ 0.358	8.581 $\pm$ –	9, 27
21265040-8140293	L3 $\gamma$	L3 $\gamma^a$	15.542 $\pm$ 0.055	14.405 $\pm$ 0.053	13.550 $\pm$ 0.041	12.910 $\pm$ 0.024	12.472 $\pm$ 0.023	11.885 $\pm$ 0.161	9.357 $\pm$ –	2, 27
21324036+1029494	—	L4 $\beta$	16.594 $\pm$ 0.138	15.366 $\pm$ 0.113	14.634 $\pm$ 0.1	14.03 $\pm$ 0.033	13.578 $\pm$ 0.042	12.383 $\pm$ 0.379	8.512 $\pm$ –	5
21543454-1055308	L4 $\beta$	L5 $\gamma^a$	16.440 $\pm$ 0.121	15.069 $\pm$ 0.082	14.200 $\pm$ 0.068	13.367 $\pm$ 0.026	12.917 $\pm$ 0.029	12.054 $\pm$ 0.316	8.426 $\pm$ –	22, 27
21544859-7459134	—	M9.5 $\beta$	14.288 $\pm$ 0.029	13.568 $\pm$ 0.042	13.084 $\pm$ 0.032	12.708 $\pm$ 0.025	12.376 $\pm$ 0.025	11.991 $\pm$ 0.211	8.913 $\pm$ –	5
21572060+8340575	L0 —	M9 $\gamma$	13.972 $\pm$ 0.026	13.066 $\pm$ 0.033	12.584 $\pm$ 0.025	12.088 $\pm$ 0.025	11.681 $\pm$ 0.021	11.077 $\pm$ 0.079	8.762 $\pm$ –	5
22025794-5605087	—	M9 $\gamma$	14.356 $\pm$ 0.034	13.616 $\pm$ 0.035	13.16 $\pm$ 0.036	12.809 $\pm$ 0.025	12.555 $\pm$ 0.025	11.728 $\pm$ 0.18	9.322 $\pm$ –	5
22064498-4217208	L4 $\gamma$	L4 $\gamma^a$	15.555 $\pm$ 0.065	14.447 $\pm$ 0.061	13.610 $\pm$ 0.055	12.823 $\pm$ 0.024	12.376 $\pm$ 0.025	11.887 $\pm$ 0.222	9.259 $\pm$ –	5, 27
22081363+2921215	L3 $\gamma$	L3 $\gamma$	15.797 $\pm$ 0.084	14.793 $\pm$ 0.070	14.150 $\pm$ 0.073	13.354 $\pm$ 0.027	12.888 $\pm$ 0.027	12.584 $\pm$ 0.391	8.498 $\pm$ –	14, 5
22134491-2136079	L0 $\gamma$	L0 $\gamma$	15.376 $\pm$ 0.032	14.404 $\pm$ 0.055	13.760 $\pm$ 0.038	13.229 $\pm$ 0.027	12.832 $\pm$ 0.029	11.552 $\pm$ 0.203	9.070 $\pm$ –	14, 6
22351658-384154	—	L1.5 $\gamma$	15.183 $\pm$ 0.051	14.272 $\pm$ 0.046	13.631 $\pm$ 0.044	13.007 $\pm$ 0.024	12.647 $\pm$ 0.027	12.535 $\pm$ 0.436	8.773 $\pm$ –	5
22353560-5906306	—	M8.5 $\beta$	14.281 $\pm$ 0.029	13.592 $\pm$ 0.037	13.168 $\pm$ 0.032	12.691 $\pm$ 0.024	12.363 $\pm$ 0.026	12.08 $\pm$ 0.309	9.094 $\pm$ –	5
2232413167+2043433	L6-5p —	L6-L8 $\gamma^a$	16.476 $\pm$ 0.140	14.999 $\pm$ 0.065	14.022 $\pm$ 0.073	12.777 $\pm$ 0.024	12.108 $\pm$ 0.024	11.136 $\pm$ 0.115	9.301 $\pm$ –	14, 6, 27
22495345+0044046	L4 $\gamma$	L3 $\beta^a$	16.587 $\pm$ 0.124	15.421 $\pm$ 0.109	14.360 $\pm$ 0.070	13.576 $\pm$ 0.027	13.144 $\pm$ 0.050	11.284 $\pm$ –	7.687 $\pm$ –	14, 6, 27
23153135+0617146	L0 $\gamma$	L0 $\gamma^a$	15.861 $\pm$ 0.082	14.757 $\pm$ 0.069	14.070 $\pm$ 0.063	13.552 $\pm$ 0.026	13.095 $\pm$ 0.031	11.671 $\pm$ 0.230	8.592 $\pm$ –	27, 36
23224684-3133231	L0 $\beta$	L3 $\gamma^a$	13.577 $\pm$ 0.027	12.789 $\pm$ 0.023	12.324 $\pm$ 0.024	11.974 $\pm$ 0.023	11.707 $\pm$ 0.023	11.253 $\pm$ 0.128	9.153 $\pm$ –	1, 6
23225299-6151275	L2 $\gamma$	L2 $\gamma^a$	15.545 $\pm$ 0.061	14.535 $\pm$ 0.062	13.860 $\pm$ 0.042	12.841 $\pm$ 0.026	12.679 $\pm$ 0.027	12.378 $\pm$ –	2, 5, 27	
23231347-0244360	M8 $\beta$	M8 $\beta$	13.58 $\pm$ 0.023	12.925 $\pm$ 0.03	12.481 $\pm$ 0.026	12.237 $\pm$ 0.025	11.948 $\pm$ 0.024	12.278 $\pm$ 0.391	8.512 $\pm$ –	3, 5
23255604-0259508	L3 —	L1 $\gamma$	15.961 $\pm$ 0.077	14.935 $\pm$ 0.069	14.115 $\pm$ 0.056	13.695 $\pm$ 0.027	13.348 $\pm$ 0.034	11.883 $\pm$ –	8.677 $\pm$ –	16, 5
23360735-3541489	—	M9 $\beta$	14.651 $\pm$ 0.025	13.809 $\pm$ 0.025	13.385 $\pm$ 0.041	13.002 $\pm$ 0.024	12.647 $\pm$ 0.026	12.518 $\pm$ 0.418	9.177 $\pm$ –	5
23433470-3646021	L3-L6 $\gamma$	L6-L8 $\gamma^a$	16.568 $\pm$ 0.13	15.011 $\pm$ 0.063	14.194 $\pm$ 0.064	13.121 $\pm$ 0.024	12.612 $\pm$ 0.027	11.698 $\pm$ 0.188	9.138 $\pm$ –	5
23453903+0055137	M9 $\beta$	M9 $\beta$	13.771 $\pm$ 0.027	13.117 $\pm$ 0.026	12.581 $\pm$ 0.028	12.212 $\pm$ 0.025	11.879 $\pm$ 0.023	11.465 $\pm$ 0.203	8.941 $\pm$ –	1, 5
23520507-1100435	M7 —	M8 $\beta$	12.84 $\pm$ 0.018	12.166 $\pm$ 0.02	11.742 $\pm$ 0.018	11.44 $\pm$ 0.025	11.146 $\pm$ 0.022	10.849 $\pm$ 0.109	8.877 $\pm$ –	3, 5

**Note.** — References: 1=Reid et al. (2008), 2=Cruz et al. (2009), 3=Cruz et al. (2007), 4=Schmidt et al. (2015b), 5=Gagné et al. (2007), 6=Allers & Liu (2013), 7=Cruz et al. (2003), 8=Faherty et al. (2012), 9=Liu et al. (2013), 10=Gizis (2002), 11=Looper et al. (2007) 12=Reid et al. (2002), 13=Faherty et al. (2009), 14=Kirkpatrick et al. (2010), 15=Kirkpatrick et al. (2014a), 16=Burgasser et al. (2014b), 17=Reid et al. (2007), 18=Kirkpatrick et al. (2009), 19=Gagné et al. (2013), 20=Teegarden et al. (2003), 21=Faherty et al. (2013), 22=Gagné et al. (2014b), 23=Scholz et al. (2005), 24=Salim & Gould (2003), 25=Burgasser et al. (2008), 26=Criado et al. (2006), 27=This paper, 28=Kirkpatrick et al. (2014b), 29=Looper et al. (2008), 30=Salmann et al. (2016), 31=Schneider et al. (2016), 32=Kellogg et al. (2016), 33=Kellogg et al. (2015), 34=Gizis et al. (2012), 35=Gizis et al. (2015).

a These sources have new infrared spectra presented in this paper. In the majority of cases we use the infrared spectral type and gravity classification diagnosed in this work. If an object had SpeX data we default to the resultant type and classification with that data.

b This source is referred to as PSO318 for the remainder of the text.

c The sources PSO318, 2M1119, and 2M1147 have photometry reported on the MKO system that we have converted to 2MASS using the relations in Stephens et al. (2009). In the case of PSO318, JHK was converted to MKO whereas for 2M119, J and H were converted and for 2M1147 only J was converted.

d Teegarden's Star.

e References are for the spectral data and gravity analysis (if different then the original spectral data reference).

f Referred to as Tully831-154910 in Tinney et al. (1995).

**Table 2**  
Details on Parallax Targets and Observations

2MASS Designation (1)	SpT OpT (2)	SpT IR (3)	Nights (4)	Frames <sup>a</sup> (5)	Ref Stars <sup>a</sup> (6)	Δt (yr) (7)	Telescope (8)	Note <sup>b</sup> (9)	Ref (10)
00452143+1634446	L2β	L2γ	4	26	24	3.0	MDM	LG	1,2
01410321+1804502	L1	L4.5	4	23	26	3.3	MDM	N	3,4,
02132880+4444453	L1.5	—	5	34	81	3.0	MDM	N	5
02235464-5815067	L0γ	—	5	48	26	4.9	DuPont	LG	1
02411151-0326587	L0γ	L1γ	6	55	20	4.9	DuPont	LG	2,13
02535980+3206373	M7β	M6	5	28	53	3.9	MDM	LG	14
03140344+1603056	L0	—	5	31	37	3.0	MDM	N	6
05002100+0330501	L4	—	5	30	61	2.8	MDM	N	6
06023045+3910592	L1	L1β	7	77	71	9.9	MDM	LG	2,15
06154934-0100415	L2	—	5	34	62	2.2	MDM	N	7
06523073+4710348	L4.5	—	5	27	49	3.0	MDM	N	5
09111297+7401081	L0	—	4	24	35	2.9	MDM	N	6
10224821+5825453	L1β	L1β	6	30	15	4.9	MDM	LG	2,13
10484281+0111580	L1	L4	3	17	14	3.0	MDM	N	8,9
13004255+1912354	L1	L3	5	47	10	2.4	MDM	N	10,11
14162408+1348263	L6	L6	5	29	11	3.3	MDM	N	12
15525906+2948485	L0β	L0β	6	27	33	5.3	MDM	LG	1,2
21265040-8140293	L3γ	L3γ	6	90	38	5.4	DuPont	LG	1

**Note.** — References: 1=Cruz et al. (2009), 2=Allers & Liu (2013), 3=Wilson et al. (2003), 4=Cruz et al. (2007), 5=Cruz et al. (2003), 6=Reid et al. (2008), 7=Phan-Bao et al. (2008), 8=Hawley et al. (2002), 9=Kendall et al. (2004), 10=Gizis et al. (2000), 11=Burgasser et al. (2008), 12=Bowler et al. (2010a), 13=Kirkpatrick et al. (2008), 14=This paper, 15=Salim & Gould (2003)

<sup>a</sup> The number of reference stars and individual image frames used in the parallax solution

<sup>b</sup> LG is a low surface gravity object and N is a field object

**Table 3**  
Results of Parallax Program

Name (1)	SpT OpT (2)	SpT IR (3)	$\mu_\alpha^a$ $'' yr^{-1}$ (4)	$\mu_\delta^a$ $'' yr^{-1}$ (5)	$\pi_{abs}$ mas (6)
00452143+1634446	L2β	L2γ	$0.355 \pm 0.01$	$-0.04 \pm 0.01$	$62.5 \pm 3.7$
01410321+1804502	L1	L4.5	$0.41 \pm 0.01$	$-0.047 \pm 0.01$	$41.0 \pm 2.8$
02132880+4444453	L1.5	—	$-0.054 \pm 0.01$	$-0.147 \pm 0.01$	$50.0 \pm 2.1$
02235464-5815067	L0γ	—	$0.0986 \pm 0.0008$	$-0.0182 \pm 0.0009$	$27.4 \pm 2.6$
02411151-0326587	L0γ	L1γ	$0.0737 \pm 0.001$	$-0.0242 \pm 0.0019$	$26.7 \pm 3.3$
02535980+3206373	M7β	M6	$0.087 \pm 0.01$	$-0.096 \pm 0.01$	$17.7 \pm 2.5$
03140344+1603056	L0	—	$-0.247 \pm 0.01$	$-0.05 \pm 0.01$	$69.0 \pm 2.4$
05002100+0330501	L4	—	$0.008 \pm 0.01$	$-0.353 \pm 0.01$	$75.2 \pm 3.7$
06023045+3910592	L1	L2β	$0.157 \pm 0.01$	$-0.504 \pm 0.01$	$88.5 \pm 1.6$
06154934-0100415	L2	—	$0.197 \pm 0.01$	$-0.055 \pm 0.01$	$49.8 \pm 2.8$
06523073+4710348	L4.5	—	$-0.118 \pm 0.01$	$0.136 \pm 0.01$	$114.9 \pm 4.0$
09111297+7401081	L0	—	$-0.2 \pm 0.01$	$-0.145 \pm 0.01$	$45.2 \pm 3.1$
10224821+5825453	L1β	L1β	$-0.807 \pm 0.01$	$-0.73 \pm 0.01$	$54.3 \pm 2.5$
10484281+0111580	L1	L4	$-0.436 \pm 0.01$	$-0.218 \pm 0.01$	$71.9 \pm 7.4$
13004255+1912354	L1	L3	$-0.793 \pm 0.01$	$-1.231 \pm 0.01$	$70.4 \pm 2.5$
14162408+1348263	L6	L6	$0.088 \pm 0.01$	$0.136 \pm 0.01$	$107.5 \pm 3.5$
15525906+2948485	L0β	L0β	$-0.162 \pm 0.01$	$-0.06 \pm 0.01$	$48.8 \pm 2.7$
21265040-8140293	L3γ	L3γ	$0.0556 \pm 0.0014$	$-0.1018 \pm 0.003$	$31.3 \pm 2.6$

<sup>a</sup> The proper motions from MDM are not corrected to absolute and have zero-point uncertainties of  $\sim 10$  mas  $yr^{-1}$ ; see Weinberger et al. (2013) for a discussion of the du Pont proper motions.

**Table 4**  
Literature Parallax Comparisons

2MASS Designation	SpT	SpT	$\mu_\alpha$ $'' yr^{-1}$	$\mu_\delta$ $'' yr^{-1}$	$\pi$ mas	Ref
(1)	(2)	(3)	(4)	(5)	(6)	(7)
00452143+1634446	L2 $\beta$	L2 $\gamma$	0.355 $\pm$ 0.01 0.3562 $\pm$ 0.00137	-0.04 $\pm$ 0.01 -0.035 $\pm$ 0.0109	62.5 $\pm$ 3.7 57.3 $\pm$ 2.0	1 2
02411151-0326587	L0 $\gamma$	L1 $\gamma$	0.0737 $\pm$ 0.001 0.084 $\pm$ 0.0117	-0.0242 $\pm$ 0.0019 -0.0224 $\pm$ 0.0086	26.7 $\pm$ 3.3 21.4 $\pm$ 2.6	1 2
10224821+5825453	L1 $\beta$	L1 $\beta$	-0.807 $\pm$ 0.01 -0.799 $\pm$ 0.0064	-0.73 $\pm$ 0.01 -0.7438 $\pm$ 0.0132	54.3 $\pm$ 2.5 46.3 $\pm$ 1.3	1 2
14162408+1348263	L6	L6	0.088 $\pm$ 0.01 0.0951 $\pm$ 0.003	0.136 $\pm$ 0.01 0.1303 $\pm$ 0.003	107.5 $\pm$ 3.5 109.9 $\pm$ 1.8	1 2
15525906+2948485	L0 $\beta$	L0 $\beta$	-0.162 $\pm$ 0.01 -0.1541 $\pm$ 0.0053	-0.06 $\pm$ 0.01 -0.0622 $\pm$ 0.0106	48.8 $\pm$ 2.7 47.7 $\pm$ 0.9	1 3

**Note.** — References: (1) This work (2) Osorio et al. 2014 (3) Dupuy & Liu 2012

**Table 5**  
New Proper Motion Measurements

2MASS (1)	SpT OpT (2)	SpT NIR (3)	$\mu_{RA}$ $\text{yr}^{-1}$ (4)	$\mu_{DEC}$ $\text{yr}^{-1}$ (5)	Ref (6)	$\Delta t$ yr (7)
00040288-6410358	L1 $\gamma$	L1 $\gamma$	0.064 $\pm$ 0.012	-0.047 $\pm$ 0.012	WISE-2MASS	10.02
00374306-5846229	L0 $\gamma$	—	0.057 $\pm$ 0.01	0.017 $\pm$ 0.005	FourStar	14.15
01174748-3403258	L1 $\beta$	L1 $\beta$	0.084 $\pm$ 0.015	-0.045 $\pm$ 0.008	FourStar	15.08
01262109+1428057	L4 $\gamma$	L2 $\gamma$	0.07 $\pm$ 0.012	-0.008 $\pm$ 0.012	WISE-2MASS	9.68
01415823-4633574	L0 $\gamma$	L0 $\gamma$	0.105 $\pm$ 0.01	-0.049 $\pm$ 0.01	FourStar	14.29
02103857-3015313	L0 $\gamma$	L0 $\gamma$	0.145 $\pm$ 0.036	-0.04 $\pm$ 0.007	FourStar	14.39
02340093-6442068	L0 $\gamma$	L0 $\beta\gamma$	0.088 $\pm$ 0.012	-0.015 $\pm$ 0.012	WISE-2MASS	10.53
03032042-7312300	L2 $\gamma$	—	0.043 $\pm$ 0.012	0.003 $\pm$ 0.012	WISE-2MASS	10.48
03231002-4631237	L0 $\gamma$	L0 $\gamma$	0.066 $\pm$ 0.008	0.001 $\pm$ 0.016	FourStar	14.30
04062677-3812102	L0 $\gamma$	L1 $\gamma$	0.009 $\pm$ 0.012	0.029 $\pm$ 0.012	WISE-2MASS	9.79
05120636-2949540	L5 $\gamma$	L5 $\beta$	-0.01 $\pm$ 0.013	0.08 $\pm$ 0.015	CAPSCam	15.14
05341594-0631397	M8 $\gamma$	M8 $\gamma$	0.002 $\pm$ 0.012	-0.007 $\pm$ 0.012	WISE-2MASS	9.52
09532126-1014205	M9 $\gamma$	M9 $\beta$	-0.07 $\pm$ 0.007	-0.06 $\pm$ 0.009	CAPSCam	15.06
09593276+4523309	—	L3 $\gamma$	-0.087 $\pm$ 0.009	-0.126 $\pm$ 0.012	WISE-2MASS	11.33
TWA 28	M8.5 $\gamma$	M9 $\gamma$	-0.06 $\pm$ 0.008	-0.014 $\pm$ 0.009	CAPSCam	14.90
11544223-3400390	L0 $\beta$	L1 $\beta$	-0.161 $\pm$ 0.008	0.012 $\pm$ 0.007	CAPSCam	14.89
14112131-2119503	M9 $\beta$	M8 $\beta$	-0.078 $\pm$ 0.009	-0.073 $\pm$ 0.011	CAPSCam	15.77
14482563+1031590	L4	L4pec	0.223 $\pm$ 0.017	-0.118 $\pm$ 0.013	CAPSCam	13.82
15382417-1953116	L4 $\gamma$	L4 $\gamma$	0.026 $\pm$ 0.007	-0.045 $\pm$ 0.007	CAPSCam	15.69
15474719-2423493	M9 $\gamma$	M0 $\beta$	-0.135 $\pm$ 0.009	-0.127 $\pm$ 0.008	CAPSCam	14.79
15575011-2952431	M9 $\delta$	L1 $\gamma$	-0.01 $\pm$ 0.012	-0.028 $\pm$ 0.012	WISE-2MASS	11.04
16154255+4953211	L4 $\gamma$	L3-L6 $\gamma$	-0.08 $\pm$ 0.012	0.018 $\pm$ 0.012	WISE-2MASS	12.11
17111353+2326333	L0 $\gamma$	L1 $\beta$	-0.063 $\pm$ 0.015	-0.035 $\pm$ 0.012	CAPSCam	16.85
18212815+1414010	L4.5	L4pec	0.226 $\pm$ 0.008	-0.24 $\pm$ 0.007	CAPSCam	15.07
19355595-2846343	M9 $\gamma$	M9 $\gamma$	0.034 $\pm$ 0.012	-0.058 $\pm$ 0.012	CAPSCam	14.79
19564700-7542270	L0 $\gamma$	L2 $\gamma$	0.009 $\pm$ 0.012	-0.059 $\pm$ 0.012	WISE-2MASS	9.72
20004841-7523070	M9 $\gamma$	M9 $\gamma$	0.069 $\pm$ 0.012	-0.11 $\pm$ 0.004	CAPSCam	13.79
20025073-0521524	L5 $\beta$	L5-L7 $\gamma$	-0.098 $\pm$ 0.005	-0.11 $\pm$ 0.008	CAPSCam	15.54
20135152-2806020	M9 $\gamma$	L0 $\gamma$	0.043 $\pm$ 0.012	-0.068 $\pm$ 0.012	WISE-2MASS	11.03
21543454-1055308	L4 $\beta$	L5 $\gamma$	0.175 $\pm$ 0.012	0.009 $\pm$ 0.012	WISE-2MASS	11.77
22064498-4217208	L4 $\gamma$	L4 $\gamma$	0.128 $\pm$ 0.013	-0.181 $\pm$ 0.008	CAPSCam	15.52
23153135+0617146	L0 $\gamma$	L0 $\gamma$	0.056 $\pm$ 0.012	-0.039 $\pm$ 0.012	WISE-2MASS	9.96
23225299-6151275	L2 $\gamma$	L3 $\gamma$	0.062 $\pm$ 0.01	-0.085 $\pm$ 0.009	FourStar	14.07

**Table 6**  
near-infrared Spectral Data

2MASS (1)	Date-Observed (2)	Instrument (3)	Mode (4)	Slit (5)	Int time (6)	Images (7)
00040288-6410358	11-Sept-2014	FIRE	Echelle	0.6	900	2
00274197+0503417	08-Aug-2014	FIRE	Echelle	0.6	900	2
00452143+1634446	08-Aug-2014	FIRE	Echelle	0.6	900	2
00550564+0134365	04-Sept-2003	SpeX	Prism	0.8	180	2
01174748-3403258	12-Sept-2014	FIRE	Echelle	0.6	900	2
01174748-3403258(2)	11-Sept-2014	FIRE	Echelle	0.6	600	2
01244599-5745379	11-Sept-2014	FIRE	Echelle	0.6	900	2
02103857-3015313	11-Sept-2014	FIRE	Echelle	0.6	750	2
02103857-3015313(2)	29-Dec-2009	TripleSpec	—	1.1x43"	300	6
02251947-5837295	28-July-2013	FIRE	Echelle	0.6	600	2
02340093-6442068	28-July-2013	FIRE	Echelle	0.6	750	2
03231002-4631237	13-Nov-2007	SpeX	Prism	0.5	180	5
03264225-2102057	13-Nov-2007	SpeX	Prism	0.5	180	6
04210718-6306022	11-Sept-2014	FIRE	Echelle	0.6	900	2
04351455-1414468	13-Nov-2007	SpeX	SXD	0.5	200	4
05012406-0010452	12-Oct-2007	SpeX	Prism	0.5	90	6
05120636-2949540	15-Nov-2013	FIRE	Echelle	0.6	500	2
05120636-2949540(2)	08-Dec-2011	SpeX	Prism	0.5	180	8
05361998-1920396	13-Dec-2013	FIRE	Echelle	0.6	650	2
07123786-6155528	15-Nov-2013	FIRE	Echelle	0.6	650	2
09532126-1014205	02-March-2009	TripleSpec	—	1.1x43"	300	6
09593276+4523309	30-Dec-2009	SpeX	Prism	0.5	180	3
11020983-3430355	12-May-2014	FIRE	Echelle	0.6	600	2
11544223-3400390	12-May-2014	FIRE	Echelle	0.6	750	2
12563961-2718455	12-May-2014	FIRE	Echelle	0.6	900	2
14112131-2119503	12-May-2014	FIRE	Echelle	0.6	500	2
14482563+1031590	13-May-2014	FIRE	Echelle	0.6	900	2
15382417-1953116	28-July-2013	FIRE	Echelle	0.6	900	2
15382417-1953116(2)	04-Sept-2003	SpeX	Prism	0.8	180	6
15515237+0941148	15-Aug-2013	FIRE	Echelle	0.6	900	2
15575011-2952431	28-July-2013	FIRE	Echelle	0.6	900	2
17111353+2326333	12-May-2014	FIRE	Echelle	0.6	800	2
17260007+1538190	12-May-2014	FIRE	Echelle	0.6	800	2
17410280-4642218	11-Sept-2014	FIRE	Echelle	0.6	1500	2
18212815+1414010	12-May-2014	FIRE	Echelle	0.6	650	2
19355595-2846343	08-Aug-2014	FIRE	Echelle	0.6	600	2
19564700-7542270	28-July-2013	FIRE	Echelle	0.6	900	4
20004841-7523070	28-July-2013	FIRE	Echelle	0.6	300	3
20025073-0521524	28-July-2013	FIRE	Echelle	0.6	600	2
20135152-2806020	12-May-2014	FIRE	Echelle	0.6	600	2
20135152-2806020(2)	08-Aug-2014	FIRE	Echelle	0.6	600	2
PSO318	13-Dec-2013	FIRE	Echelle	0.6	900	4
21265040-8140293	15-Aug-2013	FIRE	Echelle	0.6	900	2
21265040-8140293(2)	12-May-2014	FIRE	Echelle	0.6	800	2
21543454-1055308	08-Aug-2014	FIRE	Echelle	0.6	1200	2
22064498-4217208	12-May-2014	FIRE	Echelle	0.6	700	2
22064498-4217208(2)	08-Aug-2014	FIRE	Echelle	0.6	750	2
22064498-4217208(3)	21-Aug-2006	SpeX	Prism	0.5	180	5
22443167+2043433	11-Sept-2014	FIRE	Echelle	0.6	900	2
22495345+0044046	08-Aug-2014	FIRE	Echelle	0.6	1200	2
23153135+0617146	08-Aug-2014	FIRE	Echelle	0.6	750	2
23153135+0617146(2)	14-Nov-2007	SpeX	Prism	0.5	180	6

**Note.** —

**Table 7**  
Radial Velocities

Name (1)	Telescope (2)	Resolving Power (3)	Date-obs (4)	Standards Used (5)	R.V. (6)	R.V. final (7)
00325584-4405058	Magellan Clay MIKE	25000	01-Nov-2006	4.5	12.95±1.92	12.95±1.92
00332386-1521309	Gemini South Phoenix	50000	28-Oct-2009	6.7	-6.37±0.40	-6.37±0.40
00374306-5846229	Gemini South Phoenix	50000	23-Dec-2007	6.7	6.63±0.08	6.62±0.07
00374306-5846229	Keck II NIRSPEC	20000	15-Sep-2008	1.3	3.16±0.83	3.16±0.83
00452143-1-1634446	Keck II NIRSPEC	20000	14-Sep-2008	1.2,3	-2.75±0.27	-2.75±0.27
00464841+0715177	Keck II NIRSPEC	20000	14-Sep-2008	1.2,3	-1.21±0.38	-1.21±0.38
00550564-0134365	Magellan Clay MIKE	25000	02-Nov-2006	4.5	6.41±1.56	6.41±1.56
01415823-4633574	Gemini South Phoenix	50000	22-Dec-2007	6.7	7.63±0.35	7.82±0.27
02103857-3015313	Gemini South Phoenix	50000	24-Dec-2007	6.7	7.05±0.45	7.05±0.45
02103857-3015313	Gemini South Phoenix	50000	26-Dec-2007	6.7	7.96±0.16	7.96±0.16
02215494-5412054	Gemini South Phoenix	50000	27-Oct-2009	6.7	10.18±0.10	10.18±0.10
02235464-5815067	Gemini South Phoenix	50000	05-Dec-2007	6.7	9.55±0.62	10.36±0.23
02235464-5815067	Gemini South Phoenix	50000	25-Dec-2007	6.7	10.42±0.18	10.42±0.18
02340093-6442068	Gemini South Phoenix	50000	27-Oct-2009	6.7	12.56±0.14	11.76±0.72
02340093-6442068	Gemini South Phoenix	50000	29-Oct-2009	6.7	11.11±0.13	11.11±0.13
02411151-0326587 <sup>a</sup>	Keck II NIRSPEC	20000	13-Sep-2008	1.2,3	6.34±7.98	6.34±7.98
03231002-4631237	Gemini South Phoenix	50000	21-Dec-2007	6.7	13.02±0.13	13.00±0.05
03231002-4631237	Gemini South Phoenix	50000	23-Dec-2007	6.7	12.90±0.29	12.90±0.29
03393521-3525440	Magellan Clay MIKE	25000	04-Jul-2006	4.5	7.43±0.72	7.43±0.72
03572695-4417305	Magellan Clay MIKE	25000	01-Nov-2006	4.5	10.73±4.60	10.73±4.60
04210718-6306022	Gemini South Phoenix	50000	14-Dec-2007	6.7	15.81±0.53	14.70±0.33
04210718-6306022	Gemini South Phoenix	50000	15-Dec-2007	6.7	14.60±0.16	14.60±0.16
04351455-1414468	Magellan Clay MIKE	25000	01-Nov-2006	4.5	16.16±1.76	16.16±1.76
04362788-4114465	Magellan Clay MIKE	25000	02-Nov-2006	4.5	14.97±1.45	14.97±1.45
04433761+0002051	Magellan Clay MIKE	25000	01-Nov-2006	4.5	16.97±0.76	16.97±0.76
05012406-0010452	Magellan Clay MIKE	25000	02-Nov-2006	4.5	21.29±0.85	21.77±0.66
05012406-0010452	Gemini South Phoenix	50000	28-Oct-2009	6.7	22.68±1.16	22.68±1.16
05184616-2756457	Keck II NIRSPEC	20000	13-Sep-2008	1.2	24.52±0.41	24.35±0.19
05184616-2756457	Keck II NIRSPEC	20000	15-Sep-2008	1.2	24.15±0.45	24.15±0.45
06085283-2753583	Magellan Clay MIKE	25000	02-Nov-2006	4.5	28.08±1.93	26.35±0.07
06085283-2753583	Gemini South Phoenix	50000	28-Oct-2009	6.7	26.35±0.08	26.35±0.08
15474719-2423493	Magellan Clay MIKE	25000	04-Jul-2006	4.5	-6.52±0.35	-6.52±0.35
15525906-2948485	Magellan Clay MIKE	25000	04-Jul-2006	4.5	-19.90±1.38	-19.90±1.38
16154255-4953211 <sup>a</sup>	Keck II NIRSPEC	20000	13-Sep-2008	1.2,3	-25.59±3.18	-25.59±3.18
17111353-2326333	Keck II NIRSPEC	20000	14-Sep-2008	1.2,3	-20.69±0.75	-20.69±0.75
17260007-1538190	Keck II NIRSPEC	20000	15-Sep-2008	1.2,3	-20.54±0.84	-20.54±0.84
18212815-1-1414010	Magellan Clay MIKE	25000	04-Jul-2006	4.5	9.08±0.17	9.08±0.17
19350976-6200473 <sup>b</sup>	Magellan Clay MIKE	25000	04-Jul-2006	4.5	4.40±2.84	4.40±2.84
20004841-7723070	Magellan Clay MIKE	25000	04-Jul-2006	4.5	-6.53±0.24	-6.53±0.24
2013152-2806620	Gemini South Phoenix	50000	29-Oct-2009	6.7	10.03±0.49	10.03±0.49
21265040-8-140293	Keck II NIRSPEC	20000	13-Sep-2008	1.2,3	-15.59±1.93	-15.59±1.93
22081363-2921215	Magellan Clay MIKE	25000	04-Jul-2006	4.5	-4.92±4.18	-4.92±4.18
22134491-2-36079	Keck II NIRSPEC	20000	13-Sep-2008	1.2,3	-3.26±0.90	-3.26±0.90
22435345-0044046	Keck II NIRSPEC	20000	15-Sep-2008	1.2,3	-14.69±0.52	-14.69±0.52
23153135-0-617146	Gemini South Phoenix	50000	27-Oct-2009	6.7	33.86±1.11	33.86±1.11
23224684-3133231	Gemini South Phoenix	50000	28-Oct-2009	6.7	7.20±0.46	6.75±0.75
23225299-6151275	Gemini South Phoenix	50000	29-Oct-2009	6.7	5.52±0.76	5.52±0.76
23225299-6151275	Keck II NIRSPEC	20000	14-Sep-2008	1	51.95±15.04	51.95±15.04
00242463-0158201 <sup>c</sup>	Gemini South Phoenix	50000	24-Dec-2007	6.7	11.65±1.60	11.65±1.60
1224522-123835 <sup>c</sup>	Magellan Clay MIKE	25000	04-Jul-2006	4	-2.87±0.59	-2.87±0.59
01062285-5933185 <sup>c</sup>	Gemini South Phoenix	50000	27-Jul-2007	6.7	1.18±0.44	1.18±0.44
05233822-1403022 <sup>c</sup>	Gemini South Phoenix	50000	27-Oct-2009	6	12.48±0.41	12.48±0.41
05361998-1920396 <sup>c</sup>	Keck II NIRSPEC	20000	14-Sep-2008	1.2	22.07±0.70	22.07±0.70
14284323-3310391 <sup>c</sup>	Magellan Clay MIKE	25000	04-Jul-2006	5	-39.14±0.38	-39.14±0.38
18284076-1-1229207 <sup>a,c</sup>	Keck II NIRSPEC	20000	14-Sep-2008	1		

**Table 7** — *Continued*

Name (1)	Telescope (2)	Resolving Power (3)	Date-obs (4)	Standards Used (5)	R.V. (6)	R.V. final (7)
21041491-1037369 <sup>c</sup>	Gemini South Phoenix	50000	28-Oct-2009	6,7	-30.90±1.58	-30.90±1.58
21481633-4003594 <sup>c</sup>	Keck II NIRSPEC	20000	15-Sep-2008	1,2,3	-14.52±0.71	-14.52±0.71
22244381-0158521 <sup>c</sup>	Keck II NIRSPEC	20000	15-Sep-2008	1,2	-36.48±0.01	-36.48±0.01
22344161-4041387 <sup>c</sup>	Keck II NIRSPEC	20000	15-Sep-2008	1,2,3	-12.49±0.42	-12.49±0.42
23515044-2337367 <sup>a,c,d</sup>	Gemini South Phoenix	50000	28-Oct-2009	6,7	-5.68±1.82	-5.68±1.82

**Note.** — Data from 2MASS Cutri et al. (2003) and ALLWISE Cutri & et al. (2013). Standard stars are as follows: 1.) 2MASS J18212815+1414010 (+9.78 Blake et al. 2010), 2.) 2MASS J00452143+1634446 (+3.29 Blake et al. 2010), 3.) 2MASS J22244381-0158521 (-37.55 Blake et al. 2010), 4.) LHS 2924 (-37.4 Mohanty et al. 2003), 5.) BRI 1222-1221 (-4.8 Mohanty et al. 2003), 6.) 2MASS J1153952-3727350 (+45.0 Seifahrt et al. 2010), 7.) 2MASS J05233822-1403022 (+11.82 Blake et al. 2007)

a Low Quality Spectrum

b No Useable Spectrum

c No Spectroscopic Signs of Youth

d This object is listed in Filippazzo et al. (2015) with a distance and reference to Faherty+ in prep. The value in that paper was spectrophotometric and should not be regarded as a parallax.

**Table 8**  
Comparison of new and previously published RVs.

Name (1)	Telescope (2)	RV <sub>ours</sub> kms <sup>-1</sup> (3)	RV <sub>others</sub> kms <sup>-1</sup> (4)	RV ref. (5)	RV <sub>others</sub> kms <sup>-1</sup> (6)	RV ref. (7)	RV <sub>others</sub> kms <sup>-1</sup> (8)	RV ref. (9)	RV <sub>others</sub> kms <sup>-1</sup> (10)	RV ref. (11)
00242463-0158201	Gemini South Phoenix	+11.65±1.60	+10.4±3	3	+16±2	7				
00452143+1634446	Keck II NIRSPEC	+3.16±0.83	+3.29±0.43	1						
01415823-4633574	Magellan Clay MIKE	+6.41±1.56	+12±15	2						
03393521-3525440	Magellan Clay MIKE	+7.43±0.72	+7.6±3	3	+6±2	8	+5.8±2.4	5	+10±2	9
04433761+0002051	Magellan Clay MIKE	+16.97±0.76	+17.1±3	3						
05233822-1403022	Gemini South Phoenix	+12.48±0.41	+12.21±0.21	1						
06085283-2753583	Magellan Clay MIKE	+26.35±0.07	+24±1	4						
1224522-123835	Magellan Clay MIKE	-2.87±0.59	-5.8±3	3	-4.8±2	7				
14284323+3310391	Magellan Clay MIKE	-39.14±0.38	-37.4±2	7						
15525906+2948485	Magellan Clay MIKE	-19.90±1.38	-18.43±0.11	1						
18212815+1414010	Keck II NIRSPEC	+9.08±0.17	+9.78±0.21	1						
20004841-7523070	Magellan Clay MIKE	+4.40±2.84	+8±2.4	5	+11.77±0.97	6				
21041491-1037369	Gemini South Phoenix	-30.90±1.58	-21.09±0.41	1	-21.2±2.2	5				
22244381-0158521	Keck II NIRSPEC	-36.48±0.01	-37.55±0.21	1						
23515044-2537367	Gemini South Phoenix	-5.68±1.82	-10±3	3	-12.3±2.6	5				

**Note.** — References: 1. Blake et al. (2010), 2. Kirkpatrick et al. (2006), 3. Reiners (2009), 4. Rice et al. (2010), 5. Burgasser et al. (2015), 6. Gálvez-Ortiz et al. (2010), 7. Mohanty et al. (2003), 8. Basri (2000), 9. Reid et al. (2002)

**Table 9**  
Adopted near-infrared Spectral Types

Name (1)	SpT Adopted (2)	SpT Allers13 (3)	Gravity Score MedRes (4)	Gravity Type MedRes (5)	Gravity Score LowRes (6)	Gravity Type LowRes (7)
00040288-6410358	L1 $\gamma$	L2.3 ± 0.3	2221	VL-G	2211	VL-G
00274197+0503417	M8 $\beta$	M9.0 ± 0.8	2n11	INT-G	2n01	INT-G
00452143+1634446	L0 $\beta$	L1.5 ± 0.4	1211	INT-G	1211	INT-G
00550564+0134365	L2 $\gamma$	L1.0 ± 0.9	—	—	2122	VL-G
01174748-3403258	L1 $\gamma$	L2.2 ± 0.5	1211	INT-G	1211	INT-G
01174748-3403258(2)	L1 $\gamma$	L1.9 ± 0.5	2212	VL-G	2222	VL-G
01244599-5745379	L0 $\gamma$	L0.7 ± 0.5	2222	VL-G	2222	VL-G
02103857-3015313	L0 $\gamma$	L1.0 ± 0.3	2211	VL-G	2211	VL-G
02103857-3015313(2)	L0 $\gamma$	L2.2 ± 0.1	2112	VL-G	1122	VL-G
02251947-5837295	M9 $\gamma$	M9.4 ± 0.1	1n11	INT-G	1n11	INT-G
02340093-6442068	L0 $\beta/\gamma$	L0.8 ± 0.3	2211	VL-G	2211	VL-G
03231002-4631237	L0 $\gamma$	M9.0±0.4	—	—	2222	VL-G
03264225-2102057	L5 $\beta$ $\gamma$	L4.1±0.1	—	—	0n01	FLD-G
04210718-6306022	L5 $\gamma$	L4.2 ± 0.1	0n11	INT-G	0n01	FLD-G
04351455-1414468	M7 $\gamma^a$	M6.8±0.4	2n22	VL-G	2n22	VL-G
05012406-0010452	L4 $\gamma$	L2.4±0.1	—	—	2212	VL-G
05120636-2949540	L4 pec	L4.1 ± 0.8	2010	FLD-G	2010	FLD-G
05120636-2949540(2)	L5 $\beta\gamma$	L4.3 ± 0.4	—	—	0n01	FLD-G
05361993-1920396	L1 $\gamma$	L2.1 ± 0.3	1222	VL-G	1212	VL-G
07123786-6155528	L1 $\gamma$	L1.5 ± 0.5	2211	VL-G	2221	VL-G
09532126-1014205	M9 $\beta$	M9.7±0.3	2n12	VL-G	2n02	VL-G
09593276+4523309						
11020983-3430355	M9 $\gamma$	M8.3 ± 1.0	2n22	VL-G	2n22	VL-G
11544223-3400390	L1 $\beta$	L0.8 ± 0.5	1111	INT-G	1101	INT-G
12563961-2718455	L4 $\beta$	L3.4 ± 0.4	1211	INT-G	1201	INT-G
14112131-2119503	M8 $\beta$	M8.3 ± 0.1	1n11	INT-G	1n01	INT-G
14482563-1031590	L4 pec	L4.7 ± 0.8	2010	FLD-G	1010	FLD-G
15382417-1953116	L4 $\gamma$	L3.5 ± 0.9	2211	VL-G	2211	VL-G
15382417-1953116(2)	L4 $\gamma$	L2.1±0.6	—	—	1021	INT-G
15515237+0941148	> L5 $\gamma$	L3.3 ± 0.2	—	—	—	—
15575011-2952431	L1 $\gamma$	L2.3 ± 0.6	2222	VL-G	2212	VL-G
17111353+2326333	L0 pec	L0.4 ± 0.6	2211	VL-G	2211	VL-G
17260007+1538190	L3 $\beta/\gamma$	L2.6 ± 0.3	1121	INT-G	1121	INT-G
17410280-4642218	> L5 $\gamma$	L5.3 ± 0.8	—	—	—	—
18212815+1414010	L4 pec	L3.5 ± 1.3	1111	INT-G	0101	FLD-G
19355595-2846343	M9 $\gamma$	M9.3 ± 0.4	2n21	VL-G	2n11	INT-G
19564700-7542270	L2 $\gamma$	L0.9 ± 0.2	2222	VL-G	2222	VL-G
20004841-7523070	M9 $\gamma$	L0.2 ± 1.1	2n21	VL-G	2n21	VL-G
20025073-0521524	> L5 $\beta/\gamma$	L5.5 ± 0.2	—	—	—	—
20135152-2806020	L0 $\gamma$	L0.0 ± 0.4	2122	VL-G	2122	VL-G
20135152-2806020(2)	L0 $\gamma$	L0.0 ± 0.3	2122	VL-G	2122	VL-G
PSO318	L6-L8 $\gamma$	L6.8 ± 0.8	—	—	—	—
21265040-8140293	L3 $\gamma$	L2.4 ± 0.1	1221	VL-G	1221	VL-G
21265040-8140293(2)	L3 $\gamma$	L2.4 ± 0.2	1221	VL-G	1221	VL-G
21543454-1055308	L5 $\gamma$	L5.5 ± 0.8	2n11	INT-G	2n01	INT-G
22064498-4217208	L4 $\beta/\gamma$	L3.3 ± 0.2	1111	INT-G	1111	INT-G
22064498-4217208(2)	L3-4 $\beta/\gamma$	L2.7 ± 0.2	—	—	—	—

**Table 9** — *Continued*

Name (1)	SpT Adopted (2)	SpT Allers13 (3)	Gravity Score MedRes (4)	Gravity Type MedRes (5)	Gravity Score LowRes (6)	Gravity Type LowRes (7)
22064498-4217208(3)	L3 $\gamma$	L1.7 $\pm$ 0.8	—	—	1?12	INT-G
22443167+2043433	L6-L8 $\gamma$	L6.7 $\pm$ 0.8	—	—	—	—
22495345+0044046	L1 $\gamma$	L3.1 $\pm$ 0.3	2011	INT-G	2011	INT-G
23153135+0617146	L0 $\gamma$	L1.0 $\pm$ 0.5	2222	VL-G	2212	VL-G
23153135+0617146(2)	L0 $\gamma$	M9.9 $\pm$ 0.5	—	—	2222	VL-G

<sup>a</sup> Reddening E(B-V)=1.8 and SPT = M7 are a good solution, but spt/reddening is almost degenerate.

**Table 10**  
Kinematic data on Low Surface Gravity Dwarfs

2MASS Designation	SpT (OpT) (2)	SpT (IR) (3)	$\mu_{RA \cos DEC}$ ( $''$ yr $^{-1}$ ) (4)	$\mu_{DEC}$ ( $''$ yr $^{-1}$ ) (5)	$\pi$ (mas) (6)	RV (km s $^{-1}$ ) (7)	(Ref) (8)
00011217+1535355	—	L4 $\beta$	0.1352 $\pm$ 0.0107	-0.1696 $\pm$ 0.0137	—	—	10
00040288-6410358	L1 $\gamma$	L1 $\gamma^a$	0.064 $\pm$ 0.012	-0.047 $\pm$ 0.012	(17 $\pm$ 1)	(6.07 $\pm$ 2.89)	1
00182834-6703130	—	L0 $\gamma$	0.0654 $\pm$ 0.004	-0.0523 $\pm$ 0.0126	—	(6.7 $\pm$ 2.5)	1,10
00191296-6226005	—	L1 $\gamma$	0.0541 $\pm$ 0.0047	-0.0345 $\pm$ 0.0121	(21 $\pm$ 6)	(19 $\pm$ 2)	1,10
00193626+4614078	M8-	M8 $\beta$	0.14000 $\pm$ 0.006	-0.1 $\pm$ 0.05	(31 $\pm$ 3)	—	2,4
002741197+0503417	M9.5 $\beta$	L0 $\beta$	0.0105 $\pm$ 0.004	-0.0008 $\pm$ 0.003	13.8 $\pm$ 1.6	—	3
003013-1450333	L7-	L4-L6 $\beta$	0.2497 $\pm$ 0.0141	-0.0353 $\pm$ 0.015	37.4 $\pm$ 4.50	—	10.11
00325584-4405058	L0 $\gamma$	L0 $\beta$	0.12830 $\pm$ 0.0034	-0.0934 $\pm$ 0.003	21.6 $\pm$ 7.2	12.95 $\pm$ 1.92	1,5
003323.86-1521309	1.4 $\beta$	L1	0.30950 $\pm$ 0.0104	-0.0289 $\pm$ 0.0183	24.8 $\pm$ 2.5	-6.37 $\pm$ 0.40	1,6
00344300-4102266	—	L1 $\beta$	0.0939 $\pm$ 0.0079	-0.0412 $\pm$ 0.0108	—	—	10
00374306-5846229	L0 $\gamma$	—	—	—	—	6.62 $\pm$ 0.07	1
00381489-6403529	—	M9.5 $\beta$	0.0871 $\pm$ 0.005	-0.0353 $\pm$ 0.0105	(23 $\pm$ 5)	(7.22 $\pm$ 2.81)	1,10
00423923+1142104	—	M9 $\beta$	0.0929 $\pm$ 0.0038	-0.0353 $\pm$ 0.0105	—	—	10
00452143+1634446	L2 $\beta$	L2 $\gamma$	0.0929 $\pm$ 0.017	-0.0758 $\pm$ 0.0152	—	—	—
00461841+0715177	M9 $\beta$	L0 $\delta$	0.35500 $\pm$ 0.001	-0.04 $\pm$ 0.01	62.5 $\pm$ 3.7	3.16 $\pm$ 0.83	1
00470038+6803543	L7( $\gamma?$ )	L6-L8 $\gamma$	0.09800 $\pm$ 0.022	-0.051 $\pm$ 0.001	—	-2.75 $\pm$ 0.27	1,2
00550564+0134365	L2 $\gamma$	L2 $\gamma$	0.38700 $\pm$ 0.004	-0.197 $\pm$ 0.004	82 $\pm$ 3	-20 $\pm$ 1.4	7
00582253-0651239	L0-	L1 $\beta$	0.04400 $\pm$ 0.024	-0.082 $\pm$ 0.024	—	-1.21 $\pm$ 0.38	1,2
01032203+1935361	L6 $\beta$	L1 $\beta$	0.1367 $\pm$ 0.002	-0.1226 $\pm$ 0.0018	33.8 $\pm$ 4.0	—	5
01174748-3403258	L1 $\beta$	L1 $\beta^a$	0.29300 $\pm$ 0.0046	0.0277 $\pm$ 0.0047	46.9 $\pm$ 7.6	—	8
01205114-5200349	—	L1 $\gamma$	0.084 $\pm$ 0.015	-0.045 $\pm$ 0.008	(20 $\pm$ 3)	(3.96 $\pm$ 2.09)	1,10
01231125-6921379	M7.5 $\gamma$	—	0.0921 $\pm$ 0.0058	-0.0404 $\pm$ 0.0102	(24 $\pm$ 4)	(7.22 $\pm$ 2.5)	1,2
01244599-5745379	L0 $\gamma$	L0 $\gamma$	0.08278 $\pm$ 0.00174	-0.02646 $\pm$ 0.00139	21.6 $\pm$ 3.3	10.9 $\pm$ 3	4,9
01262109+1428057	L4 $\gamma$	L0 $\gamma$	0.03300 $\pm$ 0.001	0.018 $\pm$ 0.019	—	—	2
01291256-0833580	M5-	M7 $\beta$	0.07000 $\pm$ 0.012	-0.0088 $\pm$ 0.012	—	—	—
01415823-4633574	L0 $\gamma$	L0 $\gamma$	0.1007 $\pm$ 0.0084	-0.0564 $\pm$ 0.009	—	—	10
01531463-6744181	L2-	L3 $\beta$	0.105 $\pm$ 0.01	-0.049 $\pm$ 0.01	(25 $\pm$ 3)	6.409 $\pm$ 1.56	1
02103857-3015313	L0 $\gamma$	L0 $\gamma^a$	0.071 $\pm$ 0.037	-0.0166 $\pm$ 0.0127	(21 $\pm$ 7)	(10.41 $\pm$ 2.71)	1,10
02215494-5412054	M8 $\beta$	—	0.145 $\pm$ 0.036	-0.04 $\pm$ 0.007	(32 $\pm$ 8)	7.82 $\pm$ 0.274	1
0223464-5815067	L0 $\gamma$	—	0.05390 $\pm$ 0.0044	0.0137 $\pm$ 0.0045	25.4 $\pm$ 3.6	—	8
02261658-5327032	M9 $\beta$	M9 $\gamma$	0.136 $\pm$ 0.01	-0.01 $\pm$ 0.017	(31 $\pm$ 5)	10.18 $\pm$ 0.097	1,2
02292794-0532822	—	L0 $\gamma$	0.08960 $\pm$ 0.0008	-0.0182 $\pm$ 0.0009	27.4 $\pm$ 2.6	10.36 $\pm$ 0.23	1
02340093-6442068	L0 $\gamma$	L0 $\beta\gamma$	0.0936 $\pm$ 0.001	-0.0028 $\pm$ 0.0107	—	—	2
02410564-5511466	—	L1 $\gamma$	-0.00900 $\pm$ 0.098	-0.054 $\pm$ 0.202	—	—	1,10
0251947-5837295	L0 $\gamma$	L1 $\gamma$	0.088 $\pm$ 0.012	-0.015 $\pm$ 0.012	(21 $\pm$ 5)	11.762 $\pm$ 0.721	1
02530084+1652532	—	M7 $\beta$	0.0965 $\pm$ 0.0052	-0.0123 $\pm$ 0.0106	(24 $\pm$ 4)	(11.73 $\pm$ 2.44)	1,10
02539380+3206373	M7 $\beta$	M7 $\beta$	0.07370 $\pm$ 0.001	-0.0242 $\pm$ 0.0019	21.4 $\pm$ 2.6	6.34 $\pm$ 7.98	1
03032042-7312300	L2 $\gamma$	L0 $\beta$	0.0627 $\pm$ 0.0087	-0.0306 $\pm$ 0.009	30.2 $\pm$ 4.5	—	25, 10
03164512-2848521	L0-	L5 $\beta\gamma^a$	1.5124 $\pm$ 0.406	0.4305 $\pm$ 0.0447	260.63 $\pm$ 2.69	—	24
03231002-4631237	L4 $\gamma$	—	0.00900 $\pm$ 0.098	-0.054 $\pm$ 0.202	17.7 $\pm$ 2.5	—	1
03261225-2102057	M8.5-	M8.5 $\beta$	0.08700 $\pm$ 0.01	-0.015 $\pm$ 0.012	—	—	1,10
03350208-2842336	M9 $\beta$	M7.5 $\beta$	0.0625 $\pm$ 0.0098	-0.0581 $\pm$ 0.0097	—	—	1
03393521-3525440	—	L1 $\beta$	0.04300 $\pm$ 0.012	0.003 $\pm$ 0.012	—	—	10
03420931-2904317	L0 $\beta$	L0 $\gamma$	0.0952 $\pm$ 0.0082	-0.081 $\pm$ 0.0094	—	—	1,13
03421621-6817321	L4 $\gamma$	—	0.066 $\pm$ 0.008	0.001 $\pm$ 0.016	(17 $\pm$ 3)	13.001 $\pm$ 0.045	1
03550477-1032415	M8.5-	M8.5 $\beta$	0.108 $\pm$ 0.014	-0.146 $\pm$ 0.015	(41 $\pm$ 1)	(22.91 $\pm$ 2.07)	1,2
03552337+1133437	L5 $\gamma$	L3-L6 $\gamma$	0.22500 $\pm$ 0.0132	-0.63 $\pm$ 0.015	11.08 $\pm$ 4.3	11.92 $\pm$ 0.22	6,14
03573695-4417305 $b$	L0 $\beta$	L0 $\beta$	0.06400 $\pm$ 0.013	-0.02 $\pm$ 0.019	—	10.73 $\pm$ 4.60	1,2
04062677-3812102	L1 $\gamma$	L0 $\gamma$	0.00900 $\pm$ 0.012	0.029 $\pm$ 0.012	—	—	1
04183879-4507413	L3 $\gamma$	L3 $\gamma$	0.0533 $\pm$ 0.0084	-0.0082 $\pm$ 0.0126	—	—	10
04210718-6306022	L5 $\gamma$	L5 $\gamma$	0.14600 $\pm$ 0.008	0.191 $\pm$ 0.018	—	14.70 $\pm$ 0.33	1,2
04351455-1414468	M8 $\gamma$	M7 $\gamma$	0.00900 $\pm$ 0.014	0.016 $\pm$ 0.014	—	16.16 $\pm$ 1.76	1,2

Table 10 — *Continued*

2MASS Designation	Sp-T (OoP)	Sp-T (IR)	$\mu_{RA \cos DEC}$ ( $''$ yr $^{-1}$ )	$\mu_{DEC}$ ( $''$ yr $^{-1}$ )	$\pi$ (mas)	RV (km s $^{-1}$ )	(Ref)
(1)	(2)	(3)	(4)	(5)	(6)	(7)	(8)
04362788-4114465	M8 $\beta$	M9 $\gamma$	0.073 $\pm$ 0.012	0.013 $\pm$ 0.016	(23 $\pm$ 6)	14.972 $\pm$ 1.446	1,2
04400972-5126544	—	L0 $\gamma$	0.0458 $\pm$ 0.0062	0.0078 $\pm$ 0.0105	—	—	10
04433761+0002051 <sup>b</sup>	M9 $\gamma$	M9 $\gamma$	0.0280 $\pm$ 0.014	-0.099 $\pm$ 0.014	—	16.97 $\pm$ 0.76	1,2
04493288+1607226	—	M9 $\gamma$	0.0196 $\pm$ 0.0094	-0.1428 $\pm$ 0.0092	51 $\pm$ 3.7	21.77 $\pm$ 0.66	10
05012406-0010452	L4 $\gamma$	L3 $\gamma$	0.19030 $\pm$ 0.0095	-0.0399 $\pm$ 0.0106	—	—	10
05104958-1843548	—	L2 $\beta$	0.0882 $\pm$ 0.0095	—	—	—	10
05120636-2949540	L5 $\gamma$	L5 $\beta$	-0.01000 $\pm$ 0.013	0.08 $\pm$ 0.015	—	—	1
05181131-3101529	M7 $\beta$	M7 $\beta$	0.0416 $\pm$ 0.0068	0.0080 $\pm$ 0.0081	—	—	10
05184616-2756457	L1 $\gamma$	L1 $\gamma$	0.02860 $\pm$ 0.0042	-0.016 $\pm$ 0.004	21.4 $\pm$ 6.9	24.35 $\pm$ 0.19	1,8
05264316-1824315	—	M7 $\beta$	0.0247 $\pm$ 0.0093	-0.0227 $\pm$ 0.0095	—	—	10
05341594-0631397	M8 $\gamma$	M8 $\gamma$	0.00200 $\pm$ 0.012	-0.007 $\pm$ 0.012	—	—	1
05361998-1920396	L2 $\gamma$	M9 $\beta$	0.02460 $\pm$ 0.0053	-0.0306 $\pm$ 0.005	25.6 $\pm$ 9.4	22.065 $\pm$ 0.695	1,8
05402325-0906326	—	M9 $\beta$	0.0376 $\pm$ 0.0098	-0.0292 $\pm$ 0.0097	—	—	10
05575096-1359503	M7-	M7 $\gamma$	0.00000 $\pm$ 0.005	0.0 $\pm$ 0.005	1.9 $\pm$ 1	30.3 $\pm$ 2.8	12
06023045+3910592	L1-	L1 $\beta$	0.15700 $\pm$ 0.01	-0.504 $\pm$ 0.01	88.5 $\pm$ 1.6	—	1
06082283-2753583	M8.5 $\gamma$	L0 $\gamma$	0.00890 $\pm$ 0.0035	0.0107 $\pm$ 0.0035	32 $\pm$ 3.6	26.35 $\pm$ 0.07	1,8
06272161-5308428	—	L0 $\beta\gamma$	0.0104 $\pm$ 0.0066	0.0651 $\pm$ 0.0123	—	—	10
06322402-5010349	L3 $\beta$	L4 $\gamma$	-0.10020 $\pm$ 0.0052	-0.0046 $\pm$ 0.0088	—	—	1.10
06524851-5741376	M8 $\beta$	—	0.00100 $\pm$ 0.0034	0.0292 $\pm$ 0.0033	31.3 $\pm$ 3.2	—	8
07123786-61155528	L1 $\beta$	L1 $\gamma$	-0.03760 $\pm$ 0.0049	0.0791 $\pm$ 0.0048	22.9 $\pm$ 9.1	—	8
07140394+3702459	M7.5 $\beta$	M8-	-0.0984 $\pm$ 0.0069	-0.171 $\pm$ 0.0089	80.10 $\pm$ 4.8	—	26
08093903+4434216	—	L6p	-0.1833 $\pm$ 0.0081	-0.2019 $\pm$ 0.013	—	—	10
08561384-1342242	—	M8 $\gamma$	-0.0576 $\pm$ 0.0078	-0.0194 $\pm$ 0.0081	—	—	10
08575849+5708514	L8-	L8—	-0.4181 $\pm$ 0.0044	-0.3706 $\pm$ 0.0113	—	—	10
09451445-7733150	M9 $\beta$	M9 $\beta$	-0.0345 $\pm$ 0.0016	0.0436 $\pm$ 0.0119	—	—	10
09532126-1014205	M9 $\gamma$	M9 $\beta$	-0.07000 $\pm$ 0.007	-0.06 $\pm$ 0.009	—	—	1
09593276+4523309	—	L3 $\gamma$	-0.08700 $\pm$ 0.009	-0.126 $\pm$ 0.012	41 $\pm$ 4.1	2.7 $\pm$ 0.7	6
G196-3B	L3 $\beta$	L3 $\gamma$	-0.13230 $\pm$ 0.0107	-0.2021 $\pm$ 0.0137	—	—	10
10224570-2830427	M9 $\beta$	L4 $\beta\gamma$	-0.05260 $\pm$ 0.0131	-0.0375 $\pm$ 0.0163	—	—	10
1022489+0200477	M9 $\beta$	M9 $\beta$	-0.15620 $\pm$ 0.0066	-0.429 $\pm$ 0.0068	26.4 $\pm$ 11.5	-7.9 $\pm$ 4.8	8
10224821+5825453	L1 $\beta$	L1 $\beta$	-0.80700 $\pm$ 0.01	-0.73 $\pm$ 0.01	54.3 $\pm$ 2.5	19.29 $\pm$ 0.11	1
TWA28	M8.5 $\gamma$	M9 $\gamma$	-0.06720 $\pm$ 0.0006	-0.014 $\pm$ 0.0006	18.1 $\pm$ 0.5	(13.3 $\pm$ 1.8)	18
11064461-3715115	—	M9 $\gamma$	-0.0408 $\pm$ 0.0076	-0.0066 $\pm$ 0.0102	—	—	10
11083081+6830169	L1 $\gamma$	L1 $\gamma$	-0.2389 $\pm$ 0.0026	-0.1929 $\pm$ 0.0092	—	—	10
11193254-1137466	—	L7 $\gamma$	-1.451 $\pm$ 0.0149	-0.0724 $\pm$ 0.016	(35 $\pm$ 5)	8.5 $\pm$ 3.3	27
11271382-3735076	—	L0 $\delta$	-0.0613 $\pm$ 0.0138	0.0132 $\pm$ 0.0208	—	—	10
TWA26	M9 $\gamma$	M9 $\gamma$	-0.08120 $\pm$ 0.0039	-0.0277 $\pm$ 0.0021	23.82 $\pm$ 2.58	11.6 $\pm$ 2	15,16
114724-10-204021.3	—	L7 $\gamma$	-0.1221 $\pm$ 0.012	-0.0745 $\pm$ 0.0113	(32 $\pm$ 4)	(9.61 $\pm$ 1)	28
11480096-2836488	—	L1 $\beta$	-0.0743 $\pm$ 0.0135	-0.0194 $\pm$ 0.0161	—	—	10
11542223-3400390	L0 $\beta$	L1 $\beta$	-0.16100 $\pm$ 0.008	0.0124 $\pm$ 0.007	—	—	1
TWA27A	M8 $\gamma$	M8 $\gamma$	-0.06300 $\pm$ 0.002	-0.0234 $\pm$ 0.003	19.1 $\pm$ 0.4	11.2 $\pm$ 2	16,19
12074836-3900043	L0 $\gamma$	L1 $\gamma$	-0.0572 $\pm$ 0.0079	-0.0248 $\pm$ 0.0105	(15 $\pm$ 3)	(9.48 $\pm$ 1.91)	17
12271545-0636458	M9-	M8.5 $\beta$	-0.1141 $\pm$ 0.0111	-0.0646 $\pm$ 0.0109	—	—	10
TWA29	M9.5 $\gamma$	L0 $\gamma$	-0.04030 $\pm$ 0.0117	-0.0203 $\pm$ 0.0117	12.66 $\pm$ 2.07	(7.74 $\pm$ 2.04)	15
12474428-3816464	—	M9 $\gamma$	-0.03320 $\pm$ 0.0071	-0.0166 $\pm$ 0.0095	—	—	17
1253039-4211215	—	M9.5 $\gamma$	-0.0338 $\pm$ 0.009	-0.0121 $\pm$ 0.0132	—	—	10
12563916-2718455	—	L4 $\beta$	-0.0674 $\pm$ 0.0102	-0.0565 $\pm$ 0.0127	—	—	10
14112131-2119503	M9 $\beta$	M8 $\beta$	-0.0780 $\pm$ 0.009	-0.073 $\pm$ 0.011	—	-0.9 $\pm$ 2.5	1
142527798-3630229	L3-	L4 $\gamma$	-0.28489 $\pm$ 0.0014	-0.46308 $\pm$ 0.001	86.45 $\pm$ 0.83	5.37 $\pm$ 0.25	10
15104786-2818174	M9-	M9 $\beta$	-0.1092 $\pm$ 0.0081	-0.03399 $\pm$ 0.0098	—	—	10
15291017+6312539	—	M8 $\beta$	-0.1132 $\pm$ 0.0033	0.0447 $\pm$ 0.0091	—	—	10
15382417-19531116	L4 $\gamma$	L4 $\gamma$	-0.02600 $\pm$ 0.007	-0.045 $\pm$ 0.007	—	—	1
15470557-1626303A	—	M9 $\beta$	-0.0539 $\pm$ 0.0087	-0.123 $\pm$ 0.009	—	—	10
15474719-2423493	M9 $\gamma$	L0 $\beta$	-0.13500 $\pm$ 0.009	-0.127 $\pm$ 0.008	-6.52 $\pm$ 0.35	13,14	1
15512373+0941148	L4 $\gamma$	>L5 $\gamma$	-0.07000 $\pm$ 0.022	-0.05 $\pm$ 0.022	—	—	2
15522906+2948485	L0 $\beta$	L0 $\beta$	-0.16200 $\pm$ 0.01	-0.06 $\pm$ 0.01	48.8 $\pm$ 2.7	-18.43 $\pm$ 0.11	1,14
15576011-2952431	M9 $\delta$	L1 $\gamma$	-0.01000 $\pm$ 0.012	-0.028 $\pm$ 0.012	-	-	1
16154255+4953211	L4 $\gamma$	L3-L6 $\gamma$	-0.08000 $\pm$ 0.012	0.018 $\pm$ 0.012	-25.59 $\pm$ 3.18	—	1

Table 10 — *Continued*

2MASS Designation	SpT (Opt)	SpT (IR) (3)	$\mu_{RA \cos DEC}$ ( $''$ yr $^{-1}$ ) (4)	$\mu_{DEC}$ ( $''$ yr $^{-1}$ ) (5)	$\pi$ (mas) (6)	RV (km s $^{-1}$ ) (7)	(Ref) (8)
17111353+2326333	L0 $\gamma$	L1 $\beta$	-0.06300 $\pm$ 0.015	-0.0350 $\pm$ 0.012	-	-20.69 $\pm$ 0.75	1
17260007+1538190	L3.5 $\gamma$	L3 $\gamma$	-0.04310 $\pm$ 0.0071	-0.0557 $\pm$ 0.0052	28.6 $\pm$ 2.9	-20.54 $\pm$ 0.84	1,6
17410280-4632218	—	L4pec	0.23027 $\pm$ 0.00016	-0.24149 $\pm$ 0.0012	106.65 $\pm$ 0.23	9.08 $\pm$ 0.17	20
18212815+1414010	L4.5—	L1 $\gamma$	-0.0043 $\pm$ 0.0063	-0.0533 $\pm$ 0.0162	—	-5.7 $\pm$ 5.1	1,22
19350976-6200473	—	M9 $\gamma$	0.03400 $\pm$ 0.012	-0.058 $\pm$ 0.012	—	—	10
19355395-2846343	M9 $\gamma$	M9 $\gamma$	0.00900 $\pm$ 0.012	-0.059 $\pm$ 0.012	—	—	1
19564700-7542270	L0 $\gamma$	M9 $\gamma^a$	0.069 $\pm$ 0.012	-0.11 $\pm$ 0.004	(31 $\pm$ 1)	4.397 $\pm$ 2.842	1
20004841-7523070	M9 $\gamma$	L5-L7 $\gamma$	-0.09800 $\pm$ 0.005	-0.11 $\pm$ 0.008	—	—	1
20025073-0521524	L5 $\beta$	L3 $\gamma$	0.0213 $\pm$ 0.0081	-0.0713 $\pm$ 0.0145	—	—	10
20113196-5048112	—	M9 $\gamma$	0.04300 $\pm$ 0.012	-0.068 $\pm$ 0.012	—	-6.53 $\pm$ 0.24	1
20135152-2806020	—	M8.5 $\gamma$	0.0233 $\pm$ 0.0053	-0.0604 $\pm$ 0.0106	—	—	10
20282203-5637024	—	L0 $\gamma$	0.016 $\pm$ 0.0061	-0.0731 $\pm$ 0.0125	—	—	10
20334473-5635338	—	M8-	0.0485 $\pm$ 0.009	-0.0898 $\pm$ 0.009	—	—	10
20391314-1265311	M8-	M7 $\beta$	0.00160 $\pm$ 0.0038	-0.0863 $\pm$ 0.0039	70.1 $\pm$ 3.7	-24.68 $\pm$ 0.61	8
20573409-0252302	L1.5—	L6-L8 $\gamma$	0.13730 $\pm$ 0.0013	-0.1387 $\pm$ 0.0014	40.7 $\pm$ 2.4	-6.0 $^{+0.8}_{-1.1}$	21,23
PSO3.8	—	L3 $\gamma$	0.05560 $\pm$ 0.0014	-0.1018 $\pm$ 0.003	31.3 $\pm$ 2.6	10.03 $\pm$ 0.49	1
21263040-8140293	L3 $\gamma$	L4 $\beta$	0.1078 $\pm$ 0.0164	0.0297 $\pm$ 0.0181	—	—	10
21324036+1029494	—	L4 $\beta$	0.17500 $\pm$ 0.012	0.009 $\pm$ 0.012	—	—	1
21543454-1055308	L4 $\beta$	M9.5 $\beta$	0.0407 $\pm$ 0.0022	-0.0736 $\pm$ 0.0122	(21 $\pm$ 7)	(6.21 $\pm$ 3.1)	1,10
21544859-7459134	—	M9 $\gamma$	0.12496 $\pm$ 0.0008	0.0441 $\pm$ 0.0154	—	—	10
21572060+8340575	L0-	M9 $\gamma$	0.0496 $\pm$ 0.0052	-0.0696 $\pm$ 0.0103	—	—	10
22024794-5605087	—	M9 $\gamma^a$	0.128 $\pm$ 0.013	-0.181 $\pm$ 0.008	(35 $\pm$ 2)	(7.6 $\pm$ 2.0)	1
22064498-4217208	L4 $\gamma$	L4 $\gamma^a$	0.09070 $\pm$ 0.003	-0.0162 $\pm$ 0.0037	21.2 $\pm$ 0.7	-15.59 $\pm$ 1.93	1,6
22084363+2921215	L3 $\gamma$	L3 $\gamma$	0.06000 $\pm$ 0.014	-0.063 $\pm$ 0.017	(21 $\pm$ 7)	(4.39 $\pm$ 4.18)	1,2
22134491-2136079	L0 $\gamma$	L0 $\gamma$	0.0505 $\pm$ 0.0078	-0.0757 $\pm$ 0.0109	(22 $\pm$ 2)	(-4.9 $\pm$ 3.1)	10
22351658-3844154	—	L1.5 $\gamma$	0.0556 $\pm$ 0.0051	-0.081 $\pm$ 0.0108	(23 $\pm$ 5)	(1.71 $\pm$ 3.14)	1,10
22355360-5906306	—	M8.5 $\beta$	0.252 $\pm$ 0.014	-0.214 $\pm$ 0.011	(54 $\pm$ 4)	(-15.5 $\pm$ 1.7)	1,2
22443167+2043433	L6.5p-	L6-L8 $\gamma^a$	0.07500 $\pm$ 0.018	0.026 $\pm$ 0.018	—	-3.26 $\pm$ 0.90	1,2
22493345+0044046	L4 $\gamma$	L3 $\beta$	0.05600 $\pm$ 0.012	-0.039 $\pm$ 0.012	—	-14.69 $\pm$ 0.52	1
23153135+0617146	L0 $\gamma$	L0 $\gamma$	-0.19480 $\pm$ 0.0074	-0.5273 $\pm$ 0.0075	58.6 $\pm$ 5.6	33.86 $\pm$ 1.11	1,8
23224684-3133231	L0 $\beta$	L2 $\beta$	0.062 $\pm$ 0.01	-0.085 $\pm$ 0.009	(22 $\pm$ 1)	6.747 $\pm$ 0.75	1
23224799-6151275	L2 $\gamma$	L3 $\gamma^a$	0.0859 $\pm$ 0.0097	-0.0455 $\pm$ 0.0106	—	—	10
23231347-0244360	M8.5-	M8 $\beta$	0.0783 $\pm$ 0.0127	-0.0958 $\pm$ 0.011	—	—	10
23254604-0259508	L3-	L1 $\gamma$	0.0696 $\pm$ 0.0082	-0.0807 $\pm$ 0.0099	—	—	10
23360735-3541489	—	M9 $\beta$	0.087 $\pm$ 0.0083	-0.0987 $\pm$ 0.0125	—	—	10
23433470-3646021	—	L3-L6 $\gamma$	0.0841 $\pm$ 0.0134	-0.0461 $\pm$ 0.0117	—	—	10
23453903+0055137	M9-	M8 $\beta$	0.0881 $\pm$ 0.009	-0.1145 $\pm$ 0.0085	—	—	10
23520507-1100435	M7-	—	—	—	—	—	—

**Note.** — References: 1=This Paper; 2=Faherty et al. (2009); 3=Dahn et al. (2002); 4=Reiners & Basri (2009); 5=Marocco et al. (2013); 6=Zapatero Osorio et al. (2014); 7=Gizis et al. (2015); 8=Faherty et al. (2012); 9=Riedel (2015); 10=Gagné et al. (2015b); 11=Vrba et al. (2004); 12=Shkolnik et al. (2012); 13=Dieterich et al. (2014); 14=Blake et al. (2010); 15=Weinberger et al. (2013); 16=Mohanty et al. (2003); 17=Gagné et al. (2014a); 18=Duocourant et al. (2008); 19=Teixeira et al. (2014); 20=Schneider et al. (2014); 21=Liu et al. (2013); 22=Sahlmann et al. (2016); 23=Allers et al. (2016); 24=Henry et al. (2006); 25=Timney et al. (1995); 26=Dittman et al. (2014); 27=Kellogg et al. (2016); 28=Schneider et al. (2016).

a These sources have new infrared spectra presented in this paper. In the majority of cases we use the infrared spectral type and gravity classification diagnosed in this work. If an object had SpeX data we default to the resultant type and classification with that data.

b These sources were listed in Filippazzo et al. (2015) as members of associations but as has been noted in Table 12, we have downgraded them to ambiguous young objects

**Table 11**  
Kinematics for target dwarfs

Name (1)	U (2)	V (3)	W (4)	X (5)	Y (6)	Z (7)
00325584-4405058	-10.77 ± 3.85	-32.08 ± 8.55	-8.34 ± 2.26	8.96 ± 2.59	-9.24 ± 2.67	-41.15 ± 11.89
003323.86-1521309	-52.85 ± 5.68	-26.91 ± 3.93	3.23 ± 0.86	-1.86 ± 0.18	8.46 ± 0.82	-39.09 ± 3.8
00452143+1634446	-22.62 ± 1.47	-14.31 ± 1.21	-5.02 ± 0.84	-5.66 ± 0.33	9.48 ± 0.55	-11.54 ± 0.67
00470038+6803543	-8.58 ± 1.06	-27.83 ± 1.22	-13.53 ± 0.49	-6.52 ± 0.24	10.23 ± 0.37	1.1 ± 0.04
01231125-6921379	-7.92 ± 1.96	-20.39 ± 2.71	-1.82 ± 2.42	14.9 ± 2.11	-27.1 ± 3.84	-33.76 ± 4.78
02235464-5815067	-7.94 ± 0.86	-18.46 ± 1.19	-1.11 ± 0.7	4.29 ± 0.4	-20.41 ± 1.88	-29.71 ± 2.74
02411151-0326587	-9.68 ± 4.71	-11.49 ± 1.49	-1.39 ± 6.56	-21.39 ± 2.55	1.63 ± 0.19	-30.27 ± 3.6
03350208+2342356	-16.91 ± 1.77	-11.46 ± 2.11	-8.08 ± 1.95	-36.8 ± 2.02	10.13 ± 0.55	-18.31 ± 1
03393521-3525440	-13.32 ± 0.35	-4.95 ± 0.52	-0.1 ± 0.85	-2.1 ± 0.01	-3.19 ± 0.02	-5.15 ± 0.03
03552337+1133437	-5.53 ± 0.4	-26.32 ± 1.18	-15.34 ± 0.62	-7.72 ± 0.3	0.25 ± 0.01	-4.64 ± 0.18
05012406-0010452	-15.15 ± 0.83	-27 ± 1.74	-1.08 ± 1.07	-16.76 ± 1.16	-6.02 ± 0.42	-8.06 ± 0.56
05184616-2756457	-10.99 ± 0.93	-21.09 ± 1.55	-8.64 ± 1.37	-23.81 ± 6.57	-28.98 ± 8	-23.02 ± 6.35
05361998-1920396	-10.85 ± 1.41	-18.95 ± 1.83	-7.49 ± 1.06	-24 ± 7.34	-22.27 ± 6.81	-15.21 ± 4.65
05575096-1359503	-22.15 ± 7.41	-18.46 ± 8.29	-9.3 ± 9.91	-309.69 ± 83.51	-257.52 ± 69.45	-131.51 ± 35.46
06085283-2753583	-15.51 ± 0.45	-19.93 ± 0.34	-7.79 ± 0.51	-16.84 ± 1.82	-23.54 ± 2.54	-11.12 ± 1.2
10220489+0200477	14.87 ± 4.49	-53.28 ± 19.96	-49.14 ± 14.81	-11.07 ± 3.8	-20.45 ± 7.02	24.35 ± 8.36
10224821+5825453	-69.35 ± 2.74	-67.62 ± 3.48	0.1 ± 0.87	-10.57 ± 0.48	5.61 ± 0.26	13.98 ± 0.64
TWA26	-9.02 ± 1.5	-18.29 ± 1.94	-3.52 ± 1.42	9.92 ± 1.02	-35.32 ± 3.63	19.9 ± 2.04
TWA27A	-7.62 ± 0.94	-18.24 ± 1.77	-3.52 ± 1.03	19.49 ± 0.41	-44.22 ± 0.94	20.06 ± 0.42
14252798-3650229	-5.23 ± 0.21	-26.29 ± 0.27	-14.11 ± 0.19	8.56 ± 0.08	-6.42 ± 0.06	4.39 ± 0.04
15525906+2948485	-9.73 ± 0.88	-22.44 ± 1.11	-4.71 ± 0.78	8.78 ± 0.47	9.7 ± 0.52	15.74 ± 0.85
17260007+1538190	-8.66 ± 1.05	-21.01 ± 1.34	-6.26 ± 1.11	24.62 ± 2.4	19.25 ± 1.88	15.1 ± 1.48
18212815+1414010	12.91 ± 0.12	4.62 ± 0.11	-11.30 ± 0.06	6.74 ± 0.01	6.17 ± 0.01	2.11 ± 0.01
20575409-0252302	-12.44 ± 0.45	-19.97 ± 0.5	9.47 ± 0.39	8.66 ± 0.45	8.9 ± 0.47	-6.96 ± 0.36
PSO318	-10.4 ± 0.7	-16.4 ± 0.6	-9.8 ± 0.8	15.2 ± 0.6	7.2 ± 0.3	-14.6 ± 0.6
21265040-8140293	-7.02 ± 1.07	-18.57 ± 1.09	-3.67 ± 0.39	17.55 ± 1.41	-20.48 ± 1.64	-16.95 ± 1.36
22081363+2921215	-15.2 ± 0.87	-18.97 ± 1.83	-8.76 ± 1.13	3.64 ± 0.12	43.76 ± 1.4	-17.14 ± 0.55
232246843133231	40.26 ± 2.74	-30.87 ± 3.18	-24.72 ± 1.27	5.55 ± 0.51	1.46 ± 0.13	-15.97 ± 1.47

**Note.** — Data is only presented for targets with measured parallax, or measured parallax and radial velocity. While the actual uncertainties are best described by a radially-oriented ellipsoid, they are given here for comparison to other values.

**Table 12**  
Moving Group membership probabilities

Name (1)	SpT (2)	SpT (3)	BANYAN II Prob. (4)	Contam. (5)	LACEWING Group (6)	Prob. (7)	Group (8)	Prob. (9)	Convergence Prob. (10)	Group (11)	Group (12)	Decision (13)
00011217+1535355	- -	L4 $\beta$	97.4	1.1	AB DOR	35.12	AB DOR	43.1	AB DOR	99.04	AB DOR	AM
00040288-6410358	L1 $\gamma$	L1 $\gamma^a$	99.6	0	TUC-HOR	38.76	TUC-HOR	100	TUC-HOR	100	TUC-HOR	HLM
00182834-6703130	- -	L0 $\gamma$	99.9	< 0.1	TUC-HOR	48.71	TUC-HOR	76.7	TUC-HOR	99.83	TUC-HOR	AM
00191296-6226005	- -	L1 $\beta$	99.7	< 0.1	TUC-HOR	48.71	TUC-HOR	99.7	TUC-HOR	89.44	TUC-HOR	HLM
00192626-4614078	M8 -	M8 $\beta$	72	13.3	AB DOR	66.42	AB DOR	99	AB DOR	99	AB DOR	HLM
00274197+0503417	M9.5 $\beta$	L0 $\beta^a$	0	0	ARGUS	0	None	100	None	100	OLD	AM
003213-1450333	L7 -	L4-L6 $\beta$	26.5	2.6	ARGUS	29.65	AB DOR	98.1	AB DOR	97.87	ARGUS	AM
00325584-4405058	L0 $\gamma$	L0 $\beta$	67.3	1	TUC-HOR	91.3	AB DOR	96	AB DOR	100	AB DOR	HLM
003323.86-152130.9	L4 $\beta$	L1 $\delta$	0	99.8	COLUMBA	0	None	60	None	100	OLD	NM
00344300-4102266	- -	L1 $\beta$	98.7	< 0.1	TUC-HOR	41.91	TUC-HOR	70.1	TUC-HOR	100	TUC-HOR	AM
00347038+5846229	L0 $\gamma$	- -	0	99.3	BETA PIC	0	None	71	None	100	OLD	NM
00381489-6403529	- -	M9.5 $\beta$	99.9	< 0.1	TUC-HOR	62.83	TUC-HOR	58	TUC-HOR	95.91	TUC-HOR	HLM
00425923+1142104	- -	M9 $\beta$	19.6	53.1	AB DOR	0	None	64.9	AB DOR	83.02	BETA PIC	AM
00452143+1634446	L2 $\beta$	L2 $\gamma^a$	99.9	0.1	ARGUS	99.42	ARGUS	37	None	100	ARGUS	BM
00464841+0715177	M9 $\beta$	L0 $\delta$	31.3	0.1	COLUMBA	24.44	AB DOR	99	AB DOR	99	COLUMBA	AM
00470038+6803543	L7 ( $\gamma$ )	L6-L8 $\gamma$	100	0.1	AB DOR	99.95	AB DOR	56	AB DOR	100	AB DOR	BM
00550564+0134365	L2 $\gamma$	L2 $\gamma^a$	9.2	48.3	BETA PIC	0	None	68	None	100	None	NM
00584253-0651239	L0 -	L1 $\beta$	96.5	0.3	AB DOR	52.5	AB DOR	14.3	COLUMBA	91.65	BETA PIC	AM
01033203+11935361	L6 $\beta$	L6 $\beta$	51.2	15.7	ARGUS	36.95	Hyades	16	None	100	None	NM
01174748-3403258	L1 $\beta$	L1 $\beta^a$	98.4	0	TUC-HOR	30.63	TUC-HOR	100	TUC-HOR	91	TUC-HOR	HLM
01205114-5200349	- -	L1 $\gamma$	> 99.9	< 0.1	TUC-HOR	64.54	TUC-HOR	100	TUC-HOR	95.18	TUC-HOR	HLM
01231125-6921379	M7.5 $\gamma$	- -	100	0	TUC-HOR	99.97	TUC-HOR	100	TUC-HOR	100	TUC-HOR	BM
01262109+1428057	L0 $\gamma$	L0 $\gamma^a$	0	99.3	COLUMBA	0	None	0	None	100	None	NM
01294256-08235580	M5 -	M7 $\beta$	95.9	1.5	ARGUS	36.95	ARGUS	99	None	100	COLUMBA	96
01415823-4633574	L0 $\gamma$	L0 $\gamma$	100	0	TUC-HOR	99.84	TUC-HOR	100	TUC-HOR	100	TUC-HOR	HLM
01603837-3015313	L2 -	L3 $\beta$	> 99.9	< 0.1	TUC-HOR	33.25	TUC-HOR	98.8	TUC-HOR	100	TUC-HOR	HLM
0192212859-6831400	L0 $\gamma$	L0 $\gamma^a$	99.4	0.8	AB DOR	96.34	AB DOR	None	None	100	AB DOR	AM
02215494-5412054	M8 $\beta$	--	99.4	0	BETA PIC	0	TUC-HOR	99.9	TUC-HOR	100	TUC-HOR	HLM
02235464-5815067	M9 $\beta$	--	99.8	0	BETA PIC	0	TUC-HOR	99.98	TUC-HOR	100	TUC-HOR	AM
02251947-5837295	M9 $\beta$	M9 $\gamma^a$	57.5	1.2	BETA PIC	40.52	AB DOR	68	TUC-HOR	57	TUC-HOR	AM
02265658-5327032	--	L0 $\delta$	> 99.9	< 0.1	TUC-HOR	65.9	TUC-HOR	43	TUC-HOR	100	TUC-HOR	AM
02292794-00532822	--	L0 $\gamma$	79.8	1.3	BETA PIC	81.02	AB DOR	96	AB DOR	100	AB DOR	AM
02340093-6442068	L0 $\gamma$	L0 $\beta^a$	100	0	TUC-HOR	99.56	TUC-HOR	80	TUC-HOR	100	TUC-HOR	HLM
02410564-5514466	- -	L1 $\gamma$	100	0	TUC-HOR	71.24	TUC-HOR	99.9	TUC-HOR	95.36	TUC-HOR	HLM
02411151-0326587	L0 $\gamma$	L1 $\gamma$	48.5	0	TUC-HOR	0	None	35	None	100	None	NM
02501167-0151295	--	M7 $\beta$	92.9	1.1	BETA PIC	0	None	98.8	TUC-HOR	67.1	TUC-HOR	AM
02530084+1652532	--	M7 $\beta$	...	0	FIELD	0	None	0	None	100	None	NM
02535980+3206373	M7 $\beta$	M6 $\beta$	57.8	26.5	BETA PIC	20.61	AB DOR	100	AB DOR	97	BETA PIC	AM
02583123-1520536	- -	L3 $\beta$	88.9	< 0.1	TUC-HOR	0	None	77.4	None	100	None	NM
03032042-7312300	L2 $\gamma$	--	40.7	0	TUC-HOR	31.44	TUC-HOR	98	TUC-HOR	87	None	AM
03164512-2848521	L0 -	L1 $\beta$	96.9	3.2	AB DOR	50.99	TUC-HOR	99.8	AB DOR	99.25	AB DOR	AM
03264225-2102057	L0 $\gamma$	L0 $\gamma^a$	99.7	0	TUC-HOR	73.08	TUC-HOR	92	TUC-HOR	100	TUC-HOR	HLM
03350208+2342356	M8.5 -	M5 $\beta$	99.4	1	AB DOR	44.89	AB DOR	66	AB DOR	99	AB DOR	AM
03393521-3525440	M9 $\beta$	L0 $\beta$	76.2	4.9	BETA PIC	32.48	ARGUS	98	COLUMBA	79	AB DOR	AM
03420931-2904317	L4 $\gamma$	--	40.2	0.2	ARGUS	43.82	COMA BER	0	None	100	None	NM
03421621-6817321	L4 $\gamma$	--	99.8	< 0.1	TUC-HOR	27.86	TUC-HOR	99.5	TUC-HOR	98.71	TUC-HOR	HLM
03550477-1032415	M8.5 -	M8.5 $\beta$	93.8	< 0.1	TUC-HOR	0	None	99.9	TUC-HOR	93.24	COLUMBA	AM
03552337+113337	L5 $\gamma$	L3-L6 $\gamma$	99.6	1.1	AB DOR	100	AB DOR	18	TUC-HOR	100	AB DOR	BM
03572695-4417305 <sup>c</sup>	L0 $\beta$	L0 $\beta$	99.2	0	TUC-HOR	54.84	TUC-HOR	62	TUC-HOR	53	TUC-HOR	AM
04062677-3812102	L0 $\gamma$	L1 $\gamma$	0.3	79.6	COLUMBA	41.07	Octans	75	None	100	None	NM
04185879-4507413	--	L3 $\gamma$	92.7	< 0.1	TUC-HOR	28.97	AB DOR	91.6	AB DOR	64.9	BETA PIC	AM
04210718-6306022	L5 $\beta$	L5 $\gamma^a$	99.5	2.4	BETA PIC	52.74	TUC-HOR	96	BETA PIC	99	None	NM
04351455-1414468	M8 $\gamma$	M7 $\gamma^a$	93.8	0.5	BETA PIC	0	None	89	TUC-HOR	100	TUC-HOR	HLM
04362788-4114465	M8 $\beta$	M9 $\gamma$	99	0	TUC-HOR	87.97	TUC-HOR	87	TUC-HOR	100	TUC-HOR	AM

Table 12 — Continued

Name (1)	SpT (2)	SpT (3)	BANYAN II		Contam. (5)	Group (6)	LACEwING		Convergence Prob. (7)	Group (8)	BANYAN I		Group (12)	Decision (13)
			Prob. (4)	Prob. (4)			Prob. (7)	Prob. (9)			Prob. (10)	Prob. (11)		
04400972-5126544	- -	L0 $\gamma$	86.7	< 0.1	TUC-HOR	27.19	AB DOR	99.8	AB DOR	72.25	AB DOR	AM		
04433761+002051 <sup>c</sup>	M9 $\gamma$	M9 $\gamma$	99.7	3.4	BETA PIC	59.73	AB DOR	96	AB DOR	79	BETA PIC	AM		
04433768-1607226	- -	M9 $\gamma$	1.6	98.2	COLUMBA	82.87	NONE	99.9	TWHYA	82.24	BETA PIC	AM		
05012404-0010452	L4 $\gamma$	L3 $\gamma^a$	20.8	0.4	COLUMBA	23.73	AB DOR	99	TUC-HOR	100	OLD	AM		
05104958-1843548	- -	L2 $\beta$	68.6	6.6	BETA PIC	0	NONE	89.6	TWHYA	87.1	COLUMBA	AM		
05120636-2949540	L5 $\gamma$	L5 $\beta^a$	53.1	1	COLUMBA	0	NONE	6	CHA-NEAR	88	OLD	AM		
05181131-3101529	M6.5 -	M7 $\beta$	96.2	8.8	COLUMBA	0	NONE	90.4	COLUMBA	91.23	COLUMBA	BM		
05184616-2756457	L1 $\gamma$	L1 $\gamma$	99.4	0.1	COLUMBA	74.91	COLUMBA	13	COLUMBA	87	COLUMBA	BM		
05264316-1824315	- -	M7 $\beta$	93.5	12.8	COLUMBA	0	NONE	83.1	COLUMBA	88.66	COLUMBA	AM		
05341594-0631397	M8 $\gamma$	M8 $\gamma$	0	99.8	COLUMBA	0	NONE	100	BETA PIC	99	OLD	AM		
06272161-5308428	- -	L0 $\beta$ $\gamma$	99.2	0.1	COLUMBA	35.23	COLUMBA	78	BETA PIC	57	COLUMBA	AM		
06322402-5010349	L2 $\gamma$	L2 $\gamma^a$	72	16.1	COLUMBA	0	NONE	95	TUC-HOR	87.3	TWHYA	AM		
06402325-0906326	- -	M9 $\beta$	0	0	TWHYA	0	NONE	99	TWHYA	76	OLD	AM		
05575096-1359503	M7 -	M7 $\gamma$	36.4	0.8	AB DOR	46.33	AB DOR	37	COLUMBA	98	BETA PIC	AM		
06023045-3910592	L1 -	L1 $\beta$	2.4	0.8	BETA PIC	0	NONE	94	CHA-NEAR	49	BETA PIC	AM		
0608283-2753583	M8.5 $\gamma$	L0 $\gamma$	0	100	CARINA	37.72	AB DOR	90.5	CHA-NEAR	84.7	COLUMBA	AM		
06272161-5308428	- -	L0 $\beta$ $\gamma$	87.2	9.1	AB DOR	41.77	NONE	None	TWHYA	94.89	NONE	AM		
06322402-5010349	L3 $\beta$	L4 $\gamma$	29.5	76.7	AB DOR	0	NONE	98	CHA-NEAR	98	AB DOR	AM		
06524851-5741376	M8 $\beta$	- -	2.9	85.4	FIELD	30.21	HER-LYR <sub>r</sub>	4.7	Octans	83.3	BETA PIC	AM		
07123786-6155528	L1 $\beta$	L1 $\gamma^a$	78.7	37.6	BETA PIC	39.12	AB DOR	78	AB DOR	58	ARGUS	AM		
07140394-3702459	M7.5 $\beta$	M7.5 $\beta$	88.9	0.5	ARGUS	0	NONE	10.9	CHA-NEAR	87.35	CHA-NEAR	AM		
08095903-4434216	- -	L6p	80.7	27.4	ARGUS	21.49	AB DOR	15.7	AB DOR	92.79	ARGUS	AM		
085611384-1342242	- -	M8 $\gamma$	4.9	< 0.1	TWHYA	0	NONE	78.8	TWHYA	95.92	OLD	AM		
085750849-5708514	L8 -	L8 -	..	..	FIELD	41.21	HER-LYR <sub>r</sub>	4.7	Octans	93.98	AB DOR	AM		
09451445-7753150	- -	M9 $\beta$	90.4	2.8	CARINA	41.86	COMA BER	69	CHA-NEAR	67.56	OLD	AM		
09532126-1014205	M9 $\gamma$	M9 $\beta^a$	28.7	0	TWHYA	87.4	AB DOR	92	TUC-HOR	76	OLD	AM		
09532276+4523309	- -	L3 $\gamma$	2.1	0.3	TWHYA	0	NONE	92	AB DOR	69	AB DOR	AM		
G196-3B -	L3 $\beta$	L3 $\gamma$	41	23.3	AB DOR	20.19	NONE	42	COLUMBA	95	AB DOR	AM		
10212570-2830427	- -	L4 $\beta$ $\gamma$	92.4	< 0.1	TWHYA	0	NONE	97.2	AB DOR	99.3	OLD	AM		
10220489-0200477	M9 $\beta$	M9 $\beta$	6.1	6.1	AB DOR	0	NONE	0	AB DOR	100	OLD	AM		
10224821+5825453	L1 $\beta$	L1 $\beta$	0	99.9	AB DOR	0	NONE	14	AB DOR	100	TWHYA	AM		
TWA 28	M8.5 $\gamma$	M9 $\gamma^a$	99.9	0	TWHYA	100	NONE	97	TWHYA	100	TWHYA	AM		
11064461-3715115	- -	M9 $\gamma$	94.6	< 0.1	TWHYA	0	NONE	99.5	COLUMBA	99.85	TWHYA	AM		
11083081+6830169	L1 $\gamma$	L1 $\gamma$	6	89.9	CARINA	25.05	AB DOR	77.6	TWHYA	96.63	AB DOR	AM		
11193254-1137466	- -	L7 $\gamma$	92	0.0005	TWHYA	16	TWHYA	90.4	TWHYA	95.87	TWHYA	AM		
11271382-3735076	- -	L0 $\delta$	92.5	< 0.1	TWHYA	0	NONE	99.7	CHA-NEAR	99.39	TWHYA	AM		
TWA 26	M9 $\gamma$	M9 $\gamma^a$	99.9	0	TWHYA	100	NONE	97	TWHYA	100	TWHYA	AM		
114724-10-204021.3	- -	L7 $\gamma$	91.2	< 0.1	TWHYA	19	TWHYA	90	TWHYA	99.8	TWHYA	AM		
11480196-2836488	- -	L1 $\beta$	68.9	< 0.1	TWHYA	91.53	TWHYA	91	TWHYA	99.93	TWHYA	AM		
11544223-340390	L0 $\beta$	L1 $\beta^a$	91	0.6	ARGUS	76.31	TWHYA	99	CHA-NEAR	98	ARGUS	AM		
TWA 27A	M8 $\gamma$	M8 $\gamma$	100	0	TWHYA	100	TWHYA	97	TWHYA	100	TWHYA	AM		
12074836-3900043	L0 $\gamma$	L1 $\gamma$	99.6	0	TWHYA	99.72	TWHYA	92	TWHYA	100	TWHYA	AM		
12271545-0636458	M9 -	M8.5 $\beta$	1.5	0.6	TWHYA	0	NONE	100	COLUMBA	72.62	BETA PIC	AM		
TWA 29	M9.5 $\gamma$	L0 $\gamma$	91.6	0	TWHYA	76.86	TWHYA	99	TWHYA	95	TWHYA	AM		
12474428-3816464	- -	M9 $\gamma$	36.4	0	TWHYA	0	NONE	99.9	CHA-NEAR	90.45	AB DOR	AM		
12535039-421215	- -	M9.5 $\beta$	59.3	0	TWHYA	0	NONE	97.2	TWHYA	86.18	AB DOR	AM		
12563961-2718455	- -	L4 $\gamma^a$	15.9	< 0.1	TWHYA	58.05	TWHYA	75.8	TWHYA	99.14	TWHYA	AM		
14112131-2111953	M9 $\beta$	M8 $\beta^a$	0.1	27.8	TWHYA	65.16	TWHYA	86	BETA PIC	83	TWHYA	AM		
14252798-3650229	L3 -	L4 $\gamma$	99.9	0.1	AB DOR	99.99	AB DOR	39	AB DOR	100	AB DOR	AM		
15104786-2818174	M9 -	M9 $\beta$	60.2	ARGUS	0	NONE	99.1	COMA BER	100	AB DOR	AM			
15291017-6312539	- -	M8 $\beta$	79.2	AB DOR	0	NONE	81.4	HER-LYR <sub>r</sub>	19	TWHYA	AM			
15382417-1953116	L4 $\gamma$	L4 $\gamma^a$	0	100	BETA PIC	0	NONE	0	AB DOR	100	OLD	AM		
15405557-162603 A	- -	M9 $\beta$	63.4	0	AB DOR	0	NONE	97.1	TUC-HOR	98.03	AB DOR	AM		
15474719-24123493	M9 $\gamma$	L0 $\beta$	0	98.8	BETA PIC	34.23	AB DOR	17	AB DOR	97	OLD	AM		
15515237+0941148	L4 $\gamma$	>L5 $\gamma^a$	0.1	99.1	AB DOR	94.65	COMA BER	93	AB DOR	100	AB DOR	AM		
15525906+2948485	L0 $\beta$	L0 $\beta$	0	92.7	AB DOR	21.95	HER-LYR <sub>r</sub>	19	TUC-HOR	80	OLD	AM		
16154255+4953211	M9 $\delta$	L1 $\gamma^a$	0	100	BETA PIC	0	NONE	100	AB DOR	100	AB DOR	AM		
17111353+2326333	L0 $\gamma$	L1 $\beta^a$	0	100	BETA PIC	31.82	AB DOR	63	COLUMBA	63	BETA PIC	AM		
						0	NONE	92	COLUMBA	94	BETA PIC	96		

Table 12 — *Continued*

Name (1)	SpT (2)	SpT (3)	BANYAN II Prob. (4)	Contam. (5)	LACEwING Prob. (6)	Group (7)	Convergence Prob. (8)	Group (9)	BANYAN I Prob. (11)	Group (10)	BANYAN I Prob. (12)	Decision (13)
17260007+1538190	L3.5 $\gamma$	L3 $\gamma^a$	0	99.8	AB DOR	0	65	BETA PIC	80	OLD	BETA PIC	NM
17410280-4642218	—	L6-L8 $\gamma^a$	99.7	1.8	BETA PIC	78.78	94	BETA PIC	100	OLD	BETA PIC	AM
18212815+1-1414010	L4.5 —	L4 pec <sup>a</sup>	0	100	TUC-HOR	0	0	TUC-HOR	100	TUC-HOR	OLD	NM
19350976-62040473	—	L1 $\gamma$	20.8	0.2	ARGUS	0	0	ARGUS	0	TUC-HOR	97.32	AM
19355595-2846343	M9 $\gamma$	M9 $\gamma^a$	25.3	12.6	TUC-HOR	26.8	100	COLUMBA	93	TUC-HOR	OLD	AM
19564700-7542270	LO $\gamma$	L2 $\gamma^a$	53.3	0	TUC-HOR	84.05	97	BETA PIC	100	TUC-HOR	TUC-HOR	AM
200254841-7523070	M9 $\gamma$	M9 $\gamma^a$	99.4	3.5	BETA PIC	0	71	BETA PIC	100	BETA PIC	BETA PIC	HLM
200254841-7523074	L5 $\beta$	L5-L7 $\gamma^a$	0	47.8	BETA PIC	0	0	None	0	None	None	NM
20113139-5048112	—	L3 $\gamma$	42.6	< 0.1	TUC-HOR	0	0	COLUMBA	100	TUC-HOR	TUC-HOR	AM
20135152-2806020	M9 $\gamma$	L0 $\gamma^a$	77.6	39.5	BETA PIC	28.94	100	BETA PIC	100	BETA PIC	BETA PIC	AM
20282203-5637024	—	M8.5 $\gamma$	44.3	< 0.1	TUC-HOR	0	0	None	94.6	AB DOR	TUC-HOR	AM
20334473-5635338	—	L0 $\gamma$	93.4	< 0.1	TUC-HOR	0	0	None	81.7	TUC-HOR	TUC-HOR	AM
20391314-1126531	M8 —	M7 $\beta$	2.2	46.6	AB DOR	0	0	COLUMBA	100	AB DOR	AB DOR	AM
20575409-0252302	L1.5 —	L2 $\beta$	0	100	TUC-HOR	0	0	None	0	None	None	NM
FSO318	—	L6-L8 $\gamma^a$	99.7	0.1	BETA PIC	60.77	100	ARGUS	99	BETA PIC	BETA PIC	BM
21324036-1-10294.94	L3 $\gamma$	L3 $\gamma^a$	9.3	1.4	BETA PIC	76.51	26	BETA PIC	94	CHA-NEAR	CHA-NEAR	AM
2153454-1055308	L4 $\beta$	L4 $\gamma^a$	30.8	61.6	ARGUS	0	0	None	92.8	CHA-NEAR	CHA-NEAR	AM
21544859-7459134	—	M9.5 $\beta$	16.3	5.6	ARGUS	0	0	None	29	CHA-NEAR	CHA-NEAR	AM
21572060+8340575	LO —	M9 $\gamma$	99.4	< 0.1	TUC-HOR	44.34	100	TUC-HOR	100	TUC-HOR	TUC-HOR	HLM
215720794-5605087	—	M9 $\gamma$	30.8	0.1	AB DOR	0	0	None	63.3	AB DOR	AB DOR	AM
22064498-4217208	L4 $\gamma$	L4 $\gamma^a$	98.4	< 0.1	TUC-HOR	32.49	41.7	TUC-HOR	98.75	TUC-HOR	TUC-HOR	AM
22081363+2921215	L3 $\gamma$	L3 $\gamma^a$	99.1	1.4	AB DOR	41.75	89	AB DOR	96	AB DOR	AB DOR	HLM
22134491-2136079	LO $\gamma$	L0 $\gamma$	0.2	91.2	BETA PIC	0	0	None	99	TWHYA	TWHYA	AM
22351658-3844154	—	L0 $\beta$	35.4	45.8	BETA PIC	0	0	None	100	COLUMBA	COLUMBA	AM
22353560-5904306	—	L1.5 $\gamma$	96.2	< 0.1	TUC-HOR	20.7	84	TUC-HOR	94.01	TUC-HOR	TUC-HOR	HLM
22443167+2043433	L6.5p —	L6-L8 $\gamma^a$	99.4	< 0.1	TUC-HOR	50.74	99.7	AB DOR	69	AB DOR	AB DOR	HLM
22443167+2044046	L4 $\gamma$	L3 $\beta$	0.2	0.5	AB DOR	38.38	69	None	61	CHA-NEAR	CHA-NEAR	AM
23153135+0617146	LO $\gamma$	L0 $\gamma$	0	99.6	COLUMBA	0	0	None	92	COLUMBA	COLUMBA	AM
232246684-3133231	LO $\beta$	L2 $\beta$	0	54.5	AB DOR	0	0	None	0	None	None	NM
23225299-6151275	L2 $\gamma$	L3 $\gamma^a$	99.9	0	TUC-HOR	98.88	34	TUC-HOR	100	TUC-HOR	TUC-HOR	HLM
2323345+0044046	M8.5 —	M8 $\beta$	30.6	54.4	BETA PIC	0	0	None	99.9	TWHYA	TWHYA	AM
23255604-0259508	L3 —	L1 $\gamma$	73.4	12.3	AB DOR	21.28	98.5	AB DOR	91.2	AB DOR	AB DOR	AM
23360735-3541489	—	M9 $\beta$	50.8	30.3	AB DOR	30.17	74.5	TUC-HOR	74.5	AB DOR	TUC-HOR	AM
23433470-3646021	—	L3-L6 $\gamma$	68.9	4.8	AB DOR	38.46	65.9	TUC-HOR	65.9	AB DOR	56.17	AM
23453903+0055137	M9 —	M9 $\beta$	... 90.6	... 4	FIELD	0	99.6	BETA PIC	40.39	COLUMBA	COLUMBA	AM
23520507-1104335	M7 —	M8 $\beta$	... 90.6	... 4	AB DOR	27.22	57.2	AB DOR	97.85	AB DOR	AB DOR	AM

**Note.** — Computations of BANYAN I and II were done with the web calculator, without photometric data. BANYAN II and LACEwING were computed assuming the objects are young. The predicted distance and RV (as predicted by LACEwING for the final group) should be compared to the values in Table 10.

a These sources have new infrared spectra presented in this paper. In the majority of cases we use the infrared spectral type and gravity classification diagnosed in this work. If an object had SpEx data we default to the resultant type and classification with that data.

b Deacon et al. (2016) use the parallax reported in this work to show that this source is co-moving with the M dwarf TYC 9486-927-1. In that work they report a likelihood of membership in the  $\beta$  pictoris moving group, however we find this unlikely with the given kinematics. The membership of this interesting wide system remains unknown.

c These sources were listed in Filippazzo et al. (2015) as members of associations but as has been noted in Table 12, we have downgraded them to ambiguous young objects

d The source 0335+2342 is listed as a bona fide member of  $\beta$  Pictoris in Gagné et al. (2014d) using a 2MASS to WISE proper motion. Aside from the Shkolnik et al. (2012) proper motion used in this work, this source also has a PPMXL proper motion. Depending on which value is used in the kinematic analysis, the probability of membership varies. Based on its position on the various photometric and absolute magnitude diagrams in this work, we suspect this source is a  $\beta$  Pictoris member. However refined kinematics will confirm this. Furthermore, Allers & Liu (2013) list this object as an M7 VLGsource however we have chosen to list it as M7.5  $\beta$  based on the analysis in Gagné et al. (2014d).

**Table 13**  
High Confidence Moving Group Members

2MASS (1)	SpT Opt (2)	SpT NIR (3)	$\mu_{RA}$ $'' \text{ yr}^{-1}$ (4)	$\mu_{DEC}$ $'' \text{ yr}^{-1}$ (5)	$\pi$ mas (6)	RV $\text{km s}^{-1}$ (7)	$L_{bol}$ (8)	$T_{eff}$	Mass <sup>a</sup>	Ref	
<b>AB DORADUS</b>											
00192626+4614078	M8 –	M8 $\beta$	0.14000 $\pm$ 0.06	-0.1 $\pm$ 0.05	(31 $\pm$ 3)	-19.5 $\pm$ 2	-2.773 $\pm$ 0.29	2637.0 $\pm$ 371.0	66.62 $\pm$ 4.99	2,4	
00325584+4405058	L0 $\gamma$	L0 $\beta$	0.12830 $\pm$ 0.0034	-0.0934 $\pm$ 0.003	21.6 $\pm$ 7.2	12.95 $\pm$ 1.92	-3.388 $\pm$ 0.29	2066.0 $\pm$ 413.0	41.64 $\pm$ 29.47	1,5	
00470038+6803543	L7 ( $\gamma$ )	L6-L8 $\gamma$	0.38700 $\pm$ 0.004	-0.197 $\pm$ 0.04	82 $\pm$ 3	-20 $\pm$ 1.4	-4.429 $\pm$ 0.033	1230.0 $\pm$ 27.0	11.84 $\pm$ 2.63	7	
03264225+2102057	L5 $\beta$	L5 $\beta\gamma$ <sup>a</sup>	0.108 $\pm$ 0.014	-0.146 $\pm$ 0.015	(41 $\pm$ 1)	(22.91 $\pm$ 2.07)	-4.235 $\pm$ 0.022	1346.0 $\pm$ 26.0	13.77 $\pm$ 2.6	1,2	
03552337+1133437	L5 $\gamma$	L2500 $\pm$ 0.0132	-0.63 $\pm$ 0.015	110.8 $\pm$ 4.3	11.92 $\pm$ 0.22	1478.0 $\pm$ 58.0	22.52 $\pm$ 6.14	21.62 $\pm$ 6.14	6,14		
14252798-3650329	L3 –	L4 $\gamma$	-0.28489 $\pm$ 0.0014	-0.46308 $\pm$ 0.001	86.45 $\pm$ 0.83	5.37 $\pm$ 0.25	-4.038 $\pm$ 0.009	1535.0 $\pm$ 53.0	22.52 $\pm$ 6.07	13,14	
22064498-4217208	L4 $\gamma$	L4 $\gamma$ <sup>a</sup>	0.128 $\pm$ 0.013	-0.181 $\pm$ 0.008	(35 $\pm$ 2)	(7.6 $\pm$ 2.0)	-3.997 $\pm$ 0.009	1566.0 $\pm$ 59.0	23.15 $\pm$ 6.37	1	
22443167+2043433	L6.5p –	L6-L8 $\gamma$ <sup>a</sup>	0.252 $\pm$ 0.014	-0.214 $\pm$ 0.011	(54 $\pm$ 4)	(-15.5 $\pm$ 1.7)	-4.503 $\pm$ 0.007	1184.0 $\pm$ 10.0	10.46 $\pm$ 1.49	1,2	
<b>ARGUS</b>	00452143+1634446	L2 $\beta$	L2 $\gamma$ <sup>a</sup>	0.35500 $\pm$ 0.01	-0.04 $\pm$ 0.01	62.5 $\pm$ 3.7	3.16 $\pm$ 0.83	-3.405 $\pm$ 0.031	2059.0 $\pm$ 45.0	24.98 $\pm$ 4.62	1
$\beta$ Pictoris	20004841-7523070	M9 $\gamma$	M9 $\gamma$ <sup>a</sup>	0.069 $\pm$ 0.012	-0.11 $\pm$ 0.004	(31 $\pm$ 1)	4.397 $\pm$ 2.842	-2.972 $\pm$ 0.028	2375.0 $\pm$ 74.0	24.28 $\pm$ 5.63	1
PSO318	– –	L6-L8 $\gamma$ <sup>a</sup>	0.13730 $\pm$ 0.0013	-0.1387 $\pm$ 0.0014	40.7 $\pm$ 2.4	-6.0 $^{+0.8}_{-1.1}$	-4.39 $\pm$ 0.052	1213.0 $\pm$ 38.0	6.44 $\pm$ 1.29	21	
<b>COLUMBA</b>	05184616-2756457	L1 $\gamma$	L1 $\gamma$	0.02860 $\pm$ 0.0042	-0.016 $\pm$ 0.004	21.4 $\pm$ 6.9	24.35 $\pm$ 0.19	-3.575 $\pm$ 0.28	1808.0 $\pm$ 301.0	19.94 $\pm$ 9.23	1,8
<b>TUCANA HOROLOGIUM</b>											
00040288-6410358	L1 $\gamma$	L1 $\gamma$ <sup>a</sup>	0.064 $\pm$ 0.012	-0.047 $\pm$ 0.012	(17 $\pm$ 1)	(6.07 $\pm$ 2.89)	-3.48 $\pm$ 0.051	1904.0 $\pm$ 63.0	16.11 $\pm$ 2.9	1	
00191296-6226005	– –	L1 $\gamma$	0.0541 $\pm$ 0.0047	-0.0345 $\pm$ 0.0121	(21 $\pm$ 6)	(6.7 $\pm$ 2.5)	-3.644 $\pm$ 0.248	1755.0 $\pm$ 258.0	14.88 $\pm$ 4.52	1,10	
00381489-6403529	– –	M9.5 $\beta$	0.0871 $\pm$ 0.0038	-0.0353 $\pm$ 0.0105	(23 $\pm$ 5)	(7.27 $\pm$ 2.81)	-3.423 $\pm$ 0.189	22.03 $\pm$ 9.39	1,10		
01174748-2403258	L1 $\beta$	L1 $\beta$ <sup>a</sup>	0.084 $\pm$ 0.015	-0.0404 $\pm$ 0.0102	(20 $\pm$ 3)	(3.96 $\pm$ 2.09)	-3.477 $\pm$ 0.13	1903.0 $\pm$ 152.0	16.36 $\pm$ 3.69	1	
01205114-5200349	– –	L1 $\gamma$	0.0921 $\pm$ 0.0058	-0.02646 $\pm$ 0.00139	21.6 $\pm$ 3.3	(7.22 $\pm$ 2.5)	-3.737 $\pm$ 0.145	1685.0 $\pm$ 145.0	13.97 $\pm$ 3.51	1,10	
01231125-6921379	M7.5 $\gamma$	– –	0.08278 $\pm$ 0.00174	-0.0105 $\pm$ 0.001	(10.9 $\pm$ 3)	6.409 $\pm$ 1.56	-2.525 $\pm$ 0.133	2743.0 $\pm$ 317.0	55.56 $\pm$ 33.21	4,9	
01415823-4633574	L0 $\gamma$	L0 $\gamma$	0.071 $\pm$ 0.0037	-0.0166 $\pm$ 0.0127	(21 $\pm$ 7)	(10.41 $\pm$ 2.71)	-3.91 $\pm$ 0.29	1899.0 $\pm$ 123.0	16.2 $\pm$ 3.4	1	
01531463-6744181	L2 –	L3 $\beta$	0.145 $\pm$ 0.036	-0.04 $\pm$ 0.007	(32 $\pm$ 8)	7.82 $\pm$ 0.274	-3.826 $\pm$ 0.217	1545.0 $\pm$ 264.0	11.89 $\pm$ 3.36	1,10	
02103857-5015313	L0 $\gamma$	L0 $\gamma$ <sup>a</sup>	0.136 $\pm$ 0.01	-0.01 $\pm$ 0.017	(31 $\pm$ 5)	10.18 $\pm$ 0.97	—	1610.0 $\pm$ 207.0	13.03 $\pm$ 4.31	1	
02215494-5412054	M9 $\beta$	– –	0.09860 $\pm$ 0.0008	-0.0182 $\pm$ 0.0009	27.4 $\pm$ 2.6	-0.3509 $\pm$ 0.082	–	1879.0 $\pm$ 98.0	15.91 $\pm$ 3.12	1,2	
02235464-5815067	L0 $\gamma$	– –	0.098 $\pm$ 0.012	-0.015 $\pm$ 0.012	(21 $\pm$ 5)	11.762 $\pm$ 0.721	-3.538 $\pm$ 0.207	1848.0 $\pm$ 229.0	15.97 $\pm$ 4.29	1	
02410564-5511466	L1 $\gamma$	– –	0.0965 $\pm$ 0.0052	-0.0123 $\pm$ 0.0106	(24 $\pm$ 4)	(11.73 $\pm$ 2.44)	-3.679 $\pm$ 0.145	1731.0 $\pm$ 151.0	14.49 $\pm$ 3.49	1,10	
03231002-4631237	L0 $\gamma$	– –	0.066 $\pm$ 0.008	0.001 $\pm$ 0.016	(17 $\pm$ 3)	13.001 $\pm$ 0.045	-3.348 $\pm$ 0.153	2031.0 $\pm$ 201.0	23.17 $\pm$ 9.75	1	
03421621-5817321	L4 $\gamma$	– –	0.0653 $\pm$ 0.0028	0.0185 $\pm$ 0.0091	(21 $\pm$ 9)	(13.87 $\pm$ 2.62)	-3.848 $\pm$ 0.372	1590.0 $\pm$ 349.0	12.38 $\pm$ 6.11	1	
04362788-4114465	M9 $\gamma$	– –	0.073 $\pm$ 0.012	0.013 $\pm$ 0.016	(23 $\pm$ 6)	14.972 $\pm$ 1.446	-2.872 $\pm$ 0.227	2452.0 $\pm$ 404.0	38.5 $\pm$ 22.59	1,2	
21544859-7459134	M9.5 $\beta$	– –	0.0407 $\pm$ 0.0022	-0.0796 $\pm$ 0.0122	(21 $\pm$ 7)	(6.21 $\pm$ 3.1)	-3.219 $\pm$ 0.29	2118.0 $\pm$ 385.0	28.51 $\pm$ 15.15	1,10	
22351658-5844154	L1.5 $\gamma$	– –	0.0505 $\pm$ 0.0078	-0.0757 $\pm$ 0.0109	(22 $\pm$ 2)	(-4.9 $\pm$ 3.1)	—	—	—	10	
23353560-5906306	M8.5 $\beta$	– –	0.0556 $\pm$ 0.0051	-0.081 $\pm$ 0.0108	(23 $\pm$ 5)	(1.71 $\pm$ 3.14)	-3.294 $\pm$ 0.189	2076.0 $\pm$ 251.0	25.13 $\pm$ 1.58	1,10	
23225289-6151275	L2 $\gamma$	L3 $\gamma$ <sup>a</sup>	0.062 $\pm$ 0.01	-0.085 $\pm$ 0.009	(22 $\pm$ 1)	6.747 $\pm$ 0.75	-3.6063 $\pm$ 0.04	1793.0 $\pm$ 50.0	15.05 $\pm$ 2.66	1	
<b>TW HYDRAE</b>	M8.5 $\gamma$	M9 $\gamma$ <sup>a</sup>	-0.06720 $\pm$ 0.0006	-0.014 $\pm$ 0.0006	18.1 $\pm$ 0.5	(13.3 $\pm$ 1.8)	-2.561 $\pm$ 0.024	2664.0 $\pm$ 81.0	35.39 $\pm$ 10.23	18	
TWA28	M9 $\gamma$	M9 $\gamma$	-0.08120 $\pm$ 0.0039	-0.02777 $\pm$ 0.0021	23.82 $\pm$ 2.58	(11.6 $\pm$ 2)	-2.587 $\pm$ 0.094	2641.0 $\pm$ 192.0	35.33 $\pm$ 13.73	15,16	
TWA26	M8 $\gamma$	M8 $\gamma$	-0.06300 $\pm$ 0.0022	-0.023 $\pm$ 0.003	19.1 $\pm$ 0.4	11.2 $\pm$ 2	-2.602 $\pm$ 0.018	2635.0 $\pm$ 73.0	33.04 $\pm$ 9.32	16,19	
TWA27A	– –	L7 $\gamma$	-0.1451 $\pm$ 0.0149	-0.0724 $\pm$ 0.016	(35 $\pm$ 5)	8.5 $\pm$ 3.3	-4.363 $\pm$ 0.124	1223.0 $\pm$ 90.0	6.57 $\pm$ 1.94	27	
111933254-1137466	– –	L7 $\gamma$	-0.1221 $\pm$ 0.012	-0.0745 $\pm$ 0.0113	(32 $\pm$ 4)	(9.61 $\pm$ 1)	-4.346 $\pm$ 0.109	1235.0 $\pm$ 80.0	6.64 $\pm$ 1.89	28	
114724.10-2904021.3	L0 $\gamma$	L1 $\gamma$	-0.0572 $\pm$ 0.0079	-0.0248 $\pm$ 0.0105	(15 $\pm$ 3)	(9.48 $\pm$ 1.91)	-3.485 $\pm$ 0.076	1882.0 $\pm$ 84.0	13.75 $\pm$ 0.75	17	
12074856-3900043	M9.5 $\gamma$	L0 $\gamma$	-0.04030 $\pm$ 0.0117	-0.02030 $\pm$ 0.0117	12.66 $\pm$ 2.07	(7.74 $\pm$ 2.04)	-2.905 $\pm$ 0.142	2394.0 $\pm$ 236.0	24.74 $\pm$ 8.43	15	

**Note. —**

a These sources have new infrared spectra presented in this paper. In the majority of cases we use the infrared spectral type and gravity classification diagnosed in this work. If an object had SpeX data we default to the resultant type and classification with that data.

**Table 14**  
Fundamental Parameters for Young Sources

2MASS (1)	SpT OpT (2)	SpT NIR (3)	$\pi$ mas (4)	$L_{Bol}^b$ (5)	$T_{eff}^b$ K (6)	Mass <sup>b</sup> $M_{Jupiter}$ (7)
00040288-6410358	L1 $\gamma$	L1 $\gamma^a$	(17 $\pm$ 1)	-3.48 $\pm$ 0.051	1904.0 $\pm$ 63.0	16.11 $\pm$ 2.9
00191296-6226005	--	L1 $\gamma$	(21 $\pm$ 6)	-3.644 $\pm$ 0.248	1755.0 $\pm$ 258.0	14.88 $\pm$ 4.52
00192626+4614078	M8 -	M8 $\beta$	(31 $\pm$ 3)	-2.773 $\pm$ 0.129	2637.0 $\pm$ 371.0	66.62 $\pm$ 48.99
00274197+0503417	M9.5 $\beta$	L0 $\beta$	13.8 $\pm$ 1.6	-3.545 $\pm$ 0.101	1945.0 $\pm$ 197.0	31.64 $\pm$ 19.25
00303013-1450333	L7-	L4-L6 $\beta$	37.42 $\pm$ 4.50	-4.378 $\pm$ 0.105	1436.0 $\pm$ 131.0	50.89 $\pm$ 23.43
00325584-4405058	L0 $\gamma$	L0 $\beta$	21.6 $\pm$ 7.2	-3.388 $\pm$ 0.289	2066.0 $\pm$ 413.0	41.64 $\pm$ 29.47
003323.86-1521309	L4 $\beta$	L1	24.8 $\pm$ 2.5	-3.616 $\pm$ 0.088	1880.0 $\pm$ 173.0	29.68 $\pm$ 17.71
00381489-6403529	--	M9.5 $\beta$	(23 $\pm$ 5)	-3.423 $\pm$ 0.189	1957.0 $\pm$ 226.0	22.03 $\pm$ 9.39
00452143+1634446	L2 $\beta$	L2 $\gamma$	62.5 $\pm$ 3.7	-3.405 $\pm$ 0.031	2059.0 $\pm$ 45.0	24.98 $\pm$ 4.62
00470038+6803543	L7( $\gamma?$ )	L6-L8 $\gamma$	82 $\pm$ 3	-4.429 $\pm$ 0.033	1230.0 $\pm$ 27.0	11.84 $\pm$ 2.63
00584253-0651239	L0-	L1 $\beta$	33.8 $\pm$ 4.0	-3.635 $\pm$ 0.103	1860.0 $\pm$ 180.0	29.48 $\pm$ 17.76
01033203+1935361	L6 $\beta$	L6 $\beta$	46.9 $\pm$ 7.6	-4.407 $\pm$ 0.141	1223.0 $\pm$ 113.0	12.82 $\pm$ 8.43
01174748-3403258	L1 $\beta$	L1 $\beta^a$	(20 $\pm$ 3)	-3.477 $\pm$ 0.13	1902.0 $\pm$ 152.0	16.36 $\pm$ 3.69
01205114-5200349	--	L1 $\gamma$	(24 $\pm$ 4)	-3.737 $\pm$ 0.145	1685.0 $\pm$ 145.0	13.97 $\pm$ 3.51
01231125-6921379	M7.5 $\gamma$	--	21.6 $\pm$ 3.3	-2.525 $\pm$ 0.133	2743.0 $\pm$ 317.0	55.56 $\pm$ 33.21
01415823-4633574	L0 $\gamma$	L0 $\gamma$	(25 $\pm$ 3)	-3.485 $\pm$ 0.104	1899.0 $\pm$ 123.0	16.2 $\pm$ 3.4
01531463-6744181	L2 -	L3 $\beta$	(21 $\pm$ 7)	-3.91 $\pm$ 0.29	1545.0 $\pm$ 264.0	11.89 $\pm$ 5.36
02103857-3015313	L0 $\gamma$	L0 $\gamma^a$	(32 $\pm$ 8)	-3.826 $\pm$ 0.217	1610.0 $\pm$ 207.0	13.03 $\pm$ 4.31
02212859-6831400	M8 $\beta$	--	25.4 $\pm$ 3.6	--	--	--
02215494-5412054	M9 $\beta$	--	(31 $\pm$ 5)	--	--	--
02235464-5815067	L0 $\gamma$	--	27.4 $\pm$ 2.6	-3.509 $\pm$ 0.082	1879.0 $\pm$ 98.0	15.91 $\pm$ 3.12
02340093-6442068	L0 $\gamma$	L0 $\beta$ $\gamma$	(21 $\pm$ 5)	-3.538 $\pm$ 0.207	1848.0 $\pm$ 229.0	15.97 $\pm$ 4.29
02410564-5511466	--	L1 $\gamma$	(24 $\pm$ 4)	-3.679 $\pm$ 0.145	1731.0 $\pm$ 151.0	14.49 $\pm$ 3.49
02411151-0326587	L0 $\gamma$	L1 $\gamma$	21.4 $\pm$ 2.6	-3.717 $\pm$ 0.106	1787.0 $\pm$ 172.0	27.68 $\pm$ 16.67
02501167-0151295	--	M7 $\beta$	30.2 $\pm$ 4.5	-3.001 $\pm$ 0.129	2821.0 $\pm$ 242.0	103.42 $\pm$ 16.17
02530084+1652532	--	M7 $\beta$	260.63 $\pm$ 2.69	-3.193 $\pm$ 0.121	2641.0 $\pm$ 210.0	90.37 $\pm$ 13.88
02535980+3206373	M7 $\beta$	M6 $\beta$	17.7 $\pm$ 2.5	-2.788 $\pm$ 0.123	2627.0 $\pm$ 362.0	65.02 $\pm$ 47.48
03231002-4631237	L0 $\gamma$	L0 $\gamma^a$	(17 $\pm$ 3)	-3.348 $\pm$ 0.153	2031.0 $\pm$ 201.0	23.17 $\pm$ 9.75
03264225-2102057	L5 $\beta$	L5 $\beta$ $\gamma^a$	(41 $\pm$ 1)	-4.235 $\pm$ 0.022	1346.0 $\pm$ 26.0	13.77 $\pm$ 2.6
03350208+2342356	M8.5-	M7.5 $\beta$	23.6 $\pm$ 1.3	--	--	--
03393512-3525440	M9 $\beta$	L0 $\beta$	155.89 $\pm$ 1.03	-3.563 $\pm$ 0.005	1939.0 $\pm$ 142.0	29.62 $\pm$ 16.67
03421621-6817321	L4 $\gamma$	--	(21 $\pm$ 9)	-3.848 $\pm$ 0.372	1590.0 $\pm$ 349.0	12.38 $\pm$ 6.11
03552337+1133437	L5 $\gamma$	L3-L6 $\gamma$	110.8 $\pm$ 4.3	-4.104 $\pm$ 0.034	1478.0 $\pm$ 58.0	21.62 $\pm$ 6.14
04362788-4114465	M8 $\beta$	M9 $\gamma$	(23 $\pm$ 6)	-2.872 $\pm$ 0.227	2452.0 $\pm$ 404.0	38.5 $\pm$ 22.59
05012406-0010452	L4 $\gamma$	L3 $\gamma$	51 $\pm$ 3.7	-3.962 $\pm$ 0.063	1563.0 $\pm$ 116.0	22.15 $\pm$ 13.2
05184616-2756457	L1 $\gamma$	L1 $\gamma$	21.4 $\pm$ 6.9	-3.575 $\pm$ 0.28	1808.0 $\pm$ 301.0	19.94 $\pm$ 9.23
05361998-1920396	L2 $\gamma$	L2 $\gamma$	25.6 $\pm$ 9.4	-3.826 $\pm$ 0.319	1666.0 $\pm$ 334.0	27.71 $\pm$ 20.46
05575096-1359503	M7-	M7 $\gamma$	1.9 $\pm$ 1	--	--	--
060223045+3910592	L1-	L1 $\beta$	88.5 $\pm$ 1.6	-3.65 $\pm$ 0.016	1857.0 $\pm$ 133.0	27.88 $\pm$ 15.63
06085283-2753583	M8.5 $\gamma$	L0 $\gamma$	32 $\pm$ 3.6	-3.344 $\pm$ 0.098	2147.0 $\pm$ 228.0	37.85 $\pm$ 24.05
06524851-5741376	M8 $\beta$	--	31.3 $\pm$ 3.2	--	--	--
07123786-6155528	L1 $\beta$	L1 $\gamma$	22.9 $\pm$ 9.1	-3.598 $\pm$ 0.345	1861.0 $\pm$ 412.0	35.66 $\pm$ 25.8
07140394+3702459	M8-	M7.5 $\beta$	80.10 $\pm$ 4.8	-3.479 $\pm$ 0.052	2352.0 $\pm$ 97.0	77.81 $\pm$ 11.75
G196-3B	L3 $\beta$	L3 $\gamma$	41 $\pm$ 4.1	-3.752 $\pm$ 0.087	1789.0 $\pm$ 177.0	32.83 $\pm$ 20.25
10220489+0200477	M9 $\beta$	M9 $\beta$	26.4 $\pm$ 11.5	-3.323 $\pm$ 0.378	2097.0 $\pm$ 526.0	47.09 $\pm$ 35.09
10224821+5825453	L1 $\beta$	L1 $\beta$	54.3 $\pm$ 2.5	-3.682 $\pm$ 0.041	1823.0 $\pm$ 136.0	27.55 $\pm$ 15.72
TWA28	M8.5 $\gamma$	M9 $\gamma$	18.1 $\pm$ 0.5	-2.561 $\pm$ 0.024	2664.0 $\pm$ 81.0	35.39 $\pm$ 10.23
11193254-1137466	--	L7 $\gamma$	(35 $\pm$ 5)	-4.363 $\pm$ 0.124	1223.0 $\pm$ 90.0	6.57 $\pm$ 1.94
TWA26	M9 $\gamma$	M9 $\gamma$	23.82 $\pm$ 2.58	-2.587 $\pm$ 0.094	2641.0 $\pm$ 192.0	35.3 $\pm$ 13.73
114724.10-204021.3	--	L7 $\gamma$	(32 $\pm$ 4)	-4.346 $\pm$ 0.109	1235.0 $\pm$ 80.0	6.64 $\pm$ 1.89
TWA27A	M8 $\gamma$	M8 $\gamma$	19.1 $\pm$ 0.4	-2.602 $\pm$ 0.018	2635.0 $\pm$ 73.0	33.04 $\pm$ 9.32
12074836-3900043	L0 $\gamma$	L1 $\gamma$	(15 $\pm$ 3)	-3.485 $\pm$ 0.076	1882.0 $\pm$ 84.0	13.75 $\pm$ 0.75
TWA29	M9.5 $\gamma$	L0 $\gamma$	12.66 $\pm$ 2.07	-2.905 $\pm$ 0.142	2394.0 $\pm$ 236.0	24.74 $\pm$ 8.43
14252798-3650229	L3-	L4 $\gamma$	86.45 $\pm$ 0.83	-4.038 $\pm$ 0.009	1535.0 $\pm$ 53.0	22.52 $\pm$ 6.07
15525906+2948485	L0 $\beta$	L0 $\beta$	48.8 $\pm$ 2.7	-3.538 $\pm$ 0.017	1967.0 $\pm$ 153.0	30.34 $\pm$ 17.3
17260007+1538190	L3.5 $\gamma$	L3 $\gamma$	28.6 $\pm$ 2.9	-3.844 $\pm$ 0.088	1667.0 $\pm$ 146.0	24.82 $\pm$ 14.86
18212815+1414010	L4.5-	L4pec	106.65 $\pm$ 0.23	-2.801 $\pm$ 0.006	2986.0 $\pm$ 23.0	121.27 $\pm$ 6.38
20004841-7523070	M9 $\gamma$	M9 $\gamma^a$	(31 $\pm$ 1)	-2.972 $\pm$ 0.028	2375.0 $\pm$ 74.0	24.28 $\pm$ 5.63
20575409-0252302	L1.5-	L2 $\beta$	70.1 $\pm$ 3.7	-3.767 $\pm$ 0.046	2041.0 $\pm$ 88.0	69.5 $\pm$ 13.04
PSO318	--	L6-L8 $\gamma$	40.7 $\pm$ 2.4	-4.39 $\pm$ 0.052	1213.0 $\pm$ 38.0	6.44 $\pm$ 1.29
21265040-8140293	L3 $\gamma$	L3 $\gamma$	31.3 $\pm$ 2.6	-3.866 $\pm$ 0.072	1651.0 $\pm$ 132.0	24.21 $\pm$ 14.3
21544859-7459134	--	M9.5 $\beta$	(21 $\pm$ 7)	-3.219 $\pm$ 0.29	2118.0 $\pm$ 385.0	28.51 $\pm$ 15.15
22064498-4217208	L4 $\gamma$	L4 $\gamma^a$	(35 $\pm$ 2)	-3.997 $\pm$ 0.009	1566.0 $\pm$ 59.0	23.15 $\pm$ 6.37
22081363+2921215	L3 $\gamma$	L3 $\gamma$	21.2 $\pm$ 0.7	-3.705 $\pm$ 0.029	1799.0 $\pm$ 131.0	26.96 $\pm$ 15.2
22351658-3844154	--	L1.5 $\gamma$	(22 $\pm$ 2)	--	--	--
22353560-5906306	--	M8.5 $\beta$	(23 $\pm$ 5)	-3.294 $\pm$ 0.189	2076.0 $\pm$ 251.0	25.13 $\pm$ 11.58
22443167+2043433	L6.5p -	L6-L8 $\gamma^a$	(54 $\pm$ 4)	-4.503 $\pm$ 0.007	1184.0 $\pm$ 10.0	10.46 $\pm$ 1.49
23224684-3133231	L0 $\beta$	L2 $\beta$	58.6 $\pm$ 5.6	-3.85 $\pm$ 0.083	1667.0 $\pm$ 139.0	24.65 $\pm$ 14.69
23225299-6151275	L2 $\gamma$	L3 $\gamma^a$	(22 $\pm$ 1)	-3.606 $\pm$ 0.04	1793.0 $\pm$ 50.0	15.05 $\pm$ 2.66

**Table 14** — *Continued*

2MASS (1)	SpT OpT (2)	SpT NIR (3)	$\pi$ mas (4)	$L_{Bol}^b$ (5)	$T_{eff}^b$ K (6)	Mass <sup>b</sup> $M_{Jupiter}$ (7)
--------------	-------------------	-------------------	---------------------	--------------------	-------------------------	---

**Note.** —

<sup>b</sup> Lbol, Teff, and Mass are calculated as described in Filippazzo et al. (2015). Values that are slightly different from that work, have been updated using new data presented in this paper.

<sup>a</sup> These sources have new infrared spectra presented in this paper. In the majority of cases we use the infrared spectral type and gravity classification diagnosed in this work. If an object had SpeX data we default to the resultant type and classification with that data.

**Table 15**  
Average Infrared Colors of late-type M and L dwarfs

SpT	$N_{I-H}^a$ (1)	$(J-H)_{avg}$ (2)	$\sigma(J-H)$ (3)	$N_{I-K}^a$ (4)	$(J-K)_{avg}$ (5)	$N_{J-K}^a$ (6)	$(J-K)_{avg}$ (7)	$N_{J-W_1}^a$ (8)	$(J-W_1)_{avg}$ (9)	$\sigma(J-K)$ (10)	$N_{J-W_2}^a$ (11)	$(J-W_2)_{avg}$ (12)	$\sigma(J-W_1)$ (13)	$N_{H-K}^a$ (14)	$(H-K)_{avg}$ (15)	$\sigma(H-K)$ (16)
M7	1998	0.61	0.09	1976	0.97	0.10	1992	1.17	0.09	1990	1.37	0.10	1976	0.36	0.10	
M8	703	0.65	0.09	698	1.06	0.11	692	1.27	0.12	692	1.49	0.13	698	0.41	0.09	
M9	430	0.69	0.10	428	1.15	0.11	420	1.41	0.14	420	1.65	0.17	428	0.45	0.10	
L0	231	0.75	0.12	223	1.22	0.15	228	1.55	0.17	225	1.83	0.19	210	0.48	0.12	
L1	129	0.81	0.14	125	1.35	0.19	114	1.71	0.21	114	1.97	0.23	127	0.54	0.13	
L2	65	0.91	0.14	66	1.51	0.21	57	1.98	0.28	57	2.27	0.32	65	0.59	0.11	
L3	65	0.96	0.14	64	1.61	0.22	59	2.11	0.29	59	2.42	0.34	64	0.65	0.15	
L4	39	1.07	0.17	38	1.74	0.25	34	2.40	0.34	33	2.74	0.40	38	0.67	0.14	
L5	36	1.09	0.14	36	1.75	0.22	39	2.48	0.25	39	2.83	0.30	36	0.66	0.11	
L6	18	1.11	0.20	19	1.84	0.28	21	2.59	0.41	21	3.00	0.52	23	0.76	0.16	
L7	12	1.11	0.12	12	1.81	0.16	13	2.54	0.26	13	3.01	0.30	12	0.70	0.09	
L8	18	1.11	0.12	19	1.78	0.16	17	2.56	0.20	17	3.13	0.24	20	0.67	0.09	

a Only normal (non-low surface gravity, subdwarf, or young) L dwarfs with photometric uncertainty  $< 0.1$  were used in calculating the average.

**Table 16**  
Average Infrared Colors of late-type M and L dwarfs

SpT	$N_{H-W1}^a$	$(H-W1)_{avg}$	$\sigma(H-W1)$	$N_{H-W2}^a$	$(H-W2)_{avg}$	$\sigma(H-W2)$	$N_{K-W1}^a$	$(K-W1)_{avg}$	$\sigma(K-W1)$	$N_{K-W2}^a$	$(K-W2)_{avg}$	$\sigma(K-W2)$	$N_{W1-W2}^a$	$(W1-W2)_{avg}$	$\sigma(W1-W2)$
(1)	(2)	(3)	(4)	(5)	(6)	(7)	(8)	(9)	(10)	(11)	(12)	(13)	(14)	(15)	(16)
M7	1992	0.55	0.09	1988	0.76	0.10	1970	0.20	0.09	1970	0.41	0.10	1991	0.21	0.06
M8	692	0.62	0.10	692	0.84	0.12	687	0.22	0.09	687	0.44	0.11	692	0.22	0.06
M9	420	0.72	0.11	420	0.96	0.15	417	0.26	0.10	417	0.51	0.14	421	0.24	0.06
L0	222	0.81	0.13	219	1.08	0.17	223	0.34	0.12	219	0.61	0.13	229	0.27	0.08
L1	113	0.91	0.15	113	1.17	0.18	112	0.37	0.11	111	0.63	0.14	118	0.26	0.06
L2	56	1.05	0.17	56	1.34	0.22	57	0.45	0.12	57	0.74	0.16	58	0.29	0.07
L3	58	1.16	0.20	58	1.47	0.24	59	0.51	0.14	59	0.82	0.18	63	0.31	0.06
L4	34	1.34	0.24	34	1.67	0.29	34	0.68	0.14	34	1.01	0.18	35	0.34	0.07
L5	40	1.39	0.15	39	1.74	0.20	38	0.74	0.12	37	1.08	0.18	41	0.35	0.08
L6	21	1.49	0.30	21	1.92	0.38	22	0.77	0.20	22	1.19	0.26	23	0.41	0.12
L7	14	1.45	0.19	14	1.91	0.24	14	0.76	0.14	14	1.22	0.19	15	0.45	0.09
L8	19	1.46	0.16	18	2.04	0.19	19	0.80	0.11	18	1.37	0.14	19	0.56	0.11

a Only normal (non-low surface gravity, subdwarf, or young) L dwarfs with photometric uncertainty  $< 0.1$  were used in calculating the average.

**Table 17**  
Infrared Colors of low gravity late-type M and L dwarfs

Name (1)	SpT (2)	SpT (3)	(J-H) (4)	# of $\sigma_{(J-H)}$ (5)	(J-K) (6)	# of $\sigma_{(J-K)}$ (7)	(J-W1) (8)	# of $\sigma_{(J-W1)}$ (9)	(J-W2) (10)	# of $\sigma_{(J-W2)}$ (11)	(H-K) (12)	# of $\sigma_{(H-K)}$ (13)
01231125-6921379	M7.5 $\gamma$	-	0.61 ± 0.03	0.0	1.00 ± 0.03	0.3	1.26 ± 0.03	1.0	1.50 ± 0.03	1.3	0.39 ± 0.03	0.3
01294236-0823550	M5-	M7 $\beta$	0.57 ± 0.03	-0.4	0.88 ± 0.03	-0.9	1.11 ± 0.03	-0.7	1.33 ± 0.03	-0.4	0.31 ± 0.03	-0.5
02501064-0151255	-	M7 $\beta$	0.61 ± 0.03	-1.1	0.98 ± 0.03	0.1	1.20 ± 0.03	0.3	1.44 ± 0.03	0.6	0.37 ± 0.03	0.1
02533084+1652532	-	M7 $\beta$	0.51 ± 0.04	-1.6	0.81 ± 0.05	-1.6	1.07 ± 0.03	-1.1	1.34 ± 0.03	-0.3	0.30 ± 0.06	-0.6
025335980+3206373	M7 $\beta$	M6 $\beta$	0.69 ± 0.03	0.8	1.07 ± 0.03	1.0	1.29 ± 0.03	1.4	1.49 ± 0.03	1.2	0.38 ± 0.03	0.2
03350208+2342356	M8.5-	M7.5 $\beta$	0.60 ± 0.03	-0.2	0.99 ± 0.02	0.2	1.21 ± 0.03	0.4	1.48 ± 0.03	1.1	0.39 ± 0.02	0.3
033518131-3101529	M6.5-	M7 $\beta$	0.64 ± 0.03	0.4	0.98 ± 0.03	0.1	1.24 ± 0.03	0.7	1.48 ± 0.03	1.1	0.39 ± 0.03	-0.3
05264316-1824315	-	M7 $\beta$	0.52 ± 0.03	-1.0	0.91 ± 0.03	-0.6	1.16 ± 0.03	-0.1	1.41 ± 0.03	0.4	0.39 ± 0.03	0.3
05575096-1359503	M7-	M7 $\gamma$	0.73 ± 0.03	1.3	1.14 ± 0.03	1.7	1.54 ± 0.03	4.1	2.07 ± 0.03	7.0	0.41 ± 0.03	0.5
07140394+3702459	M8-	M7.5 $\beta$	0.72 ± 0.03	1.3	1.14 ± 0.03	1.7	1.41 ± 0.03	2.7	1.63 ± 0.03	2.6	0.41 ± 0.03	0.5
20391314-1126531	M8-	M7 $\beta$	0.66 ± 0.04	0.6	1.11 ± 0.04	1.4	1.33 ± 0.03	1.7	1.63 ± 0.03	0.6	0.45 ± 0.05	0.9
00192626+4614078	M8-	M8 $\beta$	0.66 ± 0.03	0.1	1.10 ± 0.02	0.4	1.34 ± 0.03	0.6	1.60 ± 0.03	0.9	0.44 ± 0.02	0.3
02212859-6831400	M8 $\beta$	-	0.69 ± 0.05	0.4	1.16 ± 0.05	0.9	1.49 ± 0.04	1.9	1.77 ± 0.04	2.2	0.47 ± 0.05	0.7
03550477-1032415	M8.5-	M8.5 $\beta$	0.62 ± 0.03	-0.4	1.11 ± 0.03	0.4	1.37 ± 0.03	0.8	1.66 ± 0.03	1.3	0.49 ± 0.03	0.9
04351455-14114468	M8 $\gamma$	M7 $\gamma$	1.26 ± 0.04	6.7	1.93 ± 0.04	7.9	2.17 ± 0.04	7.5	2.61 ± 0.04	8.6	0.67 ± 0.03	2.9
04362788-4114465	M8 $\beta$	M9 $\gamma$	0.67 ± 0.03	0.2	1.05 ± 0.03	-0.1	1.36 ± 0.03	0.7	1.64 ± 0.03	1.1	0.38 ± 0.03	-0.3
05341594-0631397	M8 $\gamma$	M8 $\gamma$	0.68 ± 0.12	0.4	1.11 ± 0.12	0.5	1.27 ± 0.08	0.0	1.80 ± 0.09	2.4	0.43 ± 0.14	0.2
06085283-2753583	M8.5 $\gamma$	L0 $\gamma$	0.70 ± 0.04	0.5	1.23 ± 0.04	1.5	1.62 ± 0.04	2.9	1.97 ± 0.03	3.7	0.53 ± 0.03	1.3
06524851-5741376	M8 $\beta$	-	0.67 ± 0.03	0.2	1.18 ± 0.03	1.1	1.48 ± 0.03	1.7	1.78 ± 0.03	2.2	0.52 ± 0.03	1.2
08651384-1342242	M8.5 $\gamma$	M8 $\gamma$	0.63 ± 0.04	-0.3	1.11 ± 0.03	0.5	1.45 ± 0.03	1.5	1.98 ± 0.03	3.8	0.49 ± 0.04	0.9
TWA28	M8.5 $\gamma$	M9 $\gamma$	0.68 ± 0.03	0.3	1.14 ± 0.03	0.8	1.60 ± 0.03	2.7	2.24 ± 0.03	5.8	0.47 ± 0.03	0.6
22353560-5906306	M8.5-	M8 $\gamma$	0.61 ± 0.04	-0.4	1.05 ± 0.04	-0.1	1.44 ± 0.04	1.5	1.99 ± 0.04	3.9	0.44 ± 0.04	0.3
23231347-0244360	M7-	M8 $\beta$	0.68 ± 0.12	0.4	1.31 ± 0.04	2.3	1.68 ± 0.04	3.4	1.94 ± 0.04	3.4	0.50 ± 0.05	1.1
23520507-110435	M7-	M8 $\beta$	0.61 ± 0.04	1.7	1.09 ± 0.03	0.3	1.35 ± 0.03	0.7	1.59 ± 0.03	0.7	0.38 ± 0.04	-0.3
122741197+0503417	M9.5 $\beta$	L0 $\beta$	0.71 ± 0.14	2.1	1.23 ± 0.15	0.7	1.57 ± 0.10	1.1	2.05 ± 0.11	2.4	0.33 ± 0.15	-1.0
15291017+6312539	-	M8 $\beta$	0.71 ± 0.04	0.6	1.09 ± 0.03	0.3	1.35 ± 0.03	0.7	1.59 ± 0.03	0.7	0.38 ± 0.04	-0.2
20242203-5637024	-	M8.5 $\gamma$	0.59 ± 0.03	-0.6	1.13 ± 0.03	0.6	1.37 ± 0.03	0.8	1.66 ± 0.03	1.3	0.53 ± 0.04	-1.4
22353560-5906306	-	M8.5 $\beta$	0.69 ± 0.05	0.4	1.11 ± 0.04	0.5	1.59 ± 0.04	2.7	1.92 ± 0.04	3.3	0.42 ± 0.05	0.2
23231347-0244360	M8.5-	M8 $\beta$	0.65 ± 0.04	0.1	1.10 ± 0.03	0.4	1.34 ± 0.03	0.6	1.63 ± 0.03	1.0	0.44 ± 0.04	0.4
002215494-54112054	M7-	M8 $\beta$	0.67 ± 0.03	0.3	1.10 ± 0.03	0.3	1.40 ± 0.03	1.1	1.69 ± 0.03	1.6	0.42 ± 0.03	0.2
02251947-5837295	M9.5 $\beta$	L0 $\beta$	0.90 ± 0.14	2.1	1.23 ± 0.15	0.7	1.57 ± 0.10	1.1	2.05 ± 0.11	2.4	0.33 ± 0.15	-0.7
00381489-6403529	-	M9.5 $\beta$	0.66 ± 0.05	-0.3	1.13 ± 0.04	-0.2	1.62 ± 0.04	1.5	1.98 ± 0.04	2.0	0.47 ± 0.06	0.2
00425023+1142104	-	M9 $\beta$	0.68 ± 0.06	-0.1	1.24 ± 0.05	0.8	1.52 ± 0.04	0.8	1.84 ± 0.05	1.1	0.56 ± 0.05	1.1
00464841+0715177	M9 $\beta$	L0 $\beta$	0.71 ± 0.04	0.2	1.34 ± 0.04	1.7	1.82 ± 0.04	2.9	2.25 ± 0.03	3.5	0.63 ± 0.04	1.8
02215494-54112054	M9 $\beta$	-	0.68 ± 0.04	-0.1	1.23 ± 0.04	0.7	1.58 ± 0.04	1.2	1.94 ± 0.04	1.7	0.55 ± 0.04	1.0
02251947-5837295	M9 $\beta$	M9 $\gamma$	0.68 ± 0.04	-0.1	1.18 ± 0.04	0.3	1.50 ± 0.03	0.7	1.81 ± 0.03	1.0	0.50 ± 0.04	0.5
03393521-3525440	M9 $\beta$	L0 $\beta$	0.71 ± 0.03	0.2	1.18 ± 0.03	0.2	1.59 ± 0.03	1.3	1.92 ± 0.03	1.6	0.47 ± 0.03	0.2
04433761+0002051	M9 $\gamma$	M9 $\gamma$	0.70 ± 0.03	0.1	1.29 ± 0.03	1.2	1.68 ± 0.03	1.9	2.03 ± 0.03	2.2	0.58 ± 0.03	1.3
04493288+1607226	-	M9 $\gamma$	0.78 ± 0.04	0.9	1.20 ± 0.04	0.4	1.54 ± 0.04	0.9	1.85 ± 0.04	1.2	0.41 ± 0.04	-0.4
05402325-0906326	-	M9 $\beta$	0.74 ± 0.05	0.5	1.26 ± 0.06	1.0	1.56 ± 0.04	1.0	1.84 ± 0.05	1.1	0.52 ± 0.06	0.7
09451445-7753150	-	M9 $\beta$	0.66 ± 0.04	-0.3	1.11 ± 0.04	-0.4	1.38 ± 0.04	-0.2	1.61 ± 0.04	-0.2	0.44 ± 0.04	-0.1
09532126-1014205	M9 $\gamma$	M9 $\beta$	0.82 ± 0.04	1.3	1.33 ± 0.03	1.6	1.71 ± 0.03	2.2	2.07 ± 0.03	2.4	0.45 ± 0.03	0.5
10220489+0200477	M9 $\beta$	M9 $\beta$	0.70 ± 0.04	0.1	1.20 ± 0.04	0.5	1.49 ± 0.04	0.6	1.76 ± 0.04	0.6	0.50 ± 0.04	0.5
11064461-3715115	-	M9 $\gamma$	0.64 ± 0.04	-0.5	1.15 ± 0.05	0.0	1.42 ± 0.04	0.0	1.73 ± 0.04	0.5	0.51 ± 0.05	0.6
15470557-1626303A	-	M9 $\beta$	0.62 ± 0.04	-0.7	1.13 ± 0.04	-0.2	1.43 ± 0.04	0.1	1.72 ± 0.04	0.4	0.51 ± 0.04	0.4
154744719-2423493	M9 $\gamma$	L0 $\gamma$	0.72 ± 0.05	0.3	1.15 ± 0.05	0.0	1.52 ± 0.04	0.8	1.90 ± 0.03	1.4	0.43 ± 0.03	-0.2
12474428-3816464	-	M9 $\gamma$	0.69 ± 0.05	0.0	1.21 ± 0.05	0.6	1.68 ± 0.04	1.9	2.26 ± 0.04	3.6	0.52 ± 0.05	0.7
12555039-4211215	-	M9.5 $\gamma$	0.70 ± 0.15	0.1	1.26 ± 0.15	1.0	1.72 ± 0.11	2.2	2.08 ± 0.11	2.5	0.56 ± 0.15	1.1
14112131-21119503	M9 $\beta$	M8 $\beta$	0.61 ± 0.03	-0.8	1.11 ± 0.03	-0.4	1.36 ± 0.03	-0.4	1.62 ± 0.03	-0.2	0.50 ± 0.03	0.5
15104786-2818174	M9-	M9 $\beta$	0.73 ± 0.04	0.4	1.15 ± 0.04	0.0	1.52 ± 0.04	0.8	1.83 ± 0.04	1.0	0.42 ± 0.04	-0.3
15470557-1626303A	-	M9 $\beta$	0.62 ± 0.04	-0.7	1.13 ± 0.04	-0.2	1.43 ± 0.04	0.1	1.72 ± 0.04	0.4	0.51 ± 0.04	0.6
154744719-2423493	M9 $\gamma$	L0 $\gamma$	0.70 ± 0.04	0.1	1.23 ± 0.03	0.7	1.56 ± 0.04	1.1	1.87 ± 0.04	1.3	0.53 ± 0.04	0.8
15575011-2952431	M9 $\delta$	M9 $\gamma$	0.87 ± 0.16	1.8	1.47 ± 0.16	2.9	1.88 ± 0.12	3.4	2.25 ± 0.13	3.5	0.60 ± 0.15	1.5
19335595-2846343	M9 $\beta$	M9 $\gamma$	0.77 ± 0.03	0.8	1.24 ± 0.04	0.8	1.61 ± 0.04	1.4	2.04 ± 0.03	2.3	0.50 ± 0.03	0.2
20004841-7523070	M9 $\gamma$	M9 $\gamma$	0.77 ± 0.03	0.8	1.22 ± 0.03	0.7	1.63 ± 0.03	1.5	1.94 ± 0.03	1.7	0.47 ± 0.03	0.1
20351512-2806020	M9 $\gamma$	L0 $\gamma$	0.78 ± 0.04	0.9	1.30 ± 0.04	1.4	1.72 ± 0.04	2.2	2.08 ± 0.04	2.5	0.52 ± 0.04	0.7
215444859-7459134	-	M9.5 $\beta$	0.72 ± 0.05	0.3	1.20 ± 0.04	0.5	1.58 ± 0.04	1.2	1.91 ± 0.04	1.5	0.48 ± 0.05	0.3
21572060+8340575	M9 $\gamma$	M9 $\beta$	0.91 ± 0.04	2.2	1.39 ± 0.04	2.2	1.88 ± 0.03	3.4	2.29 ± 0.03	3.8	0.48 ± 0.04	0.3
22025794-5605087	-	M9 $\gamma$	0.74 ± 0.05	0.5	1.20 ± 0.05	1.0	1.55 ± 0.04	1.0	1.80 ± 0.04	0.9	0.46 ± 0.05	0.4

Table 17 – *Continued*

Name (1)	SpT (2)	SpT (3)	$\langle J-H \rangle$ (4)	# of $\sigma_{(J-H)}$ <sup>a</sup> (5)	$\langle J-K \rangle$ (6)	# of $\sigma_{(J-K)}$ <sup>a</sup> (7)	$\langle J-W_1 \rangle$ (8)	# of $\sigma_{(J-W_1)}$ <sup>a</sup> (9)	$\langle J-W_2 \rangle$ (10)	# of $\sigma_{(J-W_2)}$ <sup>a</sup> (11)	$\langle H-K \rangle$ (12)	# of $\sigma_{(H-K)}$ <sup>a</sup> (13)
23360735-3541489	––	M9 $\beta$	0.84 ± 0.04	1.5	1.27 ± 0.05	1.1	1.65 ± 0.03	1.7	2.00 ± 0.04	2.1	0.42 ± 0.05	-0.3
23453903+0055137	M9–	M9 $\beta$	0.65 ± 0.04	-0.4	1.19 ± 0.04	0.4	1.56 ± 0.04	1.1	1.89 ± 0.04	1.4	0.54 ± 0.04	0.9
00325584-4405038	L0 $\gamma$	L0 $\gamma$	0.98 ± 0.08	1.9	1.75 ± 0.07	3.5	2.29 ± 0.06	4.3	2.69 ± 0.06	4.5	0.77 ± 0.07	2.4
00374306-5846229	L0 $\gamma$	L0 $\beta$	0.92 ± 0.05	1.4	1.51 ± 0.05	1.9	1.96 ± 0.04	2.4	2.29 ± 0.04	2.4	0.59 ± 0.05	0.9
01214599-5745379	L0 $\gamma$	––	1.12 ± 0.07	3.0	1.78 ± 0.07	3.8	2.25 ± 0.06	4.1	2.64 ± 0.06	4.2	0.67 ± 0.07	1.6
01415823-4633574	L0 $\gamma$	L0 $\gamma$	1.25 ± 0.14	4.2	1.99 ± 0.14	5.1	2.54 ± 0.11	5.8	2.97 ± 0.11	6.0	0.74 ± 0.12	2.2
02103857-3015313	L0 $\gamma$	L0 $\gamma$	0.96 ± 0.05	1.7	1.73 ± 0.05	3.4	2.28 ± 0.05	4.3	2.66 ± 0.05	4.4	0.78 ± 0.04	2.5
02245464-5815067	L0 $\gamma$	L0 $\gamma$	0.91 ± 0.06	1.3	1.57 ± 0.06	2.3	2.06 ± 0.05	3.0	2.41 ± 0.05	3.1	0.66 ± 0.06	1.5
02265658-5327032	––	L0 $\delta$	1.07 ± 0.06	2.6	1.65 ± 0.06	2.9	2.25 ± 0.05	4.1	2.64 ± 0.05	4.3	0.58 ± 0.06	0.9
02292794-0053282	––	L0 $\gamma$	0.74 ± 0.14	-0.1	1.31 ± 0.17	0.6	1.77 ± 0.10	1.3	2.16 ± 0.11	1.7	0.56 ± 0.17	0.7
02340932-6442068	L0 $\gamma$	L0 $\beta$	0.88 ± 0.08	1.1	1.48 ± 0.09	1.7	2.08 ± 0.07	3.1	2.42 ± 0.07	3.1	0.59 ± 0.09	0.9
02411151-0326587	L0 $\gamma$	L1 $\gamma$	0.99 ± 0.08	2.0	1.76 ± 0.08	3.6	2.16 ± 0.07	3.6	2.54 ± 0.07	3.8	0.77 ± 0.07	2.4
03231002-4631237	L0 $\gamma$	L0 $\gamma$	1.07 ± 0.09	2.7	1.69 ± 0.09	3.1	2.31 ± 0.07	4.5	2.72 ± 0.07	4.7	0.62 ± 0.08	1.2
03240931-2604317	––	L0 $\beta$	0.57 ± 0.14	-1.5	1.54 ± 0.12	2.1	1.95 ± 0.09	2.3	2.38 ± 0.09	2.9	0.98 ± 0.14	4.1
03572693-4417305	L0 $\beta$	L0 $\beta$	0.84 ± 0.04	0.7	1.46 ± 0.04	1.6	1.89 ± 0.04	2.0	2.28 ± 0.04	2.4	0.62 ± 0.04	1.2
04626777-3812102	L0 $\gamma$	L1 $\gamma$	1.06 ± 0.16	2.6	1.66 ± 0.17	2.9	2.32 ± 0.13	4.5	2.67 ± 0.13	4.4	0.60 ± 0.15	1.0
04400972-5126544	––	L0 $\gamma$	0.91 ± 0.09	1.3	1.51 ± 0.09	2.0	2.10 ± 0.07	3.2	2.49 ± 0.07	3.5	0.61 ± 0.08	1.1
06272161-5308428	––	L0 $\beta$	1.15 ± 0.15	3.3	1.70 ± 0.14	3.2	2.50 ± 0.12	5.6	2.88 ± 0.12	5.5	0.54 ± 0.13	0.5
11271382-3735076	––	L0 $\delta$	0.90 ± 0.14	1.3	1.24 ± 0.18	0.1	2.01 ± 0.10	2.7	2.37 ± 0.11	2.8	0.34 ± 0.19	-1.2
11544223-3403390	L0 $\beta$	L1 $\beta$	0.86 ± 0.04	1.0	1.35 ± 0.04	0.8	1.85 ± 0.04	1.7	2.16 ± 0.04	2.4	0.48 ± 0.04	0.0
12074836-3900043	L0 $\gamma$	L1 $\gamma$	0.89 ± 0.08	1.1	1.45 ± 0.08	1.6	1.86 ± 0.06	1.8	2.28 ± 0.06	2.4	0.57 ± 0.08	0.7
15525906+2948485	L0 $\beta$	L0 $\beta$	0.87 ± 0.03	1.0	1.46 ± 0.03	1.6	1.93 ± 0.03	2.3	2.27 ± 0.03	2.3	0.59 ± 0.04	0.9
17111353+2326333	L0 $\gamma$	L1 $\beta$	0.83 ± 0.04	0.7	1.44 ± 0.04	1.5	1.92 ± 0.03	2.2	2.27 ± 0.03	2.3	0.61 ± 0.04	1.1
19564700-7542270	L0 $\gamma$	L2 $\gamma$	1.12 ± 0.14	3.1	1.92 ± 0.12	4.7	2.46 ± 0.11	5.4	2.91 ± 0.11	5.7	0.81 ± 0.12	2.7
20334473-5635338	––	L0 $\gamma$	0.58 ± 0.14	-1.4	1.47 ± 0.12	1.7	1.90 ± 0.09	2.1	2.30 ± 0.09	2.5	0.89 ± 0.14	3.4
22134491-2136079	L0 $\gamma$	L0 $\gamma$	0.97 ± 0.06	1.9	1.62 ± 0.05	2.6	2.15 ± 0.04	3.5	2.54 ± 0.04	3.8	0.64 ± 0.07	1.4
23153135+0617146	L0 $\gamma$	L0 $\gamma$	1.10 ± 0.11	3.0	1.79 ± 0.10	3.8	2.31 ± 0.09	4.5	2.77 ± 0.09	4.9	0.69 ± 0.09	1.7
23224684-3133231	L0 $\beta$	L2 $\beta$	0.79 ± 0.04	0.3	1.25 ± 0.04	0.2	1.60 ± 0.04	0.3	1.87 ± 0.04	0.2	0.47 ± 0.03	-0.1
00040288-6410358	L1 $\gamma$	L1 $\gamma$	0.96 ± 0.10	1.0	1.78 ± 0.08	2.2	2.42 ± 0.08	3.4	2.85 ± 0.08	3.8	0.82 ± 0.09	2.2
00191296-6226005	––	L1 $\gamma$	1.02 ± 0.08	1.5	1.68 ± 0.08	1.8	2.29 ± 0.07	2.8	2.76 ± 0.07	3.4	0.66 ± 0.07	0.9
00344300-4102266	––	L1 $\beta$	0.90 ± 0.06	0.6	1.62 ± 0.09	1.1	2.11 ± 0.07	2.4	2.61 ± 0.07	2.8	0.72 ± 0.09	1.4
00554253-0651239	L0–	L1 $\beta$	0.87 ± 0.04	0.4	1.41 ± 0.04	0.3	1.75 ± 0.03	0.2	2.06 ± 0.04	0.4	0.54 ± 0.04	0.0
01174748-3403258	L1 $\beta$	L1 $\beta$	0.97 ± 0.05	1.1	1.69 ± 0.05	1.8	2.15 ± 0.04	2.1	2.56 ± 0.04	2.5	0.72 ± 0.05	1.4
01205114-520349	––	L1 $\gamma$	0.98 ± 0.10	1.2	1.89 ± 0.09	2.8	2.41 ± 0.08	3.3	2.86 ± 0.08	3.9	0.91 ± 0.09	2.8
02410564-5511466	––	L1 $\gamma$	1.06 ± 0.08	1.8	1.65 ± 0.07	1.6	2.20 ± 0.06	2.3	2.58 ± 0.06	2.6	0.59 ± 0.06	0.4
03164512-2848521	L0–	L1 $\beta$	0.81 ± 0.05	0.0	1.46 ± 0.05	0.6	1.93 ± 0.05	1.0	2.27 ± 0.05	1.3	0.66 ± 0.05	0.9
05184616-2756457	L1 $\gamma$	L1 $\gamma$	0.97 ± 0.06	1.1	1.64 ± 0.06	1.5	2.22 ± 0.05	2.4	2.60 ± 0.05	2.7	0.68 ± 0.06	1.0
06023045+3910592	L1 $\beta$	L1 $\beta$	0.85 ± 0.03	0.3	1.44 ± 0.03	0.4	1.87 ± 0.03	0.7	2.18 ± 0.03	0.9	0.59 ± 0.03	0.4
07224321+615528	L1 $\beta$	L1 $\gamma$	0.90 ± 0.07	0.7	1.63 ± 0.08	1.5	2.31 ± 0.07	2.8	2.67 ± 0.07	3.0	0.72 ± 0.06	1.4
10224321+5825453	L1 $\beta$	L1 $\beta$	0.86 ± 0.04	0.3	1.34 ± 0.03	-0.1	1.74 ± 0.03	0.1	2.00 ± 0.03	0.1	0.48 ± 0.04	-0.4
11083081+6830169	L1 $\gamma$	L1 $\gamma$	0.89 ± 0.03	0.6	1.54 ± 0.03	1.0	2.02 ± 0.03	1.5	2.37 ± 0.03	1.7	0.65 ± 0.03	0.9
11480096-2836488	––	L1 $\beta$	0.93 ± 0.11	0.8	1.55 ± 0.12	1.1	1.97 ± 0.08	1.3	2.34 ± 0.09	1.6	0.62 ± 0.12	0.6
19350976-6200473	L1 $\beta$	L1 $\beta$	0.96 ± 0.14	1.1	1.53 ± 0.14	0.9	2.20 ± 0.11	2.3	2.60 ± 0.11	2.8	0.57 ± 0.14	0.2
22351658-3844154	––	L1 $\gamma$	0.91 ± 0.07	0.7	1.55 ± 0.07	1.1	2.18 ± 0.06	2.2	2.54 ± 0.06	2.5	0.64 ± 0.06	0.8
23255604-0259508	L3–	L1 $\gamma$	1.03 ± 0.10	1.5	1.85 ± 0.10	2.6	2.27 ± 0.08	2.6	2.61 ± 0.08	2.8	0.82 ± 0.09	2.2
00452143+1634446	L2 $\beta$	L2 $\gamma$	1.00 ± 0.04	0.6	1.69 ± 0.03	0.9	2.29 ± 0.03	1.1	2.67 ± 0.03	1.2	0.69 ± 0.04	0.9
0050564+0134365	L2 $\gamma$	L2 $\gamma$	1.17 ± 0.14	1.8	2.00 ± 0.13	2.3	2.75 ± 0.12	2.8	3.23 ± 0.12	3.0	0.83 ± 0.10	2.2
03032042-7312300	L2 $\gamma$	––	1.04 ± 0.14	0.9	1.82 ± 0.14	1.5	2.36 ± 0.11	1.4	2.79 ± 0.11	1.6	0.78 ± 0.12	1.7
05104958-1843548	––	L2 $\beta$	1.01 ± 0.08	0.7	1.54 ± 0.08	0.1	2.10 ± 0.06	0.4	2.41 ± 0.06	0.4	0.53 ± 0.08	-0.6
05361998-1920396	L2 $\gamma$	L1 $\gamma$	1.08 ± 0.10	1.2	1.92 ± 0.10	1.9	2.51 ± 0.08	1.9	2.98 ± 0.08	2.2	0.84 ± 0.09	2.3
20575409-0252302	L1.5–	L2 $\beta$	0.85 ± 0.03	-0.4	1.40 ± 0.03	-0.5	1.86 ± 0.03	-0.4	2.14 ± 0.03	-0.4	0.54 ± 0.03	-0.4
23225299-6151275	L2 $\gamma$	L3 $\gamma^a$	1.01 ± 0.09	0.7	1.69 ± 0.07	0.8	2.30 ± 0.07	1.2	2.70 ± 0.07	1.4	0.68 ± 0.07	0.8
01531463-6744181	L2 $\beta$	L3 $\beta$	1.30 ± 0.16	2.4	1.99 ± 0.17	1.7	2.70 ± 0.14	2.0	3.20 ± 0.14	2.3	0.69 ± 0.13	0.2
02583123-1520536	––	L3 $\beta$	1.04 ± 0.09	0.6	1.72 ± 0.09	0.5	2.29 ± 0.08	0.6	2.71 ± 0.08	0.9	0.67 ± 0.08	0.2
04185879-4507413	––	L3 $\gamma$	1.12 ± 0.11	1.1	1.57 ± 0.12	-0.2	2.30 ± 0.09	0.7	2.71 ± 0.09	0.8	0.45 ± 0.11	-1.3
06322402-5010349	L3 $\beta$	L4 $\gamma$	0.99 ± 0.06	0.2	1.69 ± 0.05	0.3	2.41 ± 0.05	1.0	2.86 ± 0.05	1.3	0.69 ± 0.05	0.3
09593276+4523309	––	L3 $\gamma$	1.12 ± 0.10	2.7	2.21 ± 0.08	3.02	3.02 ± 0.07	3.1	3.52 ± 0.07	3.2	1.09 ± 0.08	2.9

Table 17 — *Continued*

Name (1)	SpT (2)	SpT (3)	$\langle J-H \rangle$ (4)	# of $\sigma_{(J-H)}$ <sup>a</sup> (5)	$\langle J-K \rangle$ (6)	# of $\sigma_{(J-K)}$ <sup>a</sup> (7)	$\langle J-W1 \rangle$ (8)	# of $\sigma_{(J-W1)}$ <sup>a</sup> (9)	$\langle J-W2 \rangle$ (10)	# of $\sigma_{(J-W2)}$ <sup>a</sup> (11)	$\langle H-K \rangle$ (12)	# of $\sigma_{(H-K)}$ <sup>a</sup> (13)
G196-3B	L3 $\beta$	L3 $\gamma$	1.18 ± 0.06	1.6	2.05 ± 0.06	2.0	3.13 ± 0.05	3.5	3.70 ± 0.05	3.8	0.87 ± 0.05	1.5
17260007+1538190	L3.5 $\gamma$	L3 $\gamma$	1.20 ± 0.08	1.7	2.01 ± 0.08	1.8	2.60 ± 0.07	1.7	2.98 ± 0.07	1.6	0.81 ± 0.07	1.0
210113106-5048112	—	L3 $\gamma$	1.17 ± 0.14	1.5	1.85 ± 0.14	1.1	2.41 ± 0.11	1.0	2.76 ± 0.12	1.0	0.68 ± 0.12	0.2
212650408-8140233	L3 $\gamma$	L3 $\gamma$	1.14 ± 0.08	1.3	1.99 ± 0.07	1.7	2.63 ± 0.06	1.8	3.07 ± 0.06	1.9	0.85 ± 0.07	1.4
22081363+2921215	L3 $\gamma$	L3 $\gamma$	1.00 ± 0.11	0.3	1.65 ± 0.11	0.2	2.44 ± 0.09	1.1	2.91 ± 0.09	1.4	0.64 ± 0.10	0.0
00011217+1535355	—	L4 $\beta$	1.02 ± 0.08	-0.3	1.81 ± 0.07	0.3	2.58 ± 0.07	0.5	3.01 ± 0.07	0.7	0.80 ± 0.07	0.9
003323.86-1521309	L4 $\beta$	L1	1.08 ± 0.08	0.0	1.88 ± 0.07	0.5	2.49 ± 0.06	0.2	2.81 ± 0.06	0.2	0.80 ± 0.06	0.9
01262109+1428057	L4 $\gamma$	L2 $\gamma$	0.94 ± 0.31	-0.8	1.83 ± 0.26	0.4	2.87 ± 0.22	1.4	3.41 ± 0.22	1.7	0.89 ± 0.26	1.6
03421621-6817321	L4 $\gamma$	—	1.47 ± 0.16	2.3	2.31 ± 0.16	2.3	2.90 ± 0.14	1.5	3.37 ± 0.14	1.6	0.84 ± 0.12	1.2
05012406-0010432	L4 $\gamma$	L3 $\gamma$	1.27 ± 0.05	1.2	2.02 ± 0.05	1.1	2.93 ± 0.04	1.6	3.46 ± 0.04	1.8	0.75 ± 0.05	0.6
10212570-28330427	—	L4 $\beta\gamma$	1.06 ± 0.19	0.0	1.93 ± 0.20	0.8	2.76 ± 0.16	1.0	3.24 ± 0.16	1.2	0.87 ± 0.17	1.4
125633961-2718455	—	L4 $\beta$	1.04 ± 0.18	-0.2	1.71 ± 0.16	-0.1	2.33 ± 0.13	-0.2	2.72 ± 0.13	0.0	0.67 ± 0.15	0.0
14252798-3650229	L3-	L4 $\gamma$	1.17 ± 0.04	0.6	1.94 ± 0.04	0.8	2.75 ± 0.04	1.0	3.17 ± 0.03	1.1	0.77 ± 0.03	0.7
15332417-1953116	L4 $\gamma$	L4 $\gamma$	1.08 ± 0.09	0.1	1.93 ± 0.08	0.8	2.76 ± 0.07	1.1	3.21 ± 0.07	1.2	0.85 ± 0.08	1.3
15515237+0941148	—	>L5 $\gamma$	1.21 ± 0.13	0.8	2.01 ± 0.12	1.1	2.72 ± 0.11	0.9	3.20 ± 0.11	1.1	0.80 ± 0.09	1.0
16154255+4933211	L4 $\gamma$	L3-L6 $\gamma$	1.46 ± 0.17	2.3	2.48 ± 0.15	3.0	3.59 ± 0.14	3.5	4.17 ± 0.14	3.6	1.02 ± 0.12	2.5
18212815+1414010	L4.5-	L4pec	1.04 ± 0.03	-0.2	1.78 ± 0.03	0.2	2.58 ± 0.03	0.5	2.96 ± 0.03	0.5	0.75 ± 0.03	0.5
21324036+1029494	—	L4 $\beta$	1.23 ± 0.18	0.9	1.96 ± 0.17	0.9	2.56 ± 0.14	0.5	3.02 ± 0.14	0.7	0.73 ± 0.15	0.4
21543454-1055308	L4 $\beta$	L5 $\gamma$	1.37 ± 0.15	1.8	2.24 ± 0.14	2.0	3.07 ± 0.12	2.0	3.52 ± 0.12	2.0	0.87 ± 0.11	1.4
22064498-4217208	L4 $\gamma$	L4 $\gamma$	1.11 ± 0.09	0.2	1.95 ± 0.09	0.8	2.73 ± 0.07	1.0	3.18 ± 0.07	1.1	0.84 ± 0.08	1.2
22495345+0044046	L4 $\gamma$	L3 $\beta$	1.17 ± 0.17	0.6	2.23 ± 0.14	1.9	3.01 ± 0.13	1.8	3.44 ± 0.13	1.8	1.06 ± 0.13	2.8
23433470-3646021	—	L3-L6 $\gamma$	1.56 ± 0.14	2.9	2.37 ± 0.14	2.5	3.45 ± 0.13	3.1	3.96 ± 0.13	3.0	0.82 ± 0.09	1.0
00303013-1450333	L7-	L4-L6 $\beta$	1.01 ± 0.15	-0.6	1.80 ± 0.15	0.2	2.62 ± 0.11	0.6	3.02 ± 0.12	0.6	0.79 ± 0.14	1.2
03264225-2102057	L5 $\beta$	L5 $\beta\gamma^a$	1.34 ± 0.12	1.8	2.21 ± 0.11	2.1	3.18 ± 0.10	2.8	3.70 ± 0.10	2.9	0.87 ± 0.10	1.9
03522337+1133437	L5 $\gamma$	L3-L6 $\gamma$	1.52 ± 0.04	3.1	2.52 ± 0.03	3.5	3.52 ± 0.03	4.2	4.11 ± 0.03	4.3	1.00 ± 0.03	3.1
04210718-6306022	L5 $\beta$	L5 $\gamma$	1.28 ± 0.06	1.4	2.12 ± 0.06	1.7	3.01 ± 0.05	2.1	3.43 ± 0.05	2.0	0.83 ± 0.06	1.6
0520636-2949540	L5 $\gamma$	L5 $\beta$	1.31 ± 0.07	1.5	2.17 ± 0.07	1.9	3.09 ± 0.06	2.4	3.54 ± 0.06	2.4	0.87 ± 0.06	1.9
20025073-0321524	L5 $\beta$	L5-L7 $\gamma$	1.04 ± 0.07	-0.4	1.90 ± 0.06	0.7	2.78 ± 0.05	1.2	3.23 ± 0.06	1.3	0.86 ± 0.06	1.8
00470038+6803543	L7( $\gamma^?$ )	L6-L8 $\gamma$	1.64 ± 0.08	4.4	2.55 ± 0.07	4.6	3.73 ± 0.07	4.6	4.34 ± 0.07	4.4	0.91 ± 0.05	2.4
01033203+1935361	L6 $\beta$	L3.5 $\gamma$	1.39 ± 0.10	1.4	2.14 ± 0.10	1.1	3.11 ± 0.08	1.3	3.59 ± 0.08	1.1	0.75 ± 0.08	-0.1
08095903+4434216	—	L6p	1.25 ± 0.15	0.7	2.02 ± 0.13	0.6	3.09 ± 0.12	1.2	3.63 ± 0.12	1.2	0.77 ± 0.11	0.0
08575849+5708514	L8-	L8-	1.25 ± 0.06	1.2	2.08 ± 0.05	1.9	3.02 ± 0.04	2.3	3.62 ± 0.04	2.1	0.83 ± 0.05	1.8
11193254-1137466	—	L7 $\gamma$	1.67 ± 0.07	4.7	2.71 ± 0.06	5.6	3.91 ± 0.06	5.3	4.58 ± 0.06	5.2	1.04 ± 0.04	3.7
114724.10-204021.3	—	L7 $\gamma$	1.87 ± 0.13	6.4	2.77 ± 0.06	6.0	3.92 ± 0.06	5.3	4.55 ± 0.07	5.1	0.89 ± 0.11	2.1
17410280-4642218	—	L6-L8 $\gamma$	1.25 ± 0.09	1.2	2.35 ± 0.08	3.4	3.49 ± 0.08	3.6	4.11 ± 0.08	3.7	1.10 ± 0.06	4.4
PSO318	—	L6-L8 $\gamma$	1.66 ± 0.09	4.6	2.85 ± 0.09	6.5	4.07 ± 0.08	5.9	4.82 ± 0.09	6.0	1.19 ± 0.06	5.4
22443167+2043433	L6.5p	L6-L8 $\gamma^a$	1.48 ± 0.15	1.8	2.45 ± 0.16	2.2	3.70 ± 0.14	2.7	4.37 ± 0.14	2.6	0.98 ± 0.10	1.4

<sup>a</sup> Values are the # of  $\sigma$  (as reported in Table 15) from the field sequence that each object differs. A negative (-) number indicates that the color was blueward of the field sequence average whereas a positive (+) number indicates that the color was redward of the field sequence average.

**Table 18**  
Infrared Colors of low gravity late-type M and L dwarfs

Name (1)	SpT (2)	SpT (3)	(H-W1) (4)	# of $\sigma_{(H-W1)^a}$ (5)	(H-W2) (6)	# of $\sigma_{(H-W2)^a}$ (7)	(K-W1) (8)	# of $\sigma_{(K-W1)^a}$ (9)	(K-W2) (10)	# of $\sigma_{(K-W2)^a}$ (11)	(W1-W2) (12)	# of $\sigma_{(W1-W2)^a}$ (13)
01231125-6921379	M7.5γ	--	0.65 ± 0.03	1.1	0.89 ± 0.03	1.3	0.26 ± 0.03	0.7	0.51 ± 0.03	1.0	0.24 ± 0.03	0.5
01294256-0823580	M5-	M7β	0.54 ± 0.03	-0.1	0.76 ± 0.03	0.0	0.23 ± 0.03	0.3	0.44 ± 0.03	0.3	0.22 ± 0.03	0.1
02501167-0.151295	--	M7β	0.59 ± 0.03	0.4	0.83 ± 0.03	0.7	0.22 ± 0.03	0.2	0.46 ± 0.03	0.5	0.24 ± 0.03	0.5
02530084+1652532	--	M7β	0.56 ± 0.05	0.1	0.83 ± 0.04	0.7	0.26 ± 0.05	0.7	0.53 ± 0.05	1.2	0.27 ± 0.03	0.9
02535980+3206373	M7β	M6β	0.61 ± 0.03	0.6	0.80 ± 0.03	0.4	0.23 ± 0.03	0.3	0.42 ± 0.03	0.1	0.20 ± 0.03	-0.2
0350208+2342356	M8.5-	M7.5β	0.61 ± 0.03	0.7	0.89 ± 0.03	1.3	0.22 ± 0.03	0.2	0.49 ± 0.02	0.8	0.28 ± 0.03	1.1
051.39-3.101529	M6.5-	M7β	0.59 ± 0.03	0.5	0.83 ± 0.03	0.7	0.26 ± 0.03	0.2	0.50 ± 0.03	0.9	0.24 ± 0.03	1.1
05263136-1824315	--	M7β	0.64 ± 0.03	0.9	0.89 ± 0.03	1.3	0.25 ± 0.03	0.5	0.50 ± 0.03	0.9	0.26 ± 0.03	0.8
05575096-1339503	M7-	M7γ	0.81 ± 0.03	2.9	1.34 ± 0.03	5.8	0.40 ± 0.03	2.2	0.93 ± 0.03	5.2	0.53 ± 0.03	5.4
07140394+3702459	M8-	M7.5β	0.69 ± 0.04	1.5	0.91 ± 0.03	1.5	0.27 ± 0.03	0.8	0.49 ± 0.03	0.8	0.22 ± 0.03	0.2
085192626+4614078	M8-	M8 β	0.66 ± 0.04	1.3	0.96 ± 0.04	2.0	0.22 ± 0.04	0.2	0.51 ± 0.04	1.0	0.30 ± 0.03	1.5
02212859-6831400	M8β	M8 β	0.68 ± 0.03	0.6	0.94 ± 0.03	0.8	0.24 ± 0.03	0.2	0.50 ± 0.02	0.6	0.26 ± 0.03	0.7
03501477-1632415	M8.5-	M8.5β	0.75 ± 0.03	1.3	1.08 ± 0.04	2.0	0.33 ± 0.04	1.3	0.61 ± 0.04	1.6	0.28 ± 0.03	1.0
04351455-1414468	M8γ	M7γ	0.91 ± 0.04	2.9	1.04 ± 0.03	1.6	0.26 ± 0.03	0.5	0.55 ± 0.03	1.0	0.29 ± 0.03	1.1
04362788-4114465	M8 β	M9 γ	0.69 ± 0.03	0.7	0.97 ± 0.03	1.1	0.34 ± 0.03	0.8	0.68 ± 0.03	2.2	0.44 ± 0.03	3.7
05341594-0631397	M8γ	M8γ	0.58 ± 0.10	-0.4	1.11 ± 0.11	2.3	0.15 ± 0.10	-0.7	0.59 ± 0.11	2.2	0.28 ± 0.03	1.0
06085283-2753583	M8.5γ	L0γ	0.92 ± 0.03	3.0	1.27 ± 0.03	3.6	0.39 ± 0.03	1.9	0.75 ± 0.03	2.8	0.53 ± 0.07	5.2
06524851-5741376	M8β	--	0.81 ± 0.03	1.9	1.11 ± 0.03	2.2	0.30 ± 0.03	0.9	0.59 ± 0.03	1.4	0.35 ± 0.03	2.2
08561384-1342242	--	M8γ	0.82 ± 0.04	2.0	1.36 ± 0.04	4.3	0.34 ± 0.03	1.3	0.87 ± 0.03	3.9	0.53 ± 0.03	5.2
TWA28	M8.5γ	M9γ	0.92 ± 0.03	3.0	1.56 ± 0.03	6.0	0.46 ± 0.03	2.6	1.10 ± 0.03	6.0	0.64 ± 0.03	7.0
TWA27A	M8γ	M8γ	0.83 ± 0.04	2.1	1.38 ± 0.04	4.5	0.39 ± 0.04	1.9	0.94 ± 0.04	4.6	0.55 ± 0.03	5.4
12215045-0636458	M9-	M8.5β	0.87 ± 0.04	2.5	1.13 ± 0.04	4.4	0.37 ± 0.05	1.6	0.63 ± 0.04	1.7	0.23 ± 0.03	0.6
15291017+6312539	--	M8β	0.65 ± 0.04	0.3	0.88 ± 0.04	0.3	0.26 ± 0.03	0.5	0.50 ± 0.03	0.5	0.23 ± 0.03	0.3
20282203-5637024	--	M8.5γ	0.77 ± 0.03	1.5	1.07 ± 0.04	1.9	0.24 ± 0.03	0.2	0.54 ± 0.04	0.9	0.30 ± 0.03	1.3
22353560-5906306	--	M8.5 β	0.90 ± 0.04	2.8	1.23 ± 0.05	3.2	0.48 ± 0.04	2.9	0.81 ± 0.04	3.3	0.33 ± 0.04	1.8
23231347-0244360	M8.5-	M8β	0.69 ± 0.04	0.7	0.97 ± 0.04	1.1	0.24 ± 0.04	0.3	0.53 ± 0.04	0.8	0.28 ± 0.03	1.0
23250507-110035	M7-	M8β	0.73 ± 0.03	1.1	1.02 ± 0.03	1.5	0.30 ± 0.03	0.9	0.60 ± 0.03	1.4	0.29 ± 0.03	1.2
00274197+0503417	M9.5β	L0β	0.67 ± 0.11	-0.5	1.15 ± 0.11	1.3	0.34 ± 0.12	0.8	0.83 ± 0.13	2.3	0.48 ± 0.06	4.1
00381489-6403529	--	M9.5β	0.96 ± 0.05	2.2	1.33 ± 0.05	2.5	0.49 ± 0.04	2.3	0.86 ± 0.04	2.5	0.37 ± 0.03	2.1
00425923+1142104	--	M9β	0.84 ± 0.05	1.1	1.16 ± 0.05	1.3	0.28 ± 0.04	0.2	0.60 ± 0.04	0.6	0.32 ± 0.04	1.3
004648461+0715177	M9β	L0β	1.11 ± 0.04	3.5	1.54 ± 0.04	3.9	0.48 ± 0.04	2.2	0.91 ± 0.03	2.9	0.43 ± 0.03	3.2
02215494-5412054	M9 β	--	0.90 ± 0.04	1.6	1.26 ± 0.04	2.0	0.35 ± 0.04	0.9	0.71 ± 0.04	1.4	0.36 ± 0.03	2.0
02251947-5837295	M9β	M9γ	0.82 ± 0.03	0.9	1.13 ± 0.03	1.1	0.33 ± 0.04	0.7	0.63 ± 0.03	0.9	0.31 ± 0.03	1.1
0339521-3525440	M9β	L0β	0.88 ± 0.03	1.5	1.21 ± 0.03	1.7	0.42 ± 0.03	1.6	0.74 ± 0.03	1.7	0.32 ± 0.03	1.4
04433761+0002051	M9γ	M9γ	0.98 ± 0.03	2.3	1.33 ± 0.03	2.5	0.39 ± 0.03	1.3	0.74 ± 0.03	1.7	0.35 ± 0.03	1.8
04493288+1607226	--	M9γ	0.76 ± 0.04	0.4	1.07 ± 0.04	0.7	0.35 ± 0.04	0.9	0.65 ± 0.04	1.0	0.31 ± 0.04	1.1
05402325-0906326	--	M9β	0.82 ± 0.04	0.9	1.11 ± 0.04	1.0	0.30 ± 0.05	0.4	0.59 ± 0.05	0.5	0.29 ± 0.04	0.8
09451445-7753150	--	M9β	0.72 ± 0.04	0.0	0.95 ± 0.04	0.0	0.28 ± 0.04	0.2	0.51 ± 0.04	0.0	0.23 ± 0.03	-0.1
09532126-1014205	M9β	M9β	0.89 ± 0.03	1.5	1.24 ± 0.03	1.9	0.38 ± 0.03	1.2	0.74 ± 0.03	1.6	0.35 ± 0.03	1.9
10220489+0204077	M9β	M9γ	0.79 ± 0.04	0.6	1.06 ± 0.04	0.7	0.29 ± 0.04	0.3	0.56 ± 0.04	0.4	0.27 ± 0.04	0.5
1104461-3715115	--	M9γ	0.77 ± 0.04	0.5	1.09 ± 0.04	0.9	0.27 ± 0.05	0.1	0.59 ± 0.05	0.5	0.32 ± 0.04	1.3
15470557-1626303A	--	M9β	0.84 ± 0.03	1.1	1.20 ± 0.03	1.6	0.35 ± 0.03	0.9	0.71 ± 0.03	1.4	0.36 ± 0.03	2.0
15474429-3816464	M9.5γ	L0γ	0.81 ± 0.04	0.8	1.18 ± 0.04	1.4	0.38 ± 0.04	1.2	0.75 ± 0.04	1.7	0.37 ± 0.03	2.2
12474428-4211215	--	M9.5γ	0.99 ± 0.04	2.4	1.57 ± 0.04	4.1	0.47 ± 0.05	2.1	1.05 ± 0.05	3.9	0.59 ± 0.03	5.8
14112131-21119503	M9β	M8.5	1.02 ± 0.11	2.7	1.38 ± 0.11	2.8	0.46 ± 0.11	2.0	0.82 ± 0.11	2.2	0.36 ± 0.05	2.0
15104786-2818174	M9-	M9β	0.75 ± 0.03	0.3	1.01 ± 0.03	0.3	0.25 ± 0.03	-0.1	0.52 ± 0.03	0.0	0.26 ± 0.03	0.4
2004841-7523070	M9-	M9β	0.80 ± 0.04	0.7	1.10 ± 0.04	0.9	0.37 ± 0.04	1.1	0.67 ± 0.04	1.2	0.31 ± 0.03	1.0
20135152-2806020	M9β	L0γ	0.94 ± 0.04	2.0	1.30 ± 0.04	2.3	0.30 ± 0.04	0.4	0.71 ± 0.04	1.9	0.36 ± 0.04	2.0
21544859-7459134	--	M9.5 β	0.86 ± 0.05	1.3	1.19 ± 0.05	1.5	0.38 ± 0.04	1.2	0.71 ± 0.04	1.4	0.33 ± 0.04	1.5
21572060+8340575	L0-	M9γ	0.98 ± 0.04	2.3	1.39 ± 0.04	2.8	0.50 ± 0.03	2.4	0.90 ± 0.03	2.8	0.41 ± 0.03	2.8
22025794-5605087	--	M9γ	0.81 ± 0.04	0.8	1.06 ± 0.04	0.7	0.35 ± 0.04	0.9	0.61 ± 0.04	0.7	0.25 ± 0.04	0.2

Table 18 — *Continued*

Name (1)	SpT (2)	SpT (3)	(H-W1) (4)	# of $\sigma_{(H-W1)}^a$ (5)	(H-W2) (6)	# of $\sigma_{(H-W2)}^a$ (7)	(K-W1) (8)	# of $\sigma_{(K-W1)}^a$ (9)	(K-W2) (10)	# of $\sigma_{(K-W2)}^a$ (11)	(W1-W2) (12)	# of $\sigma_{(W1-W2)}^a$ (13)
23360735-3541489	—	M9β	0.81 ± 0.03	0.8	1.16 ± 0.04	1.3	0.38 ± 0.05	1.2	0.74 ± 0.05	1.6	0.36 ± 0.04	1.9
23453903+0055137	M9-	M9β	0.91 ± 0.04	1.7	1.24 ± 0.03	1.9	0.37 ± 0.04	1.1	0.70 ± 0.04	1.4	0.33 ± 0.03	1.6
00182334-6703130	—	L0γ	1.31 ± 0.07	3.8	1.71 ± 0.07	3.7	0.54 ± 0.05	1.7	0.94 ± 0.05	2.6	0.40 ± 0.04	1.7
00325584-4405058	L0β	—	1.04 ± 0.04	1.7	1.37 ± 0.04	1.7	0.45 ± 0.04	0.9	0.78 ± 0.04	1.3	0.33 ± 0.04	0.8
00374306-5846229	L0γ	—	1.13 ± 0.06	2.5	1.52 ± 0.06	2.6	0.47 ± 0.05	1.0	0.85 ± 0.05	1.9	0.39 ± 0.04	1.5
01244599-5745379	L0γ	—	1.29 ± 0.09	3.7	1.72 ± 0.09	3.7	0.55 ± 0.09	1.7	0.98 ± 0.09	2.8	0.43 ± 0.04	2.0
0151823-4633574	L0 γ	L0 γ <sup>a</sup>	1.32 ± 0.03	4.0	1.71 ± 0.03	3.7	0.55 ± 0.04	1.7	0.93 ± 0.04	2.5	0.38 ± 0.03	1.4
02103857-3015313	L0 γ	L0 γ <sup>a</sup>	1.16 ± 0.05	2.7	1.51 ± 0.05	2.5	0.50 ± 0.05	1.3	0.85 ± 0.05	1.8	0.35 ± 0.04	1.0
02235464-5815067	L0 γ	—	1.18 ± 0.04	2.9	1.57 ± 0.04	2.9	0.60 ± 0.05	2.2	0.99 ± 0.05	2.9	0.39 ± 0.03	1.5
02265658-5327032	—	L0δ	1.13 ± 0.06	2.4	1.56 ± 0.06	2.8	0.53 ± 0.05	1.6	0.97 ± 0.05	2.8	0.44 ± 0.04	2.1
02292794-0053282	—	L0γ	1.03 ± 0.10	1.7	1.42 ± 0.11	2.0	0.46 ± 0.14	1.0	0.85 ± 0.15	1.9	0.39 ± 0.06	1.5
02340093-442068	L0 γ	L0 β <sup>a</sup> γ	1.20 ± 0.06	3.0	1.54 ± 0.06	2.7	0.60 ± 0.07	2.2	0.95 ± 0.07	2.6	0.34 ± 0.04	0.9
024111151-0326587	L0 γ	L1 γ <sup>a</sup>	1.17 ± 0.06	2.8	1.56 ± 0.06	2.8	0.40 ± 0.06	0.5	0.78 ± 0.06	1.3	0.38 ± 0.04	1.4
03231002-4631237	L0 γ	L0 γ <sup>a</sup>	1.25 ± 0.07	3.4	1.66 ± 0.07	3.4	0.63 ± 0.06	2.4	1.04 ± 0.06	3.3	0.41 ± 0.03	1.8
03420931-2904317	—	L0β	1.38 ± 0.11	4.4	1.81 ± 0.11	4.3	0.41 ± 0.09	0.6	0.84 ± 0.09	1.8	0.43 ± 0.04	2.0
03572695-4417305	L0β	—	1.06 ± 0.03	1.9	1.45 ± 0.03	2.1	0.44 ± 0.03	0.8	0.82 ± 0.03	1.6	0.39 ± 0.03	1.5
04062677-3812102	L0 γ	L1 γ <sup>a</sup>	1.26 ± 0.11	3.5	1.61 ± 0.11	3.1	0.66 ± 0.12	2.7	1.01 ± 0.12	3.1	0.35 ± 0.05	1.0
04400972-5126544	—	L0γ	1.19 ± 0.06	3.0	1.59 ± 0.06	3.0	0.59 ± 0.06	2.0	0.98 ± 0.07	2.8	0.39 ± 0.04	1.5
0622161-5308428	—	L0βγ	1.35 ± 0.09	4.2	1.73 ± 0.10	3.8	0.81 ± 0.09	3.9	1.19 ± 0.09	4.4	0.38 ± 0.04	1.4
11271382-3735076	—	L0δ	1.11 ± 0.11	2.3	1.47 ± 0.12	2.3	0.77 ± 0.16	3.6	1.13 ± 0.16	4.0	0.36 ± 0.06	1.1
11544223-3400390	L0β	—	0.98 ± 0.04	1.3	1.29 ± 0.04	1.3	0.50 ± 0.04	1.3	0.81 ± 0.04	1.6	0.31 ± 0.03	0.5
12074836-3900043	L0 γ	—	0.97 ± 0.06	1.3	1.39 ± 0.06	1.8	0.41 ± 0.07	0.5	0.82 ± 0.07	1.7	0.42 ± 0.04	1.9
15525906+2948485	L0β	—	1.06 ± 0.03	1.9	1.40 ± 0.03	1.9	0.48 ± 0.03	1.1	0.81 ± 0.03	1.6	0.34 ± 0.03	0.8
17129533+2326333	L0 γ	L1 β <sup>a</sup>	1.09 ± 0.04	2.1	1.44 ± 0.04	2.1	0.48 ± 0.04	1.2	0.83 ± 0.04	1.7	0.35 ± 0.03	1.1
19564700-7542270	L0 γ	L2 γ <sup>a</sup>	1.34 ± 0.10	4.1	1.79 ± 0.10	4.2	0.54 ± 0.07	1.6	0.98 ± 0.07	2.9	0.44 ± 0.04	2.2
20334473-5635338	—	L0γ	1.32 ± 0.11	3.9	1.72 ± 0.11	3.8	0.43 ± 0.09	0.7	0.83 ± 0.09	1.7	0.40 ± 0.04	1.7
22134491-2136079	L0γ	L0γ	1.18 ± 0.06	2.8	1.57 ± 0.06	2.9	0.53 ± 0.05	1.6	0.93 ± 0.05	2.4	0.40 ± 0.04	1.6
231531353+0611746	—	L1 β <sup>a</sup>	1.21 ± 0.07	3.0	1.66 ± 0.08	3.4	0.52 ± 0.07	1.5	0.98 ± 0.07	2.8	0.46 ± 0.04	2.3
23246684-3133231	L0β	—	0.82 ± 0.03	0.0	1.08 ± 0.03	0.0	0.35 ± 0.03	0.1	0.62 ± 0.03	0.1	0.27 ± 0.03	0.0
00040288-6410358	L1 γ	L1 γ <sup>a</sup>	1.46 ± 0.08	3.7	1.89 ± 0.08	4.0	0.64 ± 0.05	2.5	1.07 ± 0.05	3.2	0.43 ± 0.04	2.9
00191296-6222605	—	L1 γ	1.27 ± 0.06	2.4	1.74 ± 0.06	3.1	0.61 ± 0.06	2.1	1.07 ± 0.06	3.2	0.47 ± 0.04	3.5
00344223-3402266	—	L1β	1.31 ± 0.07	2.7	1.71 ± 0.07	3.0	0.59 ± 0.06	2.0	0.99 ± 0.06	2.5	0.40 ± 0.04	2.3
00584253-0651239	L0—	L1 β <sup>a</sup>	0.88 ± 0.04	-0.2	1.20 ± 0.04	0.1	0.34 ± 0.04	-0.3	0.66 ± 0.04	0.2	0.31 ± 0.04	0.9
011474748-3403258	L1 β	L1 β <sup>a</sup>	1.18 ± 0.05	1.8	1.59 ± 0.05	2.3	0.46 ± 0.04	0.8	0.87 ± 0.04	1.7	0.41 ± 0.04	2.4
01205114-5203049	—	L1 γ	1.43 ± 0.08	3.5	1.88 ± 0.08	4.0	0.52 ± 0.06	1.4	0.97 ± 0.06	2.5	0.45 ± 0.04	3.2
02424881-5511466	—	L1 γ	1.14 ± 0.06	1.0	1.52 ± 0.06	1.9	0.55 ± 0.04	1.7	0.93 ± 0.05	2.1	0.38 ± 0.03	1.9
03164512-2848521	L0—	L1 β <sup>a</sup>	1.12 ± 0.04	1.4	1.46 ± 0.04	1.6	0.47 ± 0.04	0.9	0.80 ± 0.04	1.2	0.34 ± 0.03	1.3
05181616-2736457	L1 γ	—	1.25 ± 0.05	2.3	1.63 ± 0.05	2.6	0.57 ± 0.05	1.9	0.96 ± 0.05	2.4	0.38 ± 0.04	2.1
06023045+3910592	L1—	L1 β <sup>a</sup>	1.02 ± 0.03	0.7	1.33 ± 0.03	0.9	0.43 ± 0.03	0.5	0.74 ± 0.03	0.8	0.31 ± 0.03	0.8
07123076-6155528	L1 β	—	1.40 ± 0.05	3.3	1.77 ± 0.05	3.3	0.68 ± 0.05	2.8	1.04 ± 0.05	3.0	0.37 ± 0.03	1.8
10224821+5825453	L1β	—	0.88 ± 0.04	-0.2	1.15 ± 0.04	-0.1	0.40 ± 0.03	0.3	0.66 ± 0.03	0.2	0.27 ± 0.03	0.1
11083081+6830169	L1 γ	—	1.13 ± 0.03	1.5	1.48 ± 0.03	1.7	0.48 ± 0.03	1.0	0.83 ± 0.03	1.4	0.35 ± 0.03	1.5
11480096-2836488	—	L1 β <sup>a</sup>	1.05 ± 0.09	0.9	1.41 ± 0.09	1.3	0.42 ± 0.09	0.5	0.79 ± 0.09	1.1	0.37 ± 0.05	1.8
13950976-6200473	—	L1 γ	1.23 ± 0.10	2.2	1.64 ± 0.10	2.6	0.67 ± 0.10	2.7	1.07 ± 0.11	3.2	0.41 ± 0.05	2.0
22351658-3844154	—	L1 γ	1.27 ± 0.05	2.4	1.63 ± 0.05	2.5	0.62 ± 0.05	2.3	0.98 ± 0.05	2.5	0.36 ± 0.04	1.7
23255604-0295908	L3—	L1 β <sup>a</sup>	1.24 ± 0.07	2.2	1.59 ± 0.08	2.3	0.42 ± 0.06	0.5	0.77 ± 0.07	1.0	0.35 ± 0.04	1.4
00452143+1634446	L2β	—	1.29 ± 0.04	1.4	1.67 ± 0.04	1.5	0.60 ± 0.03	1.3	0.98 ± 0.03	1.5	0.38 ± 0.03	1.2
0050564+0134365	L2γ	—	1.59 ± 0.08	3.2	2.07 ± 0.08	3.3	0.76 ± 0.07	2.6	1.24 ± 0.08	3.1	0.48 ± 0.04	2.7
03032042-7312300	L2γ	—	1.32 ± 0.09	1.6	1.75 ± 0.09	1.8	0.54 ± 0.09	0.8	0.97 ± 0.09	1.4	0.43 ± 0.04	2.0
05104958-1843548	—	L2β	1.09 ± 0.06	0.2	1.40 ± 0.06	0.3	0.56 ± 0.06	0.9	0.87 ± 0.06	0.8	0.32 ± 0.04	0.4
05361998-1920396	L2γ	—	1.43 ± 0.07	2.2	1.90 ± 0.08	2.6	0.59 ± 0.07	1.1	1.06 ± 0.07	2.0	0.47 ± 0.04	2.6
20575409-0292302	L1.5—	L2β	1.01 ± 0.03	-0.3	1.29 ± 0.03	-0.2	0.74 ± 0.03	0.0	0.46 ± 0.03	0.1	0.28 ± 0.03	-0.1
232323299-6151275	L2 γ <sup>a</sup>	—	1.29 ± 0.07	1.4	1.69 ± 0.07	1.6	0.62 ± 0.05	1.4	1.02 ± 0.05	1.7	0.40 ± 0.04	1.6
01531463-6744181	L2—	L3 β	1.40 ± 0.09	1.2	1.89 ± 0.09	1.8	0.71 ± 0.11	1.4	1.21 ± 0.11	2.2	0.50 ± 0.04	3.1
02583123-1520536	—	L3 β <sup>a</sup>	1.24 ± 0.07	0.4	1.67 ± 0.07	0.8	0.57 ± 0.06	0.4	1.00 ± 0.06	1.0	0.43 ± 0.04	2.0
04181587-4507413	L3 γ	—	1.18 ± 0.08	0.1	1.59 ± 0.08	0.5	0.73 ± 0.09	0.6	1.14 ± 0.09	1.8	0.41 ± 0.04	1.7
06322402-5010349	L4β	—	1.42 ± 0.04	1.3	1.86 ± 0.04	1.6	0.73 ± 0.04	1.6	1.17 ± 0.04	1.9	0.44 ± 0.03	2.2
09593276+4523309	L3 γ	—	1.90 ± 0.07	3.7	2.40 ± 0.07	3.9	0.81 ± 0.05	2.2	1.31 ± 0.05	2.7	0.50 ± 0.04	3.1

Table 18 — Continued

Name (1)	SpT (2)	SpT (3)	(H-W1) (4)	# of $\sigma_{(H-W1)}^a$ (5)	(H-W2) (6)	# of $\sigma_{(H-W2)}^a$ (7)	(K-W1) (8)	# of $\sigma_{(K-W1)}^a$ (9)	(K-W2) (10)	# of $\sigma_{(K-W2)}^a$ (11)	(W1-W2) (12)	# of $\sigma_{(W1-W2)}^a$ (13)
G196-3B	L3 $\beta$	L3 $\gamma$	1.95 ± 0.05	3.9	2.51 ± 0.05	4.4	1.08 ± 0.04	4.1	1.64 ± 0.04	4.6	0.57 ± 0.03	4.3
17260007+1538190	L3.5 $\gamma$	L3 $\gamma$	1.39 ± 0.05	1.2	1.77 ± 0.05	1.3	0.59 ± 0.06	0.6	0.97 ± 0.06	0.8	0.38 ± 0.04	1.1
20113196-5048112	- -	L3 $\gamma$	1.25 ± 0.09	0.4	1.59 ± 0.09	0.5	0.57 ± 0.09	0.4	0.91 ± 0.09	0.5	0.34 ± 0.05	0.5
21265040-8140293	L3 $\gamma$	L3 $\gamma$	1.50 ± 0.06	1.7	1.93 ± 0.06	1.9	0.64 ± 0.05	0.9	1.08 ± 0.05	1.4	0.44 ± 0.03	2.1
22081363+2821215	L3 $\gamma$	L3 $\gamma$	1.44 ± 0.08	1.4	1.91 ± 0.08	1.8	0.80 ± 0.08	2.0	1.26 ± 0.08	2.5	0.47 ± 0.04	2.6
00011217+1535355	- -	L4 $\beta$	1.57 ± 0.06	0.9	1.99 ± 0.06	1.1	0.77 ± 0.05	0.7	1.19 ± 0.05	1.0	0.42 ± 0.03	1.2
003323.86-1521309	L4 $\beta$	L1	1.41 ± 0.06	0.3	1.73 ± 0.06	0.2	0.61 ± 0.05	-0.5	0.93 ± 0.05	-0.4	0.32 ± 0.04	-0.3
01262109+1428057	L4 $\gamma$	L2 $\gamma$	1.94 ± 0.22	2.5	2.47 ± 0.22	2.8	1.04 ± 0.15	2.6	1.58 ± 0.15	3.2	0.54 ± 0.05	2.8
03421621-6817321	L4 $\gamma$	- -	1.43 ± 0.09	0.4	1.90 ± 0.09	0.8	0.59 ± 0.09	-0.7	1.06 ± 0.09	0.3	0.47 ± 0.04	1.9
05012406-0010452	L4 $\gamma$	L3 $\gamma$	1.66 ± 0.04	1.3	2.20 ± 0.04	1.8	0.91 ± 0.04	1.6	1.44 ± 0.04	2.4	0.53 ± 0.03	2.7
10212570-2830427	- -	L4 $\beta\gamma$	1.69 ± 0.12	1.5	2.17 ± 0.12	1.7	0.82 ± 0.13	1.0	1.30 ± 0.13	1.6	0.48 ± 0.05	2.0
12563961-2718455	- -	L4 $\beta$	1.29 ± 0.12	-0.2	1.68 ± 0.12	0.0	0.62 ± 0.10	-0.4	1.01 ± 0.10	0.0	0.39 ± 0.04	0.8
14252798-3650229	L3-	L4 $\gamma$	1.58 ± 0.03	1.0	2.00 ± 0.03	1.1	0.81 ± 0.03	0.9	1.23 ± 0.03	1.2	0.42 ± 0.03	1.2
153824117-1953116	L4 $\gamma$	L4 $\gamma$	1.68 ± 0.07	1.4	2.13 ± 0.07	1.6	0.83 ± 0.06	1.1	1.28 ± 0.06	1.5	0.45 ± 0.04	1.6
15515237+0941148	L4 $\gamma$	>L5 $\gamma$	1.51 ± 0.08	0.7	1.99 ± 0.08	1.1	0.71 ± 0.06	0.2	1.19 ± 0.06	1.0	0.48 ± 0.04	2.0
16115255+4953211	L4 $\gamma$	L3-L6 $\gamma$	2.13 ± 0.10	3.3	2.71 ± 0.10	3.6	1.11 ± 0.07	3.1	1.69 ± 0.07	3.8	0.58 ± 0.03	3.4
18212815+1414010	L4.5-	L4pec	1.54 ± 0.03	0.8	1.92 ± 0.03	0.9	0.80 ± 0.03	0.8	1.18 ± 0.03	0.9	0.38 ± 0.03	0.5
21324036+1029494	- -	L4 $\beta$	1.34 ± 0.12	0.0	1.79 ± 0.12	0.4	0.60 ± 0.11	-0.5	1.06 ± 0.11	0.3	0.45 ± 0.05	1.6
21543454-1055308	L4 $\beta$	L5 $\gamma$	1.70 ± 0.09	1.5	2.15 ± 0.09	1.7	0.83 ± 0.07	1.1	1.28 ± 0.07	1.5	0.45 ± 0.04	1.6
22064498-4217208	L4 $\gamma$	L4 $\gamma^a$	1.62 ± 0.07	1.2	2.07 ± 0.07	1.4	0.79 ± 0.06	0.8	1.23 ± 0.06	1.2	0.45 ± 0.03	2.0
22495345+0044046	L4 $\gamma$	L3 $\beta$	1.85 ± 0.11	2.1	2.28 ± 0.12	2.1	0.78 ± 0.08	0.7	1.22 ± 0.09	1.1	0.43 ± 0.06	1.3
23433470-3646021	- -	L3-L6 $\gamma$	1.89 ± 0.07	2.3	2.40 ± 0.07	2.5	1.07 ± 0.07	2.8	1.58 ± 0.07	3.2	0.51 ± 0.04	2.4
00303013-1450333	L7-	L4-L6 $\beta$	1.62 ± 0.10	1.5	2.01 ± 0.11	1.4	0.82 ± 0.10	0.7	1.22 ± 0.11	0.8	0.39 ± 0.04	0.6
03264225-2102057	L5 $\beta$	L5 $\beta\gamma^a$	1.84 ± 0.08	3.0	2.36 ± 0.08	3.1	0.97 ± 0.07	1.9	1.49 ± 0.07	2.3	0.51 ± 0.03	2.1
03550337+1133437	L5 $\gamma$	L3-L6 $\gamma$	2.00 ± 0.04	4.1	2.59 ± 0.04	4.2	1.00 ± 0.03	2.2	1.59 ± 0.03	2.8	0.59 ± 0.03	2.9
04210718-6306022	L5 $\gamma$	L5 $\gamma$	1.73 ± 0.05	2.2	2.15 ± 0.05	2.0	0.89 ± 0.05	1.3	1.32 ± 0.05	1.3	0.42 ± 0.03	0.9
05120636-2949540	L5 $\gamma$	L5 $\beta$	1.78 ± 0.05	2.6	2.24 ± 0.05	2.5	0.91 ± 0.05	1.4	1.37 ± 0.05	1.6	0.46 ± 0.03	1.3
20025073-0521524	L5 $\beta$	L5-L7 $\gamma$	1.75 ± 0.06	2.4	2.19 ± 0.06	2.2	0.89 ± 0.04	1.2	1.33 ± 0.04	1.4	0.44 ± 0.03	2.4
00470038+6803543	L7( $\gamma^?$ )	L6-L8 $\gamma$	2.09 ± 0.05	3.4	2.70 ± 0.05	3.3	1.18 ± 0.04	3.0	1.79 ± 0.04	3.0	0.61 ± 0.03	1.8
01033203+1935361	L6 $\beta$	L6 $\beta$	1.72 ± 0.06	0.8	2.20 ± 0.06	0.7	0.97 ± 0.06	1.0	1.45 ± 0.06	1.0	0.48 ± 0.04	0.6
08095903+4434216	- -	L6p	1.84 ± 0.10	1.2	2.37 ± 0.10	1.2	1.07 ± 0.06	1.5	1.61 ± 0.06	1.6	0.53 ± 0.04	1.0
08575849+5708514	L8-	L8-	1.77 ± 0.05	1.9	2.38 ± 0.05	1.8	0.94 ± 0.04	1.3	1.55 ± 0.04	1.3	0.60 ± 0.03	0.4
11193254-1137466	- -	L7 $\gamma$	2.24 ± 0.04	4.2	2.91 ± 0.04	4.1	1.20 ± 0.03	3.2	1.87 ± 0.03	3.4	0.67 ± 0.04	2.4
114724.10-204021.3	- -	L7 $\gamma$	2.05 ± 0.11	3.1	2.67 ± 0.12	3.2	1.15 ± 0.03	2.8	1.78 ± 0.03	3.0	0.63 ± 0.04	2.0
17410280-4642218	- -	L6-L8 $\gamma$	2.23 ± 0.06	4.1	2.86 ± 0.06	4.0	1.14 ± 0.04	2.7	1.76 ± 0.04	2.9	0.63 ± 0.03	2.0
PSO318	- -	L6-L8 $\gamma$	2.41 ± 0.05	5.0	3.16 ± 0.05	5.2	1.22 ± 0.05	3.3	1.97 ± 0.05	4.0	0.75 ± 0.04	3.4
22443167+2043433	L6.5p-	L6-L8 $\gamma^a$	2.22 ± 0.07	2.4	2.89 ± 0.07	2.6	1.25 ± 0.08	2.4	1.91 ± 0.08	2.8	0.67 ± 0.03	2.2

<sup>a</sup> Values are the # of  $\sigma$  (as reported in Table 16) from the field sequence that each object differs. A negative (-) number indicates that the color was blueward of the field sequence average whereas a positive (+) number indicates that the color was redward of the field sequence average.

**Table 19**  
Coefficients of Polynomial Fits for M6 -T9 Dwarfs

$M_{Filter}$	x	rms	$c_0$	$c_1$	$c_2$	$c_3$	$c_4$	$c_5$	$c_6$
$M_J$ FLD	$6.0 < \text{SpT} < 29.0$	0.402	-8.350e+00	7.157e+00	-1.058e+00	7.771e-02	-2.684e-03	3.478e-05	...
$M_J$ YNG	$7.0 < \text{SpT} < 17.0$	0.647	4.032e-03	-1.416e-01	2.097e+00	8.478e-01	...	...	...
$M_J$ GRP	$7.0 < \text{SpT} < 17.0$	0.660	-3.825e-03	1.370e-01	-9.279e-01	10.141e+00	...	...	...
$M_H$ FLD	$6.0 < \text{SpT} < 29.0$	0.389	-7.496e+00	6.406e+00	-9.174e-01	6.551e-02	-2.217e-03	2.841e-05	...
$M_H$ YNG	$7.0 < \text{SpT} < 17.0$	0.634	2.642e-03	-1.049e-01	1.753e+00	1.207e+00	...	...	...
$M_H$ GRP	$7.0 < \text{SpT} < 17.0$	0.603	-3.909e-03	1.346e-01	-9.347e-01	9.728e+00	...	...	...
$M_{Ks}$ FLD	$6.0 < \text{SpT} < 29.0$	0.537	-6.704e+00	5.970e+00	-8.481e-01	5.978e-02	-1.997e-03	2.540e-05	...
$M_{Ks}$ YNG	$7.0 < \text{SpT} < 17.0$	0.640	-1.585e-02	7.338e-01	4.537e+00	...	...	...	...
$M_{Ks}$ GRP	$7.0 < \text{SpT} < 17.0$	0.556	-4.006e-03	1.378e-01	-1.031e+00	9.916e+00	...	...	...
$M_{W1}$ FLD	$6.0 < \text{SpT} < 29.0$	0.365	-1.664e-01	2.991e+00	-3.603e-01	2.258e-02	-6.897e-04	8.337e-06	...
$M_{W1}$ YNG	$7.0 < \text{SpT} < 17.0$	0.648	-1.397e-02	5.955e-01	5.247e+00	...	...	...	...
$M_{W1}$ GRP	$7.0 < \text{SpT} < 17.0$	0.551	-4.483e-03	1.505e-01	-1.208e+00	10.403e+00	...	...	...
$M_{W2}$ FLD	$6.0 < \text{SpT} < 29.0$	0.398	-5.043e-01	3.032e+00	-3.655e-01	2.283e-02	-6.938e-04	8.190e-06	...
$M_{W2}$ YNG	$7.0 < \text{SpT} < 17.0$	0.694	-1.507e-02	5.944e-01	5.061e+00	...	...	...	...
$M_{W2}$ GRP	$7.0 < \text{SpT} < 17.0$	0.616	-6.821e-03	2.322e-01	-2.133e+00	13.322e+00	...	...	...
$M_{W3}$ FLD	$6.0 < \text{SpT} < 29.0$	0.446	6.462e+00	3.365e-01	1.520e-02	-2.573e-03	9.477e-05	-1.024e-06	...
$M_{W3}$ YNG	$7.0 < \text{SpT} < 17.0$	0.717	-1.003e-04	-1.670e-03	2.023e-01	7.529e+00	...	...	...
$M_{W3}$ GRP	$7.0 < \text{SpT} < 17.0$	0.427	-5.684e-03	1.993e-01	-1.987e+00	13.972e+00	...	...	...
$T_{eff}$ FLD	$6.0 < \text{SpT} < 29.0$	113.431	4.747e+03	-7.005e+02	1.155e+02	-1.191e+01	6.318e-01	-1.606e-02	1.546e-04
$T_{eff}$ YNG	$7.0 < \text{SpT} < 17.0$	180.457	1.330e+00	-66.8637	1235.42	-10068.8	32766.4	...	...
$T_{eff}$ YNG2	$7.0 < \text{SpT} < 28.0$	197.737	2.795e+04	-9.183e+03	1.360e+03	-1.066e+02	4.578e+00	-1.016e-01	9.106e-04
$T_{eff}$ GRP	$7.0 < \text{SpT} < 17.0$	172.215	7.383e+00	-344.522	4879.86	...	...	...	...
$L_{bol}$ FLD	$7.0 < \text{SpT} < 28.0$	0.133	2.787e+00	-2.310e+00	3.727e-01	-3.207e-02	1.449e-03	-3.220e-05	2.736e-07
$L_{bol}$ YNG	$7.0 < \text{SpT} < 17.0$	0.335	-6.514e-03	2.448e-01	-3.113e+00	9.492e+00	...	...	...
$L_{bol}$ YNG2	$7.0 < \text{SpT} < 28.0$	0.206	2.059e-01	9.585	-3.985	4.923e-01	-3.048e-02	9.134e-04	-1.056e-05
$L_{bol}$ GRP	$7.0 < \text{SpT} < 17.0$	0.221	6.194e-03	-3.757e-01	2.728e-02	...	...	...	...
$M_{L\text{converted}}^a$	$7.0 < \text{SpT} < 28.0$		-3.46623e-01	3.40366e-02	-3.072e-03				

**Note.** — Relations use 2MASS or WISE magnitudes. Polynomial fits to optical M/L dwarfs and NIR T dwarfs (L dwarfs with no optical spectral type have NIR spectral types) excluding subdwarfs, low-gravity dwarfs, and binaries for the field (FLD) relations. We present polynomials inclusive of (1) all  $\gamma$  and  $\beta$  sources under the YNG polynomials as well as (2) only High Likelihood/bonafide moving group members under the GRP polynomials (see Table 13). The function is defined as  $M_{J,H,Ks,W1,W2,W3,Lbol,Teff} = \sum_{i=0}^n c_i (\text{SpT})^i$  and is valid for varying spectral types M6-T9 where 6=M6, 10=L0, 20=T0, etc. An FTTEST was used to determine the goodness of fit for each polynomial. In the case of all FLD polynomials, the sample of Filippazzo et al. (2015) is used. In the case of all YNG or GRP polynomials, they are valid from M7 - L7. We list a second  $L_{bol}$  and Teff for the YNG polynomial (captioned YNG2) that includes planetary mass companions (e.g. HN Peg b, Gu Psc b, Ross 458C, etc) from Filippazzo et al. (2015) and allows us to extend the polynomial from M7-T8.

<sup>a</sup> Add W1 photometry to SpT polynomial conversion:  $M_{L\text{converted}} = W1 + \sum_{i=0}^n c_i (\text{SpT})^i$

This publication has made use of the Carnegie Astrometric Program parallax reduction software as well as the data products from the Two Micron All-Sky Survey, which is a joint project of the University of Massachusetts and the Infrared Processing and Analysis Center/California Institute of Technology, funded by the National Aeronautics and Space Administration and the National Science Foundation. This research has also made use of the NASA/IPAC Infrared Science Archive, which is operated by the Jet Propulsion Laboratory, California Institute of Technology, under contract with the National Aeronautics and Space Administration. Furthermore, this publication makes use of data products from the Wide-field Infrared Survey Explorer (WISE), which is a joint project of the University of California, Los Angeles, and the Jet Propulsion Laboratory/California Institute of Technology, and NEOWISE, which is a project of the Jet Propulsion Laboratory/California Institute of Technology. WISE and NEOWISE are funded by the US National Aeronautics and Space Administration. Australian access to the Magellan Telescopes was supported through the National Collaborative Research Infrastructure and Collaborative Research Infrastructure Strategies of the Australian Federal Government. CGT acknowledges the support in this research of Australian Research Council grants DP0774000 and DP130102695. JRT gratefully acknowledges support from NSF grants AST-0708810 and AST-1008217

## REFERENCES

- Ackerman, A. S. & Marley, M. S. 2001, ApJ, 556, 872
- Aganze, C., Burgasser, A. J., Faherty, J. K., Choban, C., Escala, I., Lopez, M. A., Jin, Y., Tamiya, T., Tallis, M., & Rockward, W. 2016, AJ, 151, 46
- Allard, F. & Hauschildt, P. H. 1995, ApJ, 445, 433
- Allard, F., Hauschildt, P. H., Alexander, D. R., Tamai, A., & Schweitzer, A. 2001, ApJ, 556, 357
- Aller, K. M., Liu, M. C., Magnier, E. A., Best, W. M. J., Kotson, M. C., Burgett, W. S., Chambers, K. C., Hodapp, K. W., Flewelling, H., Kaiser, N., Metcalf, N., Tonry, J. L., Wainscoat, R. J., & Waters, C. 2016, ApJ, 821, 120
- Allers, K. N., Gallimore, J. F., Liu, M. C., & Dupuy, T. J. 2016, ArXiv e-prints
- Allers, K. N., Jaffe, D. T., Luhman, K. L., Liu, M. C., Wilson, J. C., Skrutskie, M. F., Nelson, M., Peterson, D. E., Smith, J. D., & Cushing, M. C. 2007, ApJ, 657, 511
- Allers, K. N. & Liu, M. C. 2013, ApJ, 772, 79
- Anglada-Escudé, G., Boss, A. P., Weinberger, A. J., Thompson, I. B., Butler, R. P., Vogt, S. S., & Rivera, E. J. 2012, ApJ, 746, 37
- Apai, D., Radigan, J., Buenzli, E., Burrows, A., Reid, I. N., & Jayawardhana, R. 2013, ApJ, 768, 121
- Artigau, É., Gagné, J., Faherty, J., Malo, L., Naud, M.-E., Doyon, R., Lafrenière, D., & Beletsky, Y. 2015, ApJ, 806, 254
- Baraffe, I., Homeier, D., Allard, F., & Chabrier, G. 2015, A&A, 577, A42
- Barenfeld, S. A., Bubar, E. J., Mamajek, E. E., & Young, P. A. 2013, ApJ, 766, 6
- Barman, T. S., Macintosh, B., Konopacky, Q. M., & Marois, C. 2011a, ApJ, 733, 65
- . 2011b, ApJL, 735, L39
- Basri, G. 2000, ARA&A, 38, 485
- Bessell, M. S. 1990, PASP, 102, 1181
- Best, W. M. J., Liu, M. C., Magnier, E. A., Deacon, N. R., Aller, K. M., Redstone, J., Burgett, W. S., Chambers, K. C., Draper, P., Flewelling, H., Hodapp, K. W., Kaiser, N., Metcalfe, N., Tonry, J. L., Wainscoat, R. J., & Waters, C. 2015, ApJ, 814, 118
- Binks, A. S. & Jeffries, R. D. 2014, MNRAS, 438, L11
- Blake, C. H., Charbonneau, D., & White, R. J. 2010, ApJ, 723, 684
- Blake, C. H., Charbonneau, D., White, R. J., Marley, M. S., & Saumon, D. 2007, ApJ, 666, 1198
- Bochanski, J. J., Hennawi, J. F., Simcoe, R. A., Prochaska, J. X., West, A. A., Burgasser, A. J., Burles, S. M., Bernstein, R. A., Williams, C. L., & Murphy, M. T. 2009, PASP, 121, 1409
- Bonnefoy, M., Boccaletti, A., Lagrange, A.-M., Allard, F., Mordasini, C., Beust, H., Chauvin, G., Girard, J. H. V., Homeier, D., Apai, D., Lacour, S., & Rouan, D. 2013, A&A, 555, A107
- Bonnefoy, M., Chauvin, G., Rojo, P., Allard, F., Lagrange, A.-M., Homeier, D., Dumas, C., & Beuzit, J.-L. 2010, A&A, 512, A52
- Bonnefoy, M., Marleau, G.-D., Galicher, R., Beust, H., Lagrange, A.-M., Baudino, J.-L., Chauvin, G., Borgniet, S., Meunier, N., Rameau, J., Boccaletti, A., Cumming, A., Helling, C., Homeier, D., Allard, F., & Delorme, P. 2014, A&A, 567, L9
- Boss, A. P., Weinberger, A. J., Anglada-Escudé, G., Thompson, I. B., Burley, G., Birk, C., Pravdo, S. H., Shaklan, S. B., Gatwood, G. D., Majewski, S. R., & Patterson, R. J. 2009, PASP, 121, 1218
- Bowler, B. P., Liu, M. C., & Dupuy, T. J. 2010a, ApJ, 710, 45
- Bowler, B. P., Liu, M. C., Dupuy, T. J., & Cushing, M. C. 2010b, ApJ, 723, 850
- Bowler, B. P., Liu, M. C., Shkolnik, E. L., & Dupuy, T. J. 2013, ApJ, 774, 55
- Buenzli, E., Apai, D., Radigan, J., Reid, I. N., & Flateau, D. 2014, ApJ, 782, 77
- Buenzli, E., Saumon, D., Marley, M. S., Apai, D., Radigan, J., Bedin, L. R., Reid, I. N., & Morley, C. V. 2015, ApJ, 798, 127
- Burgasser, A. J., Cruz, K. L., Cushing, M., Gelino, C. R.,Looper, D. L., Faherty, J. K., Kirkpatrick, J. D., & Reid, I. N. 2010a, ApJ, 710, 1142
- Burgasser, A. J., Gillon, M., Faherty, J. K., Radigan, J., Triaud, A. H. M. J., Plavchan, P., Street, R., Jehin, E., Delrez, L., & Opitom, C. 2014, ApJ, 785, 48
- Burgasser, A. J., Kirkpatrick, J. D., Brown, M. E., Reid, I. N., Burrows, A., Liebert, J., Matthews, K., Gizis, J. E., Dahn, C. C., Monet, D. G., Cutri, R. M., & Skrutskie, M. F. 2002a, ApJ, 564, 421
- Burgasser, A. J., Liu, M. C., Ireland, M. J., Cruz, K. L., & Dupuy, T. J. 2008, ApJ, 681, 579
- Burgasser, A. J., Logsdon, S. E., Gagné, J., Bochanski, J. J., Faherty, J. K., West, A. A., Mamajek, E. E., Schmidt, S. J., & Cruz, K. L. 2015, ApJS, 220, 18
- Burgasser, A. J., Marley, M. S., Ackerman, A. S., Saumon, D., Lodders, K., Dahn, C. C., Harris, H. C., & Kirkpatrick, J. D. 2002b, ApJL, 571, L151
- Burgasser, A. J., Simcoe, R. A., Bochanski, J. J., Saumon, D., Mamajek, E. E., Cushing, M. C., Marley, M. S., McMurtry, C., Pipher, J. L., & Forrest, W. J. 2010b, ApJ, 725, 1405
- Burrows, A., Hubbard, W. B., Lunine, J. I., & Liebert, J. 2001, Reviews of Modern Physics, 73, 719
- Canty, J. I., Lucas, P. W., Roche, P. F., & Pinfield, D. J. 2013, MNRAS, 435, 2650
- Chauvin, G., Lagrange, A.-M., Dumas, C., Zuckerman, B., Mouillet, D., Song, I., Beuzit, J.-L., & Lowrance, P. 2004, A&A, 425, L29
- Chauvin, G., Lagrange, A.-M., Zuckerman, B., Dumas, C., Mouillet, D., Song, I., Beuzit, J.-L., Lowrance, P., & Bessell, M. S. 2005, A&A, 438, L29
- Crifo, F., Phan-Bao, N., Delfosse, X., Forveille, T., Guibert, J., Martín, E. L., & Reylé, C. 2005, A&A, 441, 653
- Cruz, K. L., Kirkpatrick, J. D., & Burgasser, A. J. 2009, AJ, 137, 3345
- Cruz, K. L., Reid, I. N., Kirkpatrick, J. D., Burgasser, A. J., Liebert, J., Solomon, A. R., Schmidt, S. J., Allen, P. R., Hawley, S. L., & Covey, K. R. 2007, AJ, 133, 439
- Cruz, K. L., Reid, I. N., Liebert, J., Kirkpatrick, J. D., & Lowrance, P. J. 2003, AJ, 126, 2421
- Currie, T., Burrows, A., Itoh, Y., Matsumura, S., Fukagawa, M., Apai, D., Madhusudhan, N., Hinz, P. M., Rodigas, T. J., Kasper, M., Pyo, T.-S., & Ogino, S. 2011, ApJ, 729, 128
- Currie, T., Daemen, S., Debes, J., Lafreniere, D., Itoh, Y., Jayawardhana, R., Ratzka, T., & Correia, S. 2014, ApJL, 780, L30

- Cushing, M. C., Kirkpatrick, J. D., Gelino, C. R., Griffith, R. L., Skrutskie, M. F., Mainzer, A., Marsh, K. A., Beichman, C. A., Burgasser, A. J., Prato, L. A., Simcoe, R. A., Marley, M. S., Saumon, D., Freedman, R. S., Eisenhardt, P. R., & Wright, E. L. 2011, *ApJ*, 743, 50
- Cushing, M. C., Vacca, W. D., & Rayner, J. T. 2004, *PASP*, 116, 362
- Cutri, R. M. & et al. 2013, VizieR Online Data Catalog, 2328
- Cutri, R. M., Skrutskie, M. F., van Dyk, S., Beichman, C. A., Carpenter, J. M., Chester, T., Cambresy, L., Evans, T., Fowler, J., Gizis, J., Howard, E., Huchra, J., Jarrett, T., Kopan, E. L., Kirkpatrick, J. D., Light, R. M., Marsh, K. A., McCallon, H., Schneider, S., Stiening, R., Sykes, M., Weinberg, M., Wheaton, W. A., Wheelock, S., & Zácarias, N. 2003, 2MASS All Sky Catalog of point sources., ed. Cutri, R. M., Skrutskie, M. F., van Dyk, S., Beichman, C. A., Carpenter, J. M., Chester, T., Cambresy, L., Evans, T., Fowler, J., Gizis, J., Howard, E., Huchra, J., Jarrett, T., Kopan, E. L., Kirkpatrick, J. D., Light, R. M., Marsh, K. A., McCallon, H., Schneider, S., Stiening, R., Sykes, M., Weinberg, M., Wheaton, W. A., Wheelock, S., & Zácarias, N.
- Dahn, C. C., Harris, H. C., Vrba, F. J., Guetter, H. H., Canzian, B., Henden, A. A., Levine, S. E., Luginbuhl, C. B., Monet, A. K. B., Monet, D. G., Pier, J. R., Stone, R. C., Walker, R. L., Burgasser, A. J., Gizis, J. E., Kirkpatrick, J. D., Liebert, J., & Reid, I. N. 2002, *AJ*, 124, 1170
- Deacon, N. R., Schlieder, J. E., & Murphy, S. J. 2016, ArXiv e-prints
- Delorme, P., Gagné, J., Malo, L., Reylé, C., Artigau, E., Albert, L., Forveille, T., Delfosse, X., Allard, F., & Homeier, D. 2012, *A&A*, 548, A26
- Dieterich, S. B., Henry, T. J., Jao, W.-C., Winters, J. G., Hosey, A. D., Riedel, A. R., & Subasavage, J. P. 2014, *AJ*, 147, 94
- Dittmann, J. A., Irwin, J. M., Charbonneau, D., & Berta-Thompson, Z. K. 2014, *ApJ*, 784, 156
- Ducourant, C., Teixeira, R., Galli, P. A. B., Le Campion, J. F., Krone-Martins, A., Zuckerman, B., Chauvin, G., & Song, I. 2014, *A&A*, 563, A121
- Dupuy, T. J. & Liu, M. C. 2012, ArXiv e-prints
- Eggen, O. J. & Iben, I. J. 1989, *AJ*, 97, 431
- Faherty, J. K., Beletsky, Y., Burgasser, A. J., Tinney, C., Osip, D. J., Filippazzo, J. C., & Simcoe, R. A. 2014a, *ApJ*, 790, 90
- Faherty, J. K., Burgasser, A. J., Cruz, K. L., Shara, M. M., Walter, F. M., & Gelino, C. R. 2009, *AJ*, 137, 1
- Faherty, J. K., Burgasser, A. J., Walter, F. M., Van der Blieck, N., Shara, M. M., Cruz, K. L., West, A. A., Vrba, F. J., & Anglada-Escudé, G. 2012, *ApJ*, 752, 56
- Faherty, J. K., Rice, E. L., Cruz, K. L., Mamajek, E. E., & Núñez, A. 2013, *AJ*, 145, 2
- Faherty, J. K., Tinney, C. G., Skemer, A., & Monson, A. J. 2014b, *ApJL*, 793, L16
- Filippazzo, J. C., Rice, E. L., Faherty, J., Cruz, K. L., Van Gordon, M. M., &Looper, D. L. 2015, *ApJ*, 810, 158
- Fuhrmann, K. & Chini, R. 2015, *ApJ*, 806, 163
- Gagné, J., Burgasser, A. J., Faherty, J. K., Lafrenière, D., Doyon, R., Filippazzo, J. C., Bowsher, E., & Nicholls, C. P. 2015a, *ApJL*, 808, L20
- Gagné, J., Faherty, J. K., Cruz, K., Lafrenière, D., Doyon, R., Malo, L., & Artigau, É. 2014a, *ApJL*, 785, L14
- Gagné, J., Faherty, J. K., Cruz, K. L., Lafrenière, D., Doyon, R., Malo, L., Burgasser, A. J., Naud, M.-E., Artigau, É., Bouchard, S., Gizis, J. E., & Albert, L. 2015b, *ApJS*, 219, 33
- Gagné, J., Lafrenière, D., Doyon, R., Artigau, É., Malo, L., Robert, J., & Nadeau, D. 2014b, *ApJL*, 792, L17
- Gagné, J., Lafrenière, D., Doyon, R., Malo, L., & Artigau, É. 2014c, *ApJ*, 783, 121
- . 2014d, *ApJ*, 783, 121
- . 2015c, *ApJ*, 798, 73
- Gálvez-Ortiz, M. C., Clarke, J. R. A., Pinfield, D. J., Jenkins, J. S., Folkes, S. L., Pérez, A. E. G., Day-Jones, A. C., Birmingham, B., Jones, H. R. A., Barnes, J. R., & Pokorný, R. S. 2010, *MNRAS*, 409, 552
- Gauza, B., Béjar, V. J. S., Pérez-Garrido, A., Rosa Zapatero Osorio, M., Lodieu, N., Rebolo, R., Pallé, E., & Nowak, G. 2015, *ApJ*, 804, 96
- Gillon, M., Triaud, A. H. M. J., Jehin, E., Delrez, L., Opitom, C., Magain, P., Lendl, M., & Queloz, D. 2013, *A&A*, 555, L5
- Gizis, J. E. 2002, *ApJ*, 575, 484
- Gizis, J. E., Allers, K. N., Liu, M. C., Harris, H. C., Faherty, J. K., Burgasser, A. J., & Kirkpatrick, J. D. 2015, *ApJ*, 799, 203
- Gizis, J. E., Faherty, J. K., Liu, M. C., Castro, P. J., Shaw, J. D., Vrba, F. J., Harris, H. C., Aller, K. M., & Deacon, N. R. 2012, *AJ*, 144, 94
- Gizis, J. E., Monet, D. G., Reid, I. N., Kirkpatrick, J. D., Liebert, J., & Williams, R. J. 2000, *AJ*, 120, 1085
- Golimowski, D. A., Leggett, S. K., Marley, M. S., Fan, X., Geballe, T. R., Knapp, G. R., Vrba, F. J., Henden, A. A., Luginbuhl, C. B., Guetter, H. H., Munn, J. A., Canzian, B., Zheng, W., Tsveltanov, Z. I., Chiu, K., Glazebrook, K., Hoversten, E. A., Schneider, D. P., & Brinkmann, J. 2004, *AJ*, 127, 3516
- Gorlova, N. I., Meyer, M. R., Rieke, G. H., & Liebert, J. 2003, *ApJ*, 593, 1074
- Hallinan, G., Littlefair, S. P., Cotter, G., Bourke, S., Harding, L. K., Pineda, J. S., Butler, R. P., Golden, A., Basri, G., Doyle, J. G., Kao, M. M., Berdyugina, S. V., Kuznetsov, A., Rupen, M. P., & Antonova, A. 2015, *Nature*, 523, 568
- Hawley, S. L., Covey, K. R., Knapp, G. R., Golimowski, D. A., Fan, X., Anderson, S. F., Gunn, J. E., Harris, H. C., Ivezić, Ž., Long, G. M., Lupton, R. H., McGehee, P. M., Narayanan, V., Peng, E., Schlegel, D., Schneider, D. P., Spahn, E. Y., Strauss, M. A., Szkody, P., Tsvetanov, Z., Walkowicz, L. M., Brinkmann, J., Harvanek, M., Hennessy, G. S., Kleinman, S. J., Krzesinski, J., Long, D., Neilson, E. H., Newman, P. R., Nitta, A., Snedden, S. A., & York, D. G. 2002, *AJ*, 123, 3409
- Hayashi, C. & Nakano, T. 1963, *Progress of Theoretical Physics*, 30, 460
- Henry, T. J., Jao, W.-C., Subasavage, J. P., Beaulieu, T. D., Ianna, P. A., Costa, E., & Méndez, R. A. 2006, *AJ*, 132, 2360
- Hinkley, S., Bowler, B. P., Vigan, A., Aller, K. M., Liu, M. C., Mawet, D., Matthews, E., Wahhaj, Z., Kraus, S., Baraffe, I., & Chabrier, G. 2015, *ApJL*, 805, L10
- Hinz, P. M., Rodigas, T. J., Kenworthy, M. A., Sivanandam, S., Heinze, A. N., Mamajek, E. E., & Meyer, M. R. 2010, *ApJ*, 716, 417
- Johnson, D. R. H. & Soderblom, D. R. 1987, *AJ*, 93, 864
- Kellogg, K., Metchev, S., Gagne, J., & Faherty, J. 2016, ArXiv e-prints
- Kellogg, K., Metchev, S., Geißler, K., Hicks, S., Kirkpatrick, J. D., & Kurtev, R. 2015, *AJ*, 150, 182
- Kendall, T. R., Delfosse, X., Martín, E. L., & Forveille, T. 2004, *A&A*, 416, L17
- Kirkpatrick, J. D. 2005, *ARA&A*, 43, 195
- Kirkpatrick, J. D., Barman, T. S., Burgasser, A. J., McGovern, M. R., McLean, I. S., Tinney, C. G., & Lowrance, P. J. 2006, *ApJ*, 639, 1120
- Kirkpatrick, J. D., Cruz, K. L., Barman, T. S., Burgasser, A. J., Looper, D. L., Tinney, C. G., Gelino, C. R., Lowrance, P. J., Liebert, J., Carpenter, J. M., Hillenbrand, L. A., & Stauffer, J. R. 2008, *ApJ*, 689, 1295
- Kirkpatrick, J. D., Cushing, M. C., Gelino, C. R., Griffith, R. L., Skrutskie, M. F., Marsh, K. A., Wright, E. L., Mainzer, A., Eisenhardt, P. R., McLean, I. S., Thompson, M. A., Bauer, J. M., Benford, D. J., Bridge, C. R., Lake, S. E., Petty, S. M., Stanford, S. A., Tsai, C.-W., Bailey, V., Beichman, C. A., Bloom, J. S., Bochanski, J. J., Burgasser, A. J., Capak, P. L., Cruz, K. L., Hinz, P. M., Kartaltepe, J. S., Knox, R. P., Manohar, S., Masters, D., Morales-Calderón, M., Prato, L. A., Rodigas, T. J., Salvato, M., Schurr, S. D., Scoville, N. Z., Simcoe, R. A., Stapelfeldt, K. R., Stern, D., Stock, N. D., & Vacca, W. D. 2011, *ApJS*, 197, 19
- Kirkpatrick, J. D., Looper, D. L., Burgasser, A. J., Schurr, S. D., Cutri, R. M., Cushing, M. C., Cruz, K. L., Sweet, A. C., Knapp, G. R., Barman, T. S., Bochanski, J. J., Roellig, T. L., McLean, I. S., McGovern, M. R., & Rice, E. L. 2010, *ApJS*, 190, 100
- Kirkpatrick, J. D., Reid, I. N., Liebert, J., Gizis, J. E., Burgasser, A. J., Monet, D. G., Dahn, C. C., Nelson, B., & Williams, R. J. 2000, *AJ*, 120, 447

- Knapp, G. R., Leggett, S. K., Fan, X., Marley, M. S., Geballe, T. R., Golimowski, D. A., Finkbeiner, D., Gunn, J. E., Hennawi, J., Ivezić, Z., Lupton, R. H., Schlegel, D. J., Strauss, M. A., Tsvetanov, Z. I., Chiu, K., Hoversten, E. A., Glazebrook, K., Zheng, W., Hendrickson, M., Williams, C. C., Uomoto, A., Vrba, F. J., Henden, A. A., Luginbuhl, C. B., Guetter, H. H., Munn, J. A., Canzian, B., Schneider, D. P., & Brinkmann, J. 2004, AJ, 127, 3553
- Kraus, A. L., Ireland, M. J., Cieza, L. A., Hinkley, S., Dupuy, T. J., Bowler, B. P., & Liu, M. C. 2014, ApJ, 781, 20
- Kumar, S. S. 1963, ApJ, 137, 1121
- Kuzuhara, M., Tamura, M., Kudo, T., Janson, M., Kandori, R., Brandt, T. D., Thalmann, C., Spiegel, D., Biller, B., Carson, J., Hori, Y., Suzuki, R., Burrows, A., Henning, T., Turner, E. L., McElwain, M. W., Moro-Martín, A., Suenaga, T., Takahashi, Y. H., Kwon, J., Lucas, P., Abe, L., Brandner, W., Egner, S., Feldt, M., Fujiwara, H., Goto, M., Grady, C. A., Guyon, O., Hashimoto, J., Hayano, Y., Hayashi, M., Hayashi, S. S., Hodapp, K. W., Ishii, M., Iye, M., Knapp, G. R., Matsuo, T., Mayama, S., Miyama, S., Morino, J.-I., Nishikawa, J., Nishimura, T., Kotani, T., Kusakabe, N., Pyo, T.-S., Serabyn, E., Suto, H., Takami, M., Takato, N., Terada, H., Tomono, D., Watanabe, M., Wisniewski, J. P., Yamada, T., Takami, H., & Usuda, T. 2013, ApJ, 774, 11
- Lagrange, A.-M., Bonnefoy, M., Chauvin, G., Apai, D., Ehrenreich, D., Boccaletti, A., Gratadour, D., Rouan, D., Mouillet, D., Lacour, S., & Kasper, M. 2010, Science, 329, 57
- Liu, M. C., Magnier, E. A., Deacon, N. R., Allers, K. N., Dupuy, T. J., Kotson, M. C., Aller, K. M., Burgett, W. S., Chambers, K. C., Draper, P. W., Hodapp, K. W., Jedicke, R., Kaiser, N., Kudritzki, R.-P., Metcalfe, N., Morgan, J. S., Price, P. A., Tonry, J. L., & Wainscoat, R. J. 2013, ApJL, 777, L20
- Lodders, K. 1999, ApJ, 519, 793
- Looper, D. L., Burgasser, A. J., Kirkpatrick, J. D., & Swift, B. J. 2007, ApJL, 669, L97
- Looper, D. L., Kirkpatrick, J. D., Cutri, R. M., Barman, T., Burgasser, A. J., Cushing, M. C., Roellig, T., McGovern, M. R., McLean, I. S., Rice, E., Swift, B. J., & Schurr, S. D. 2008, ApJ, 686, 528
- Lucas, P. W., Roche, P. F., Allard, F., & Hauschildt, P. H. 2001, MNRAS, 326, 695
- Luhman, K. L. 2014, ApJL, 786, L18
- Luhman, K. L., Peterson, D. E., & Megeath, S. T. 2004, ApJ, 617, 565
- Mace, G. N., Kirkpatrick, J. D., Cushing, M. C., Gelino, C. R., McLean, I. S., Logsdon, S. E., Wright, E. L., Skrutskie, M. F., Beichman, C. A., Eisenhardt, P. R., & Kulas, K. R. 2013, ApJ, 777, 36
- Macintosh, B., Graham, J. R., Barman, T., De Rosa, R. J., Konopacky, Q., Marley, M. S., Marois, C., Nielsen, E. L., Pueyo, L., Rajan, A., Rameau, J., Saumon, D., Wang, J. J., Ammons, M., Arriaga, P., Artigau, E., Beckwith, S., Brewster, J., Bruzzone, S., Bulger, J., Birmingham, B., Burrows, A. S., Chen, C., Chiang, E., Chilcote, J. K., Dawson, R. I., Dong, R., Doyon, R., Draper, Z. H., Duchêne, G., Esposito, T. M., Fabrycky, D., Fitzgerald, M. P., Follette, K. B., Fortney, J. J., Gerard, B., Goodsell, S., Greenbaum, A. Z., Hibon, P., Hinkley, S., Hufford, T., Hung, L.-W., Ingraham, P., Johnson-Groh, M., Kalas, P., Lafreniere, D., Larkin, J. E., Lee, J., Line, M., Long, D., Maire, J., Marchis, F., Matthews, B. C., Max, C. E., Metchev, S., Millar-Blanchaer, M. A., Mittal, T., Morley, C. V., Morzinski, K. M., Murray-Clay, R., Oppenheimer, R., Palmer, D. W., Patel, R., Patience, J., Perrin, M. D., Poyneer, L. A., Rafikov, R. R., Rantakyrö, F. T., Rice, E., Rojo, P., Rudy, A. R., Ruffio, J.-B., Ruiz, M. T., Sadakuni, N., Saddlemeyer, L., Salama, M., Savransky, D., Schneider, A. C., Sivaramakrishnan, A., Song, I., Soummer, R., Thomas, S., Vasisht, G., Wallace, J. K., Ward-Duong, K., Wiktorowicz, S. J., Wolff, S. G., & Zuckerman, B. 2015, ArXiv e-prints
- Madhusudhan, N., Burrows, A., & Currie, T. 2011, ApJ, 737, 34
- Males, J. R., Close, L. M., Morzinski, K. M., Wahhaj, Z., Liu, M. C., Skemer, A. J., Kopon, D., Follette, K. B., Puglisi, A., Esposito, S., Riccardi, A., Pinna, E., Kompero, M., Briguglio, R., Biller, B. A., Nielsen, E. L., Hinz, P. M., Rodigas, T. J., Hayward, T. L., Chun, M., Ftacras, C., Toomey, D. W., & Wu, Y.-L. 2014, ApJ, 786, 32
- Malo, L., Doyon, R., Feiden, G. A., Albert, L., Lafrenière, D., Artigau, É., Gagné, J., & Riedel, A. 2014, ApJ, 792, 37
- Malo, L., Doyon, R., Lafrenière, D., Artigau, É., Gagné, J., Baron, F., & Riedel, A. 2013, ApJ, 762, 88
- Marley, M. S., Saumon, D., Cushing, M., Ackerman, A. S., Fortney, J. J., & Freedman, R. 2012, ArXiv e-prints
- Marocco, F., Andrei, A. H., Smart, R. L., Jones, H. R. A., Pinfield, D. J., Day-Jones, A. C., Clarke, J. R. A., Sozzetti, A., Lucas, P. W., Buccarelli, B., & Penna, J. L. 2013, AJ, 146, 161
- Marois, C., Macintosh, B., Barman, T., Zuckerman, B., Song, I., Patience, J., Lafrenière, D., & Doyon, R. 2008, Science, 322, 1348
- Marois, C., Zuckerman, B., Konopacky, Q. M., Macintosh, B., & Barman, T. 2010, Nature, 468, 1080
- McGovern, M. R., Kirkpatrick, J. D., McLean, I. S., Burgasser, A. J., Prato, L., & Lowrance, P. J. 2004, ApJ, 600, 1020
- McLean, I. S., Becklin, E. E., Bendiksen, O., Brims, G., Canfield, J., Figer, D. F., Graham, J. R., Hare, J., Lacayanga, F., Larkin, J. E., Larson, S. B., Levenson, N., Magnone, N., Teplitz, H., & Wong, W. 1998, in Society of Photo-Optical Instrumentation Engineers (SPIE) Conference Series, Vol. 3354, Infrared Astronomical Instrumentation, ed. A. M. Fowler, 566–578
- Metchev, S. A., Heinze, A., Apai, D., Flateau, D., Radigan, J., Burgasser, A., Marley, M. S., Artigau, É., Plavchan, P., & Goldsmith, B. 2015, ApJ, 799, 154
- Metchev, S. A. & Hillenbrand, L. A. 2006, ApJ, 651, 1166
- Mohanty, S., Jayawardhana, R., & Barrado y Navascués, D. 2003, ApJL, 593, L109
- Mohanty, S., Jayawardhana, R., Huéamo, N., & Mamajek, E. 2007, ApJ, 657, 1064
- Oppenheimer, B. R., Baranec, C., Beichman, C., Brenner, D., Burruss, R., Cady, E., Crepp, J. R., Dekany, R., Fergus, R., Hale, D., Hillenbrand, L., Hinkley, S., Hogg, D. W., King, D., Ligon, E. R., Lockhart, T., Nilsson, R., Parry, I. R., Pueyo, L., Rice, E., Roberts, J. E., Roberts, Jr., L. C., Shao, M., Sivaramakrishnan, A., Soummer, R., Truong, T., Vasit, G., Veitch, A., Vescelus, F., Wallace, J. K., Zhai, C., & Zimmerman, N. 2013, ApJ, 768, 24
- Patience, J., King, R. R., De Rosa, R. J., Vigan, A., Witte, S., Rice, E., Helling, C., & Hauschildt, P. 2012, A&A, 540, A85
- Patten, B. M., Stauffer, J. R., Burrows, A., Marengo, M., Hora, J. L., Luhman, K. L., Sonnett, S. M., Henry, T. J., Raghavan, D., Megeath, S. T., Liebert, J., & Fazio, G. G. 2006, ApJ, 651, 502
- Persson, S. E., Murphy, D. C., Smee, S., Birk, C., Monson, A. J., Uomoto, A., Koch, E., Shectman, S., Barkhouse, R., Orndorff, J., Hammond, R., Harding, A., Scharfstein, G., Kelson, D., Marshall, J., & McCarthy, P. J. 2013, PASP, 125, 654
- Phan-Bao, N., Bessell, M. S., Martín, E. L., Simon, G., Borsenberger, J., Tata, R., Guibert, J., Crifo, F., Forveille, T., Delfosse, X., Lim, J., & de Batz, B. 2008, MNRAS, 383, 831
- Pickles, A. J. 1998, PASP, 110, 863
- Radigan, J., Jayawardhana, R., Lafrenière, D., Artigau, É., Marley, M., & Saumon, D. 2012, ApJ, 750, 105
- Radigan, J., Lafrenière, D., Jayawardhana, R., & Artigau, E. 2014, ApJ, 793, 75
- Reid, I. N., Cruz, K. L., & Allen, P. R. 2007, AJ, 133, 2825
- Reid, I. N., Cruz, K. L., Kirkpatrick, J. D., Allen, P. R., Mungall, F., Liebert, J., Lowrance, P., & Sweet, A. 2008, AJ, 136, 1290
- Reid, I. N., Kirkpatrick, J. D., Liebert, J., Gizis, J. E., Dahn, C. C., & Monet, D. G. 2002, AJ, 124, 519
- Reiners, A. 2009, ApJL, 702, L119
- Reiners, A. & Basri, G. 2009, ApJ, 705, 1416
- Rice, E. L., Faherty, J. K., Cruz, K., Barman, T., Looper, D., Malo, L., Mamajek, E. E., Metchev, S., & Shkolnik, E. L. 2011, ArXiv e-prints
- Rice, E. L., Faherty, J. K., & Cruz, K. L. 2010, ApJL, 715, L165
- Riedel, A. 2015, TBD
- Rodriguez, D. R., Zuckerman, B., Kastner, J. H., Bessell, M. S., Faherty, J. K., & Murphy, S. J. 2013, ApJ, 774, 101
- Sahlmann, J., Lazorenko, P. F., Bouy, H., Martín, E. L., Queloz, D., Ségransan, D., & Zapatero Osorio, M. R. 2016, MNRAS, 455, 357
- Salim, S. & Gould, A. 2003, ApJ, 582, 1011
- Saumon, D. & Marley, M. S. 2008, ApJ, 689, 1327

- Schmidt, S. J., Cruz, K. L., Bongiorno, B. J., Liebert, J., & Reid, I. N. 2007, AJ, 133, 2258
- Schmidt, S. J., West, A. A., Hawley, S. L., & Pineda, J. S. 2010, AJ, 139, 1808
- Schneider, A., Melis, C., & Song, I. 2012a, ApJ, 754, 39
- Schneider, A., Song, I., Melis, C., Zuckerman, B., & Bessell, M. 2012b, ApJ, 757, 163
- Schneider, A. C., Cushing, M. C., Kirkpatrick, J. D., Mace, G. N., Gelino, C. R., Faherty, J. K., Fajardo-Acosta, S., & Sheppard, S. S. 2014, AJ, 147, 34
- Schneider, A. C., Windsor, J., Cushing, M. C., Kirkpatrick, J. D., & Wright, E. L. 2016, ArXiv e-prints
- Scholz, R.-D., McCaughrean, M. J., Zinnecker, H., & Lodieu, N. 2005, A&A, 430, L49
- Seifahrt, A., Reiners, A., Almaghrbi, K. A. M., & Basri, G. 2010, A&A, 512, A37
- Shkolnik, E. L., Anglada-Escudé, G., Liu, M. C., Bowler, B. P., Weinberger, A. J., Boss, A. P., Reid, I. N., & Tamura, M. 2012, ApJ, 758, 56
- Shkolnik, E. L., Liu, M. C., Reid, I. N., Dupuy, T., & Weinberger, A. J. 2011, ApJ, 727, 6
- Simcoe, R. A., Burgasser, A. J., Schechter, P. L., Fishner, J., Bernstein, R. A., Bigelow, B. C., Pipher, J. L., Forrest, W., McMurtry, C., Smith, M. J., & Bochanski, J. J. 2013, PASP, 125, 270
- Skemer, A. J., Hinz, P. M., Esposito, S., Burrows, A., Leisenring, J., Skrutskie, M., Desidera, S., Mesa, D., Arcidiacono, C., Mannucci, F., Rodigas, T. J., Close, L., McCarthy, D., Kulesa, C., Agapito, G., Apai, D., Argomedo, J., Bailey, V., Boutsia, K., Briguglio, R., Brusa, G., Busoni, L., Claudi, R., Eisner, J., Fini, L., Follette, K. B., Garnavich, P., Gratton, R., Guerra, J. C., Hill, J. M., Hoffmann, W. F., Jones, T., Krejny, M., Males, J., Masciadri, E., Meyer, M. R., Miller, D. L., Morzinski, K., Nelson, M., Pinna, E., Puglisi, A., Quanz, S. P., Quiros-Pacheco, F., Riccardi, A., Stefanini, P., Vaiteeswaran, V., Wilson, J. C., & Xompero, M. 2012, ApJ, 753, 14
- Skemer, A. J., Morley, C. V., Zimmerman, N. T., Skrutskie, M. F., Leisenring, J., Buenzli, E., Bonnefoy, M., Bailey, V., Hinz, P., DeFrere, D., Esposito, S., Apai, D., Biller, B., Brandner, W., Close, L., Crepp, J. R., De Rosa, R. J., Desidera, S., Eisner, J., Fortney, J., Freedman, R., Henning, T., Hofmann, K.-H., Kopytova, T., Lupu, R., Maire, A.-L., Males, J. R., Marley, M., Morzinski, K., Oza, A., Patience, J., Rajan, A., Rieke, G., Schertl, D., Schlieder, J., Stone, J., Su, K., Vaz, A., Visscher, C., Ward-Duong, K., Weigelt, G., & Woodward, C. E. 2015, ArXiv e-prints
- Stauffer, J. R., Schultz, G., & Kirkpatrick, J. D. 1998, ApJL, 499, L199
- Stephens, D. C., Leggett, S. K., Cushing, M. C., Marley, M. S., Saumon, D., Geballe, T. R., Golimowski, D. A., Fan, X., & Noll, K. S. 2009, ApJ, 702, 154
- Teegarden, B. J., Pravdo, S. H., Hicks, M., Lawrence, K., Shaklan, S. B., Covey, K., Fraser, O., Hawley, S. L., McGlynn, T., & Reid, I. N. 2003, ApJL, 589, L51
- Teixeira, R., Ducourant, C., Chauvin, G., Krone-Martins, A., Song, I., & Zuckerman, B. 2008, A&A, 489, 825
- Thompson, M. A., Kirkpatrick, J. D., Mace, G. N., Cushing, M. C., Gelino, C. R., Griffith, R. L., Skrutskie, M. F., Eisenhardt, P. R. M., Wright, E. L., Marsh, K. A., Mix, K. J., Beichman, C. A., Faherty, J. K., Tolosa, O., Ferrara, J., Apodaca, B., McLean, I. S., & Bloom, J. S. 2013, PASP, 125, 809
- Thorstensen, J. R. 2003, AJ, 126, 3017
- Thorstensen, J. R., Lépine, S., & Shara, M. 2008, AJ, 136, 2107
- Tinney, C. G., Burgasser, A. J., & Kirkpatrick, J. D. 2003, AJ, 126, 975
- Tinney, C. G., Faherty, J. K., Kirkpatrick, J. D., Cushing, M., Morley, C. V., & Wright, E. L. 2014, ApJ, 796, 39
- Tinney, C. G., Faherty, J. K., Kirkpatrick, J. D., Wright, E. L., Gelino, C. R., Cushing, M. C., Griffith, R. L., & Salter, G. 2012, ApJ, 759, 60
- Tinney, C. G., Reid, I. N., Gizis, J., & Mould, J. R. 1995, AJ, 110, 3014
- Tokunaga, A. T. & Kobayashi, N. 1999, AJ, 117, 1010
- Torres, C. A. O., Quast, G. R., Melo, C. H. F., & Sterzik, M. F. 2008, Young Nearby Loose Associations, ed. Reipurth, B., 757
- Tremblin, P., Amundsen, D. S., Chabrier, G., Baraffe, I., Drummond, B., Hinkley, S., Mourier, P., & Venot, O. 2016, ApJL, 817, L19
- Tsuji, T., Ohnaka, K., & Aoki, W. 1996a, A&A, 305, L1
- Tsuji, T., Ohnaka, K., Aoki, W., & Nakajima, T. 1996b, A&A, 308, L29
- Vacca, W. D., Cushing, M. C., & Rayner, J. T. 2003, PASP, 115, 389
- Vrba, F. J., Henden, A. A., Luginbuhl, C. B., Guetter, H. H., Munn, J. A., Canzian, B., Burgasser, A. J., Kirkpatrick, J. D., Fan, X., Geballe, T. R., Golimowski, D. A., Knapp, G. R., Leggett, S. K., Schneider, D. P., & Brinkmann, J. 2004, AJ, 127, 2948
- Weinberger, A. J., Anglada-Escudé, G., & Boss, A. P. 2013, ApJ, 762, 118
- West, A. A., Hawley, S. L., Bochanski, J. J., Covey, K. R., Reid, I. N., Dhital, S., Hilton, E. J., & Masuda, M. 2008, AJ, 135, 785
- Wilson, J. C., Miller, N. A., Gizis, J. E., Skrutskie, M. F., Houck, J. R., Kirkpatrick, J. D., Burgasser, A. J., & Monet, D. G. 2003, in IAU Symposium, Vol. 211, Brown Dwarfs, ed. E. Martín, 197
- Woitke, P. & Helling, C. 2004, A&A, 414, 335
- Zapatero Osorio, M. R., Béjar, V. J. S., Miles-Páez, P. A., Peña Ramírez, K., Rebolo, R., & Pallé, E. 2014, A&A, 568, A6
- Zuckerman, B. & Song, I. 2004, ARA&A, 42, 685
- Zuckerman, B., Song, I., & Bessell, M. S. 2004, ApJL, 613, L65